Effects of Gadolinium-Based Nanoparticles AGuIX on Ionizing Radiation-Elicited Macrophage Functional Reprogramming

Zeinaf Muradova

université PARIS-SACLAY

Effects of Gadolinium-based nanoparticles AGuIX on ionizing radiation-elicited macrophage functional reprogramming

Effets des nanoparticules à base de Gadolinium AGuIX sur la reprogrammation fonctionnelle des macrophages induite par les rayonnements ionisants

Thèse de doctorat de l'université Paris-Saclay

École doctorale n°582 : cancérologie : biologie - médecine - santé (CBMS)
Spécialité de doctorat : aspects moléculaires et cellulaires de la biologie
Graduate School : Sciences de la vie et santé. Référent : Faculté de médecine

Thèse préparée dans l'unité de recherche **Radiothérapie Moléculaire et Innovation Thérapeutique (Université Paris-Saclay, Institut Gustave Roussy, Inserm)**, sous la direction **de Jean-Luc PERFETTINI**, Directeur de recherche, Université Paris-Saclay

Thèse soutenue à Paris-Saclay, le 29 novembre 2021, par

Zeinaf MURADOVA

Composition du Jury

Sandrine LACOMBE Professeure, Université Paris-Saclay	Présidente
François PARIS Directeur de recherche, Université de Nantes	Rapporteur & Examinateur
Serge CANDEIAS Chercheur, Université Grenoble-Alpes	Rapporteur & Examinateur
Awatef ALLOUCH Chercheuse, Université Paris-Saclay	Examinatrice
Olivier TILLEMENT Professeur, Université de Lyon	Examinateur
Jean-Luc PERFETTINI Directeur de recherche, Université Paris-Saclay	Directeur de thèse

THESE DE DOCTORAT

NNT : 2021UPASL097

This thesis work has been supported by
University of Paris-Saclay and
INSERM UMR 1030

université PARIS-SACLAY

ÉCOLE DOCTORALE
Cancérologie : biologie - médecine - santé (CBMS)

Title : Effects of Gadolinium-based nanoparticles AGuIX on ionizing radiation-elicited macrophage functional reprogramming

Keywords : TAMs, nanoparticles, AGuIX, cancer, AMPK, radiotherapy

Abstract : Tumor-associated macrophages (TAMs) are essential components of the inflammatory microenvironment of tumors and are associated with poor clinical outcomes in the majority of cancers. TAMs mainly exhibit anti-inflammatory functions that promote and support the tissue remodeling, the immune suppression, and the tumor growth. Converting anti-inflammatory TAMs into pro-inflammatory phenotype recently emerged as a therapeutic opportunity to improve the efficacy of anticancer treatments such as radiotherapy. Here we show that gadolinium-based nanoparticles AGuIX alone and in combination with ionizing radiation induce DNA damage and an Ataxia telangiectasia mutated (ATM)-DNA-damage response in human macrophages and trigger their pro-inflammatory reprogramming. This process is associated with the activating phosphorylation of the Adenosine Monophosphate (AMP) activated protein kinase on threonine 1972 (AMPKT172*) and the modulation of mitochondrial dynamic. Interestingly, we demonstrate that the depletion of the AMPK reduces the mitochondrial fragmentation and the pro-inflammatory reprogramming of macrophages elicited by gadolinium-based nanoparticles AGuIX and their combination with ionizing radiation, thus revealing that the AMPK plays a central role for the pro-inflammatory macrophage reprogramming. Altogether, our results identify a novel signaling pathway induced by gadolinium-based nanoparticles AGuIX and their combined treatment with ionizing radiation that target macrophage polarization, skew macrophage function toward the pro-inflammatory phenotype and may enhance the effectiveness of radiotherapy.

université PARIS-SACLAY | ÉCOLE DOCTORALE Cancérologie : biologie - médecine - santé (CBMS)

Titre : Effets des nanoparticules à base de gadolinium AGuIX sur la reprogrammation des macrophages induite par les rayonnements ionisants

Mots clés : TAMs, nanoparticules, AGuIX, cancer, AMPK, radiothérapie

Résumé : Les macrophages associés aux tumeurs (TAMs) sont des composants essentiels du microenvironnement inflammatoire des tumeurs et sont associés à de mauvais pronostics cliniques dans la majorité des cancers. Les TAMs présentent principalement des fonctions anti-inflammatoires qui favorisent et soutiennent le remodelage tissulaire, la suppression immunitaire et la croissance tumorale. La conversion des TAMs anti-inflammatoires en phénotype pro-inflammatoire est récemment apparue comme une opportunité thérapeutique pour améliorer l'efficacité des traitements anticancéreux tels que la radiothérapie. Dans cette thèse, nous démontrons que les nanoparticules à base de gadolinium AGuIX seules et en combinaison avec des rayonnements ionisants, induisent des dommages à l'ADN, une réponse aux dommages à l'ADN induite par l'ataxie télangiectasie (ATM) dans les macrophages humains et déclenchent une reprogrammation pro-inflammatoire des macrophages. Ce processus, est associé à la phosphorylation de la protéine kinase active sur l'adénosine monophosphate (AMP) de la thréonine 1972 (AMPKT172*) et à la modulation de la dynamique mitochondriale. Nous démontrons également que l'extinction de l'AMPK réduit la fragmentation mitochondriale et la reprogrammation pro-inflammatoire des macrophages induits par les nanoparticules à base de gadolinium AGuIX et leur combinaison avec les rayonnements ionisants. Ce phénomène, révèle ainsi que l'AMPK joue un rôle central pour la reprogrammation pro-inflammatoire des macrophages. Dans l'ensemble, nos résultats identifient une nouvelle voie de signalisation induite par les nanoparticules à base de gadolinium AGuIX et leur traitement combiné avec des rayonnements ionisants, ciblent la polarisation des macrophages, altèrent la fonction des macrophages vers le phénotype pro-inflammatoire et améliorent l'efficacité de la radiothérapie.

TABLE OF CONTENT

AKNOWLEDGEMENT

First and foremost, I would like to extend my sincere gratitude to my PhD supervisor Dr. Jean-Luc PERFETTINI for his assistance and support at every stage of the research project. I also would like to thank Dr. Awatef ALLOUCH for her insightful comments and suggestions in setting up experimental methods and analysis of the results during the course of my PhD degree. This work would not have been possible without the constant support of both of you.

I would like to acknowledge Dr. Serge CANDEIAS, Dr. François PARIS, Dr. Olivier TILLEMENT, and Dr. Sandrine LACOMBE for being in my thesis evaluation committee. I am extremely grateful for your time, guidance and suggestions.

I am especially thankful to all my colleagues and friends at Institute Gustave Roussy: Ali, Aurelia, Emmie, Deborah, Desiree, Kevin, Nathalie, Constance, Luca, Winchign, Lydia, Dorine, Melanie, Murat, Umit, Regina, Zakia, and Larissa. You all have given me a tremendous support and have been always ready to help with any questions that I had.

Further, I would like to thank Doctoral School n° 582 of the University of Paris-Saclay for the provided studentship that allowed me to conduct this thesis. I would like also to thank the assistant of the doctoral school Lea POISOT, for her continuous help throughout of my education.

Last but not the least, I would like to say a heartfelt thank to my family: my parents, my grandma and grandpa, my brothers, Emil and Osman, my sister, Etar, and my nephew, Turgut, as well as my friends: Aliya, Celia, Aktoti, Sonya, Aziza, Shokhista, Gulaiim, Dana, Aygerim, Marjan, Rachael, Thuy, Oriana, Yiwen, Akzhan, Carlos, and Luca for always believing in me and encouraging me to follow my dreams. Your love and prayers kept me going during this challenging period of my life and I dedicate this work to all of you.

Zeinaf Muradova

September 2021

ABBREVATIONS

15-HETE	15-hydroxyeicosatetraenoic acid
15-LOX	15-lipoxygenase
3DCRT	3D conformal radiotherapy
7AAD	7-amino-actinomycin D
ACs	Apoptotic cells
AD	Activation domain
AHFRT	Ablative hypofractionated radiation therapy
AID	Autoinhibitory domain
ALDA	Aldolase
AMPK	AMP-activated protein kinase
ANG-2	Angiopoietin-2
AP-1	Activator protein 1
APTES	Aminopropyl triethoxysilane
ASL	Argininosuccinate lyase
ASS1	Argininosuccinate synthase
ATM	Ataxia-telangiectasia mutated
ATMs	Adipose tissue macrophages
ATP	Adenosine triphosphate
ATR	ATM and Rad3-related
ATRIP	ATR-interacting protein
BMDMs	Bone-marrow-derived macrophages
BPs	Bisphosphonates
C/EBPs	CCAAT/enhancer-binding proteins
CAD	Cell-autonomous death
CAF	Cancer-associated fibroblasts
CaMKKβ	Calcium/calmodulin-dependent protein kinase β
CAT 1	Cationic amino acid transporters 1
CAT 2	Cationic amino acid transporters 2
CBM	Carbohydrate-binding module
CBS	Cystathionine β synthase
CCK8	Cell counting kit-8
CCR2	C–C chemokine receptor type 2
cDCs	Conventional DCs
CDK	Cyclin-dependent kinases
CFRT	Conventional fractionated radiation therapy
cGAS	cGMP-AMP synthase
Chk1	Checkpoint kinase 1
CHO	Chinese hamster ovary
CLUT	Glucose transporters
cMoPs	Common monocyte progenitors
CNS	Central nervous system

COX-2	Cyclooxygenase-2
CRT	Calreticulin
CSF-1	Colony-stimulating factor-1
CTD	C-terminal domain
CTFs	Collaborating transcription factors
DAMPs	Damage-associated molecular patterns
DAP12	DNAX-activating protein of 12 kDa
DDR	DNA damage response
DEF	Dose enhancement factor
DEG	Diethylene glycol
DOTAGA	1,4,7,10-tetra- azacyclododecane-1-glutaric anhydride- 4,7,10-triacetic acid
Drp1	Dynamin-related protein 1
DSBs	Double-strand breaks
dsDNA	Double-stranded DNA
EBRT	External beam radiation therapy
ECM	Extracellular matrix
EGF	Epidermal growth factor
EIMs	Erythroblastic island macrophages
EMPs	Erythro-myeloid progenitors
EMT	Epithelial-mesenchymal transition
ENO1	Enolase 1
ENOL	Enolase
EPR	Enhanced permeability and retention
ER	Endoplasmic reticulum
ET	Endothelin
FAO	Fatty acid oxidation
FGF	Fibroblast growth factor
Fis1	Mitochondrial fission 1
GAS	Gamma-activated sequence
Gd	Gadolinium
GLS	Glutaminase
GLUD1	Glutamate dehydrogenase
GM-CSF	Granulocyte-macrophage colony-stimulating factor
GMPs	Granulocyte/macrophage precursors
H3K27	Histone 3 Lys 27
H3K4me3	Histone 3 lysine 4 trimethylation
HIFs	Hypoxia-inducible factors
HK2	Hexokinase 2
HMGB1	High mobility group B1
HSCs	Hematopoietic stem cells
HSPs	Heat shock proteins
ICD	Immunologic cell death
ICP-MS	Inductively coupled plasma-mass spectroscopy

ICSBP	IFN consensus sequence binding protein
ID	Injected dose
IDO	Indoleamine2,3-dioxygenase
IFN-γ	Interferon-γ
IGF-1	Insulin-like growth factor-1
IGF-1	Insulin-like growth factor–1
IGF-1R	Insulin-like growth factor–1 receptor
IL-34	Interleukin 34
ILC2s	Type 2 innate lymphoid cells
IMCs	Immature myeloid cells
IMRT	Intensity-modulated radiation therapy
iNOS	Inducible nitric oxide synthase (iNOS)
IRF-8	Interferon regulatory factor-8
IRFs	Interferon regulatory factors
ISGF3	IFN-stimulated gene factor 3
ISGs	Interferon-stimulated genes
ISREs	Interferon-stimulated response elements
iTregs	Induced regulatory T cells
JAKs	Janus tyrosine kinases
Jmjd3	Jumonji domain-containing 3
KCs	Kupffer cells
KD	Kinase domain
KLF-4	Kruppel-like Factor 4
LDHA	Lactate dehydrogenase-A
LDTFs	Lineage determining transcription factors
LIBS	Laser-induced breakdown spectroscopy
LKB1	Liver kinase B1
LPS	Lipopolysaccharides
LSPR	Localized surface plasmon resonance
LT-HSCs	Long-term HSCs
LYVE-1	Lymphatic vessel endothelial hyaluronan receptor 1
M-CSF	Macrophage colony-stimulating factor
MARCO	Macrophage receptor with collagenous structure
MCP-1	Monocyte chemoattractant protein-1
MDPs	Macrophage/DC precursors
MDSCs	Myeloid-derived suppressor cells
MFF	Mitochondrial fission factors
MFN1	Mitofusin 1
miRNAs	MicroRNAs
MM	Meningeal macrophages
MMMs	Marginal metallophilic macrophages
MMPs	Matrix metalloproteinases
MMPs	Matrix metalloproteinases

moDCs	Monocyte-derived DCs
MPPs	Multipotent HSCs
MRI	Magnetic resonance imaging
mROS	Mitochondrial ROS
Mtg 16	Myeloid translocation gene on chromosome 16
MZMs	Marginal zone macrophages
NCAD	Non-cell-autonomous death
NCS	Neocarzinostatin
NIK	NF-κB-inducing kinase
NK	Natural killer
NKG2D	Natural killer group 2 member D
NLC	Nanostructured lipid carriers
NPs	Nanoparticles
Nrf2	NF-E2 related factor 2
NSLC	Non-small lung cancer
nTregs	Natural regulatory T cells
OI	Optical imaging
OPA1	Optic atrophy 1
OPN	Osteopontin
OXPHOS	Oxidative phosphorylation
PAI-1	Plasminogen activator inhibitor-1
PAMPs	Pathogen associated pattern molecules (PAMPs)
PDAC	Pancreatic ductal adenocarcinoma
pDCs	Plasmacytoid DCs
PDGF	Platelet-derived growth factor
PEG	Polyethylene glycol
PEG-PGlu	Poly(ethylene glycol)-b-poly(glutamic acid)
PFKL	Glycolytic enzymes PFK-liver type
PGK1	Phosphoglycerate kinase-1
PGs	Prostaglandins
PIKK	Phosphatidylinositol-3-kinase-related kinases
PINK1	Phosphatase and tensin homolog-induced kinase1
PLGA	Poly(lactic-co-glycolic acid)
PPARG	Peroxisome proliferator-activated receptor-gamma
PPP	Pentose-phosphate pathway
PRRs	Pattern-recognition receptors
PSCs	Pancreatic stellate cells
PVA	Polyvinyl alcohol
PVM	Perivascular macrophages
QDs	Quantum dots
RA	Rheumatoid arthritis
RLR	Retinoic acid-inducible gene-I-like receptor
ROS	Reactive Oxygen Species

RPA	Replication protein A
RPMs	Red pulp macrophages
SABR	Stereotactic ablative radiotherapy
SBRT	Stereotactic body radiation therapy
SCA-1	Stem cell antigen-1
SCFAs	Short-chain fatty acids
SCS	Subcapsular sinus
SDS	Sodium dodecylsulfate
SDTFs	Signal-dependent transcription factors
SER	Sensitizing enhancement ratio
SF	Survival fraction
SHIP1	Src homology-2 domain-containing inositol 5-phosphatase 1
Siglec-1	Sialic acid-binding Ig-like Lectin-1
SLE	Systemic lupus erythematosus
SLN	Solid lipid nanoparticles
SR-DUV	Synchrotron Radiation Deep UV
SSBs	Single-strand breaks
ssDNA	single-stranded DNA
ST-HSCs	Short-term HSCs
STAT	Signal transducer and activator of transcription
STING	Stimulator of IFN genes
TAMs	Tumor-associated macrophages
TANs	Tumor-associated neutrophils
TCA	Tricarboxylic acid
TEM	Transmission electron microscopy
TEMs	TIE2-expressing monocytes
TGF-β	Transforming growth factor-beta
TLRLs	Toll-like receptor ligands
TLRs	Toll-like receptors
TME	Tumor microenvironment
TNF	Tumor necrosis factor
TNF-α	Tumor necrosis factor-α
TNFR	TNF receptor
Tregs	Regulatory T cells
TREM2	Triggering receptor expressed on myeloid cells 2
TSS	Transcription start sites
VCAM-1	Vascular cell adhesion molecule-1
VEGF	Vascular endothelial growth factor
VEGF-A	Vascular endothelial growth factor A
WASP	Wiskott-Aldrich syndrome protein
WAVE2	WASP-family verprolin homologous 2
WBRT	Whole-brain radiotherapy
α-KG	α-ketoglutarate

LIST OF FIGURES

LIST OF TABLES

RESUME DE THESE

Effets des nanoparticules à base de gadolinium AGuIX sur la reprogrammation des macrophages induite par les rayonnements ionisants

Contexte

Le microenvironnement tumoral (TME) est très hétérogène et se compose de diverses cellules, dont des macrophages. Ces macrophages résidant dans les tissus sont caractérisés par une grande plasticité et peuvent se différencier en deux formes : les macrophages activés de manière classique (également appelés M1) et les macrophages activés alternativement (M2). Les macrophages M1 présentent un phénotype pro-inflammatoire et anti-tumoral, tandis que les macrophages M2 ont tendance à développer des réponses anti-inflammatoires et pro-tumorales. Les macrophages abondants dans le TME sont principalement polarisés en phénotype de type M2 et sont appelés macrophages associés aux tumeurs (TAMs). L'accumulation de preuves indique que les TAMs proviennent principalement de monocytes dérivés de la moelle osseuse recrutés sur le site de la tumeur. Les fonctions pro-tumorales des TAMs comprennent la promotion de l'invasion des cellules tumorales, des métastases, de l'angiogenèse, du remodelage de la matrice extracellulaire et de l'immunosuppression tumorale. Ces fonctions pro-tumorales des TAMs en font une cible thérapeutique intéressante pour les thérapies anticancéreuses. L'une des stratégies émergentes pour cibler les TAMs comprend la reprogrammation des TAMs d'un phénotype pro-tumoral de type M2 en un phénotype anti-tumoral de type M1. Plusieurs études ont démontré que les rayonnements ionisants (IR) pouvaient repolariser les TAMs vers un phénotype pro-inflammatoire en induisant une réponse aux dommages de l'ADN.

Plusieurs nanoparticules à base de métal ont été développées pour améliorer le dépôt de doses de rayonnement dans les sites tumoraux. Sous l'exposition de l'IR, ces nanoparticules métalliques produisent des photons et des électrons Auger qui améliorent les dommages à l'ADN et génèrent des espèces réactives de l'oxygène (ROS). Outre les propriétés radiosensibilisantes, les nanoparticules métalliques à base de gadolinium, comme AGuIX (activation et guidage de l'irradiation par rayons X), ont été largement utilisées en clinique comme agents de contraste positifs pour l'IRM en raison de leurs propriétés paramagnétiques. Après des études précliniques approfondies, les nanoparticules AGuIX en association avec la radiothérapie sont actuellement testées dans de multiples essais cliniques chez des patientes

présentant des métastases cérébrales et un cancer avancé du col de l'utérus. Bien que la combinaison d'AGuIX avec l'IR ait démontré l'efficacité potentielle dans les traitements contre le cancer, leur impact combiné sur les cellules immunitaires est mal compris. L'objectif de ce doctorat. La thèse est d'évaluer l'impact des nanoparticules AGuIX en combinaison avec l'IR sur le phénotype des TAMs.

Résultats

1. Les nanoparticules AGuIX à base de gadolinium et leur combinaison avec les rayonnements ionisants déclenchent des cassures double brin de l'ADN et activent la réponse aux dommages à l'ADN dépendant de l'ATM dans les macrophages humains anti-inflammatoires.

Plusieurs études ont démontré que les nanoparticules AGuIX en combinaison avec la radiothérapie augmentent les dommages à l'ADN dans les cellules cancéreuses. Nous avons déjà montré que les dommages à l'ADN des macrophages sont essentiels à leur activation. Ici, nous avons utilisé des macrophages humains THP1 différenciés au phorbol-12-myristate13-acétate (PMA) pour démontrer que différentes doses de nanoparticules AGuIX seules et en combinaison avec une faible dose de rayonnement X (0,2 Gy) étaient capables d'induire la phosphorylation du variant d'histone H2AX sur la sérine 139 (H2AXS139*) (également connu sous le nom de foyers γ-H2AX^{+}) qui est une caractéristique des cassures double brin (DSB) de l'ADN. Les dommages détectés à l'ADN étaient particulièrement graves dans les traitements combinés de l'IR avec des doses plus élevées d'AGuIX. De plus, nous avons illustré que les traitements avec des nanoparticules AGuIX seules et en combinaison avec l'IR déclenchaient une réponse aux dommages à l'ADN (DDR) via la phosphorylation activatrice de la kinase Ataxia télangiectasie mutée (ATM) sur la sérine 1981 (ATMS1981*). Ainsi, nos résultats montrent que les nanoparticules AGuIX seules et en combinaison avec l'IR induisent des DSB et activent la DDR dans les macrophages humains anti-inflammatoires.

2. Les nanoparticules AGuIX à base de gadolinium et leur association aux rayonnements ionisants favorisent la reprogrammation des macrophages anti-inflammatoires en macrophages pro-inflammatoires.

Nos travaux antérieurs ont démontré que le DDR et l'ATM contrôlent l'activation des macrophages pro-inflammatoires. Dans cette thèse, nous avons évalué si les dommages à

l'ADN et l'activation de l'ATM induits par AGuIX et leur combinaison avec l'IR avaient un impact sur le phénotype des macrophages pro-inflammatoires. Nos résultats ont démontré que les macrophages THP1 humains différenciés par PMA irradiés avec 0,2 Gy en combinaison ou non avec différentes concentrations d'AGuIX surexprimaient l'oxyde nitrique synthase (iNOS), une enzyme fonctionnelle importante qui régule sélectivement le phénotype des macrophages M1. Pour confirmer ces résultats, nous avons également montré que la combinaison de l'IR avec 100 nM, 200 nM, 0,6 mM ou 1,2 mM d'AGuIX augmentait l'expression du facteur de transcription interféron Regulatory Factor 5 (IRF5), qui est le régulateur principal de la différenciation M1. Dans l'ensemble, ces résultats indiquent qu'AGuIX seul et en combinaison avec l'IR reprogramme les macrophages anti-inflammatoires en phénotype pro-inflammatoire.

3. Les rayonnements ionisants, les nanoparticules à base de gadolinium AGuIX et les traitements combinés activent l'AMPK et déclenchent la fragmentation mitochondriale dans les macrophages anti-inflammatoires.

Des études antérieures ont montré que l'IR peut modifier la dynamique mitochondriale. Ces changements métaboliques sont étroitement associés au phénotype et à la fonction des TAM. Nous avons analysé la forme des mitochondries dans les macrophages THP1 différenciés par PMA en suivant l'expression de la translocase de la protéine de la membrane mitochondriale externe 20 (TOM20). Nos résultats ont montré que la dose unique de 0,2 Gy et les traitements avec 100 nM, 200 nM, 0,6 mM ou 1,2 mM d'AGuIX entraînaient l'accumulation de mitochondries raccourcies et fragmentées de manière dose-dépendante avec la concentration d'AGuIX. La dynamique des mitochondries est étroitement contrôlée par le complexe protéine kinase activée par l'AMP (AMPK), qui intervient dans de nombreux processus métaboliques via l'activation ou la suppression de protéines cibles clés. Nous avons révélé que ces traitements activaient et phosphorylaient l'AMPK sur la thréonine 172 (AMPKT172*) dans les macrophages THP1 différenciés par PMA. Ainsi, ces résultats démontrent que l'exposition à AGuIX seul et en combinaison avec l'IR induit une fragmentation mitochondriale et active l'AMPK dans les macrophages anti-inflammatoires.

4. L'activation de l'AMPK contrôle la dynamique mitochondriale et la reprogrammation pro-inflammatoire des macrophages traités par IR, AGuIX et leur combinaison.

Dans cette étude, nous avons cherché à savoir si la fragmentation mitochondriale et l'activation de l'AMPK induites par l'IR, AGuIX et leur combinaison jouaient un rôle central dans la

polarisation des macrophages pro-inflammatoires. Nous avons traité des macrophages THP1 différenciés par PMA avec une irradiation à dose unique de 0,2 Gy et 200 nM d'AGuIX en présence de 10 μM d'inhibiteur d'AMPK Dorsomorphine (DRS). Nos résultats ont démontré que la dorsomorphine inhibe la phosphorylation d'AMPKT172* et altère la régulation positive de l'expression d'IRF5. Nous avons ensuite inactivé génétiquement la sous-unité régulatrice 2 de l'AMPK (AMPKα2) en utilisant de petits ARN interférents. L'épuisement spécifique de l'AMPKα2 a réduit la fréquence des mitochondries fragmentées, supprimé la phosphorylation d'ATMS1981* et diminué la régulation positive de l'IRF5. Ensemble, ces résultats démontrent le rôle essentiel de l'AMPK lors de la reprogrammation des macrophages anti-inflammatoires en macrophages pro-inflammatoires déclenchée par l'IR, AGuIX et leur combinaison.

Conclusion

Pour conclure, nous avons démontré que différentes concentrations d'AGuIX seul et en combinaison avec de faibles doses de rayonnement X induisent une activation des macrophages pro-inflammatoires. Nous avons révélé que l'activation de l'AMPK sur T172 au niveau de la sous-unité catalytique α2 est essentielle pour la reprogrammation pro-inflammatoire des macrophages. L'AMPK contrôle la fragmentation mitochondriale, la phosphorylation de l'ATM et la surexpression d'IRF5 observées dans les macrophages anti-inflammatoires traités avec AGuIX seul et en combinaison avec l'IR. Ainsi, nos résultats révèlent une nouvelle voie de signalisation (AMPKT172* → Fragmentation mitochondriale → ATMS1981* → IRF5) qui joue un rôle central dans la reprogrammation pro-inflammatoire des macrophages en réponse à l'IR, AGuIX et leur combinaison. Ces découvertes ouvrent la voie à de nouvelles cibles thérapeutiques qui peuvent être développées pour cibler l'activation des macrophages.

Chapter 1 Biology of Macrophages

1.1. Origin of macrophages

Macrophages are phagocytic cells which were first discovered by the zoologist and pathologist Elie Metchnikoff who has been consequently awarded a Noble Prize in Physiology and Medicine in 1908 [1]. Metchnikoff made first microscopic observations of macrophage phagocytosis of foreign materials, pathogens and host apoptotic cells. This discovery has laid a foundation to a variety of different fields ranging from developmental biology, immunology, probiotics, and gerontology [2]. Since then, the field has evolved tremendously and expanded to form a unique system known as "the mononuclear phagocyte system" which includes cells such as monocytes, dendritic cells, and macrophages [3]. Until recently, most phagocytic cells have been thought to evolve distinctly from bone marrow-derived monocytes. This concept has been challenged as many studies demonstrated that distinct tissue-resident macrophages arise from embryonic progenitors, such as the yolk sac and fetal liver, during embryogenesis, and retain their self-renewal properties throughout lifespan [4].

Recent studies suggested that tissue-macrophage populations are predominantly developed during early embryogenesis and can be described in three sequential waves (Figure 1). The first wave in embryonic hematopoiesis occurs around embryonic day 7 (E7) in rodents when the embryonic blood circulation has not yet developed. During this wave, erythro-myeloid progenitors (EMPs) arise from blood islands in the yolk sac and differentiate into pre-macrophages (pMacs) independently from c-Myb which is a master transcriptional regulator of hematopoiesis [3].

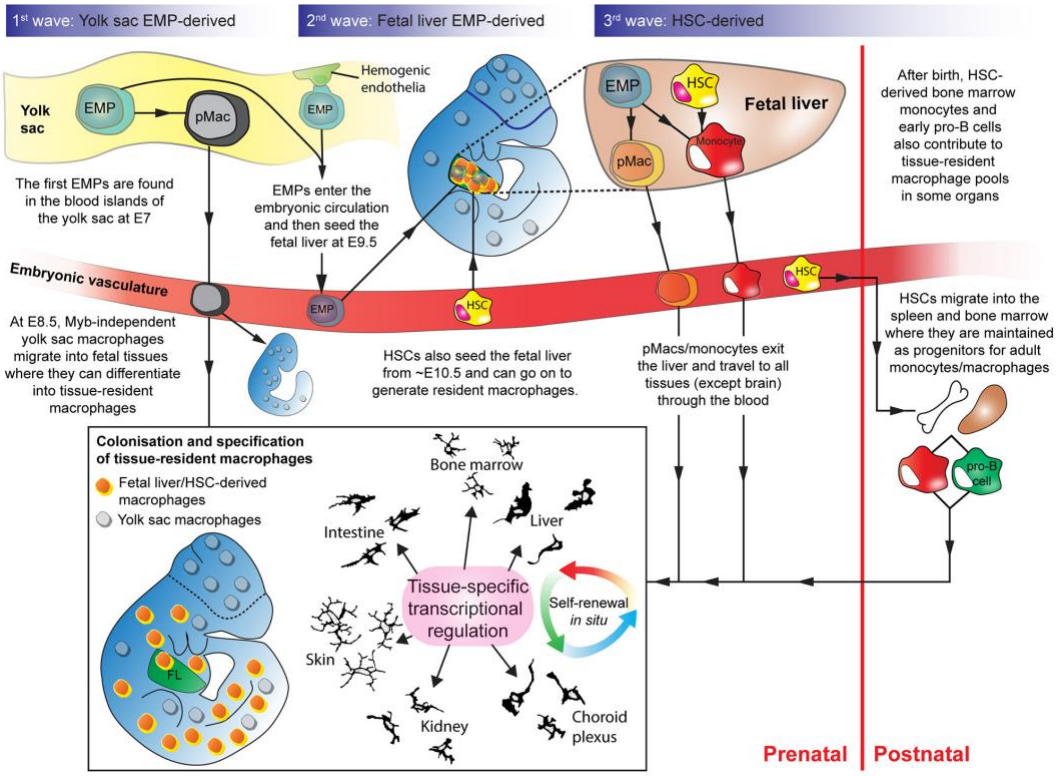

Figure 1. Macrophage development process.

Macrophage progenitors colonize developing embryos in three waves. During the first wave, erythro-myeloid progenitors (EMPs) originated from the yolk sac differentiate into pre-macrophages (pMacs) and migrate into embryonic vasculature. A second wave EMPs derived from hemogenic endothelium seeds the fetal liver, where they differentiate into pMacs and monocytes. During the third wave, hematopoietic stem cells (HSCs) developed from the aorta-gonad-mesonephros region enter the fetal liver. At this stage, pMacs and monocytes travel through the bloodstream and seeds all the tissue, except the brain. EMP, erythro-myeloid progenitor; HSC, hematopoietic stem cell; pMac, pre-macrophage. Adapted from *Munro and Hughes (2017)* [3].

Around E8.5 when embryonic blood circulation connects the yolk sac with the entire embryo, the second wave of macrophage development starts. During this second phase, c-Myb independent pMacs seed throughout the embryo and start to differentiate into tissue-specific macrophages. At the same time, the second type of EMPs develops at the hemogenic endothelial in a c-Myb dependent manner and seeds the fetal liver. In the fetal liver, EMPs rapidly expand and differentiate into pMacs and monocytic intermediates. At E11.5, these pMacs and monocytes enter the embryonic vasculature system and reside almost in all developing organs, except the brain due to the blood-brain barrier [3,4].

During the third wave of macrophage development, around E10.5, hematopoietic stem cells (HSCs) arise from several anatomical sites such as the yolk sac, the aorta-gonad mesonephros region, and the placenta and reside in the fetal liver [5]. Besides contributing to the population of tissue-resident macrophages, HSCs populate the spleen and bone marrow of the embryo and continue to produce monocytes during the postnatal period. Even though prenatal tissue-resident macrophage progenitors have an unlimited capacity for self-renewal during lifespan, HSCs derived monocytes remain the main source to replenish macrophages in organs, except the brain, during injury and/or inflammation [6,7].

Thus, during the prenatal period, tissue-resident macrophages develop mainly from the embryonic yolk sac and fetal liver precursors and retain their self-maintaining capacity during lifetime. After birth, bone marrow monocytes and pro-B cell-derived macrophages may contribute to the population of tissue-resident macrophages to sustain the tissue homeostasis during injury and inflammation.

1.2. Regulation of macrophage development and tissue specialization

1.2.1. Regulation of tissue-resident macrophage development

Maturation of embryonic macrophage progenitors into complete functioning tissue-resident macrophages is regulated by a combined action of lineage-determining transcription factors (LDTFs), collaborating transcription factors (CTFs), signal-dependent transcription factors (SDTFs) and epigenetic modulation of enhancer regions of target genes through the acetylation of lysine 27 of histone 3 (H3K27) (Figure 2) [8].

Tissue-specific macrophage development during prenatal life depends on CTFs such as PU.1 and LDTFs, like interferon regulatory factor family members and CCAAT/Enhancer-Binding-Protein (Cebp)-α [8]. Among them, the most studied is PU.1 transcription factor. Many studies involving PU.1 knockout model demonstrated its crucial role in the maturation of myeloid progenitors into functional cells: loss of PU.1 expression resulted in lack of common myeloid progenitor, defective granulocytic neutrophil production, and an absence of mature macrophages [9]. Expression of PU.1 is regulated by RUNX1 (also known as AML1) and it controls the differentiation process in a dose-dependent manner [10]. A low level of PU.1 expression activates both neutrophil and macrophage lineage-specific genes. However, a certain PU.1 threshold level induces the expression of Egr-2 and the transcriptional repressor Nab-2, both those transcription factors are needed to repress the expression of Gfi-1, a

transcription factor which controls neutrophil differentiation. Thus, repression of Gfi-1 silences neutrophil genes and promotes macrophage differentiation [9]. In addition to PU.1, other LDTFs such as MYB, c-MAF, MAFB, and ZEB2 have shown to play a crucial role in pre-macrophage development in distinct types of human and murine tissue-resident macrophages [10]. Together, these transcription factors form a unique fingerprint in a form of cell surface receptors shared by a majority of human and murine tissue-resident macrophages [10] (common human mouse macrophage markers include: EMR1-F4/80 [11], and CD64 [12]).

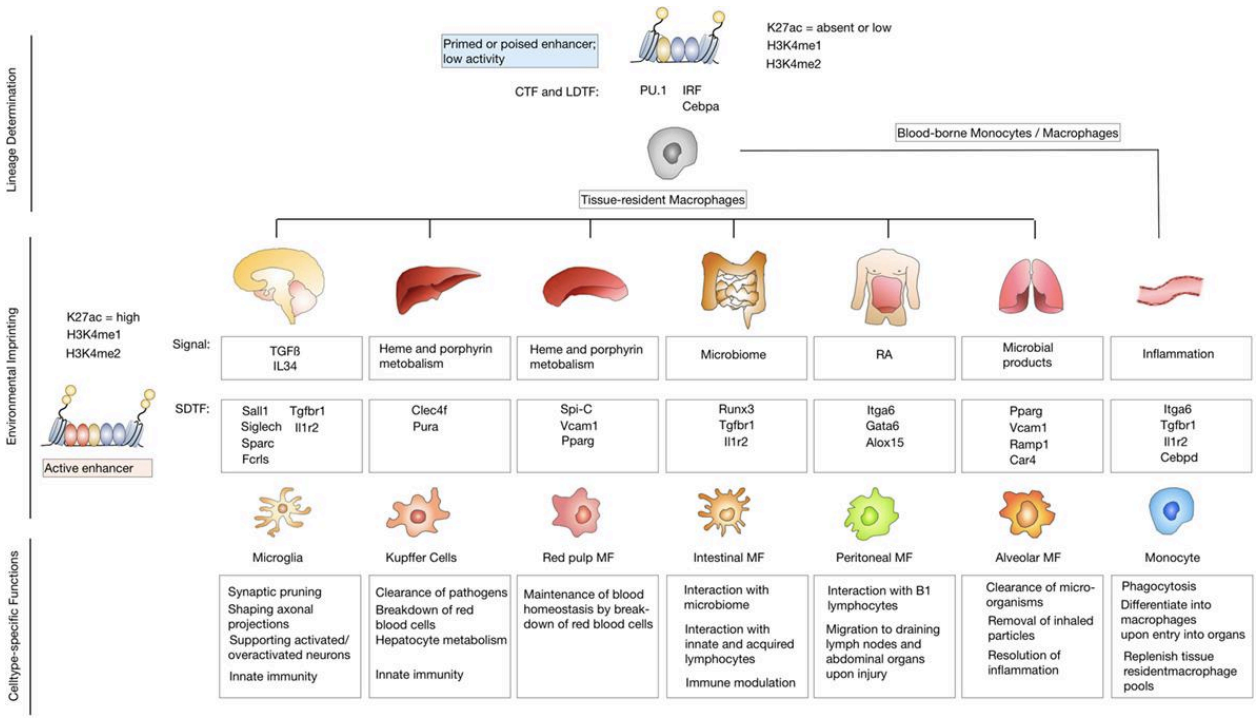

Figure 2. Regulation of tissue-resident macrophage development.

Lineage determination of tissue-resident macrophages initially is governed by LDTFs and CTFs which can bind to the enhancer region of the gene of interest and turn them into primed or poised stage. Later during development, unique environmental cues activate SDTFs and regulate tissue-specific functions of different macrophage subpopulations. LDTFs, lineage-determining transcription factors; SDTFs, signal-dependent transcription factors; CTFs, collaborating transcription factors; H3K4me1, histone lysine 4 monomethylation; H3K4me2, histone lysine 4 dimethylation; H3K27me3, histone H3 lysine 27 trimethylation. Adapted from *Sevenich (2018)* [8].

Beside LDTFs, environmental signals arising from pre-macrophage tissue environment determine the fate of tissue-resident macrophages (Figure 2) [8]. During organogenesis, pre-macrophages populate certain organs, which provide niche-specific signals and facilitate tissue-dependent macrophage differentiation. These niche signals can include cytokines,

metabolites, cell-cell contact, inflammation and can activate SDTFs [10]. Most of SDTFs are designed to convert poised or primed enhancers into active by directly activating signature genes or by inducing epigenetic chromatin remodeling [13].

Among macrophage subsets, differentiation of red pulp macrophages (RPMs) localized in the splenic red pulp has been shown to be regulated the heme metabolite released after erythrocyte degradation [14]. Heme induces proteasomal degradation of BACH1 the transcriptional repressor of Spi-C, which is a crucial transcription factor for RPMs differentiation through the transactivation of Vcam1 RPM expressed gene [10].

In contrast to RPMs, the differentiation of microglia, the tissue-resident macrophages of the central nervous system (CNS) is dependent on brain environmental cytokines such as colony-stimulating factor-1 (CSF-1), interleukin 34 (IL-34), and transforming growth factor-beta (TGF-β) [15]. Cytokine TGF-β controls microglia development through phosphorylation of the Smad2 and Smad3 cytosolic proteins, initiating further interaction with Smad4 and consequently the formation of a Smad2/3-Smad4 active hetero-complex which then translocate into the nucleus and regulate expression of target genes [16]. CSF-1 and IL-34 are both ligands to CSF-1R receptor and formation of CSF-1/CSF-1R or IL-34/ CSF-1R complex promotes a rapid monomer to dimer transition of CSF-1R receptor causing a series of tyrosine phosphorylation which eventually activates downstream complexes responsible for regulating macrophage survival, proliferation, and differentiation genes [17].

The microbiome niche of the intestine is also contributing to the development of intestinal macrophages. Due to a high turnover rate of tissue-resident macrophages in the intestinal lining, the majority of aged embryo-derived intestinal macrophages are replaced by bone-marrow-derived monocytes [18]. After birth, the microbiota of the gut contributes to macrophage development by releasing mainly polysaccharides and short-chain fatty acids (SCFAs). For example, n-butyrate can repress IL-6, IL-12b, and Nos2 expression in intestinal macrophages located in the colon region by inhibiting histone deacetylases [19]. Even though many bacterial metabolites have been identified to be important in macrophage differentiation, more work is required to understand the exact molecular mechanism governing this process.

In addition to the above-mentioned types of tissue-resident macrophages, other tissues such as skin (Langerhans cells), lung (alveolar macrophages), bone (osteoclasts), liver (Kupffer cells), and peritoneum (peritoneal macrophages) are populated with tissue-specific macrophages as

well [10]. Cytokine TGF-β has been shown to control Langerhans cells development by regulating the expression of RUNX3 and ID2 transcription factors, while in osteoclasts it controls RANKL-induced differentiation [10]. Moreover, TGF-β regulates the expression of ID1 and ID3 which play an essential role during Kupffer cell development. The fate of alveolar macrophages, in contrast, is determined by alveolar type II epithelial cells producing granulocyte-macrophage colony-stimulating factor (GM-CSF) which induces the expression of PPARγ. Lastly, the development of peritoneal macrophages is partially regulated by local tissue-derived retinoic acid which controls the expression of zinc finger transcription factor GATA6 [20].

In summary, differentiation of tissue-resident macrophages is governed distinct combination of transcription factors and tissue-specific environment stimuli. Lineage-specific transcription factors play a vital role during early embryonic development and distribution of pre-macrophages, while signals arising from the tissue environment facilitate further organ-specific differentiation of macrophages during prenatal development and after birth.

1.2.2. Regulation of monocyte development

Monocytes during embryogenesis develop from erythro-myeloid precursors (EMPs) in the fetal liver and after birth, they arise from bone marrow (BM)-derived hematopoietic stem cells (HSCs) [21,22]. HSCs are a highly heterogeneous population and can be sub-divided into categories such as long-term HSCs (LT-HSCs), short-term HSCs (ST-HSCs), and multipotent HSCs (MPPs). LT-HSCs have a self-renewal capacity and give rise to ST-HSCs, which then differentiate into MPPs. MPPs have a less self-renewal ability and they are the main progenitors of monocytes (Figure 3) [23].

Monocyte development from MPPs in murine model happens in several intermediate stages and is tightly regulated by specific transcription factors (Figure 3) [24]. The first precursor of MPPs is the common myeloid precursors (CMPs), which are characterized by the expression of surface glycoprotein CD34 and by losing the expression of stem cell antigen-1 (SCA-1) receptor. The next intermediate cells are granulocyte/macrophage precursors (GMPs) which express Fcγ receptors such as CD16 and CD32 [24]. GMPs are followed by macrophage/DC precursors (MDPs) which are characterized by the expression of CD115 (CSF-1R/M-CSFR), CX3CR1, and Flt-3 (CD135) receptors [25]. These cells, in turn, can differentiate into the common monocyte progenitors (cMoPs) which maintain the expression of CD115 and

CX3CR1 receptors and gain the expression of Ly6C receptor. Several studies demonstrated that cMoPs give rise to Ly6C^{hi} monocytes which then give rise to other subsets of monocytes [24].

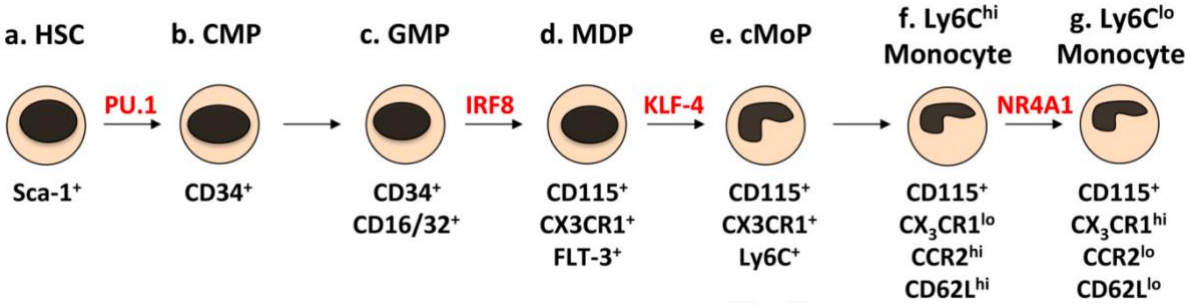

Figure 3. Monocyte development pathway in murine model.

Sca-1^{+} hematopoietic stem cells (HSC) (a) give rise to CD34^{+} common myeloid precursors (CMP) (b) followed by granulocyte/macrophage precursors (GMP) (c) macrophage/DC precursors (MDP) (d) common monocyte progenitor (cMoP) (e) Ly6C^{hi} monocyte (f) and Ly6C^{low} monocyte (g). Key transcription factors involved in differentiation process are highlighted in red. Adapted from *Terry and Miller (2014)* [24].

The transcription factor PU.1 plays a crucial role at various stages of monocyte differentiation. The up-regulation of PU.1 has been shown to induce the expression of Interferon regulatory factor-8 (IRF8), Kruppel-like Factor 4 (KLF-4), Erg-2 and Nab-2 and to inhibit the expression of neutrophil differentiation genes such as GATA-1, GATA-2, and C/EBPα [26,27]. Then IRF-8 has been shown to form a heterodimer with PU.1 and activate several monocyte-related genes such as cystatin C and cathepsins [28]. The IRF-8/PU.1 complex demonstrated to control as well the expression of the KLF-4 factor by binding to its promoter region [29]. Activated Erg-2 and Nab-2, together inhibit the expression of the Gfi-1 gene involved in promoting neutrophil differentiation [30].

Depending on surface markers and chemokine receptors human monocytes could be subdivided into three subsets, classical, intermediate, and non-classical (Table 1). Human classical monocytes express high levels of CD14 and do not express CD16 (CD14^{++}CD16^{-}) and have high levels of chemokine receptor CCR2 and low levels of CX3CR1 (CCR2^{high}CX3CR1^{low}) [21]. Intermediate monocytes express higher levels of CD14 and low CD16 (CD14$^{+(+)}$CD16^{+}). Whereas, non-classical monocytes express low levels of CD14 and high levels of CD16 (CD14^{+}CD16^{++}) [31,32]. Both intermediate and non-classical human monocytes express low levels of CCR2 and high levels of CX3CR1 (CCR2^{low}CX3CR1^{high}) [33].

Similarly, murine monocytes could be subdivided into the same three functionally different subsets (Table 1). All three subsets, classical, intermediate and non-classical express CD11b and CD115 receptors, the difference rises from Ly6C expression: classical monocytes express high levels of Ly6C ($Ly6C^{hi}CD11b^{+}CD115^{+}$), intermediate express lower levels of Ly6C ($Ly6C^{intermediate}CD11b^{+}CD115^{+}$) and non-classical monocyte express some levels of Ly6C ($Ly6C^{low}CD11b^{+}CD115^{+}$) [33,34].

Subset	Markers	Chemokine receptors	Main functions
Human			
Classical	$CD14^{++}CD16^{-}$	$CCR2^{high}CX3CR1^{low}$	Immune response Phagocytosis
Intermediate	$CD14^{+(+)}CD16^{+}$	$CCR2^{low}CX3CR1^{high}$	Proinflammatory Wound healing
Nonclassical	$CD14^{+}CD16^{++}$	$CCR2^{low}CX3CR1^{high}$	Patrolling role Fibrosis
Mouse			
Classical/intermediate (∗)	$Ly6C^{+}CD11b^{+}CD115^{+}$	$CCR2^{high}CX3CR1^{low}$	Proinflammatory Phagocytosis
Nonclassical	$Ly6C^{-}CD11b^{+}CD115^{+}$	$CCR2^{low}CX3CR1^{high}$	Patrolling Tissue repair

(∗) Murine $Ly6C^{+}$ (classical/intermediate) monocytes are sometimes further divided into $Ly6C^{high}$ and $Ly6C^{intermediate}$ monocytes.

Table 1: Human and murine monocyte subsets.

Adapted from *Sprangers, Vries, and Everts (2016)*[33].

Thus, during embryogenesis monocyte initially arises from the fetal liver erythromyeloid progenitors and these immature HSCs seed the bone marrow. Only after birth, bone-marrow-derived HSCs start to differentiate into functional monocytes via several distinct progenitors. Development of HSCs into monocyte is controlled by several transcription factors and produce functionally distinct monocyte subsets which will be further explored in the upcoming sections.

1.2.2. Regulation of tissue hematopoietic macrophage development

Tissue-resident macrophages have a strong self-renewal capacity, longevity and resistance to stress signals, which enable their long survival. However, under steady-state homeostasis, as well as during a "stress" situation, bone marrow (BM) derived monocyte could also contribute to the population of tissue-resident macrophages [35,36]. The distribution of BM monocyte-derived tissue-resident macrophages varies from tissue to tissue with a minor contribution to microglia population in the brain and with a substantial input to the macrophages resident in the peritoneum, intestine, and dermis (Figure 4) [37]. Tissue-resident macrophages developed from the yolk sac and fetal liver differ from BM-derived monocyte by expression of surface markers, self-renewal capacity, and longevity. Murine blood monocyte-derived macrophages generally express low levels of F4/80 surface marker, have a short lifespan, and have a limited

self-renewal capacity while the majority of embryonically derived macrophages express a high level of F4/80, are long-lived, and have a high self-renewal capacity [36–38].

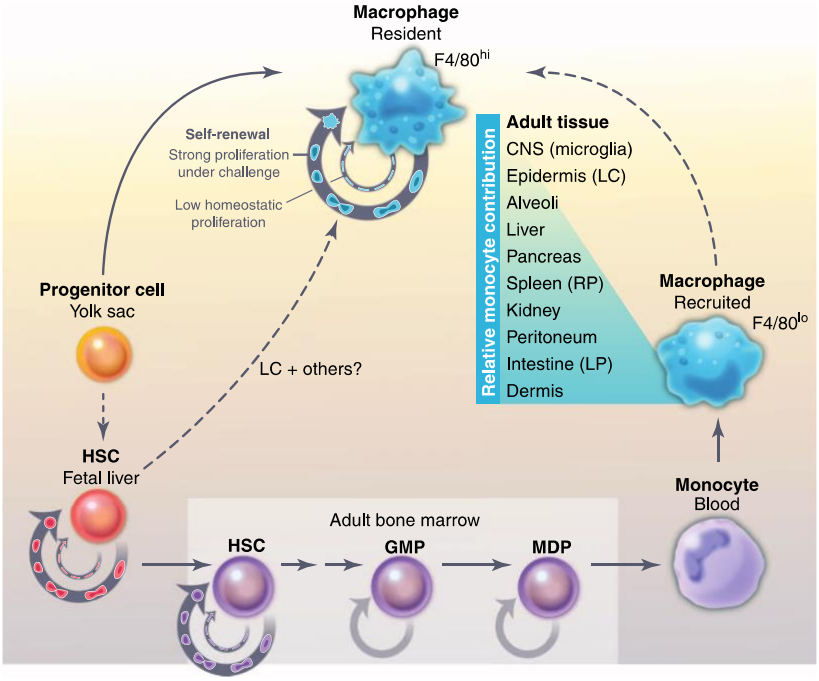

Figure 4. Origin and self-renewal of tissue-resident murine macrophage population.

Murine tissue-resident macrophages initially rise from embryonic progenitors in the yolk sac and fetal liver and can maintain strong self-renewal property (thick arrows) throughout life. Later in life macrophages are derived from monocyte seed tissues with high turn-over (highlighted with blue background) and these macrophages have limited self-renewal capacity (dotted arrows), instead, tissue-resident macrophages in those tissues constantly replenish from recruited monocytes. GMP, granulocyte-macrophage progenitor; MDP, macrophage-dendritic progenitor; LC, Langerhans cells; RP, red pulp; LP, lamina propria. Adapted from *Sieweke and Allen (2013)* [37].

Little is known about the process of differentiation of monocytes into fully functional tissue-specific macrophages under physiological conditions. In cardiac tissue, for example, $CCR2^-$ population of macrophages are renewed by self-proliferation, while $CCR2^+$ sub-population are replenished by blood monocyte [39,40] and its proliferation depends on the expression of the transcriptional co-repressor myeloid translocation gene on chromosome 16 (Mtg16) [41]. However, most of the monocyte under physiological conditions remain circulating in the blood or stay undifferentiated in the tissue periphery [22]. Monocyte to macrophage activation occurs mainly under pathological conditions or microbial sensing and results in high macrophage infiltration in the tissue, creating specific pro-inflammatory or/and anti-inflammatory immune responses [38].

1.2.3. Characteristics of macrophage phenotypes

Tissue-resident and circulating macrophages display remarkable plasticity and functional diversity. Depending on signals received from the surrounding environment or the phagocytized body, macrophages can be polarized into pro-inflammatory (M1 like) and anti-inflammatory (M2 like), also referred as classical M1 and alternative M2 activated macrophages. Anti-inflammatory macrophages could be further classified into three sub-populations M2a, M2b, and M2c [42–44]. Some specific surface markers, stimuli, and functions of these macrophage subsets are summarized in Figure 5. Murine specific marker include F4/80 [45], and markers such as CD206 and CD163 are common for both human and mouse species [46,47].

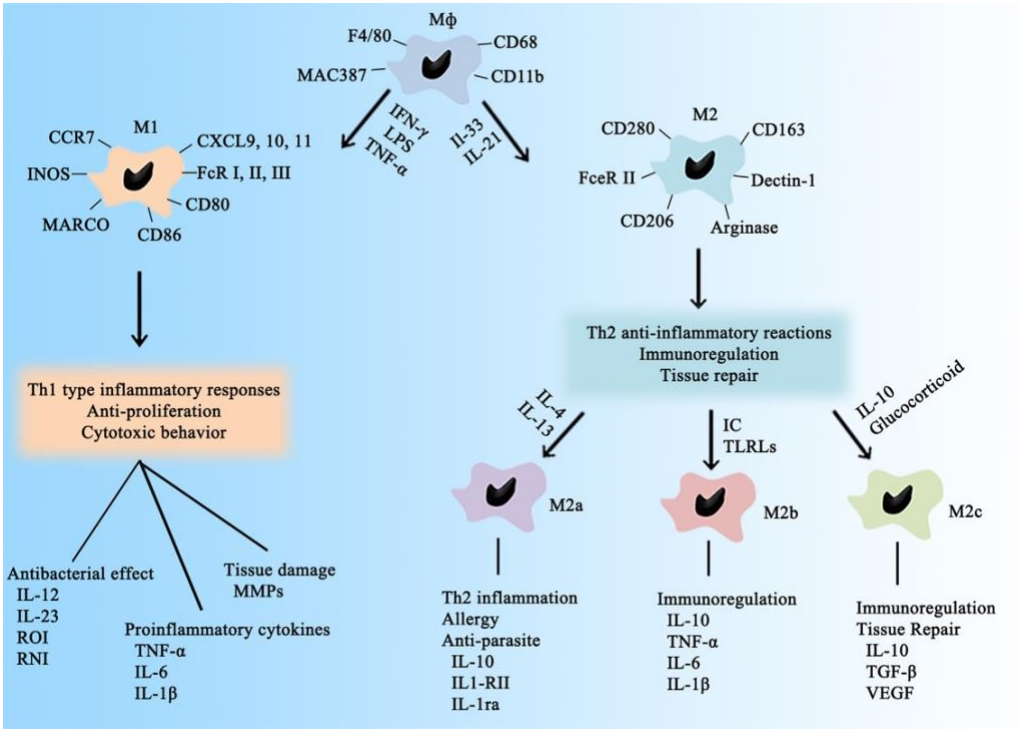

Figure 5. Surface markers, activators, and functions of different polarized macrophage populations in human and/or murine models.

Depending on the sensed stimuli (illustrated next to black arrows) macrophages could switch into pro-inflammatory M1-type or anti-inflammatory M2-type macrophages. M1 and M2 macrophages differ in expression of surface markers (highlighted next to cells images) and secreted soluble factors (listed down the functions in rows). M2-like macrophages further could be subdivided into M2a, M2b, and M2c phenotypes. Adapted from *Chen et al. (2016)* [43].

Pro-inflammatory macrophage activation is induced by Th1 cytokines such as interferon-γ (IFN-γ) and tumor necrosis factor-α (TNF-α), granulocyte-macrophage colony-stimulating

factor (GM-CSF) and by pathogen associated pattern molecules (PAMPs) such as bacterial lipopolysaccharide (LPS). Pro-inflammatory activated macrophages are characterized by the expression of surface receptors (CD80, CD86, CCR7 and high levels of major histocompatibility complex (MHC) class II (MHCII) HLA-DR) and the secretion of interleukins (IL-12 and IL-23), inflammatory cytokines and mediators (IL-1β, TNF-α, IL-6, iNOS) and chemokines (CXCL9, CXCL10, and CXCL13) [42]. They were shown to produce also reactive oxygen and nitrogen metabolism intermediates (ROI and RNI) [43,48]. Moreover, pro-inflammatory macrophages were demonstrated to secrete enzymes from the matrix metalloproteinases (MMPs) family, such as MMP14, which was shown responsible for the induction of pro-inflammatory genes [49]. Hence, classically activated macrophages were shown to possess strong microbiocidal, tumoricidal and phagocytic activities and involved in antigen presentation to Th1 cells and their stimulation and in the clearance of apoptotic cells [44,50–52].

By contrast, anti-inflammatory macrophage activation could occurs in response to anti-inflammatory stimuli such as IL-33 IL-21, IL4, IL13, M-CSF, transforming growth factor-β (TGF-β) and is distinguished by up-regulation of surface markers such as mannose receptor CD206, scavenger receptor CD163, and arginase I receptor and down-regulating MHCII HLA-DR receptor [53,54]. They secrete high levels of anti-inflammatory cytokines, namely IL-10 and TGF-β [44,50].

As mentioned before, anti-inflammatory macrophages could be subdivided into M2a, M2b, and M2c. M2a macrophages obtained upon stimulation with IL-4 or IL-13 were shown to secrete CCL24, CCL22, CCL17, and CCL18 chemokines and to recruit Th2 cells, eosinophils, and basophils. Hence, they were demonstrated to play crucial roles in mediating Th2 inflammation, allergic responses, and parasitic infections. M2b macrophages activated by stimulation with immune complexes (IC) and Toll-like receptor ligands (TLRLs) were shown to produce both pro-inflammatory and anti-inflammatory cytokines such as TNF-α, IL-1β, IL-6, and IL-10 and express high levels of chemokine CCL1 which interacts with CCR8 expressed on the surface of eosinophils, regulatory T cells (Treg), Th2 cells, and skin-homing T cells. By controlling the level of expression of cytokines and chemokines, M2b macrophages mainly regulate the immune response by suppressing or promoting inflammation. M2c macrophages activated by stimulation with IL-10 and glucocorticoid hormones were demonstrated to produce IL-10, TGF-β, CCL16, and CCL18 and involved in the clearing of apoptotic cells [43,44,51]. M2d type macrophages, which were distinguished by some reports to be an extension

to M2c, are activated by TLR antagonists and IL-10 and were shown to release vascular endothelial growth factor (VEGF) which promotes angiogenesis and tumor progression [42,55].

It is crucial to note that even though M1 like and M2 like classification types have been a useful tool for *in vitro* studies, macrophage plasticity *in vivo* is more diverse than thought before. In tissue environment macrophages were shown to acquire a wide range of phenotypes which could elongate between extremes of fully pro-inflammatory and anti-inflammatory phenotypes [50,56].

1.2.4. Molecular mechanisms of macrophage activation

1.2.4.1. Transcriptional mechanisms

In this section, key effectors of transcriptional signaling pathways and cascades involved in macrophage activation are explored. Some of them are illustrated in Figure 6 and are explained in detail in the corresponding sections below.

1.2.4.1.1. NF-kB/Rel proteins. Nuclear factor-kB/Rel is a family of transcription factors composing of five monomers, including NF-κB1 (also named p50), NF-κB2 (also named p52), RelA (also named p65), RelB, and c-Rel [57,58]. NF-kB monomers dimerize into homo- or heterodimers and interact with cytoplasmic regulatory IkB consensus domain, which composed of five inhibitory proteins (IκBα, β, ε, γ, and δ) [59]. In recent years, it has become clear that along with a diverse range of dimers, the activation of the NF-kB transcription factor is governed by two separate strategies, known as "canonical" and "non-canonical" (or "alternative") signaling pathways. Both of these signaling pathways could be activated by a variety of stimuli (including cytokines, bacterial and viral products, physical and chemical stress agents) and play an essential role in regulating immune responses driven by macrophage activation [59,60].

The canonical NF-kB pathway is initiated by several stimuli which activate cell surface receptors such as pattern-recognition receptors (PRRs), TNF receptor (TNFR) superfamily, and various cytokine receptors, for instance, IL1Rs [59]. There are four members of PRRs expressed by innate immune cells, including toll-like receptors (TLRs), RIG-I-like receptors, NOD-like receptors (NLRs), and C-type lectin-like receptors. These PRRs can detect pathogen-associated molecular patterns (PAMPs) derived from microbes and damage-associated molecular patterns (DAMPs) released from damaged and dying cells [61].

The primary mechanism of the canonical NF-kB pathway was shown to involve activation of receptors, which in turn lead to the phosphorylation of a secondary cellular messenger, an IKK complex. The IKK complex consists of a regulatory subunit IKKγ (also known as NEMO) and two serine-threonine kinases (IKKα and IKKβ). Activation of the canonical pathway requires the IKKγ and phosphorylated IKKα/β subunits which leads to the phosphorylation of the IkB proteins. Consequently, IkBs become poly-ubiquitinated and degraded by proteasome causing the release of NF-κB dimers which eventually translocate into the nuclear region and activate the transcription of target pro-inflammatory genes, including primary response genes such as *TNF* and *IL1B* genes [59,62].

On the contrary, activation of the non-canonical pathway involves binding of specific ligands to receptors of tumor necrosis factor (TNF) superfamily such as BAFFR (also known as BLyS), LTβR, CD40, and RANK [63,64]. Stimulation of these receptors demonstrated to lead to the activation of NF-κB-inducing kinase (NIK), which the,n cooperates with downstream kinase, IκB kinase-α (IKKα) to mediate p100 phosphorylation, leading to p100 ubiquitination and proteasomal degradation [64]. Processing of p100 results in the generation of functional p52 protein and triggers the formation of RelB/p52 heterodimer, which in turn translocates to nucleus and regulates genes involved in immune cell maturation, differentiation, and lymphoid organogenesis [57,65].

Overall, the NF-kB signaling pathway plays an essential role in controlling pro-inflammatory macrophage activation and inflammation. Particularly, NF-kB is involved in regulating inflammatory genes such as TNF-α, IL-1β, IL-6, IL-12p40, and cyclooxygenase-2. It is also essential in pro-inflammatory macrophage-mediated Th1, Th17, and Treg cells maturation [66,67].

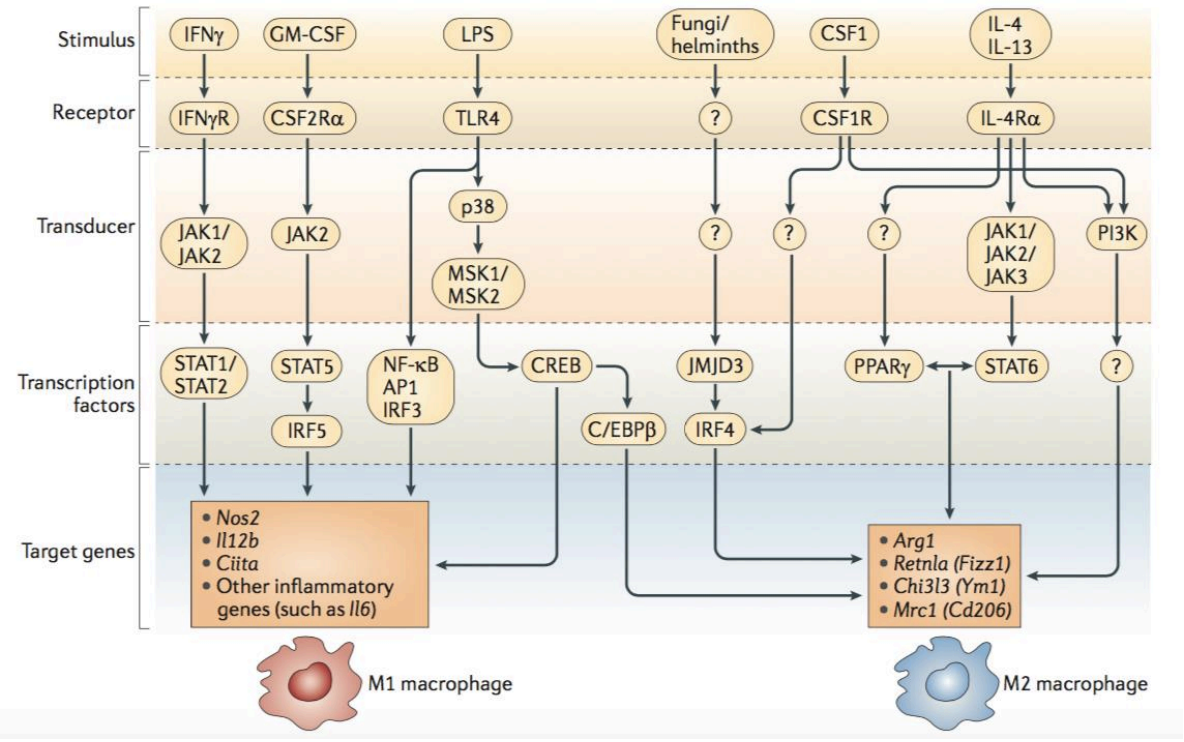

Figure 6. Signaling pathways leading to M1 and M2 macrophage polarization.

Certain stimuli activate receptors on macrophage surfaces leading to activation of transducers and transcription factors, which then trigger the expression of target genes leading to pro-inflammatory (M1) or anti-inflammatory (M2) macrophage phenotype development. *Arg1, arginase 1*; C/EBPβ, CCAAT/enhancer-binding protein-β; *Chi3l3*, chitinase 3-like 3; *Ciita*, MHC class II transactivator; CREB, cAMP-responsive element-binding protein; CSF, colony-stimulating factor; IFNγ, interferon-γ; IL, interleukin; IRF, interferon-regulatory factor; JAK, Janus kinase; LPS, lipopolysaccharide; *Mrc1*, macrophage mannose receptor 1; MSK, mitogen- and stress-activated kinase; NF-κB, nuclear factor-κB; *Nos2*, nitric oxide synthase 2; PI3K, phosphoinositide 3-kinase; PPARγ, peroxisome proliferator-activated receptor-γ; *Retnla*, resistin-like-α; STAT, signal transducer and activator of transcription; TLR4, Toll-like receptor 4. Adapted from *Lawrence and Natoli (2011)* [68].

1.2.4.1.2. JAK/STAT signaling. The signal transducer and activator of transcription (STAT) proteins family consists of seven transcription factors (STAT1, 2, 3, 4, 5A, 5B, and 6) and functionally linked to the Janus tyrosine kinases (JAKs) protein family consisting of four members (JAK1, 2, 3, and tyrosine kinase 2 (TYK2)) [69]. JAKs proteins were shown recruited to the intracellular domains of several cell-surface receptors of interferons (such as INF-β and INF-γ) and cytokines (like GM-CSF, CSF1, IL1, and IL13) upon extracellular ligand and receptor association [66,68]. JAKs, which are then trans-phosphorylated and activated further recruit and phosphorylate downstream STAT proteins, leading to their dimerization and nuclear translocation. STATs dimers alone or in complexes with other transcription factors

(including IRFs) could control pro-inflammatory and anti-inflammatory macrophage activation [70].

STAT1 and STAT2 phosphorylation are involved in the activation of macrophages toward the pro-inflammatory phenotype [68]. Indeed, the binding of IFN-γ to its receptor (IFNGR) was demonstrated to activate JAK1 and JAK2 complex which then phosphorylates STAT1 transcription factor [71]. Upon phosphorylation, STAT1 forms a homodimer and translocates into the nucleus, where it activates the interferon-gamma-activated sequence (GAS) and its downstream targets, the interferon-stimulated genes (ISGs), encoding for proteins such as NOS2, the MHC class II transactivator (CIITA), and IL-12, which reprogram macrophages toward pro-inflammatory phenotype [68,71]. Although the INF-β signaling pathway was shown induced by STAT1 activation and targets the same set of genes, it stimulates other transducers and transcription factors for macrophage activation [68]. INF-β triggers IFNAR1/IFNAR2 receptors which activate JAK1 and TYK2 kinases, which in turn phosphorylate STAT1 and STAT2 leading to their heterodimer formation [71]. STAT1/STAT2 heterodimer then recruits IRF9 and forms an IFN-stimulated gene factor 3 (ISGF3) complex [72]. After translocation into the nuclear region, ISGF3 binds into interferon-stimulated response elements (ISREs), which are abundant in pro-inflammatory related genes, like *Nos2, Ciita, and Il12b* [68,73].

In contrast, STAT3 and STAT6 signaling pathways are directly associated with anti-inflammatory macrophage activation [74]. Cytokines IL-4 and IL-13 are acting through their receptors IL-4Rα and IL-13Rα, respectively, to activate STAT6 homodimer, while IL-10 and its receptor IL-10R triggers STAT3 dimerization [75]. Interestingly, it has been shown that in murine bone marrow-derived macrophages, IL-4 establishes an M2 activation by up-regulating genes, such as *Klf4*, *Hbegf*, and *Edn1*, and by repressing other genes, like *Abca1, Clec4d, Fos, Tlr2,* and *Cd14* [76]. Whereas, in the macrophages treated by IL-13, high expression levels of SOCS1, DC-SIGN, CCL18, CD23, and SERPINE were shown associated with alternative macrophage activation as well [77]. In similar manner, stimulation of macrophages with IL-10 demonstrated to initiate JAK2 mediated STAT3 phosphorylation and consequently its dimerization. After nuclear translocation, STAT3 complex regulates transcription of anti-inflammatory genes, such as vascular endothelial growth factor A (VEGF-A), basic fibroblast growth factor-2, and placental growth factor [78].

1.2.4.1.3. IRFs signalings. Nine protein members of the interferon regulatory factors (IRFs) family have been identified. Most of them are ubiquitously expressed, except IRF-4 and ICSBP (also known as IRF8) which were shown expressed only in lymphoid and myeloid cells [79,80].

It has been demonstrated that IRF1, IRF3, IRF5, IRF8, and IRF9 are involved in classical pro-inflammatory macrophage activation (Figure 6) [69,81]. Upon activation of TLR9 receptor, IRF1 was shown activated by binding MyD88 cytosolic adapter enabling its migration to the nucleus, where it induces the expression of IFNβ, iNOS, and IL12p35 [82,83]. Whereas IRF3 could be induced by TLR3 and TLR4, several PRRs, including the cytosolic RNA helicase retinoic acid-inducible gene-I (RIG-I)-like receptor (RLR) family members and cytosolic DNA sensors, such as cGMP-AMP synthase (cGAS) and stimulator of IFN genes (STING) [84]. Activated IRF3 directly targets type I IFN genes and several cytokines, such as CXCL10, RANTES, IFN-stimulated gene 56, IL-12p35, IL-15, CCL5, and arginase II [81,83]. Endosomal TLR7, TLR8, and TLR9 and their signaling adapter MyD88 are involved in IRF5 activation, a major determinant of pro-inflammatory macrophage activation [85]. IRF5 controls the expression of several key pro-inflammatory cytokines, such as IL-6, TNF, IL-12p40, IL-12p35, and IL-23p19, and is involved in the suppression of anti-inflammatory cytokine IL-10 [86,87]. Another member of the IRFs family, IRF8, also known as IFN consensus sequence binding protein (ICSBP), is activated by IFNs and LPS [83]. Induction of IRF8 is essential for IL-12 and iNOS synthesis [74]. Moreover, IRF8 is involved in NLRC4, NLRP3, AIM2, and Pyrin inflammasomes activation [88]. The role of IRF9 in the pro-inflammatory macrophage activation downstream STAT1 and STAT2 activation was already described above (in the section 1.2.5.1.2).

In the contrary, IRF4 overexpression was shown strongly associated with anti-inflammatory macrophage polarization (Figure 6) [89,90]. Expression of IRF4 in macrophages is regulated by IL-4 induced STAT6 activation [76]. STAT6 binds to the Jumonji domain-containing 3 (Jmjd3) promoter and facilitates IRF4 expression. Active Jmjd3 removes an inhibitory trimethyl group from a histone 3 Lys 27 (H3K27) demethylase at IRF4 promoter and initiates its transcription [69,91]. It has been demonstrated that IRF4 controls CCL17 chemokine production in macrophages [92] . However, its most important role remains in increasing IL-4 promoter activity and subsequently promoting a positive loop of endogenous IL-4 cytokine production [93].

1.2.4.1.4. C/EBP proteins. CCAAT/enhancer-binding proteins (C/EBPs) are members of bZIP (basic region leucine zipper) transcription factors, which activate gene expressions during

inflammation and macrophage activation [94,95]. Among different members of the C/EBPs family, C/EBPε expression level is notably low in macrophages, while C/EBPα and C/EBPβ are abundantly expressed [79]. Studies done on C/EBPα conditional knockout mice demonstrated that C/EBPα is able to control both pro- and anti-inflammatory activation in macrophages. Although, no differences were observed in the endogenous expression level of the pro-inflammatory markers, such as TNFα, IL-6, and CD11 between C/EBPα knockout mice and control mice, upon LPS stimulation TNFα and IL-6 mRNA levels were significantly decreased. Besides, endogenous expression of anti-inflammatory markers, such as Arg1, Mgl1, Chi3l3, Mrc1, and IL-10, were significantly lower in C/EBPα-deficient macrophages and were further diminished upon IL-4 treatment [96]. Accordingly, it has been shown that activation of C/EBPβ controlled expression of anti-inflammatory related genes such as *Msr1, Il10, Il13ra*, and *Arg-1* and did not affect pro-inflammatory associated genes, like *Il1b, Il6, Il12b,* and *Tnfa* [97]. Altogether, these studies indicate that C/EBPα plays roles in macrophage activation in response to pro-inflammatory and immunosuppressive stimuli.

1.2.4.1.5. MicroRNAs. MicroRNAs (miRNAs) are short non-coding single-stranded RNA molecules (20-24 nucleotide length) which account for approximately 1-2% of all genes in mammals [98]. MiRNAs control gene expression by binding to the 3′ untranslated region (3′UTR) of mRNAs, leading to mRNA degradation or translational blockage [79,99].

Several miRNAs have been shown to regulate macrophage activation through regulating the NF-KB signaling pathway. Particularly, miR-210 was shown to negatively regulate LPS-induced pro-inflammatory cytokines TNF-α and IL-6 production by increasing Iκ-Bα level and reducing the p65 expression [94]. Interestingly, up-regulation of miR-26b in LPS-induced bovine alveolar macrophages was shown to increase mRNA levels of pro-inflammatory cytokines TNF-α, IL-1β, and IL-8 and to inhibit IL-6 production [100]. In contrast, some miRNAs, such as miR-301a initiate a positive regulatory loop by elevating NF-KB activity through inhibition of NF-κB-repressing factor (Nkrf) [101].

Overexpression of miR-155 was shown to lead to an increased phosphorylation of STAT1 and STAT3 and diminished activation of STAT6 [102]. Several studies indicated that miR-155 down-regulates the suppressor of cytokine signaling-1 (SOCS1) and Src homology-2 domain-containing inositol 5-phosphatase 1 (SHIP1), the negative regulators of the JAK-STAT pathway [103]. miR-155 was described involved in the upregulation of either pro-inflammatory

TNF-α mRNA or anti-inflammatory cytokine IL-10 [104]. IL-10 activation, in turn, was shown to repress the miR-155 transcription via STAT3 [105]. Moreover, miR-155 demonstrated to inhibit IL-13 receptor (IL-13 Rα1) causing an inhibition in STAT6 activity and thus inducing a pro-inflammatory phenotype [99].

Likewise, several studies showed a crucial role of miRNAs in controlling expression of IRFs. For instance, miR-146b transcription was impaired in IL-10 and Rag1 double knockout mice. Further studies showed that IL-10 induces miR-146b production which then decreases IRF5 level and consequently favors anti-inflammatory macrophage activation [106]. Another study showed that down-regulation of miR-22-3p increases IRF5 expression level and favors the accumulation of pro-inflammatory cytokines TNF-α and IL-1β [107]. The expression of IRF4, an essential mediator of anti-inflammatory macrophage activation, was demonstrated regulated mainly by miR-125b and miR-210. Accumulation of miR-125b in macrophages targets IRF4 mRNA and protein levels, while in B cells it causes complete IRF4 gene deletion [108]. Whereas miR-210 diminishes IRF4 level through down-regulation of an 18S rRNA base methyltransferase (DIMT1), a key regulator of 18S rRNA synthesis [109].

Some miRNAs were shown to regulate macrophage activation by interfering with the C/EBPs family. For example, miR-124 represses C/EBP-α by directly binding into its 3′UTR region [110]. Overexpression of miR-124 downregulates pro-inflammatory markers and cytokines, such as CD86, MHC class II HLA-DR, TNF-α, and NOS2, and activates anti-inflammatory macrophage phenotype, particularly by increasing accumulation of TGF-β1, Arg-1, and FIZZ1 [94]. Besides miR-124, miR-181a binds to the 3′UTR region of C/EBP-α mRNA and promotes immunosuppressive activation [111]. Previously mentioned STAT family regulator miR-155 regulates C/EBP-β at mRNA and protein level by directly binding to their functional units [99].

An increasing list of miRNAs involved in the regulation of pro-inflammatory or anti-inflammatory macrophage activation is continuously described. Among them, miR-9, miR-127, and miR-21 were shown to enhance classical pro-inflammatory activation. Whereas miR-34a, let-7c, miR-132, miR-146a, and miR-125a-5p have been shown to induce anti-inflammatory phenotype in macrophages [99]. Altogether, these studies underlined the roles of miRNAs, beside transcription factors, in the determination of the immune plasticity of macrophages in response to microenvironment stimuli.

1.2.4.2. Metabolic mechanisms

Metabolic pathways are complex interconnected biochemical reactions responsible for providing the cell with energy, fatty acids, and essential amino acids [112]. Macrophages can adapt their metabolism depending on the resources available in their microenvironment [113]. These metabolic adaptations control transcriptional and post-transcriptional modifications and lead to specific cell phenotypes that can be used to distinguish pro-inflammatory and anti-inflammatory macrophages [114]. Key metabolic signatures of pro-inflammatory and anti-inflammatory macrophages are summarized in Figure 7 and the most relevant metabolic pathways are further explained in the section below.

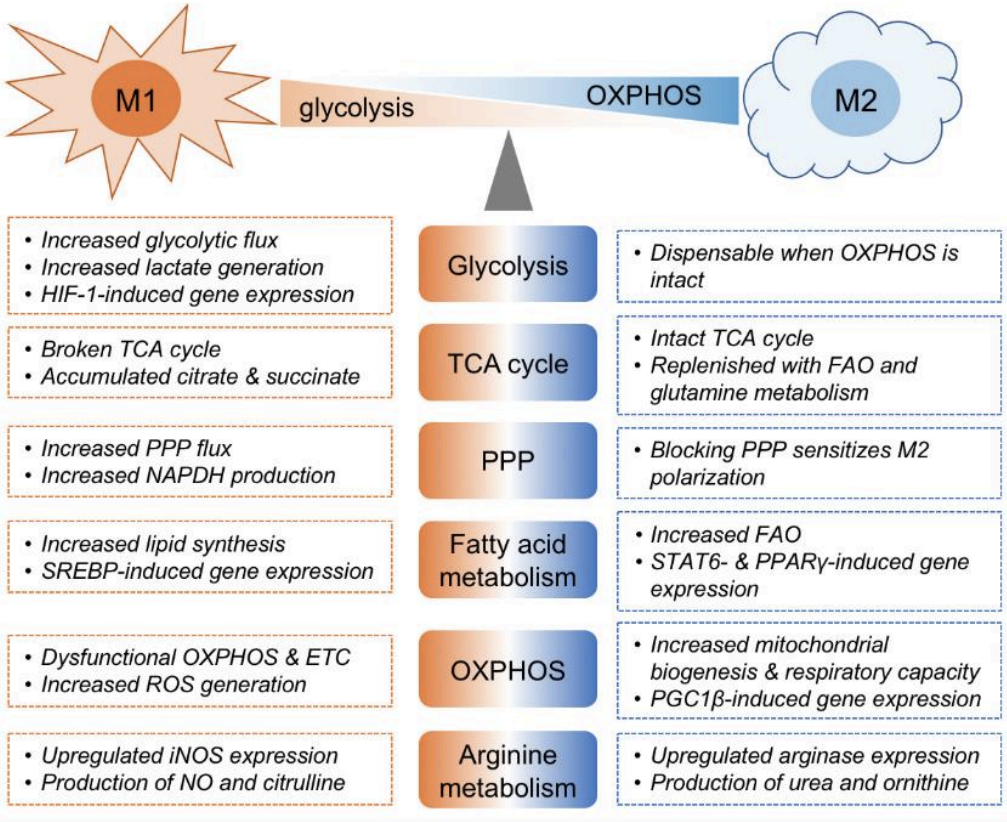

Figure 7. Metabolic profile of anti-inflammatory and pro-inflammatory macrophages.

Metabolic signatures of classically activated pro-inflammatory (M1) and alternatively activated anti-inflammatory (M2) macrophages are highlighted. OXPHOS, oxidative phosphorylation; TCA cycle, tricarboxylic acid cycle; PPP, pentose monophosphate pathway; FAO, fatty acid oxidation; ETC, electron transport chain. Adapted from *Thapa and Lee (2019)* [115].

1.2.4.2.1. Energy metabolism. Pro-inflammatory macrophages described to use glycolysis to meet their energy requirements, while anti-inflammatory macrophages were shown to rely on oxidative phosphorylation (OXPHOS) pathways [116]. During glycolysis, after extracellular

glucose uptake, a six-carbon glucose molecule breaks down into a three-carbon pyruvate molecule in the cytosol of the cell and does not consume oxygen molecules [113]. Overall, the process of glycolysis consists of 10 regulatory enzymatic steps and produces per one molecule of glucose two molecules of pyruvate, two ATP, and two NADH [114,117]. Also, glycolysis generates other intermediate metabolites, such as glucose-6-phosphate which is then used in the pentose-phosphate pathway (PPP) to produce fatty acids. It has been shown that in pro-inflammatory macrophages most of the generated pyruvate molecules are then converted into lactate [118]. Conversely, in anti-inflammatory macrophages most pyruvate molecules were shown to be further converted into Acetyl CoA, which is then enters into the tricarboxylic acid (TCA) cycle [117]. TCA cycle produces intermediates such as alpha-ketoglutarate (α-KG), citrate and succinate metabolites. It also provides electron carriers NADH and FADH2 for the electron transport chain for the oxidative phosphorylation (OXPHOS) pathway [118]. In addition to pyruvate, glutamine and fatty acids can be used as a carbon source for the TCA cycle. Glutamine is directly converted into TCA cycle intermediate α-KG, while fatty acids enter the fatty acid oxidation pathway (FAO) and become converted into acetyl-CoA, NADH, and FADH2. OXPHOS utilizes oxygen, NADH, and FADH2 to produce in total thirty-six molecules of ATP. Hence, anti-inflammatory macrophages demonstrated to rely on high energy OXPHOS metabolism which is often associated with long-living cells [113,118].

1.2.4.2.2. Arginine metabolism. Arginine is a non-essential amino acid synthesized from another amino acid citrulline mainly in the small intestine. In pro-inflammatory macrophages, arginine is converted into nitric oxide and citrulline by an enzyme inducible nitric oxide synthase (also known as iNOS or NOS2). Pro-inflammatory signals such as IFN-γ, TNF-α, and IL-1β control iNOS expression via STAT1 [53,119]. Interestingly, it has been demonstrated that in LPS-treated pulmonary macrophages miR-34a is responsible for controlling iNOS expression through the STAT3 activation [120]. Even though the main source of arginine remains the extracellular transport, when requirements for nitric oxide (NO) increase, macrophages could convert citrulline into arginine by the two enzymesargininosuccinate synthase (ASS1) and argininosuccinate lyase (ASL) [119]. In contrast, anti-inflammatory macrophages were shown to use arginase 1 to convert arginine into ornithine and urea. Ornithine is further metabolized into proline and polyamines [53]. The expression of arginase 1 was demonstrated controlled by anti-inflammatory cytokines IL-4, IL-13, IL-10, and TGF-β through activation of transcription factors STAT3, STAT6, and C/EBPβ. Hence, iNOS and arginase 1 competing for arginine dictate the fate of the macrophage activation, underlying the fact that the

availability of arginine is a major factor regulating the immune response outcome [119]. During macrophage activation, cationic amino acid transporters 1 and 2 (CAT1 and CAT2) are responsible for transporting l-arginine into the intracellular region. It has been shown that CAT2 expression is increased during pro-inflammatory and anti-inflammatory cytokine stimulations, while the level of CAT1 remains unaffected [121].

1.2.4.2.3. Hypoxia. Hypoxia, which is a cell condition under low availability of oxygen, is characterized by triggering the accumulation of transcription factors, known as hypoxia-inducible factors (HIFs) 1, 2, and 3. HIFs have distinct α subunits and common β subunit [122,123]. HIF-1α and HIF-2α under hypoxia condition translocate into the nucleus and form a complex with HIF-1β subunit, the formed complex then activates transcription of hypoxia-induced genes [124]. Whereas increased oxygen availability induces their rapid degradation. HIF-3α subunit (also called inhibitory PAS domain protein – IPAS) is a negative regulator of HIF-1α and HIF-2α [125]. In pro-inflammatory macrophages hypoxia environment was demonstrated to promote HIF-1α accumulation, which leads to increased glycolysis and suppression of the OXPHOS pathway. Particularly, HIF-1α was reported to upregulate genes encoding for glucose transporters (GLUT)1 and GLUT3, glycolytic enzymes PFK-liver type (PFKL), aldolase (ALDA), phosphoglycerate kinase-1 (PGK1), enolase (ENOL), and lactate dehydrogenase-A (LDHA) [124]. Moreover, it has been shown that HIF-1α directly binds to the iNOS promoter and increases its accumulation [126,127]. Some studies reported that HIF-1α could negatively control OXPHOS by promoting mitophagy, which is a selective process of defective mitochondria degradation by autophagy, and thereby reducing the level of mitochondrial ATP and reactive oxygen species (ROS) production (CHEK THE REFs). On the contrary, HIF-2α was described to promote the anti-inflammatory macrophage phenotype by inducing arginase 1 expression, which reduces NO accumulation and down-regulates pro-inflammatory cytokines IL-1β and TNF-α production [128,129]. Furthermore, HIF-2α diminishes the phagocytic activity of macrophages and promotes arteriogenesis. HIF-2α activation was associated with increased OXPHOS and reduced mitochondrial ROS production [129]. Taken together, these reports showed that in response to hypoxia HIF-1α accumulation favors pro-inflammatory phenotype, while HIF-2α expression increases anti-inflammatory macrophage activation.

1.2.4.2.4. Mitochondrial dynamics and the role of AMPK kinase. Mitochondria are highly dynamic organelles responsible for ATP production through the OXPHOS process, metabolite

synthesis, and mitochondrial ROS (mROS) generation [130,131]. The shape of mitochondria is controlled by fusion and fission processes and dysfunctional mitochondria are removed selectively by autophagy in a process named mitophagy. Key proteins involved in mitochondrial fusion, fission, and mitophagy processes are summarized in Figure 8 and their roles in macrophage activation are further discussed in this section.

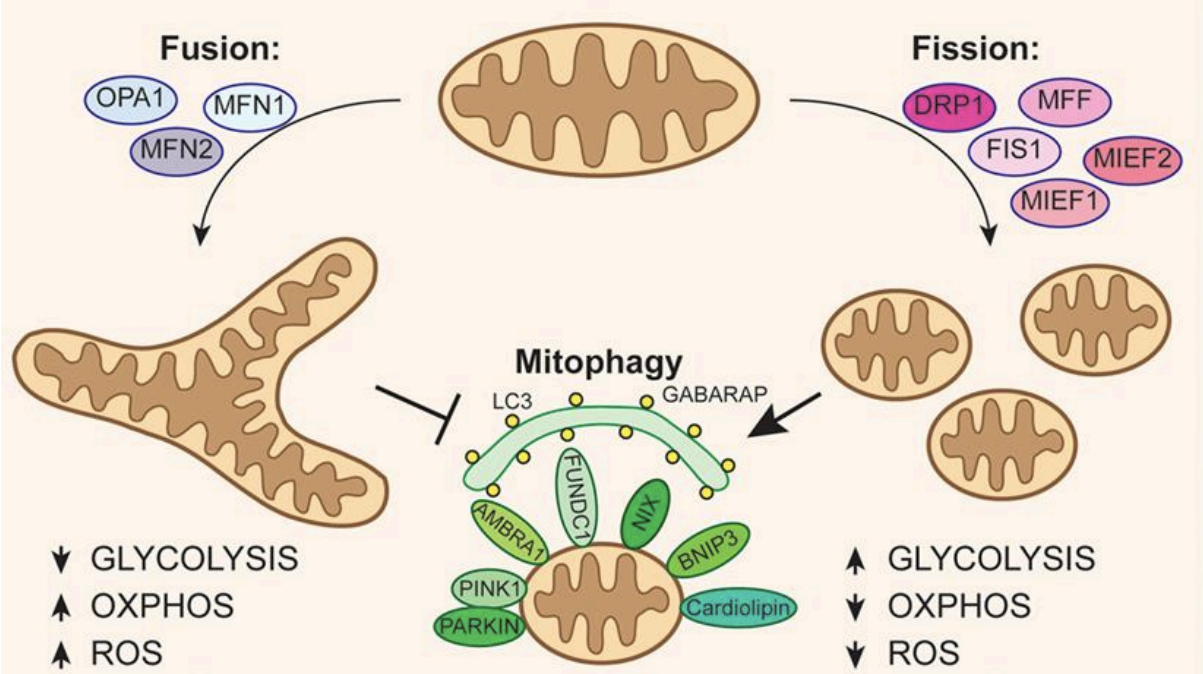

Figure 8. Mitochondrial dynamics affect cellular metabolism.

Mitochondrial fusion mediated by optic atrophy 1, mitofusin 1, and 2 leads to increased oxidative phosphorylation and reactive oxygen species production. On the other hand, mitochondrial fission mediated by dynamin-related protein-1 and fission factors FIS1, Mief1, and Mief2 decreases oxidative phosphorylation and promotes a switch to glycolysis. DRP1, dynamin-related protein-1; OPA1, optic atrophy-1; OXPHOS, oxidative phosphorylation; MFN1, mitofusin 1; MFN2, mitofusin 2; MFF, mitochondrial fission factors; ROS, reactive oxygen species. Adapted from *Bordi, Nazio, and Campello (2017)* [132].

Mitochondria respond to changes in metabolism by adjusting their morphology through the fusion and fission processes [133,134]. The fusion phase is orchestrated by several dynamin-related GTPases, such as mitofusin 1 (MFN1), MFN2, optic atrophy 1 (OPA1), FAM73a, and FAM73b [135,136]. Studies have demonstrated that mitochondrial fusion is essential for expanding mitochondrial mass and volume, which results in increased OXPHOS and mROS production [132,137,138]. Furthermore, mitochondria have their circular DNA encoding for key proteins required for ATP synthesis and any occasional mutations may cause devastating effects [137]. By promoting fusion, the cell may combine mutated mitochondria with wild type and compensate

for defects [139]. The role of fusion in macrophage activation has been highlighted in several studies. Particularly, two independent reports demonstrated that in LPS induced macrophages MFN2, but not MFN1, is essential for the expression of pro-inflammatory cytokines (TNF-α and IL-6) and NO synthesis [140,141]. Another study showed that bone marrow derived macrophages (BMDMs) from *FAM73b* knockout mice have increased the secretion of the pro-inflammatory cytokine IL-12 and inhibited the expression of the ant-inflammatory cytokine IL-10. Accordingly, genetic ablation of FAM73b and FAM73a also resulted in the stabilization of IRF1, a key transcription factor of pro-inflammatory macrophages [136]. Thus, the protein regulators of mitochondria fusion are associated with anti-inflammatory macrophage activation.

Mitochondrial fission instead is mainly controlled by a cytosolic dynamin-related protein 1 (Drp1), mitochondrial fission 1 (Fis1), and mitochondrial fission factors (MFF) [138,142]. A shift toward fission favors mitochondria fragmentation into small pieces, increases its mass, and enhances glycolysis [143,144]. Recently, several studies have demonstrated the crucial role of Drp1 S616 phosphorylation in the LPS induced pro-inflammatory cytokine release [145,146]. LPS stimulation induces TLR-4 activation leading to STAT1 phosphorylation, which then activates the Drp1 protein. Drp1 phosphorylation initiates the fission process, causing a decrease in mitochondrial membrane potential, loose of structural cristae, and fragmentation [146]. As a result of these metabolic changes, the cell shifts from ATP production to ROS generation, resulting in NF-kB mediated transcription of pro-inflammatory cytokines, such as IL-6, IL-1β, and TNF-α [146,147]. Hence, mitochondrial fission seems to be associated with pro-inflammatory macrophage activation.

Extensive ROS production during the fission process could activate mitophagy, a crucial mechanism that selectively removes damaged mitochondria by autophagy [143]. Mitophagy of damaged mitochondria starts with binding of phosphatase and tensin homolog-induced kinase1 (PINK1) to the outer mitochondrial membrane of the organelle, following by recruitment of E3 ubiquitin ligase Parkin [148]. Once there, Parkin promotes ubiquitination of outer membrane proteins, which then may undergo proteasomal degradation or bind to ubiquitin-binding adaptor p62 (also known as SQSTM1) [149,150]. A recent study suggests that p62 controls NF-kB mediated NLRP3-inflammasome suppression through induction of mitophagy [151]. Macrophages deficient in p62 showed a high accumulation of damaged mitochondria and excessive IL-1β-dependent inflammation associated with cell death. Suggesting that p62

induced mitophagy is essential for controlling an excessive inflammasome activation in macrophages [151]. Interestingly, activation of another mitophagy mediator protein kinase B, or Akt1, has been associated with prolonged survival of macrophages as well. Moreover, Akt1 activation increased anti-inflammatory cytokine TGF-β1 expression, which induces anti-inflammatory phenotype in macrophages through activating the Smad2/3-mediated and Smad1/5-mediated signaling pathway [152].

Mitochondria dynamics are closely controlled by the Adenosine Monophosphate (AMP)-activated protein kinase (AMPK) complex, an ultimate energy sensor of the cell [153]. Low ATP level triggers AMPK activation which results in a metabolic shift towards increased catabolism and decreased anabolism. As shown in Figure 9, AMPK controls numerous other metabolic processes via activating or suppressing key target proteins to rewire the cellular metabolism [154]. AMPK is serine and threonine kinase composed of three subunits, a catalytic α-subunit, and two regulatory subunits, β and γ. In mammals, there are two isoforms of α-subunit (α1 and α2), two of β-subunit (β1 and β2), and three of γ-subunit (γ1, γ2, and γ3). Thus, potentially AMPK could form up to 12 different αβγ complexes in a 1:1:1 ratio [153,154]. The catalytic α-subunit is the main functional part of the AMPK complex and it consists of three domains: N-terminal serine/threonine kinase domain (KD), a putative autoinhibitory domain (AID), and β subunit-interacting C-terminal domain (α-CTD) [153,154]. Interestingly, α subunit determines AMPK complex subcellular localization as well. It has been demonstrated that α1 isoform mainly instructs for non-nucleus localization and α2 could be found in both the nucleus and cytoplasm [154]. Activation of AMPK requires phosphorylation of threonine (Thr) residue, which lies within an "activation loop" of KD domain. AMPK subunit α1 is composed of 559 amino acid residues and its activation site is Thr183 (or Thr174), while subunit α2 contains 552 amino acid residues with primary activation site at Thr172 [154,155]. AMPK activation through Thr172 phosphorylation could be catalyzed by two main upstream kinases, calcium/calmodulin-dependent protein kinase β (CaMKKβ) and liver kinase B1 (LKB1) [156,157]. Moreover, it has been shown that physical binding of ADP and AMP to γ-subunit protects from dephosphorylation at Thr172, allowing prolonged activation [155,158]. The β-subunit has two main domains: a glycogen-binding carbohydrate-binding module (CBM) which allows binding to glycogen and a scaffolding C-terminal domain (β-CTD), which connects the γ subunit and the α-CTD [159,160]. The γ subunit senses AMP level and contains two domains: the N-terminal domain, to whose amino acid length varies γ1, γ2 and γ3 isoforms, and a tandem domain

containing four evolutionarily conserved cystathionine β synthase (CBS) repeats which functions as nucleotide binding sites [154,159,160]. Thus, AMPK has a complex structure, and its activity is tightly regulated.

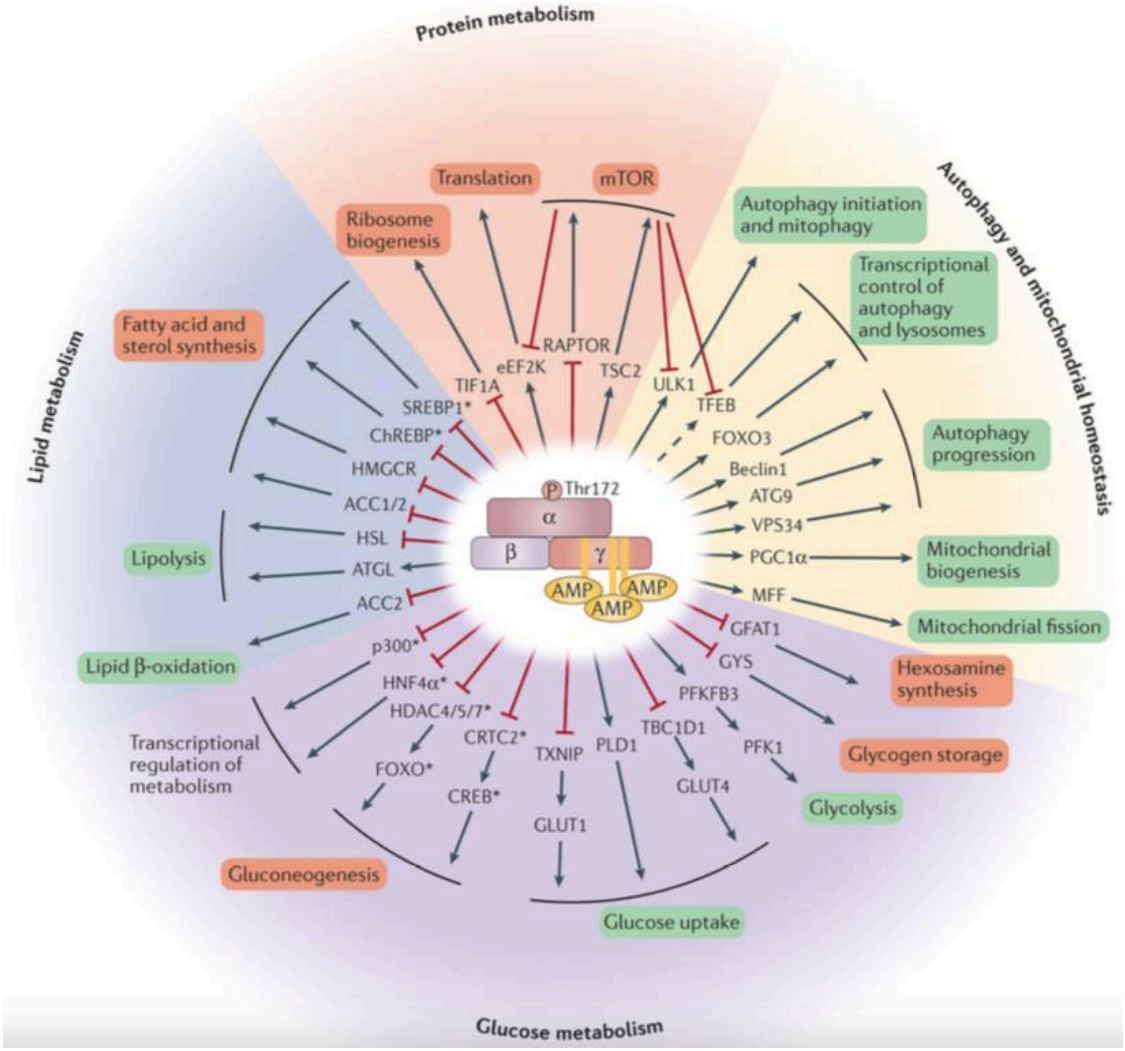

Figure 9. Role of AMPK in regulating various metabolic processes.

The AMP-activated protein kinase (AMPK) complex could directly phosphorylate several cellular targets indicated in the first intrinsic circle. Phosphorylation could be activating (black arrows) or inhibitory (red arrows). The box color indicates whether the metabolic processes are generally activated (green) or inhibited (red). ChREBP, carbohydrate-responsive element-binding protein; CREB, cAMP response element-binding protein; FOXO, forkhead box protein O; HDAC, histone deacetylase; HMGCR, HMG-CoA reductase; HNF4α, hepatocyte nuclear factor 4α; MFF, mitochondrial fission factor; PGC1α, peroxisome proliferator-activated receptor-γ co-activator 1α; PLD1, phospholipase D1; SREBP1, sterol regulatory element-binding protein 1; TFEB, transcription factor EB. Adapted from *Herzig and Shaw (2018)* [160].

Even though the crucial role of AMPK in metabolic processes is well established, very little is known about its contribution to macrophage activation. Some reports described a regulatory role of AMPK activation in inflammatory signaling pathways in macrophages. For example, the inhibition of AMPKα1 phosphorylation in macrophages was demonstrated to increase the LPS-induced TNF-α and IL-6 secretion and decrease IL-10 release [157]. These findings suggested that AMPKα1 activation promotes anti-inflammatory functional phenotype in macrophages. Furthermore, studies on macrophages derived from AMPKα1-deficient mice showed that AMPK phosphorylation at Thr172 is required for IL-10 induced STAT3 direct phosphorylation and indirect phosphorylation through induction of mTORC1 signaling pathway. Phosphorylation of STAT3 transcription factor leads to its stabilization and SOCS3 gene expression, which then blocks the transcription of pro-inflammatory cytokines TNF-α and IL-6 [161,162]. Altogether, these studies further support that AMPKα1 phosphorylation leads to anti-inflammatory macrophage activation.

1.3. Functions of macrophages

Macrophages are main effectors of innate immunity and important initiators and stimulators of adaptive immune response. They are specialized phagocytes, of pathogens and apoptotic cells, and could achieve a variety of functions in homeostasis and immune response enabling them to play crucial roles in the development of diseases, tumorigenesis and pathogenesis [163,164]. In this section, we discuss some of the crucial functions of macrophages involved in tissue homeostasis and disease.

1.3.1. Physiological functions of macrophages

Tissue macrophages, as it is shown in Figure 10, are strategically populated throughout the body, where they engulf foreign bodies, pathogens, dead and deregulated cells and establish hemostasis [165,166]. Besides their organ-specific functions, macrophages also modulate the immune system by recruiting monocytes and presenting antigens to lymphocytes [167]. Here, we summarize how tissue-specific macrophages sustain homeostasis within the organ they reside.

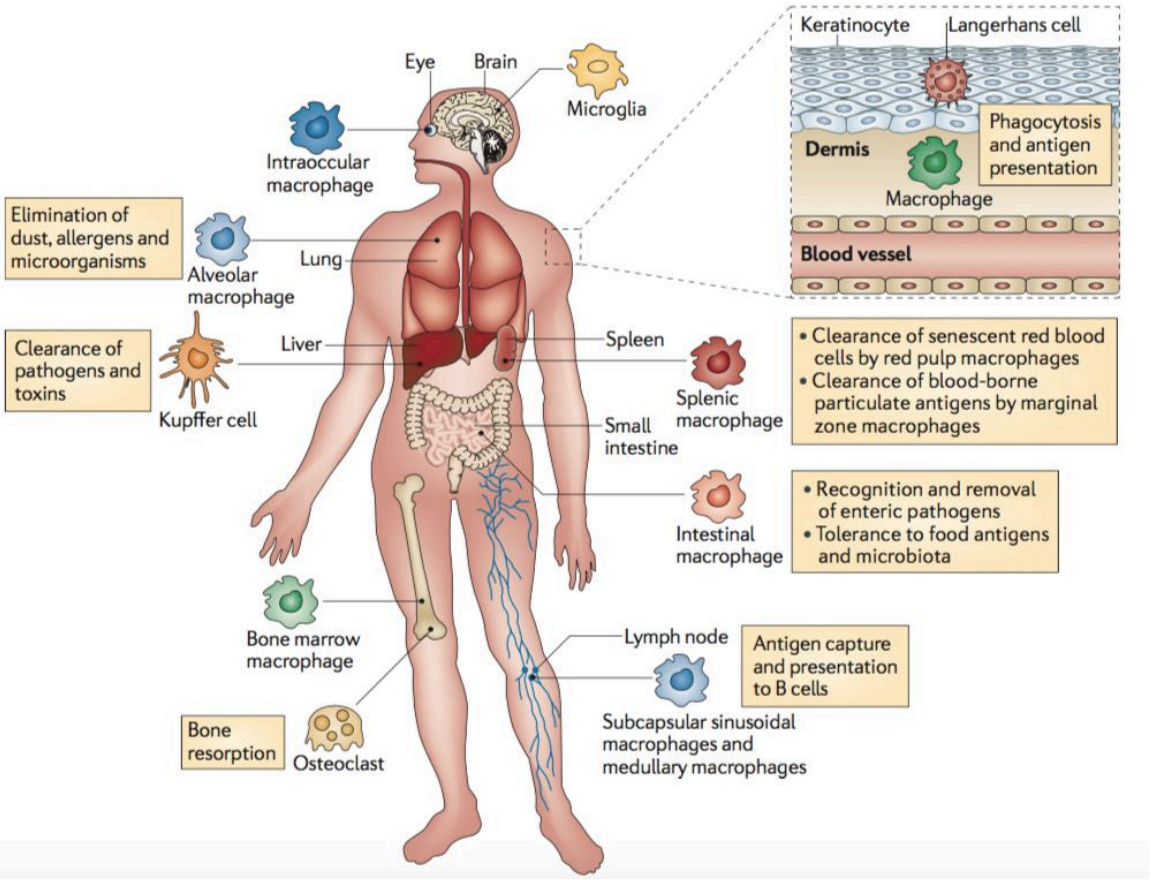

Figure 10. Homeostatic functions of tissue-specific macrophages.

Tissue-specific macrophages perform various functions, including clearance of foreign bodies, pathogens, dead, senescent and deregulated cells, antigen presentation to B cells, to maintain tissue homeostasis. Adapted from *Murray and Wynn (2011)* [165].

1.3.1.1. Adipose tissue. Adipose tissue macrophages were shown to acquire an anti-inflammatory phenotype of (ATMs) promoted by eosinophils and type 2 innate lymphoid cells (ILC2s), which reside in adipose tissue and secrete Th2 cytokines IL-4 and IL-13, respectively [168,169]. ATMs were demonstrated to secrete anti-inflammatory cytokines, such as IL-10, IL-4, Il-1RA, TGF-β, and involved in the resolution of inflammation [169]. Moreover, ATMs promote insulin sensitivity through the peroxisome proliferator-activated receptor-gamma (PPARγ) and sustains thermogenesis through the production of catecholamines [170,171].

1.3.1.2. Central nervous system: CNS includes various types of macrophages, including microglia, perivascular macrophages (PVM), and meningeal macrophages (MM) [168]. Among them, the most abundant and fully studied are microglia [172]. Depending on the signals and stimuli of the tissue environment, microglia could develop both pro-inflammatory and anti-inflammatory phenotypes and are known for their plasticity to shift from one type to another [173]. Microglia were shown mainly involved in synaptogenesis, neuronal survival, and

degeneration [174]. Proper synaptic function depends on the microglial receptors involved in phagocytosis, such as the triggering receptor expressed on myeloid cells 2 (TREM2), and the DNAX-activating protein of 12 kDa (DAP12) [174,175]. Whereas survival of V cortical neurons depends on insulin-like growth factor-1 (IGF-1) released mainly from microglia cells [174]. IGF-1 promotes repair and regenerative anti-inflammatory microglial cells while inhibiting neurotoxic ROS generation from pro-inflammatory microglia [176]. Chronic pro-inflammatory macroglia activation results in uncontrolled release of pro-inflammatory cytokines, such as IL-1, IL-6, IFN-γ, and TNF-α, which causes the progression of neurodegenerative pathologies, including Alzheimer's disease, Parkinson's disease, and Amyotrophic lateral sclerosis [177,178].

1.3.1.3. Spleen. Spleen has three different subpopulations of macrophages, marginal metallophilic macrophages (MMMs), marginal zone macrophages (MZMs), and red pulp macrophages (RpMs) [179]. Murine MMMs express sialic acid-binding Ig-like Lectin-1 (Siglec-1, Sialoadhesin, CD169) and MOMA-1, while MZMs express C-type lectin SIGN-related 1 (SIGNR1) and macrophage receptor with collagenous structure (MARCO) [35,179]. Both macrophage subpopulations are responsible for removing blood-borne pathogens and clearance of apoptotic T and B lymphocytes [35,180]. MMMs can cross transfer pathogens, such as adenovirus, to splenic dendritic cells, which then educate cytotoxic T cells [181]. RpMs recycle iron from phagocytized senescent and damaged erythrocytes. Moreover, RpMs were shown able to induce Type I interferon response through activation of TLR9/MyD88/IRF7 signaling pathway [14,182]. RpMs were demonstrated to produce TGF-β as well, which induces Foxp3 expression in naïve $CD4^+$ T cells, resulting in the generation of functional regulatory $Foxp3^+$ T cells [183].

1.3.1.4. Liver. Kupffer cells (KCs) are liver resident macrophages involved in maintaining liver functioning. They have high phagocytic activity giving to the abundant expression of complement receptors, which enable them to remove gut bacteria, bacterial toxins and debris coming from the gastrointestinal tract [184]. Kupffer cells contribute with hepatocytes to the filtration of the blood from chemical and harmful substances and also recycle heme into iron, biliverdin, and carbon monoxide [185]. Constant exposure to harmless dietary and commensal antigens requires the liver immune system to develop immunological tolerance rather than immunity [186]. KCs help to maintain the immune tolerance by expressing lower levels of MHCII, B7.1, B7.2, and CD40, which makes them poor stimulators of T cells [187]. They also known to induce apoptosis of activated $CD8^+$ T cells [188,189].

1.3.1.5. Lymph nodes. Based on the anatomical location, phenotype, and function, macrophages populating lymph nodes are mainly divided into two subpopulations, the subcapsular sinus (SCS) and the medullary sinus (MS) macrophages [190,191]. SCS macrophages abundantly express sialic acid-binding Ig-like lectin 1 (Siglec1 or CD169), the integrin Mac1 (CD11b/CD18), and MCH II, however, they lack the expression of murine macrophage marker F4/80, suggesting that SCS macrophages have the low phagocytic capacity and high antigen-presenting capabilities [190,192]. Together with lymphatic endothelial cells (LECs), SCS macrophages form a tight physical barrier in the entry of afferent lymphatic vessels, where they capture pathogens and antigens entering the lymph node [191]. SCS macrophages further translocate antigens to B cells, causing B cell maturation and humoral immune response [193]. Moreover, SCS macrophages directly activate natural killer T cells through CD1d receptor [191]. They are also involved in type I interferon production and recruitment of other immune cells, such as T cells, monocytes and neutrophils [190]. In contrast, MS murine macrophages express F4/80, the lymphatic vascular endothelial marker LYVE-1, SIGNR1, and MARCO [191]. These macrophages are highly phagocytic and involved in the clearance of lymph-borne antigens, dying plasma cells, and immune cells, such as eosinophils [192].

1.3.1.6. Bone and bone marrow. Bone and bone marrow resident macrophages are broadly classified into four categories: osteoclast, osteomacs, erythroblastic island macrophages (EIMs), and hematopoietic stem cell (HSC) niche macrophages [194,195]. Osteoclasts contribute in bone remodeling by releasing hydrochloric acid and cathepsin K [196]. Whereas osteomacs are involved in bone development, tissue repair, and remodeling processes [197]. EIMs promote proliferation and differentiation of erythroid progenitor cells by producing cytokines, such as IL-3 and GM-CSF [198]. Whereas, HSC niche macrophages produce chemokine CXCL12, responsible for HSC retention in the bone marrow [199,200].

1.3.1.7. Lung tissues. Pulmonary macrophages are the first line of defense against inhaled pathogens, dangerous or innocuous particles, toxins, and allergens, coming from inhaled air or blood flow [201]. Lung macrophages are highly heterogeneous and based on the anatomical location within the organ can be subdivided into two distinct populations in humans: alveolar and interstitial macrophages [202,203]. Alveolar macrophages reside in the airway lumen, close to the blood vessels and the type I and type II alveolar epithelial cells [204]. Pathogens or environmental particles activate pattern-recognition receptors in alveolar macrophages, triggering phagocytosis and the secretion of pro-inflammatory cytokines [205,206]. To avoid

overstimulation of the immune system, alveolar macrophages develop airway tolerance by coexpressing TGF-β and retinal dehydrogenases (RALDH1 and RALDH 2) that results in the generation of Foxp3^{+} Treg cells [207]. Interstitial macrophages reside within the lung parenchyma and under physiological conditions, they function as immunosuppressive cells that release cytokine IL-10 through activation of the TLR4/MyD88 pathway [208,209].

1.3.2. Macrophages in human pathologies

Circulating monocytes in the blood could increase or decrease under pathological conditions and monitoring this phenomenon is crucial for patient diagnosis and management [163]. Both decrease and increase of monocytes and macrophage populations contribute to pro-inflammatory or anti-inflammatory phenotype development and consequently to the inflammatory immune responses [164]. Thus, monocytes and macrophages play crucial role in disease development. Here, we discuss the roles of monocytes and macrophages in several pathological conditions.

1.3.2.1. Infectious diseases. Pathogens activate pattern-recognition receptors on macrophages, which initiate pro-inflammatory cytokine production and activate them toward the pro-inflammatory phenotype. These cytokines then are contributing to inflammatory processes and pathogen clearance [210]. Nonetheless, several pathogens have evolved mechanisms to evade the host immune responses and ensure their survival and disease progression. For example, upon bacterial infection with *Mycobacterium tuberculosis* (*M. tuberculosis*), macrophages produce TNF-α, IL-1β, IL-12, CCL2, and CXCL18 and are skewed toward pro-inflammatory phenotype [211]. However, *M. tuberculosis* was shown to interfere with phagosome-lysosome fusion and dictate macrophage activation toward the anti-inflammatory phenotype in both necrotic and non-necrotic tuberculosis granulomas, which is associated with reduced bactericidal activity of macrophages [212,213]. Several other pathogens, such as bacteria *Helicobacter pylori* and fungus *Candida albicans* target pro-inflammatory and anti-inflammatory plasticity of macrophages to circumvent their clearance and maintain their replication in the specific tissues [210].

Beside bacteria, viruses are able to infect macrophages and dictate their functional reprogramming and survival to ensure viral body spread and persistence. For instance, at early acute phase of HIV-1 infection macrophages produce pro-inflammatory chemokines such as CCL3, CCL4, and CCL5 and Th1 cytokines such as IFN-γ, IL-2, IL-12. Pro-inflammatory

activation of HIV-1 infected macrophages was shown to down-regulate CD4 and DC-SIGN, membrane receptors which bind HIV-1, thus avoiding superinfection and enabling viral expansion [210,214]. However, at chronic HIV-1 infection phases, secretions of IL-4 and IL-13 induce the anti-inflammatory reprogramming of macrophages, which is associated with high permissiveness to HIV-1 infection and AIDS progression. HIV-1 was also demonstrated to modulate the expression of apoptosis signal-regulating kinase-1 (ASK1) in macrophages, which in turn lead to the inhibition of Fas- and TNF receptor-mediated apoptosis [214]. Thus, the long lived HIV-1 infected macrophages, with memory CD4 T cells, are the major viral reservoir and main source of HIV-1 relapses after anti-retroviral (ART) therapy [210,215]. WONG HIV

1.3.2.2. Autoimmune diseases. Autoimmune disorders are often characterized by the pathologic role of antigen-specific T and B lymphocytes, which fail to distinguish between "self" and "non-self" antigens [216]. However, recent observations over the last decade have also demonstrated the important modulatory role of macrophages in autoimmune diseases, including systemic lupus erythematosus (SLE) and rheumatoid arthritis (RA) [217]. SLE is a systemic autoimmune disorder, where autoantibodies attack nuclear components, such as double-stranded DNA (dsDNA), ribonucleoproteins, and histones, resulting in chronic inflammation and damage to vital organs [218]. The role of macrophages in the pathological development of SLE is mainly driven by defective phagocytosis and imbalanced activation [216,219]. Particularly, in SLE macrophages were demonstrated to secrete an abnormal amount of type I interferon, which inhibits their ability of clearance of apoptotic cells. Accumulation of apoptotic cells was shown to promote autoantigens release and consequently autoreactive B cell activation [219]. It has been found that the propagation of type I inflammation in SLE is supported by pro-inflammatory macrophages, which secrete TNF-α, IFN-γ, and GM-CSF [220]. Furthermore, pro-inflammatory macrophages appear to play a pivotal role in RA, a chronic inflammation of the joints, which results in cartilage and bone destruction [221,222]. RA progression is in part caused by the pro-inflammatory activated macrophages through inducing the secretion of the inflammatory cytokine and chemokine, the production of the inflammatory metabolites (reactive oxygen species (ROS) and nitric oxide (NO)), and the release of matrix-degrading enzymes [223].

1.3.2.3. Metabolic diseases. Obesity is discussed here because it is an outstanding example of metabolic disorders. Indeed, obesity is considered as low-grade chronic inflammation driven

by an imbalance between caloric intake and energy expenditure, which results in excessive body fat and causes obesity-related health problems, including insulin resistance, type 2 diabetes mellitus, dyslipidemia, coronary heart disease, hypertension, cerebral vasculopathy, gallbladder lithiasis, and fatty liver disease [224,225]. It has been demonstrated that obesity is characterized by an increased monocyte recruitment into adipose tissue, which predominantly differentiate into classically pro-inflammatory activated macrophages [226]. These pro-inflammatory macrophages then govern the chronic inflammation by producing the pro-inflammatory cytokines TNF-α, IL-1β, IL-6, IL-17 and other inflammatory factors, such as CCL2 [224,227].

1.3.2.4. Cancer. The tumor microenvironment (TME) is highly heterogeneous, composing of endothelial cells, cancer-associated fibroblasts, and different populations of immune cells, including macrophages. Tumor-associated macrophages (TAMs) are a major component of TME could represent up to 80% of the tumor. TAMs play crucial roles in the tumorigenesis and in the response to cancer therapies. Thus, several aspects on the biology and the roles of TAMs are discussed in detail in the next section (1.4).

1.4. Tumor-associated macrophages

The TME is highly heterogeneous milie consisting of various cells, including tumor cells, T cells, B cells, natural killer (NK) cells, TAMs, myeloid-derived suppressor cells (MDSCs), mast cells, granulocytes, dendritic cells (DCs), tumor-associated neutrophils, cancer-associated fibroblasts (CAFs), adipocytes, vascular endothelial cells, stem cells, granulocytes, and pericytes [228,229]. In fact, the TME promotes the antitumor immune responses and play a critical role in tumor growth, invasion, and metastasis, as well as in acquired resistance of cancers to various therapies [228,230,231].Tumor-associated macrophages (TAMs) are particularly abundant immune infiltrates in the TME. High TAMs infiltration has been associated with poor prognosis and clinical outcomes in distinct cancer types, including lymphoma, cervical, bladder and breast cancers [232,233]. Interestingly, a clinical exception was observed in colorectal cancer where high TAMs accumulation in tumor stroma was associated with favorable 5-year overall survival [234]. These conflicting functions of TAMs are due to their complex phenotypes and functional characteristics, rising from distinct tumor microenvironments. In this section, we discuss the development and functions of TAMs and their roles in cancer therapies.

1.4.1. Origin of tumor-associated macrophages

It has been recently demonstrated that depending on the type of tumor TAMs could be originated from both embryonic-derived resident macrophages and monocytes-originated macrophages. Interestingly, TAM populations could be derived from monocytes recruited from both bone marrow and liver [235]. It was established that tissue-resident macrophages could be originated from either an embryonic precursor (yolk sac, fetal liver) or a monocyte precursor from hematopoiesis and could retain self-renewal and proliferation capacities throughout their lifespan [236,237]. The recruitment of monocyte into tissue site was shown to be induced mainly by monocyte chemoattractant protein-1 (MCP-1/CCL2) and its receptor C–C chemokine receptor type 2 (CCR2) [238]. Indeed, the early studies on solid tumors have demonstrated that blocking CCL2/CCR2 axis has significantly reduced TAMs population in the tumor microenvironment suggesting that the main origin of TAMs is the CCR2+ monocyte precursors recruited from both bone marrow and liver [235,239]. However, blocking CCL2/CCR2 axis does not result in the complete deletion of TAMs, suggesting that another origin might exist [235]. Indeed, recent studies have shown that TAMs could be originated from resident macrophages of embryonic origin as well [235,240,241]. For instance, it has been shown that murine TAMs which infiltrate pancreatic ductal adenocarcinoma (PDAC) are originated from both embryonic and $Ly6C^{hi}$ monocytes-derived macrophages [240]. Similar observations were shown in murine lung tumor, where TAMs are derived from $Ly6C^{hi}$ monocytes differentiated into $Ly6C^{low}CD64^{+}FLT1^{+}$ TAMs and from yolk sac–derived interstitial $Ly6C^{low}CD64^{+}$ resident macrophages acquiring $Ly6C^{low}CD64^{+}FLT1^{+}VCAM1^{+}$ pro-tumorigenic macrophage phenotype [241]. However, in the majority of human cancers high accumulation of $CD16^{+}$ monocytes was observed and associated with a worse prognosis [233]. For instance, the elevated level of $CD14^{+}CD16^{+}$ monocytes in cholangiocarcinoma was associated with high infiltration of monocyte-derived TAMs [242]. Accordingly, $CD14^{+}CD16^{+}$ monocyte frequency was suggested as a marker of breast cancer diagnosis because it was significantly increased in these cancer patients as compared to healthy individuals [243]. Altogether, these results suggest that TAM populations in TME are predominantly monocyte-derived macrophages and with less frequency are derived from the embryonic tissue-resident macrophages, though they play pro-tumorigenic role as well.

1.4.2. Recruitment and development of TAMs

The formation of functional monocyte-derived TAMs involves several stages, such as recruitment, differentiation, and self-renewal and each step is regulated by distinct mechanisms. The recruitment of monocytes in the tumors was shown to be mediated mainly by the help of specific chemokines, cytokines, and certain vasoactive and mitogenic peptides [123,233]. The CCL2 and CCL5 chemokines, which are secreted from the cancer cells, macrophages, fibroblasts, and endothelial cells of the TME, were demonstrated highly involved in monocyte infiltration in the tumor [244]. CCL2 is chemo-attractive that bind CCR2 receptor on the monocyte surface and recruit them to the tumor site. It was shown that CCL2 activate JAK2/STAT3, MAP kinase, and PI3K signaling pathways, which are associated with stimulating cell migration and phospholipase-C-mediated calcium release [238]. Besides chemoattractant properties, CCL2 also promotes macrophages-associated chemoresistance by inducing the expression of the immunosuppressive molecular MCP-1-induced protein (MCPIP1) through activation of the JAK2-STAT3 signaling pathway [245].

Similarly, CCL5 was demonstrated to target a variety of receptors, including CCR1, CCR3, CCR4, CCR5, CD44, and GPR75. CCL5 binding to the specific receptors on target monocytes triggers downstream NF-kB signaling pathway, in which STAT3 activation is likely to play an important role [246–248]. CCL5 recruited monocytes are differentiated in TME toward immunosuppressive M2-like macrophages, which express PD-L1 and CD206 and produce anti-inflammatory cytokines IL-10 and TGF-β [249,250]. Other chemokines, such as CCL3, CCL4, CCL8, and CCL22 also been shown involved in monocyte recruitment to tumors [244].

As well as chemokines, cytokines, including CSF1 (M-CSF) and VEGF, have been implicated in monocyte recruitment and their differentiation into immunosuppressive TAMs in TME [244]. Both, macrophages and tumors can secrete CSF1 [251] and VEGF [252]. CSF1 triggers monocyte spreading and migration via activating actin nucleators Wiskott-Aldrich syndrome protein (WASP) and WASP-family verprolin homologous 2 (WAVE 2) (REFS). Moreover, CSF1 controls macrophage differentiation through the activation of its own receptor CSF-1R by phosphorylation (CSF-1R pTyr-807), , which ultimately activates MEK and PI3K pathway in a dose-dependent manner. CSF1 also promotes macrophage survival by triggering the CSF-1R pTyr721/PI3K pathway [17]. VEGF cytokine and its main isoform VEGF-A its most common isoform were involved in the infiltration of TAMs [253,254]. VEGF-A binds to two receptor tyrosine kinases, VEGFR1 and VEGFR2 [254]. A recent study showed that VEGFR1 controls

macrophage migration and proliferation through PLCγ and PI3K pathways [255]. It has been also reported that VEGF controls PD-L1 expression in macrophages likely through VEGFR2 [256,257]. (REFS). Accordingly, simultaneous inhibition of PD-L1 and VEFR2 induced strong anti-tumor response.

Accumulation of several vasoactive and mitogenic peptides in tumors has been associated with high TAMs infiltration as well [244]. For instance, endothelins, 1-3 (ET-1, -2, and -3) were shown to be highly expressed in several types of human tumors [258]. ET-1 and ET-2 were demonstrated able to attract monocytes and macrophages [259]. Moreover, ET-1 was shown able to enhance macrophage adhesion to tumor cells via increasing integrin αV and integrin β1 mRNA expression through activating Elk-1/STAT3/NF-kB signaling pathway [260].

Overall, recruitment and development of TAMs in the TME is a complex mechanism involving numerous cytokines, growth factors, active mitogenic proteins, and chemicals, which trigger vital cellular processes, including migration, proliferation, differentiation, and survival.

1.4.3. Metabolic modulations of TAMs

Based on metabolic and phenotypic differences macrophages are generally subdivided into two subtypes anti-tumorigenic pro-inflammatory M1-like type and pro-tumorigenic anti-inflammatory M2-like type macrophages. However, recent studies demonstrate that TAMs could exhibit mixed features of pro-inflammatory and anti-inflammatory phenotypes during cancer development. Moreover, depending on the tumor microenvironment TAMs form a distinct phenotypic and functional subset, which have predominantly an anti-inflammatory phenotype expressing some pro-inflammatory gene and metabolic signatures.

1.4.3.1. Glucose metabolism. Similarly to pro-inflammatory macrophages, TAMs were demonstrated to use glycolysis as a key metabolic pathway [261,262]. Indeed, TAMs have an upregulated level of glycolytic enzymes, including hexokinase 2 (HK2), phosphofructokinase, and enolase1 (ENO1) [263]. Enhanced glycolysis is associated with a high production of lactic acid, which plays an important role in regulating anti-inflammatory macrophage activation. High lactate level increases HIF1α and HIF2α activation by distinct mechanisms. Lactate and hypoxia activate HIF1α, resulting in VEGF and Arg1 overexpression and IFNγ secretion [262,264]. Lactate could also decrease lysosomal degradation of HIF2α, which induces the expression of *VEGF, Mrc1, Arg1*, and *Retnla* genes. In patients with head and neck squamous cell carcinomas the expression of ARG1 mRNA was associated with low overall survival rate [265].

Moreover, a high lactate level directly activates homeostatic gene expression, through histone lactylation and histone demethylases KDM6A and KDM5A [262].

1.4.3.2. Lipid metabolism. Fatty acid (FA) synthesis is essential for energy production, generation of cellular membranes and production of signaling metabolites. FA synthesis is fueled from different sources, including citrate TCA cycle product, which is converted into AcCoA in the cytoplasm [266]. FA synthesis in TAMs was shown to be associated with both protumoral and antitumoral macrophage activation. Antitumoral phenotype is triggered by IFN-β signaling cascade, which is controlled by epidermal fatty acid-binding protein (E-FABP), an intracellular lipid chaperone [263]. Whereas several other FA signaling pathways enhance infiltration and protumoral phenotypic reprogramming in TAMs. For instance, the accumulation of eicosanoid 15-hydroxyeicosatetraenoic acid (15-HETE), which synthesized by 15-lipoxygenase (15-LOX) during arachidonic acid metabolism, is associated with CCL2 and IL-10 production [263,267]. Moreover, overexpression of Cyclooxygenase-2 (COX-2) enzyme, which converts AA into different prostaglandins (PGs) including prostaglandin E_2 (PGE_2), plays a crucial role in antitumoral activation of TAMs [268]. PGE2 primarily targets EP4 receptors on macrophages, resulting in VEGF production and ERK1/2 phosphorylation [269]. Interestingly, it has been demonstrated that tumor cells induce PD-L1 expression on macrophages through modulating the COX-2/PGE_2 signaling pathway [270].

1.4.3.3. Amino acid metabolism. Amino acids, especially glutamine, arginine, and tryptophane were shown to play a critical role in the development of TAMs [266]. Glutamine is converted into glutamate by the enzyme glutaminase (GLS), and further catabolized to α-ketoglutarate (α-KG) by glutamate dehydrogenase (GLUD1) [271]. GLS is highly expressed in IL-10 treated macrophages and several types of malignancies including colon, esophagus, liver, stomach, thyroid, and head and neck cancer [261,272]. Blocking glutamine catabolism is associated with less monocyte recruitment and antitumor TAMs infiltration [273]. Even though the exact mechanism remains largely unknown, it was shown that glutamine fuels one-third of all carbons in the TCA cycle and it is necessary for T cell activation [263,266]. TAMs metabolize arginine through upregulating arginase I expression, which competes for arginine with iNOS, as a result, arginase I establish anti-inflammatory activation through inhibiting iNOS-induced pro-inflammatory reprogramming [119,266]. Furthermore, TAMs have a high expression of indoleamine2,3-dioxygenase (IDO), an enzyme that converts tryptophan to kynurenine. High

IDO levels limit tryptophan availability for T cells and NK cells, which is necessary for biomass regeneration [261,263].

Overall, TAMs exhibit diverse metabolic profile, which highly depends on extracellular characteristics of the TME. The heterogeneous factors and mediators present at the TME can reprogram TAMs into pro-inflammatory or anti-inflammatory phenotype.

1.4.4. Roles of TAMs in tumor growth and metastasis

Considering that in many solid and hematological tumors, the TME is often highly populated with TAMs, the identification of the molecular mechanisms defining their functions provides new insights and novel targets for efficient cancer therapies. These innovative strategies could be able to overcome issues of refractoriness to cancer treatments caused by immunosuppressive TAMs and to enhance the effectiveness of conventional therapies. In this section, we attempt to describe key functions exhibited by TAMs and elaborate their role in tumor progression.

1.4.4.1. Cancer initiation and promotion. It has been demonstrated that TAMs play a crucial role in promoting tumor development and initiation by secreting distinct soluble factors in TME including growth factors, chemokines and cytokines. Particularly TAMs are known to secrete a large number of growth factors including TGF-β, VEGF, and platelet-derived growth factor (PDGF), epidermal growth factor (EGF), fibroblast growth factor (FGF), cytokines such as M-CSF, IL-10, and C-X-C motif chemokine ligands (CXCLs), which directly or through epithelial cells activate tumor growth [239,274]. For instance, in ovarian cancer EGF secreted by TAMs promoted tumor progression by suppressing LIMT (lncRNA inhibiting metastasis) through the EGFR-ERK signaling pathway [275]. Moreover, the chemokine CXCL8 accumulation was associated with breast cancer, colorectal cancer, non-small cell lung cancer, gastric cancer, and melanoma development [276]. In endometrial cancer CXCL8 secreted by TAMs cause tumor progression through inducing ERα loss via HOXB13 [277].

1.4.4.2. Tumor invasion and metastasis. TAMs were involved almost in every step of metastasis, including preparation of premetastatic niches, extravasation, invasion, vascularization, protecting and supporting persistent growth of metastatic cells [278,279]. Several studies suggested that TAMs support tumor invasion through releasing various soluble factors, such as IL-1β, IL-8, TNF-α, and (TGF-β), which modulate the epithelial-mesenchymal transition (EMT) [279]. Moreover, TAMs promote extracellular matrix (ECM) degradation by

secreting proteolytic enzymes such as cathepsins, MMPs, and serine proteases and thereby allowing cancer cell migration [280]. TAMs also activate survival and protective mechanisms in newly disseminated cancer cells. For example, breast cancer cells expressing vascular cell adhesion molecule-1 (VCAM-1) primarily metastasize in lung tissue by tethering to α4-integrin expressed on the surface of tissue-resident pro-tumoral macrophages. As a result, VCAM-1 engagement promotes Ezrin phosphorylation which leads to activation of the PI3K/Akt survival pathway [279,281]. This study also indicates that the premetastatic niches in the host tissues are populated by TAMs before the arrival and engraftment of metastatic cells. Indeed, it has been shown that primary tumors release VEGF-A, TNF-α, TGF-β, and LOX which reprogram tissue-resident macrophages, such as osteoclast (bone), Kupffer cell (liver), or alveolar (lung) into protumoral macrophages, which then secrete IL-6, CCL2, COX-2, and MMPs and create premetastatic niches [278,282].

1.4.5. Roles of TAMs in tumor immunosuppression and angiogenesis

1.4.5.1. Immunosuppression. It was well established that TAMs release cytokines, chemokines, enzymes, and express specific receptors to modulate multiple immune cells, including $CD8^+$ and $CD4^+$ T cells, induced regulatory T cells (iTregs), and natural Tregs (nTregs) [274]. For example, CCL2 chemokine secreted by TAMs in TME inhibits $CD8^+$ T cells trafficking and thus prevents from reaching and removing tumor cells [283,284]. Moreover, TAMs express PD-L1 and PD-L2 ligands which bind to the T cell inhibitory PD-1 receptor, resulting in exhausted and dysfunctional $CD8^+$ T cells. Another important T cell inhibitory receptor involved in $CD8^+$ T cells exhaustion is cytotoxic T-lymphocyte-associated antigen-4 (CTLA-4) which binds to CD80 and CD86 receptors expressed in TAMs [285,286]. TAMs secrete cytokines IL-10 and TGF-β which can directly suppress $CD8^+$ T cells function or recruit immunosuppressive $FoxP3^+$ $CD4^+$ Tregs cells [287]. IL-10 also suppresses IL-12 expression in intratumoral dendritic cells, which is necessary to induce IFN-γ production by $CD4^+$ T cells, NK, and $CD8^+$ T cells [288,289].

TAMs also modulate the expression of MHC class I molecules to inhibit the anti-tumor immune responses [290]. MHC class I encodes two sets of HLA class I (HLA-I) molecules [291], which are named as classical (includes HLA-A, -B, and -C molecules) [292] and non-classical molecules (such as HLA-E, -F,-G) [293]. Both classical and non-classical MHC class I molecules are expressed on macrophages [290]. It was shown that soluble forms of HLA-A, -B,-C, and -G molecules were able to trigger apoptosis in CD8+ T lymphocytes and in CD8+ NK cells by

ligating to the CD8 receptor, which lead to the up-regulation of Fas ligand (FasL) and consequently Fas-mediated apoptosis [291]. Similarly, HLA-E binds to the inhibitory CD94/NKG2A receptor, which impairs IL2 receptor-dependent proliferation of tumor-infiltrating T cells [294]. HLA-F positivity in breast cancer was associated with increased tumor size and poor clinical outcomes [295].

1.4.5.2. Angiogenesis and lymphangiogenesis. In the beginning tumor cells usually do not have vascular and lymphatic vessels and they grow under hypoxia. When a tumor reaches a certain size "angiogenic switch" occurs, which results in the formation of new blood vessels and lymph nodes [279,296]. During tumor angiogenesis, endothelial cells release cytokine angiopoietin-2 (ANG-2) and attract new subsets of TAMs known as TIE2-expressing monocytes (TEMs). TEMs express chemokine receptor CXCR4 and can be recruited to tumors by chemokine CXCL12 as well. TEMs express a high level of pro-angiogenic factors, including MMP9, VEGF-A, COX-2, and Wnt5a, and are already programmed to induce angiogenesis [274,297]. Moreover, ANG-2 stimulates M2 like phenotype in TEMs by increasing IL-10 and mannose receptor expression and diminishing TNF-α and IL-12 expression [280]. TAMs promote lymphangiogenesis by secreting prolymphangiogenic factors which can either induce proliferation of already existing lymphatic endothelial cells or cause trans-differentiation of macrophages into lymphatic endothelial vessels [298,299]. Prolymphangiogenic factors, including VEGFR-3 and its ligands, VEGF-C and VEFG-D are abundantly expressed in TAMs [297]. Phosphorylation of VEGFR-3 activates PI3K/AKT and PKC/ ERK1/2 signaling pathways leading to the proliferation of lymphatic endothelial cells [300]. TAMs expressing a marker of lymphatic vessels LYVE-1 (lymphatic vessel endothelial hyaluronan receptor 1) can transdifferentiate and integrate into lymphatic vessels, however, the exact molecular mechanism of this process remains elusive [301].

Overall, TAMs play a crucial role from tumor inception to its invasion and metastasis. The main protumoral functions of TAMs arise from their ability to secrete a variety of soluble factors and their plasticity to acquire different functional phenotypes.

1.4.5.3. Resistance to cancer treatments.

TAMs can promote treatment resistance and limit the efficacy of cytoreductive therapies, such as chemotherapy and radiotherapy [302]. Chemoresistance to cisplatin and carboplatin is promoted by TAMs that release IL-6 via activation of the STAT3 signaling pathway. Released

IL-6 triggers cancer cells to produce more PGE2 and IL-6 that promote tumor cell growth and skew macrophages toward M2-like phenotype [303]. While paclitaxel (Taxol) chemotherapy causes macrophages to overexpress cysteine cathepsin proteases, which protect tumor cells from apoptosis and promote metastasis in breast cancer [304]. Radiation therapy combined with TAMs depletion and immune checkpoint blockades improved tumor suppression [305,306], suggesting that TAMs also promote resistance to radiation therapy. M1 macrophages are more sensitive to IR, comparing M2 macrophages [307], thus radiation therapy affects the ratio of M2 macrophages. Radiotherapy also increases the production of IL-6, IL-8, and MCP-1 and infiltration of myeloid cells [308]. One of the mechanisms of radioresistance involves the high expression of SIRPα on TAMs surface, as the depletion of SIRPα on intratumoral macrophages improved efficacy of radiotherapy in treatment-resistant colorectal and pancreatic tumors [309].

Conclusively, TAMs sustain pro-tumoral functions associated with worse prognosis and poor clinical outcome leading them in the last decades to be a highly attractive target for anti-tumor strategies.

1.4.5. TAMs as a therapeutic target in cancer treatment

Considering the crucial roles of TAMs in tumor progression, inhibition of anti-tumor immune responses and contribution to the resistance to anti-cancer treatments, targeting TAMs raises hope for successful cancer therapies and long-term disease control [310,311]. As depicted in Figure 11, current therapeutic strategies to target TAMs mainly include reprogramming of macrophages toward an anti-tumoral phenotype, depleting, and limiting monocyte recruitment [312]. In this section, we summarize current knowledge available on TAMs-targeting therapeutic strategies.

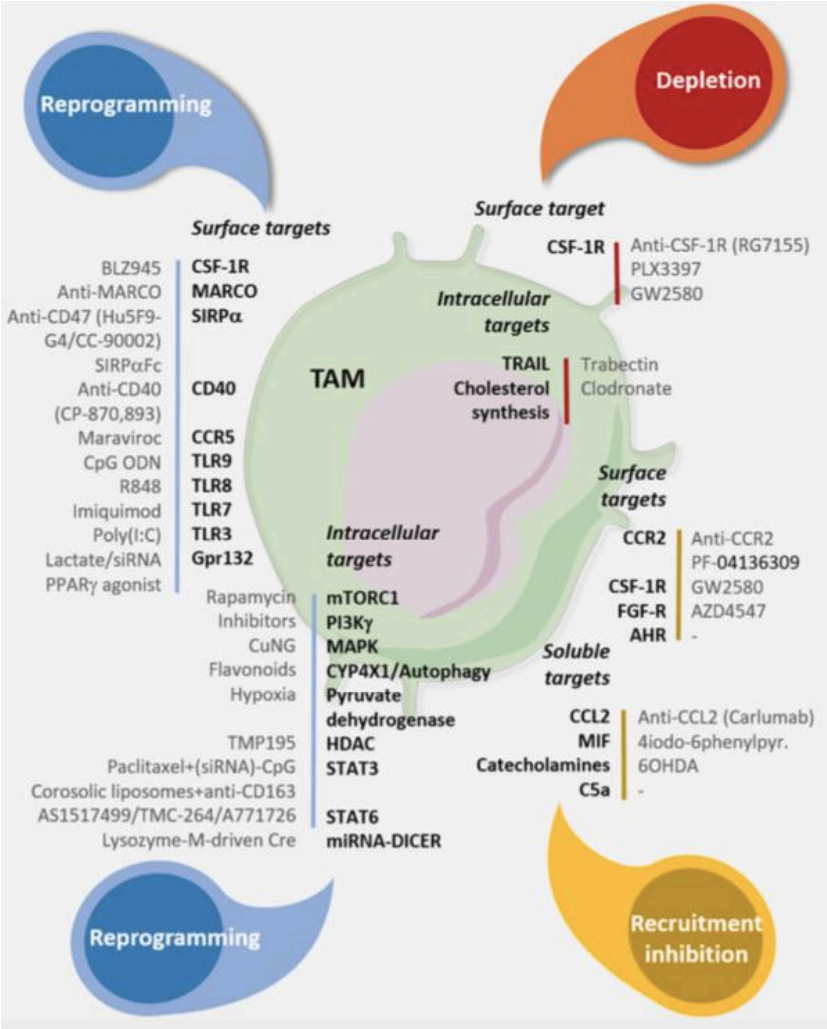

Figure 11. Therapeutic strategies targeting pro-inflammatory reprogramming, depletion and recruitment inhibition of TAMs.

Summary of antibodies and small molecules against the surface and intracellular targets that have been designed for TAMs reprogramming, recruitment, and depletion. Adapted from *Laplagne et al. (2020)*[312].

1.4.5.1. Strategies of reprogramming and re-education of TAMs. Several approaches to target TAM receptors have been shown to successfully reprogram pro-tumoral macrophages into anti-tumoral macrophages [312]. For instance Toll-like receptors (TLRs) are highly expressed in TAMs and their activation can reprogram macrophages toward the pro-inflammatory M1 phenotype [312,313]. TLR3 recognizes dsRNA, TLR7 and TLR8 bind to ssRNA, and TLR9 senses dsDNA [314,315]. Two TLR3 agonists made of synthetic dsRNA analogs, polyI: CLC (also known as Hiltonol™) and polyI: C12U (also known as Ampligen™) are currently involved in eight different clinical trials at different phases in individuals with metastatic prostate cancer, breast cancer, melanoma, mesothelioma, and colorectal cancer [316]. There are six ongoing clinical studies for different TLR7 agonists, two for TLR8 and two other studies that involve drugs

targeting both of those receptors [317]. So far, only TLR7 agonist Imiquimod, best known as Aldara or R-837, has been approved by FDA for treatment of basal cell carcinoma and genital warts [318,319].

1.4.5.2. Strategies to deplete TAMs. Strong pieces of evidence suggest that targeting the CSF-1/CSF-1R axis could significantly reduce TAMs recruitment to tumors and enhance $CD8^+/CD4^+$ T-cell immune responses [320,321]. Currently, numbers of CSF-1/CSF-1R inhibiting molecules including ARRY-382, PLX7486, BLZ945, and JNJ-40346527 and monoclonal antibodies such as emactuzumab, AMG820, IMC-CS4 (also referred to as LY3022855), cabiralizumab, MCS110, and PD-0360324 are under clinical development and testing [320,322]. Among CSF-1R-specific inhibitors, only pexidartinib (also known as PLX3397) has been approved by FDA for the treatment of c-KIT-mutated melanoma, prostate cancer, glioblastoma, classical Hodgkin lymphoma, neurofibroma, sarcoma, and leukemia [322].

Another way to deplete TAMs is to use bisphosphonates (BPs), which are anti-resorptive agents that are subdivided into non nitrogen-containing and nitrogen-containing BPs [310,323]. Once internalized in cells BPs induce cellular apoptosis through inhibiting farnesyl diphosphonate synthase, a key enzyme involved in cholesterol biosynthesis and post-transitional protein prenylation [312]. BPs can also inhibit MMP-9, VEGF, and PDGF production [320,324]. Currently, there are two nitrogen-containing BPs, Pamidronate and Zoledronate, that have been initially used for the treatment of osteoporosis and then approved for management of multiple myeloma and bone metastasis from solid tumors, such as breast cancer [321,325]. While clodronate, a non-nitrogen BP, has been widely used for macrophage depletion in pre-clinical studies, however, its high toxicity toward tissue-resident macrophages limits clodronate translational to clinics [310,313].

Macrophage depletion may also have toxic effects. For instance, frequently reported adverse effects after treatment with CSF1R inhibitors to include elevated liver enzymes, pneumonia, periorbital oedema, lupus erythematosus, erythema, dermohypodermitis, asthenia, pruritus, rash, nausea/vomiting, headache, dry skin, increased lacrimation, and decreased appetite [326–328]. Long-lasting CSFR1 depletion can lead to an acquired resistance and tumor recurrence as well [328]. Using genetic mouse models of glioblastoma, it was shown that the TME promotes resistance to CSF-1R by elevating the levels of macrophage-derived insulin-like growth factor–1 (IGF-1) and tumor cell IGF-1 receptor (IGF-1R), which activate the PI3K signaling pathway. Therefore, the combination of IGF-1R or PI3K blockade with CSF-1R inhibitors improved the

overall survival rate [329]. CSF-1R depletion also activates the expression of HDAC2 in CAF, increasing the accumulation of tumor-promoting polymorphonuclear myeloid-derived suppressor cells that neutralize the anti-tumor effect of CSF1 receptor blockade [330].

1.4.5.3. Strategies to inhibit the recruitment of TAMs. Chemokine CCL2 facilitates TAMs colonization in TME by recruiting $CCR2^+$ inflammatory monocytes from the bone marrow. Inhibition of CCL2/CCR2 signaling has shown positive results in various experimental cancer models and clinical trials [313,320]. Depleting CCL2 by monoclonal antibody Carlumab in combination with chemotherapy was evaluated in phase Ib clinical study in patients with advanced solid tumors. This combination, however, did not yield a steady depletion of CCL2 and was not recommended for further clinical evaluations [331]. In contrast, CCR2 inhibitor PF-04136309 in combination with nab-paclitaxel and gemcitabine was evaluated in phase Ib clinical trial in metastatic pancreatic ductal adenocarcinoma patients and showed a significant decrease of $CD14^+CCR2^+$ circulating monocytes in the serum [332]. Another dual CCR2 and CCR5 inhibitor BMS-813160 in combination with chemotherapy and immunotherapy are currently evaluated in phase Ib/II study in patients with pancreatic or colorectal cancer [310,311].

1.4.5.4. Strategies of targeting immune checkpoints of TAMs. Furthermore, inhibiting the macrophage SIRPα/CD47 signaling axis has been proven to be successful in several preclinical studies and clinical trials [312,333]. SIRPα controls phagocytosis of cancer cells by binding to CD47 receptor that regulates cell migration and survival. CD47 is overexpressed on the surface of many tumors and it blocks cancer cell removal by transducing "don't eat me signal" [320]. Currently, in several clinical trials, CD47/SIRPα axis is targeted by a variety of methods including humanized anti-CD47 antibodies, such as Hu5F9-G4, CC-90002, and SRF231, and recombinant SIRPα proteins, like ALX148, TTI-621, and TTI-622 [313,320]. Monotherapy with anti-CD47 showed little efficacy in various cancer types. However, substantially higher efficacy on tumor regression was observed in combination with other existing therapies targeting PD-1/PD-L1 immune checkpoint blockers or CD20 surface marker of non-Hodgkin lymphoma B-cells using the therapeutic anti-CD20 antibodies (Rituximab) [313,333,334].

Chapter 2: Nanomedicine, Ionizing Radiation, and Immune Response

2.1. A brief introduction to nanomedicine

The term "nano" takes its origin from the Greek word "nanos" which can be translated as "dwarf" [335]. While nanoparticles (NPs) are defined as extremely small substances with a size in one or more dimensions in the range of 1 to 100 nm [336]. NPs can be manufactured in different sizes and morphologies, including spheres, cages, wires, rods, cubes, *etc*. [337]. Modifying nanoparticle size, shape, and the surface can give them unique physical and chemical properties that can be used to achieve desired behaviors *in vivo*, such as biopersistence, better pharmacokinetics, and targeting specific cell mechanisms [336,337]. Nanomedicine is a field of advanced medicine that uses nano-sized particles for the diagnosis, prevention, and treatment of various diseases [338].

2.1.1. Types of nanoparticles

NPs are complex molecules and can be composed of two or three layers: the surface area, the shell, and the core [339]. The surface area of NPs can be functionalized with metal ions (such as sodium) small molecules (such as citrate and thiopropanoic acid) surfactants (such as sodium dodecylsulfate (SDS)), and polymers (such as polyethylene glycol (PEG)) [340]. NPs with charged surfaces are easily dispersed in aqueous media [341]. The shell area is made of chemically different material from the core material and can be virtually composed of any compound [340]. For example, magnetic particles can be synthesized by iron oxide core and covered by silica shell, which protects the core from oxidation [342]. The core layer is a major part of NPs and usually, NPs are called by core material because their key properties are often related to the exceptional characteristics of the core composition [339]. NPs can be divided into various categories based on their shape, size, composition, and properties [339]. Here, we discuss the most well-known classes of NPs that are used in biomedical researches, such as the polymeric, lipid-based, and inorganic NPs.

2.1.1.1. Polymeric nanoparticles. Polymeric NPs can be assembled spontaneously into core/shell micelle from two copolymers of different hydrophobicity in an aqueous solution or synthesized from monomers [341]. Different production methods, such as solvent evaporation and nanoprecipitation, can be used to assembly polymeric NPs into nanocapsules and

nanospheres [339,343]. These NPs designs provide a stable environment for loading and delivering various cargos, including small drug molecules, proteins, and nucleic acids [343]. Another important advantage of polymeric NPs includes the controlled and slow release of the drug at specific target sites. For instance, delivering a drug to the eye entails has many challenges because of the anatomy and physiology of the organ and requires special delivery systems. Several types of polymeric micelles have been developed for that purpose, including poly(lactic-co-glycolic acid) (PLGA) formulated with polyvinyl alcohol (PVA) to deliver drugs like bevacizumab, dexamethasone, and fenofibrate [344]. Moreover, polymeric NPs loaded with anti-cancer drugs are currently tested in the clinics and they are especially proven efficient for delivering chemotherapy drugs. For example, the poly(ethylene glycol)-b-poly(glutamic acid) (PEG-PGlu) nanocarrier incorporated with drug cisplatin in combination gemcitabine has enrolled into phase III clinical trials in patients with solid tumors [345].

Another type of synthetic polymers is dendrimers that have 3D architecture resembling a branched tree connected to one point [346,347]. Dendrimers can be synthesized from a variety of elements, including amino acids, sugars, and nucleotides and by using two main synthesis methods, divergent and convergent growth [341,346]. Due to their outstanding biomedical characteristics, dendrimers can be used as sensors, drug, and gene delivery vehicles [341]. Currently, the pharmaceutical company Starpharma is conducting several clinical trials with Dendrimer Enhanced Product® (DEP®), which is a poly-l-lysine dendrimer formulated with a drug attached to its surface through by PEG linker. The toxicity DEP® docetaxel formulation is currently being tested under phase II clinical studies. For the other two formulations, DEP® cabazitaxel and DEP® irinotecan, phase II clinical trials are now at the stage of recruitment [348].

2.1.1.2. Lipid-based nanoparticles. Lipid-based NPs include liposomes, ethosomes, solid lipid NPs (SLN), and nanostructured lipid carriers (NLC) [349,350]. Unique advantages of lipid-based NPs are their high temporal and thermal stability, low toxicity, and high loading capacity [351]. Moreover, their large-scale industrial production is relatively low cost as they can be manufactured from natural sources, such as bola-amphiphiles, phospholipids, sphingolipids, cholesterol, and cholesteryl hemisuccinate [351,352]. Among lipid-based NPs, liposomes are the most studied and used nanocarriers in drug delivery. Liposomes are made of amphipathic phospholipids which spontaneously form a bilayer spherical vehicle with an internal aqueous cavity [353]. This structure can encapsulate hydrophobic drugs in the phospholipid bilayer and hydrophilic drugs in the aqueous region [350]. Moreover, the liposome's surface can be

functionalized with specific antibodies that only target the cells of interest. They also can be synthesized with stimulus-sensitive design and release drugs at a certain temperature, pH, and magnetic field [351]. Currently, several liposomes are used in the clinic to deliver anti-cancer, anti-fungal, anti-inflammatory drugs, viral vaccines, and therapeutic genes. For example, a liposomal product DaunoXome® is used to deliver chemotherapy medication daunorubicin in patients with advanced HIV-associated Kaposi's sarcoma. Also, liposomal vaccines Epaxal® and Inflexal® V are currently used to deliver inactivated hepatitis A virus (strain RGSB) and influenza virus (strains A and B), respectively [353].

2.1.1.3. Inorganic nanoparticles. Inorganic NPs are very stable and resistant to enzymatic degradation. They also can be synthesized in ultrasmall sizes (<20 nm) that allow them renal or fecal elimination from the body. There are several classes of inorganic NPs, including semiconductors, plasmonic, magnetic, and upconversion nanocarriers [336]. They all share a similar core/shell structure. The core usually contains metals, such as iron oxide and gold, or fluorescence dyes, while the shell region can be made from metals or organic polymers [354].

Among semiconductors, quantum dots (QDs), also known as inorganic nanocrystals, have gained a lot of interest in the field of nano-theranostics [355]. QDs have unique photo-electric properties which allow them to have broad excitation spectra, narrow emission spectra, tunable emission peaks, greater quantum yields, and longer photostability [356]. Popular examples of plasmonic NPs are nanostructures with a core made of noble metals, such as gold and silver [336]. Free electrons on the surface of metallic NPs can collectively oscillate when exposed to the photonic energy of the same resonant frequency [357]. This phenomenon of collective oscillation is known as localized surface plasmon resonance (LSPR) and it is widely exploited in the development of high sensitivity bioassays and biosensors [358,359]. Magnetic nanocarriers have other unique properties that are used in developing bioseparation and biosensing devices, as well as magnetic field-controlled drug and gene delivery [360]. Finally, upconversion NPs are designed as a guest-host system, where guests are trivalent lanthanide ions (such as Ho^{3+}, Yb^{3+}, Tm^{3+}, and Gd^{3+}) and hosts are dielectric lattice (such as $NaYF_4$) [336]. Upconversion is an optical process that converts low-energy input photons into high-energy output photons and this intense emission can be used in *in vitro* and *in vivo* imaging, as well as in cancer therapies [361].

Overall, NPs can be constructed from various materials, in different sizes and shapes and can be exploited for diverse biomedical purposes, including diagnosis and therapy of a variety of diseases.

2.1.2. Medical application of inorganic nanoparticles

As stated earlier, inorganic NPs possess unique optical, magnetic, electronic, and catalytic properties that give them several key advantages as compared with their organic and polymeric counterparts [362]. Over the last few decades, a wide range of inorganic NPs with different composition and functionality have been synthesized and tested in preclinical studies, however, as it is shown in Figure 12, only a few have made its way to clinic [363,364]. In this section, we discuss the application of inorganic NPs as detecting tools, contrast agents as well as therapeutic vehicles in clinical practices.

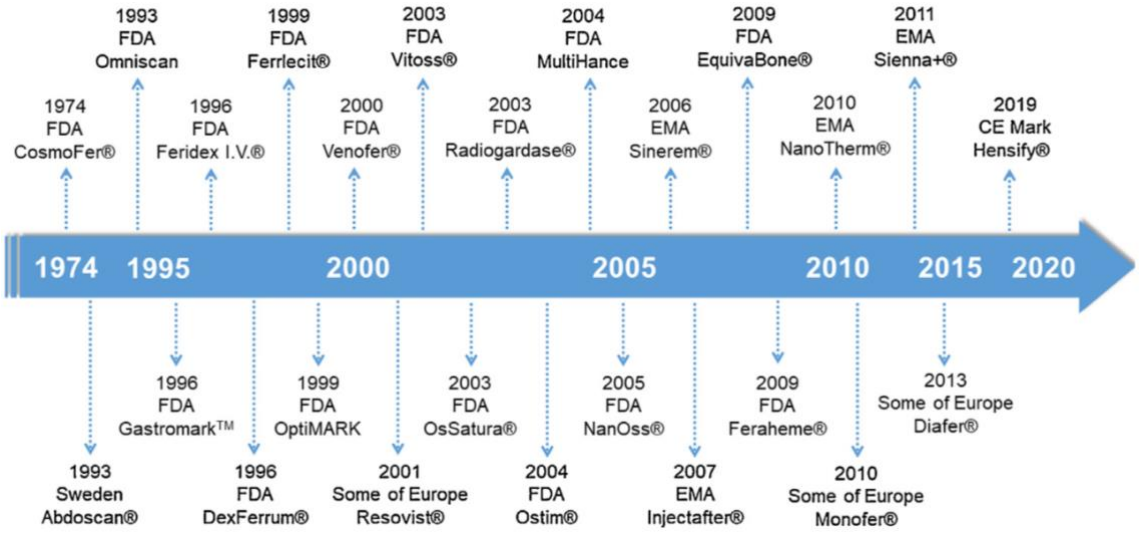

Figure 12.Timeline of marketed inorganic nanomedicines (1974-2020).

Up to this day twenty-five, inorganic nanocarriers have been approved for medical uses by several health organizations. Adapted from *Huang et al. (2020)* [364].

2.1.2.1. Therapeutic agents. Several inorganic materials have been intensively studied as therapeutic agents for anticancer therapies, iron-replacement therapies, and antibacterial agents [364]. The majority of current clinical and/or preclinical studies for antitumor therapies are based on inorganic NPs made of iron, gold, and hafnium metals [363,364]. Iron-based nanoparticle NanoTherm® commercialized by Magforce Nanotech company is the first nanotherapeutic approved by the European Medicines Agency (EMA) in 2010 for treatment of glioblastoma [363,365]. NanoTherm® is made of iron oxide (Fe_3O_4) core and coated with aminosilane. After intratumoral injection, an externally applied magnetic field induces rapid rotation of the NPs causing the increase of the temperature within the tumor cells. Consequently, heat induces irreversible damage to cancer cells [363,366]. Another iron-based nanoparticle Magnablate, which

operates similarly to NanoTherm®, was tested in phase I clinical trial in patients with prostate cancer in 2015, however, the results of this study have not yet been published [367].

Among gold NPs, CYT-6091, a type of gold nanoshells functionalized with thiolated PEG and human recombinant TNFα, was developed for targeting solid tumors [364,367]. CYT-6091, also known as Aurimune, was successfully tested in phase I clinical trial on patients with advanced or refractory solid tumor malignancies [367]. Currently, CYT-6091 is evaluated in phase II clinical trials for non-small lung cancer (NSLC) [363].

Another inorganic nanoparticle in clinical development is Hensify®/NBTXR3, which has been approved in Europe since April 2019 for the treatment of locally advanced sarcoma [364]. NBTXR3 is 50 nm size nanocarrier with the core made of hafnium oxide (HfO_2) NPs and coated with the negatively charged surface [368]. NBTXR3 is injected intratumorally and activated by irradiation. Activated HfO_2 NPs produce high-energy electrons, which then fuel the production of free radicals and the generation of ROS. As a result, tumor cells that internalized HfO_2 NPs experience stress and severe DNA damage, which eventually leads to the destruction of the cells (Bayda et al. 2017; Weissig and Guzman-Villanueva 2015).

2.1.2.2. Diagnostic imaging. Inorganic NPs-based probes are particularly used in magnetic resonance imaging (MRI) and optical imaging (OI) [364]. MRI is a powerful non-invasive imaging technique based on the nuclear magnetic resonance (NMR) theory [369,370]. Under the applied magnetic field, hydrogen atoms align their magnetic moments along the longitudinal axis. After removal of the external magnetic field, the time it takes for hydrogen atoms to reach their original equilibrium state is called a relaxation time and it is affected by the presence of nearby magnetic materials [369,371]. Contrast agents that enhance longitudinal proton relaxation are called T_1 contrast agents and agents that affect transverse proton relaxation are known as T_2 contrast agents [371]. The most selected T_1 contrast agents are Gd-based nanoformulations [372,373]. Currently, several Gd-based NPs have been approved for use in humans by the EMA and/or FDA, including gadoxetate disodium, gadodiamide, gadofosveset trisodium, *etc.* [371,372]. Due to their supermagnetic properties, iron oxide NPs have been extensively used as T_2 contrast agents for more than two decades [364,371]. Unfortunately, most iron-based contrast agents were withdrawn from the market because of their relatively low sensitivity as compared to Gd-based products [374]. Today, the only commercialized superparamagnetic iron oxide NPs-based MRI contrast agent is Lumirem/GastroMARK, which is administered orally for imaging the gastrointestinal tract [364,372].

Attributing to the favorable optical characteristics carbon- and semiconductor-based inorganic NPs have been continuously employed for optical imaging in clinical trials [364]. Carbon nanotubes have been widely used as a lymphatic tracer in harvesting lymph nodes and currently, they are tested in eight different clinical trials [364,375]. Carbon nanotubes are unable to penetrate blood vessels. However, due to the large gaps in the endothelial lining at the lymph nodes region, carbon nanotubes can enter lymphatic vessels and lymphatic capillaries and be internalized by macrophages [364,376]. As a result, lymph nodes, but not parathyroid part, become stained in black and remain colored for at least six months, which helps surgeons to identify the regions for dissection [364,377,378]. Among semiconductor quantum dots, CdS/ZnS core-shell quantum dots coated with a drug veldoreotide and formulated as a topical cream is currently tested in phase I clinical trial in patients with breast and skin cancers [364,379].

2.1.2.3. Theranostic agents. Theranostic NPs are a type of nanomedicines designed to combine diagnostic and therapeutic capabilities into a single platform [380]. The majority of theranostic NPs are synthesized for passive targeting and activated by external stimuli, such as light, magnetic field, ultrasound, radiofrequency, and radiation [381]. Currently, several inorganic NPs are being tested in clinical trials, including iron oxide-based NPs Ferumoxytol, Ferumoxtran-10, and SENTINAC-01 [381,382]. Apart from them, Gd-based contrast agents previously approved for MRI imaging are currently widely investigated as theranostic agents in different clinical trials [364]. Gd-based contrast agents available for clinical use include Omniscan, Magnevist, MultiHance, Gadovist, Eovist, ProHance, and Dotarem [383]. However, only two radiation-enhancing NPs, hafnium oxide NPs (NBTXR3) and gadolinium-based NPs (AGuIX), are currently under investigation in clinical trials [384].

2.2. Gadolinium based nanoparticles (AGuIX)

The gadolinium (Gd) complexes have unique magnetic properties that have been extensively utilized in the clinic for MRI contrast imaging and radiosensitization [385,386] . The paramagnetic properties of the trivalent Gd^{+3} ion come from its seven unpaired electrons that can organize their spin magnetic moments in parallel [387]. Gadolinium-based paramagnetic contrast agents (also referred to as T1 or positive contrast agents) enhance the contrast between different soft tissues and provide anatomic and structural information [386,388]. Moreover, gadolinium-based NPs have a high Z-atomic number and are proven to be effective radiosensitizing agents, as after interaction with radiation energy these NPs can undergo photoelectric effect and generate low energy Auger electrons [389,390] . In 2013, Mignot et al. synthesized a new type of ultrasmall

and multifunctional gadolinium-based silica NPs, AGuIX, which since then has been extensively studied in various pre-clinical and clinical studies [391] . Here, we provide a concise summary of AGuIX synthesis and characterization, as well as its use in pre-clinical and clinical studies.

2.2.1. Synthesis and characterization of AGuIX

NPs must meet three main requirements for clinical applications as theranostic agents: 1) long circulation in the blood to ensure accumulation in the tumor region, 2) small size distribution to facilitates rapid renal elimination, and 3) simultaneously display therapeutic and imaging properties [392]. However, achieving the development of NPs meeting all previously mentioned requirements remains a great challenge and requires constant optimization of synthesis methods. That is why an original top-down method was developed to synthesize ultrasmall AGuIX NPs [391].

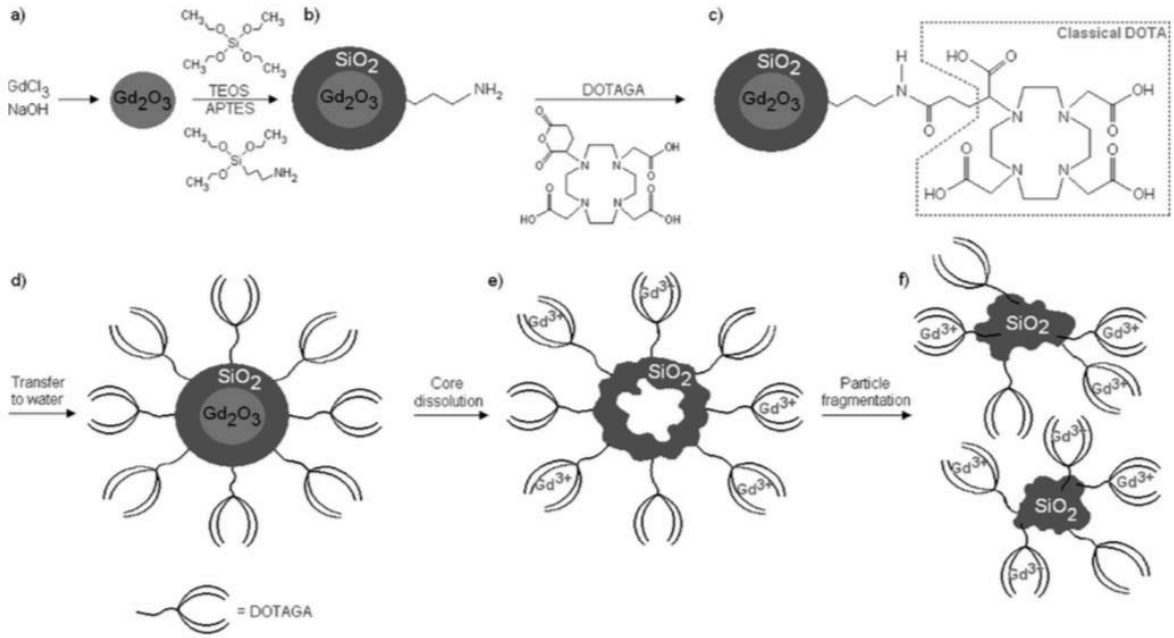

Figure 13.The top-down synthesis method of AGuIX NPs.

The synthesis of AGuIX NPs can be subdivided into six main steps: a) synthesis of a gadolinium oxide Gd_2O_3 core, b) encapsulation in a polysiloxane shell, c) grafting with DOTAGA ligands, d) dissolving in water, e) dissolution of the gadolinium oxide Gd_2O_3 core, and f) polysiloxane fragmentation. Adapted from *Mignot et al. (2013)* [391].

As shown in Figure 13, the top-down synthesis method involves six main steps [391]. First, a colloidal gadolinium oxide Gd_2O_3 core is precipitated from rare-earth gadolinium chloride in a presence of high boiling alcohol, diethylene glycol (DEG) [393]. In the second step, the

gadolinium oxide core is encapsulated by polysiloxane shell in a controlled manner via hydrolysis-condensation of a mixture of aminopropyl triethoxysilane (APTES) and tetraethyl orthosilicate [391,394]. Because of the presence of amine functions of APTES in the polysiloxane network, during the next synthesis step DOTAGA (1,4,7,10-tetra- azacyclododecane-1-glutaric anhydride- 4,7,10-triacetic acid) molecule can be grafted to the core-shell particles via an amide linkage [391,395]. Finally, the nano formulation is transferred to the water where the gadolinium oxide core dissociates and releases Gd^{3+} ions that are captured and efficiently chelated to the DOTAGA molecules on the surface. At the same time, the polysiloxane shell collapse on itself and split into several fragments, forming a polysiloxane core with both DOTAGA and DOTAGA–Gd^{3+} chelates. To enrich non-chelated DOTAGA molecules with Gd3+ ions, before purification AGuIX NPs were incubated with excess Gd^{3+} ions for additional time, which resulted in approximately 100% complexed ligands [391].

Deep characterization of a synthesized AGuIX nanoparticle revealed a global chemical formula Gd7APTES16TEOS10.5DOTAGA10.5 with an average molecular mass of 8500 kDa and size distribution below 5 nm. The relaxivity measurements of AGuIX NPs showed that the longitudinal relaxivity r1 is 11.9 s^{-1} mm^{-1} per Gd molecule at 60 MHz [391]. Finally, the biodegradation of AGuIX NPs was followed by measuring the hydrodynamic radius with dynamic light scattering technique and demonstrated that NPs have a half-life of about 19.6 minutes at physiological pH [394].

2.2.2. *In vitro* studies with AGuIX

Most *in vitro* studies involving AGuIX NPs were aimed to evaluate cellular internalization, toxicity, and the radiosensitization capacity in different cellular models. In this section, we describe the most relevant studies investigating cellular uptake and toxicity, subcellular localization, and radiosensitization of AGuIX NPs.

2.2.2.1. Cellular uptake and toxicity. The cellular internalization of AGuIX NPs was studied on epithelial and immune cancer cell lines, as well as on murine and on human primary cell cultures by applying various techniques [396,397]. TEM and confocal images revealed that AGuIX NPs are internalized via macropinocytosis and passive diffusion [397]. A Luchette et al. quantified AGuIX NPs uptake in HeLa cells by using inductively coupled plasma mass spectroscopy (ICP-MS) technique and identified that after one-hour incubation with 0.5 mM nanoparticle suspension, the intracellular concentration of gadolinium was 0.059 mM [398]. Similar results

were observed in Panc1 pancreatic cancer cells, where AGuIX uptake was measured by MRI and crosschecked by ICP-MS [390]. Štefančíková et al. investigated AGuIX uptake in U87 glioblastoma cells by using Synchrotron Radiation Deep UV (SR-DUV) microscopy and observed complete internalization of the NPs and accumulation in the cytoplasm of the targeted cells [399]. Similar findings were made by Kotb et al., where they used AGuIX conjugated to FITC and confocal microscopy to study the NPs uptake in mouse B16F10 skin melanoma cells and observed high accumulation of the NPs in the cytoplasm of targeted cells [400].

Several other studies evaluated simultaneously cellular uptake and viability after AGuIX treatment. For instance, Miladi et al. treated SQ20B squamous carcinoma cells with AGuIX conjugated to Cy5.5 fluorescence dye to study the cellular internalization by confocal microscopy and observed accumulation in the cytoplasm as well. They also used cell counting kit-8 (CCK8) proliferation assay to evaluate cellular viability and observed no cytotoxicity after 72 h of treatment with 0.6 mM AGuIX NPs [395]. The immunotoxicity effect was studied on murine primary dendritic cells and Jurkat human T lymphocyte cell line [401,402]. Briefly, dendritic cells extracted from the bone marrow of C57BL/6 mice were incubated with different concentration of AGuIX NPs and apoptosis was accessed by 7-amino-actinomycin D (7AAD) staining and flow cytometry. The consequent analysis demonstrated that AGuIX NPs induce no significant apoptosis at low concentrations with AGuIX NPs and LD50 (quantity required to kill 50% of cells) is close to 5 mM after 24 h of incubation [391]. Apoptosis of Jurkat human T lymphocytes treated with RITC-labeled AGuIX was accessed by FITC–annexin V and propidium iodide (PI) staining and demonstrated no cellular toxicity after NPs exposure [402].

2.2.2.2. Subcellular distribution. Transmission electron microscopy (TEM) images from several independent studies demonstrated that AGuIX NPs are actively captured in endosomal vacuoles and accumulated into the cytoplasm of the targeted cells without penetrating the nuclear membrane [397,399,403] . These results were confirmed with fluorescence-labeled AGuIX NPs and confocal microscopy [399,400]. Co-localization studies performed on U87 cells with confocal microscopy revealed that after 20 h of incubation, Cy5.5-labeled AGuIX NPs are predominantly co-localized within lysosomes (Figure 14 A, B, and C), but not in the mitochondrial region (Figure 14 D, E, and F). Interestingly, no significant mitochondrial co-localization was observed after 37 h of incubation as well [399]. Similar observations were made on human SQ20B larynx carcinoma cells treated with Cy5.5-labeled AGuIX for 24 h [404].

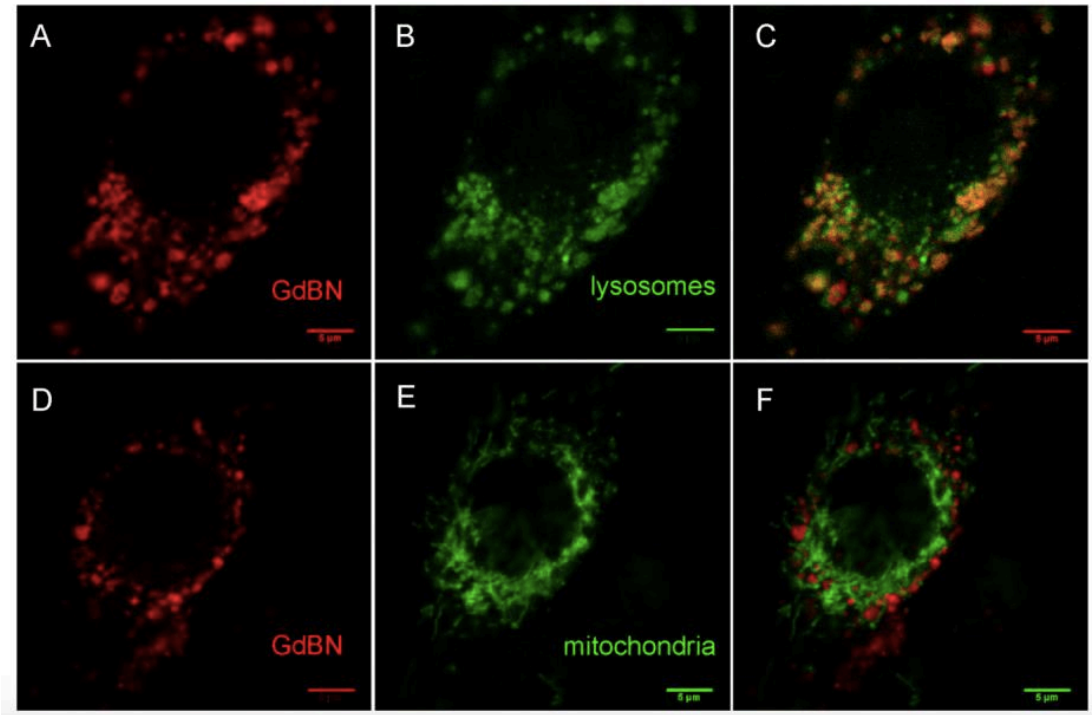

Figure 14. The representative images highlighting the subcellular localization of Cy5.5-labeled AGuIX NPs within U87 cells.

U87 cells were pretreated with Lysotracker-green (Figure 14 A, B, and C) or Mitotracker-green (Figure 14 D, E, F) for 45 min before the incubation with 1 mM Cy5.5-labeled AGuIX NPs for 1 h. Adapted from *Štefančíková et al. (2014)* [399].

2.2.2.3. Radiosensitization. *In vitro* studies the radiosensitization capacity of NPs is assessed by calculating the sensitizing enhancement ratio (SER), which is a ratio of the survival fraction (SF) of the control group (irradiation only) over the treated group (cells are treated with NPs prior the irradiation). SER values between 1.1 and 2.5 are considered significant [385]. Another important coefficient is a dose enhancement factor (DEF), which represents a ratio of the dose deposited in the presence of NPs divided by the dose deposited without NPs [405].

Several experiments have demonstrated that the radiosensitization capacity of AGuIX NPs depends on the concentration of gadolinium and radiation energy applied. For instance, Detappe et al. studied the radiosensitization effect of low-energy (220 kVp) beam, and two high energy radiation methods used in the clinic, a standard 6 MV beam (STD) and a flattening filter-free 6 MV beam (FFF) on radioresistant Panc 1 pancreatic cells incubated with 0.5 mM AGuIX for 1 h. The results demonstrated that high energy FFF beam significantly improves cell killing (SER at 4 Gy was 1.20 ± 0.04 and DEF at 20 % survival was 1.30 ± 0.05), comparing to the STD beam (SER at 4 Gy was 1.12 ± 0.04 and DEF at 20 % survival was 1.23 ± 0.03) [390]. In another study involving SQ20B head and neck carcinoma cells incubated with

0.4 mM or 0.6 mM AGuIX for 1 h followed by 250 kV photon irradiation, showed that increasing the dose of NPs improves the dose deposition (SER for 0.4mM was 1.22 and for 0.6mM was 2.14) [385,406].

To evaluate the impact of different irradiation sources on the radiosensitization capacity of AGuIX NPs, irradiation with various ion beams was used. Porcel et al. used Chinese hamster ovary (CHO) cells to test two ion sources, He^{2+} and C^{6+}. The CHO cells were incubated with 0.1 mM NPs for 1 h before irradiation and survival fractions were calculated. Consequent analysis showed that irradiating with different ion sources lead to the same order of SER (SER for He^{2+} ion source was 1.14 and for C^{6+} beam was 1.50) [385,407]. Comparison between 0.3 mM or 0.6 mM treated SQ20B cells irradiated with C6+ beam demonstrated the same dose enhancement effect as with high-energy photon irradiation, but with a higher efficacy [385,408].

Overall, a large variety of *in vitro* experiments have been performed to study AGuIX nanoparticle's internalization, accumulation, and radiosensitization capacity. The uptake studies demonstrate efficient cellular internalization and cytoplasmic accumulation. AGuIX NPs show high radiosensitization capacity at low and high concentrations in combination with different radiation doses, with slight deviations in radiation sources.

2.2.3. *In vivo* studies with AGuIX

The successful translation of nanomedicines into clinics depends widely on *in vivo* studies. The designed experiments should define the optimal doses and safe routes of administrations, as well as the mechanism of action and elimination. In this section, we summarize preclinical studies where the biodistribution and safety of AGuIX NPs were assessed.

2.2.3.1. Biodistribution in tumor free animals. In preliminary *in vivo* studies, the biodistribution of AGuIX NPs was extensively studied in healthy animals of different species (rodents and nonhuman primates) by using different routes of administrations, such as intravenous, intratumoral, and via airways [385,392]. Long-term clearance of AGuIX NPs was studied in mice model by using intravenous injection of a therapeutic dose of 8 μmol of gadolinium per animal. The renal kinetics and mechanism of elimination were evaluated by using laser-induced breakdown spectroscopy (LIBS) and revealed a rapid AGuIX accumulation in kidneys after 5 min of injection. After 24 h of injection, approximately 10% of a fraction of the injected dose (ID) was still concentrated in kidneys, while 0.2% of the total ID was distributed in other organs. One week post-injection, most of the particles were

eliminated, suggesting an effective clearance from the body via urine [409]. The administration via airways was also studied in healthy mice by using an ultrashort echo time (UTE) MRI imaging. The analysis of the axial slices of the lungs revealed that AGuIX NPs pass through lungs with an accumulation lifetime of 149 ± 51 min. Further analysis demonstrated the elimination via kidneys and bladder and no accumulation was detected in the liver or spleen [385].

To verify further the renal elimination, the AGuIX NPs were conjugated with a radioactive isotope of indium, ^{111}In [385,410]. The labeled NPs were injected intravenously into healthy C57Bl6/J mice and the biodistribution at 3 h and 24 h was monitored in all organs. This study confirmed that after 3 h and 24 h of post-injection AGuIX NPs accumulate in all organs with less than 0.2% and most of the particles are concentrated in the kidney and bladder regions [385]. The detailed distribution studies of ^{111}In -labeled AGuIX NPs from 15 min to 3 h post-injection showed a gradual increase in the bladder and the kidney regions, followed by a simultaneous decrease in the blood [410].

In parallel, the pharmacokinetics of AGuIX NPs was evaluated in nonhuman cynomolgus monkey primates [396]. After intravenous administration of a total of 200 mg/kg of AGuIX NPs to healthy male monkeys, the MRI images acquired during the first minutes demonstrated a rapid distribution of NPs throughout the blood vessels and vital organs, such as the heart, liver, and kidneys. Then, the images at 35 min showed the enhanced signals at kidneys and ureters, validating the rapid renal clearance [396]. The blood half-life of NPs was approximately 2 h. These results confirmed that AGuIX NPs primarily accumulate in the kidneys, liver, and ureters and that there is no significant uptake in other organs [392,396].

2.2.3.2. Biodistribution in tumor-bearing animals. In the contest of tumor-bearing animals, small NPs after the systematic administration primarily concentrate in the tumor region [385,392]. This phenomenon is known as enhanced permeability and retention (EPR) effect and has been widely exploited in pre-clinical studies [411]. Besides excellent MRI contrast agent properties, AGuIX NPs have demonstrated an efficient EPR-mediated tumor targeting in various tumor models [412].

Preclinical studies on brain tumors were performed on three different tumor models: 9L gliosarcoma xenografts bearing rats, U87MG glioblastoma xenografts bearing mice, and B16F10 brain melanoma metastases bearing mice [392,412]. In 9L gliosarcoma-bearing rats,

AGuIX NPs were administered intravenously and followed by MRI after 1, 4, 7, and 24 h of injections. After approximately 7 hours of AGuIX injection at days 14 and 17 of tumor implantation, the tumors were irradiated with 10 Gy by using a 6-MV medical irradiator. The MRI results demonstrated that AGuIX NPs concentrate mainly in the tumor region after the first hours of injection and remain there up to 24 h of post-administration. On day 17 after treatment, the tumor volume in the group treated with AGuIX plus irradiation was reduced by 26% compared to the irradiated group alone. The mean survival times were 26 ± 0.5 days for the control group, 39 ± 2 days for the irradiated group, and 72.9 ± 35.5 days for the AGuIX plus irradiation group [413]. More precise biodistribution experiments were performed on U87MG glioblastoma xenografts bearing mice treated with ^{68}Ga and ^{89}Zr labeled AGuIX NPs and showed similar retention patterns on tumor region and rapid renal elimination [414,415]. The study on B16F10 brain melanoma metastases bearing mice also showed that after intravenous injection, AGuIX NPs accumulate in the tumor region up to 24 h and it was positively correlated with the increased life spans of the animals [400].

In addition, the accumulation and retention of the AGuIX NPs have been studied in animals bearing pancreatic, colorectal, chondrosarcoma, breast, and lung tumors [392,412]. Particularly, the study on immunodeficient mice inoculated with luciferase-modified human NSCLC H358 cells showed that after orotracheal or intravenous administration, the AGuIX NPs accumulate in the tumor region up to 72 h after administration. Moreover, this study compared the efficiency between two routes of administration and demonstrated that for lung cancer the orotracheal administration improves the MRI contrast signal up to twofold with four times less Gd^{3+} [416]. In another study, the AGuIX contrast agent capacity was evaluated in a rat model of hepatic colorectal cancer metastases after intravenous injection. The study showed that AGuIX provides high enhancement properties for MRI-guided detection of malignant focal liver lesions and is efficiently eliminated via renal excretion [417].

2.2.3.3. Biodegradation and toxicity. Animal preliminary toxicology studies have been performed in mice, rats, and monkeys [392,418]. Single intravenous injection of 8 μmol AGuIX in mice showed a slight increase in the serum creatinine concentration after 30 min of injection, however, the serum level returned to physiological normal after 1 h and remained unchanged up to 8 weeks [409]. In the dose-escalation studies, rats were intravenously injected with 250, 500, or 750 mg/kg/day twice at a 1-week interval. The results showed no visible AGuIX-related side effects on vital organs, except on one female rat treated with 750 mg/kg/ day experienced

slight vacuolation after 10 weeks of post-treatment [413]. A similar study was performed on cynomolgus monkeys. The protocol involved two intravenous injections of 150, 300, or 450 mg/kg once a week for two weeks period. The results showed no observable side effects, including vacuolation [396]. Altogether, these results were used to establish the range of 100mg/kg as the safe dose for clinical studies in humans [385].

2.2.4. AGuIX in clinical trials

AGuIX NPs were evaluated in two clinical trials in France, NanoRAD (NCT02820454) and NanoCOL (NCT03308604) [392]. NanoRAD, is a phase I study designed to evaluate the safety and the tolerability of AGuIX NPs in combination with standard whole-brain radiotherapy (WBRT) in patients with multiple brain metastases. In 15 patients the five escalation doses were evaluated, 15, 30, 50, 75, and 100mg/kg [418]. The treatment protocol consists of a single intravenous injection followed by 10 fractionated all brain irradiation (total 30 Gy in 10 sessions of 3 Gy). The first irradiation is delivered after 4 h of AGuIX administration (NCT02820454). The results of NanoRaD study showed administration of AGuIX was safe and feasible, and 14 patients out 15 showed stabilization or decrease in tumor volume [419]. Currently, the phase II clinical study, also known as NanoRAD 2, is under recruitment status. This randomized study aims to recruit 100 patients and evaluate 3 intravenous injections at 100mg/kg in combination with 10 fractionated all brain irradiation (total 30 Gy in 10 sessions of 3 Gy) (NCT03818386). The second clinical trial NanoCOL is a phase Ib clinical trial designed to evaluate the safety and tolerability of AGuIX NPs in combination with radiation, cisplatin, and brachytherapy in patients with locally advanced cervical cancer. The tested escalation doses of AGuIX NPs are 20, 30, and 50 mg/kg that will be administered intravenously at different stages during the treatment [392]. The study involves 18 patients, and the estimated date of completion is May 2021 (NCT03308604).

2.3. Ionizing radiation and cellular response

Radiation is a form of energy that travels as waves or particles [420]. Based on the nature of radiation, it can be classified as ionizing and non-ionizing [421]. Non-ionizing radiation represents electromagnetic radiation with photon energy less than 10 eV, which corresponds to wavelengths longer than 100 nm [422]. Whereas, ionizing radiation is highly energetic and has the capacity of inducing atomic ionization. There are four main sources of ionizing

radiation alpha particles, beta particles, X-rays, and gamma rays, and all of them are successfully utilized for therapeutic purposes, especially in cancer treatments [421,423].

Despite the remarkable progress in cancer treatments, cancer incidences increase every year, and cancer remains the leading cause of death worldwide [424,425]. According to the GLOBOCAN study, which collected data for 36 types of cancer in 185 countries, in 2020, there were 19.3 million new cases of cancer and about 10.0 million reported deaths, with lung cancer remaining the number one cause of cancer-related deaths [424]. Currently, there are various cancer treatment modalities available in clinics, including radiation therapy, surgery, chemotherapy, targeted therapy, immunotherapy, and hormonal therapy [425,426]. Among them, radiation therapy alone or in combination with other treatments is used in approximately 50% of all cancer patients and contributes to 40% of all radiation-treated survivors [425]. Since the discovery of radiation therapy, many technological advances have been made in the field of how radiation treatments are delivered. The most innovative approaches currently used in the clinics include 3D conformal radiotherapy (3DCRT), intensity-modulated radiation therapy (IMRT), image-guided radiotherapy (IGRT), and stereotactic body radiation therapy (SBRT) [425–427].

The success of radiation therapy in cancer treatment can be attributed to the fact that radiation can directly or indirectly damage the DNA inside the tumor cells [425,428]. The direct damage is predominantly caused by high-energy radiation and it causes changes in the molecular structure of the DNA [429,430]. The indirect DNA damage is caused by free radicals, which are generated from ionization or excitation of the water molecules and other organic components of the cell [425,431]. Free radicals, including hydroxyl (HO•) and alkoxy (RO2•) radicals, have a highly reactive unpaired electron in their structure, which can react with DNA molecule and induce structural damage [429,431]. The ultimate result of severe direct and indirect DNA structural changes can lead to cell damage or even cell death [425,429].

2.3.1. DNA damage and DNA damage responses (DDR)

All living cells develop various strategies to modulate and repair DNA damages. These mechanisms rapidly sense the DNA damage and activate the DNA damage response (DDR), which is crucial for activation of the DNA-repair machinery and the cell-cycle checkpoints [432,433]. A wide diversity of DNA lesions can be induced by different external triggers, including ionizing radiation, ROS, oncogenes, and mutagens [433,434]. Ionizing radiation

mostly induces base modifications, interstrand crosslinks, single-strand breaks (SSBs), and double-strand breaks (DSBs) [435]. As shown in Figure 15, depending on the type of DNA lesions, different DNA damage sensors and apical kinases are activated [434]. Particularly two members of the PIKK (phosphatidylinositol-3-kinase-related kinases) family, ATM (ataxia-telangiectasia mutated) and ATR (ATM and Rad3-related) coordinate a broad spectrum of cellular responses during DNA damage, including cell-cycle arrest, apoptosis, and senescence [435–437].

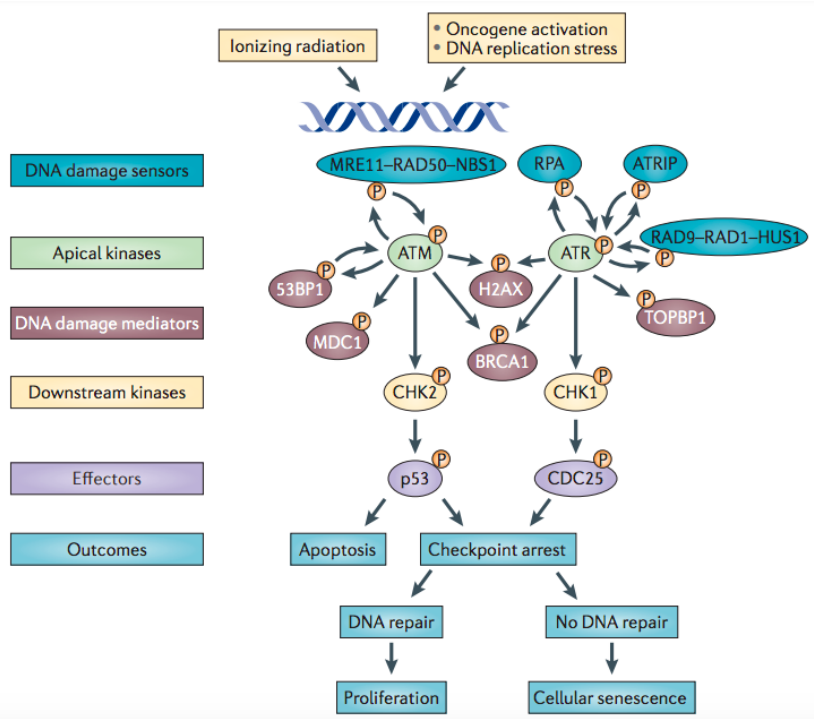

Figure 15. DNA-damage response pathways.

Upon DNA damage, cells activate certain sensors, kinases, and effectors to mediate cellular apoptosis or checkpoint arrest. RPA, replication protein A; ATM, ataxia telangiectasia mutated; ATR, ataxia telangiectasia and Rad3-related; ATRIP, ATR-interacting protein; γ-H2AX, phosphorylation of the Ser-139 residue of the histone variant H2AX; MDC1, mediator of DNA damage checkpoint 1; 53BP1, p53-binding protein 1; CDC25, cell division cycle 25. Adapted from *Sulli, Di Micco, and Di Fagagna (2012)* [434].

2.3.1.1. ATR activation. Among the different types of DNA damages, SSBs are the most observed and they have a tremendous impact on the cell fate [437,438]. The presence of single-stranded DNA (ssDNA) is sensed by replication protein A (RPA), which rapidly coat the ssDNA and recruits two protein complexes, ATRIP (ATR-interacting protein) associated with ATR and the RAD17/RFC2–5 complex [436,437]. After, the RAD17/RFC2–5 protein

loads the RAD9–HUS1–RAD1 (9–1–1) clamp complex, which then recruits and positions TopBP1 protein in the proximity to the ATR-ATRIP complex [436]. The TopBP1 protein has an activation domain (AD) that binds and activates ATR, which then phosphorylates other downstream effectors, including Chk1 (Checkpoint kinase 1) and Claspin [436,439]. Activated Chk1 further phosphorylates cyclin-dependent kinases (CDK), such as Cdc25, which induce the cell cycles arrest from G1 into S-phase, and from G2 into mitosis [440,441]. Moreover, several kinds of research have demonstrated that Chk1 phosphorylates p73 at serine-47, which induces p73 overexpression and promotes p53-independent cellular apoptosis [440,442]. Like Chk1, activated Claspin protein monitors replication during S-phase and ensures whether the cell undergoes DNA repair or apoptosis [443]. Collectively, these processes determine the cellular responses to SSBs and play an essential role in maintaining genomic integrity.

2.3.1.2. ATM activation. Comparing to SSBs, DSBs are particularly toxic types of DNA damage that activate numerous DDR pathways [433,444]. One of the initial responses to DSBs is a recruitment of the MRN complex, containing Mre11, Rad50, and Nbs1components to the site of the DNA lesion [445,446]. Several studies demonstrated that the C terminus of Nbs1protein and Mre11–Rad50 complex can directly interact with ATM kinase and activate it [446,447]. The ATM kinase is predominantly a nuclear protein, where it exists as a catalytically inactive homodimer [447]. Interestingly, treatment with neocarzinostatin (NCS) and IR can activate ATM kinase in MRN independent manner via autophosphorylation at serine (S)1981, which at the same time induces monomerization of ATM [447–449]. IR can also induce autophosphorylation at several other sites in ATM, including serines 367, 1893, and 2996 [449,450]. Activated ATM is a major kinase responsible for phosphorylation of histone H2A variant at serine 139, also known as γ-H2AX foci, which is a relevant biomarker for DNA DSBs [444,451]. The formation of γ-H2AX foci is essential for the activation of cell-cycle arrest proteins and recruitment of the DNA damage signaling and repair proteins to the site of DSBs [452,453]. Moreover, γ-H2AX foci are involved in the recruitment of cohesion proteins, which are necessary to hold together the broken sister chromatids and ensure post-replicational DNA repair [454]. Claspin can as well trigger cellular apoptosis and its inactivation is tightly associated with tumor progression [443].

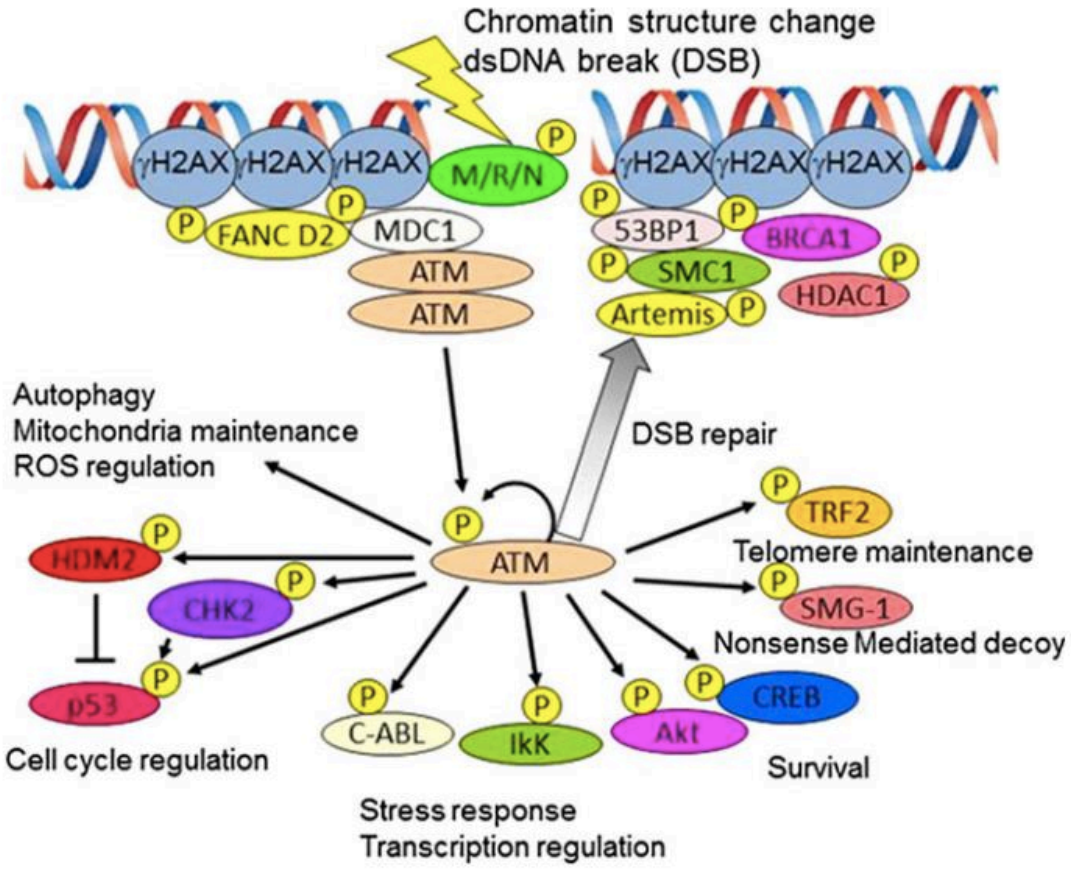

Figure 16. Mechanism of ATM activation and its function in DNA damage response.

In response to DNA double-strand breaks, ATM is activated through autophosphorylation and/or MRN complex. Activated ATM further phosphorylates and activates numerous substrates that mediate the cell cycle control, stress response, cell survival, mitochondrial biogenesis, DNA repair, and telomere maintenance. BRCA1, breast cancer type 1 susceptibility protein; γ-H2AX, phosphorylation of the Ser-139 residue of the histone variant H2AX; MDC1, mediator of DNA damage checkpoint 1; 53BP1, p53-binding protein 1; HDM2, human homolog of double minute 2; IkK, IκB kinase; CREB, cAMP response element-binding protein; TRF2, telomeric repeat binding factor 2; SMC1, structural maintenance of chromosomes protein 1; HDAC1, histone deacetylase 1; FANC D2, Fanconi anemia group D2. Adapted from *Mizutani and Takagi (2013)* [455].

ATM also plays a key role in the activation of several downstream effector kinases involved in cell-cycle arrest [433,456]. Figure 16 illustrates some of the most-studied ATM substrates and their function [455]. One of the ways that ATM uses to regulate the cell cycle is through the stabilization of a tumor-suppressor protein p53 [457]. p53 is involved in numerous cellular processes, including cell-cycle arrest, apoptosis, autophagy, senescence, glycolysis, and ribosomal biogenesis [458]. ATM can stabilize p53 by directly phosphorylating its serine-15 residue or by indirectly phosphorylating Chk2 kinase, which then phosphorylates p53 on

serine-20 [459,460]. Interestingly, ATM can make a complex and phosphorylate HDM2 (the human homolog of murine MDM2), the negative regulator of p53 [457,461]. HDM2 is an E3 ubiquitin ligase, that can associate with p53 and block its transcriptional activity, as well as promote its proteasomal degradation [461,462]. In addition, activated Chk2 kinase phosphorylates substrates, such as CDC25A and CDC25C, which are involved in G1 into S-phase and in G2 into M-phase transitions, respectively [463].Several studies have demonstrated that ATM is essential for activation of NF-κB signaling pathway as well [464]. For instance, it was shown that IR-induced DSBs trigger ATM-dependent IKK complex activation, which is required for stimulating of NF-κB pathway [465]. Moreover, the DNA-dependent protein kinase, another serine/threonine protein kinase, was shown to phosphorylate IkB-α and IkB-β, causing NF-κB nuclear translocation [466].

Several studies have highlighted the important role of ATM activation in mitochondrial biogenesis and in the regulation of ribonucleotide reductase [448,467]. For instance, ATM-deficient lymphoblastoid cells had a low mitochondrial respiratory activity compared to wild-type cells, and the expression level of DNA-encoded genes involved in oxidative damage responses, such as polymerase gamma, mitochondrial topoisomerase I, peroxiredoxin 3, and manganese superoxide dismutase, were elevated [468]. Another study showed that the ATM deficiency in thymocytes had led to an elevated level of aberrant mitochondria, increased ROS accumulation, and decreased mitophagy [469]. Under stress conditions, such as irradiation, the mitochondria homeostasis can be maintained between cell-to-cell direct communication, where healthy organelles are transferred to damaged cells through nanotubular highways [470,471]. Interestingly, it was demonstrated that in co-culture between irradiated and non-irradiated cells, ATM controls the bilateral transfer of mitochondria through membrane nanotubes [472]. ATM was also implicated in controlling and maintaining the expression of R1, R2, and p53R2 subunits of ribonucleotide reductase, an enzyme required for the synthesis of deoxyribonucleoside triphosphates, which are essential for the synthesis and repair of DNA [473]. Collectively, these results suggest that ATM plays a significant role in modulating mitochondrial homeostasis, disfunction of which can be a contributing factor to the cancer-prone phenotype observed in ATM-deficient patients.

2.3.2. Ionizing radiation and tumor microenvironment

The tumor microenvironment (TME) is a complex system composed of stromal cells (cellular part) and ECM components (non-cellular). The cellular components include tumor

cells, stromal cells including cancer-associated fibroblasts (CAF), endothelial cells, and immune cells, such as TAMs with the anti-inflammatory phenotype, tumor-associated neutrophils (TANs) with the N2 phenotype, MDSCs (myeloid-derived suppressor cells), mast cells, regulatory T cells (Tregs), and natural killer (NK) cells [474–476]. The non-cellular components of ECM include collagen, fibronectin, hyaluronan, and laminin [474,477]. The TME is also enriched by soluble factors, such as growth factors, matrix metalloproteinases (MMPs), chemokines, enzymes, RNA, DNA, and metabolites [476,477]. Depending on the immune responses the TME can be classified into two types, immune responsive "hot tumor", and immune-suppressive tumor "cold tumor" [478,479]. Radiotherapy can turn the TME either into an immunostimulant or immunosuppressive phenotype and trigger a systemic effect of a local radiotherapy [480]. The consequent phenotype largely depends on the dose, timing, and fractionation pattern [481]. Indeed, the ionizing radiation mainly modulates the TME by killing cancer cells through distinct cell death modalities that can be cell-autonomous (CAD), or non-cell-autonomous (NCAD) (Figure 17) [482]. IR can also induce endothelial cell damage and hypoxic environment (Figure 18) [481,483].

2.3.2.1. Radiotherapy elicited cell death modalities. Radiotherapy can simultaneously induce CAD and NCAD in cancer cells [482]. CAD is executed in a cell-autonomous manner and includes type I and type II cell death (or apoptosis, autophagic cell death, pyroptosis, and mitotic death), and type III cell death (or necrosis and necroptosis). Whereas NCAD is initiated after the engulfment of live cells by other living cells and classified as a type IV cell death (or emperipolesis, entosis, cannibalism, emperitosis, and phagoptosis) (Figure 17) [482,484]. Apoptosis is characterized by cytoplasmic shrinkage, reduction of cellular and nuclear volume (pyknosis), nuclear fragmentation (karyorrhexis), and plasma membrane blebbing [485]. Morphological characteristics of autophagic cell death include the formation of large intracellular double-membraned vacuoles and activation of autophagic signaling pathways [486]. While pyroptotic cell death is defined by pore formation in the plasma membrane, that cause cell to swell, lyse, and release the cytosolic contents [487]. Premature or aberrant entry of cells into mitosis results in a mitotic catastrophe that is characterized by the accumulation of multiple micronuclei and multinucleated giant cells [488]. (Necroptosis and necrosis exhibit similar morphological characteristics, such as quick swelling of the cells, plasma membrane rupture, and release of cell contents [489,490]. Radiotherapy can also induce other CAD, such as methuosis and iron-dependent cell death [491].

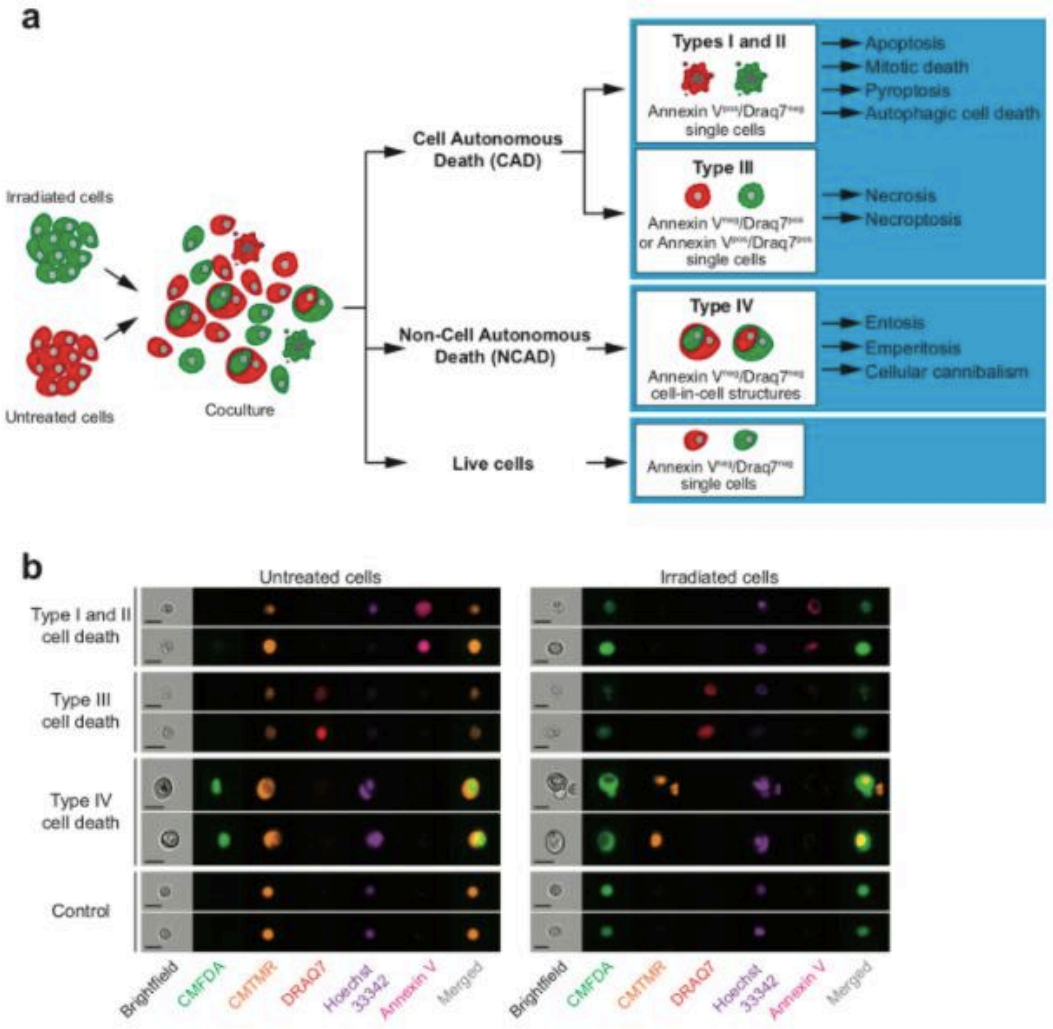

Figure 17. Irradiation-induced cell-autonomous and non-cell-autonomous death.

a) Graphical representation of the cell death profiling assay designed to detect cell-autonomous (CAD) and non-cell-autonomous death (NCAD) by using multispectral imaging flow-cytometry. Before co-culture, untreated cancer cells have been labeled with the red fluorescent probe 5-(and-6)-(((4-chloromethyl)benzoyl)amino) tetramethylrhodamine (CMTMR) and irradiated isogenic cancer cells have been labeled with the green fluorescent probe 5-chloromethylfluorescein diacetate (CMFDA). The phosphatidylserine (PS) exposure was detected by using Biotin-AnnexinV and BV786-Streptavidin, the loss of plasma integrity by DRAQ7 uptake, and the DNA content by using Hoechst 33342. b) Simultaneous detection of cell death modalities by flow cytometry on HCT116 cell line treated by γ-irradiation. Adapted from *Martins et al. (2018)* [482].

Among NCAD emperipolesis, entosis and cellular cannibalism are closely related in their characteristic appearances but fundamentally different in their mechanisms [492]. Emperipolesis is a process where a live cell penetrates another living cell without causing

structural or functional harm for either of them [493]. The molecular mechanism of emperipolesis involves the Ezrin, LFA-1, and ICAM-1 proteins and after emperipolesis, the

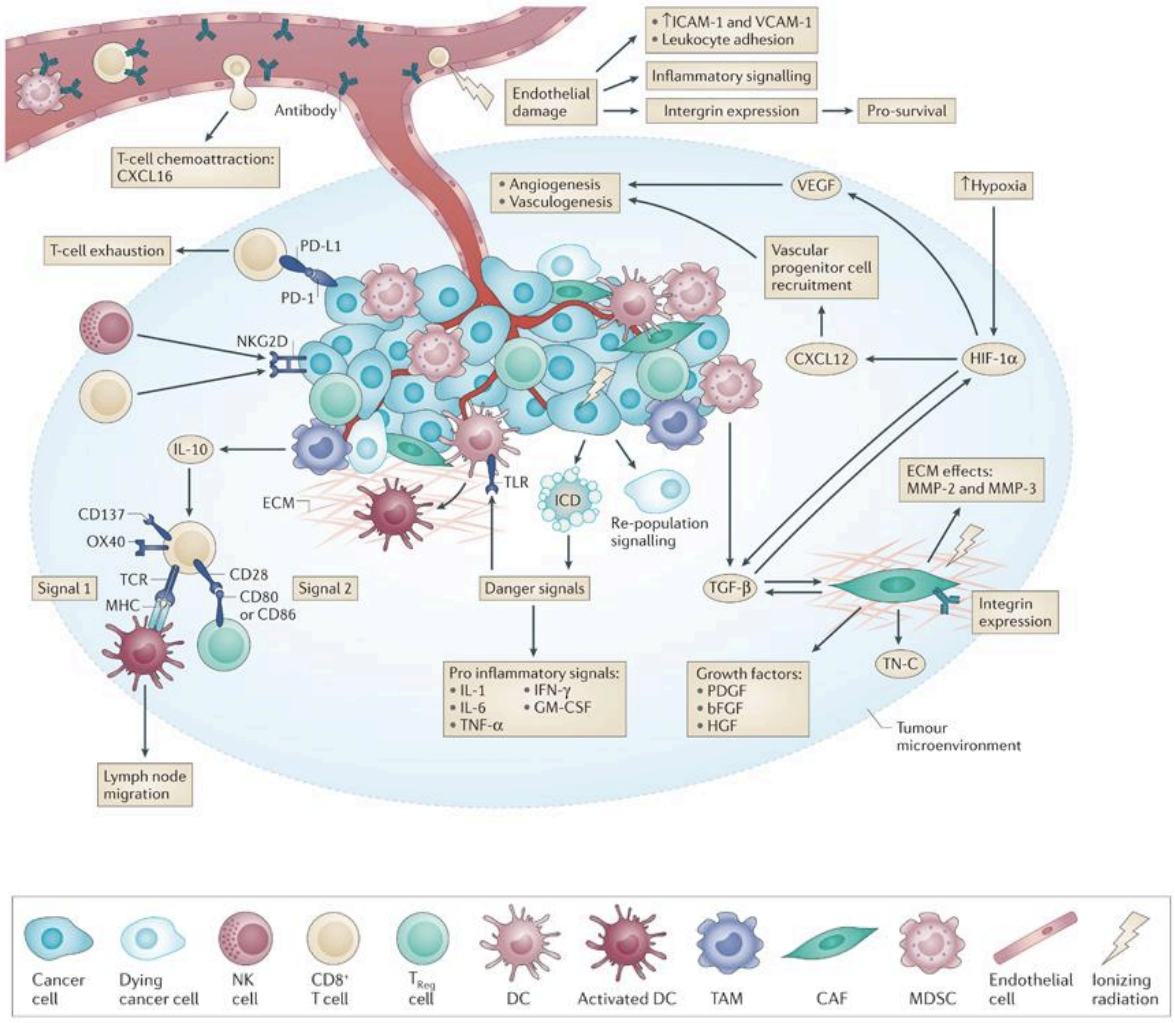

Figure 18. Ionizing radiation modifies the tumor microenvironment.

Ionizing radiation affects the tumor microenvironment (TME) in numerous ways. Damage of the endothelial cells leads to intercellular adhesion molecule 1 (ICAM-1) and vascular cell adhesion molecule 1 (VCAM-1) expressions, which facilitates leucocytes adhesion and inflammation. The destruction of the vascular system causes hypoxia, leading to activation of HIF-1 signaling, which activates pro-angiogenic and pro-vasculogenic pathways through VEGF and CXCL12 expressions. Radiation simultaneously induces distinct modalities of death (CAD and NACD) that are associated with the release of danger-associated signals, which activates DAMP-PRR mediated damage response and causes the release of pro-inflammatory cytokines and shifts the TME toward immunoreactive phenotype. Therapeutic radiation also promotes cancer-associated fibroblasts (CAF) co-ordinated extracellular matrix (ECM) remodeling, through the release of growth factors. Adopted *Barker et al. (2015)* [483].

internal cell can escape, or both host and internal cell may die [494]. Entosis is similar to emperipolesis, however, here both engulfing and internalized cells are the same type [484,492]. Entosis is induced by the expression of epithelial cadherin proteins (E- or P-cadherin) and involves the overactivation of RhoA or ROCK I/II [495] and AMPK [496] within the entotic cells. Following the entosis, the internalized cell can be either released or undergo lysosomal degradation [497]. In the process of cellular cannibalism, the host cell internalizes another living cell of its type or another in a vacuolated space and degrades the engulfed cell [494,498]. This process is mediated by caveolins, ezrin, and specific lytic enzymes, such as cathepsin [499].

Radiation therapy can also induce a peculiar type of cell death that activates an adaptive immune system, known as immunogenic cell death (ICD), that consequently triggers a stable anticancer immunity [500,501]. As opposed to non-immunogenic cell death, during ICD cancer cells undergo cell swelling and bursting, which leads to the emission of specific DAMPs, including the exposure of endoplasmic reticulum (ER) proteins, such as calreticulin (CRT) on the cell surface, extracellular secretion of adenosine triphosphate (ATP), the passive release of heat shock proteins (HSPs), like HSP70 and HSP90, and a non-histone chromatin-binding protein, known as a high mobility group B1 (HMGB1) [500,502]. In the pro-apoptotic stage CRT, which is a Ca^{2+} ion binding protein, co-translocates to the cellular membrane together with another ER stress protein, the disulfide isomerase ERp57[503,504]. At the cell surface, CRT/ERp57 complex acts as an “eat me” signal and initiates the engulfment of cancer cells by dendritic cells (DCs), promoting further DCs activation and antigen presentation to tumor-specific CTL [502,503,505]. Similarly, extracellular ATP acts as a "find me” signal and binds to P2X7 receptors on DCs, causing the activation of the NALP3-ASC-inflammasome, which leads to the release of pro-inflammatory cytokine IL-1β [506–508].

In the late stages stressed and dying cells release endogenous danger molecules, such as HMGB1 and HSP70/90, which have immunostimulatory properties as well [502]. HMGB1 binds to TLR4 receptor, expressed abundantly on the surface of DCs [509]. The interaction between HMGB1 and TLR4 leads to DCs maturation, enhanced phagocytosis, and cross-presentation of the tumor-antigens through MHC class I and class II molecules to specific T cells [509,510]. HSPs function as antigen carriers (chaperoning) for APCs and provide a link between innate and adaptive immune systems [511,512]. Complexes of HSP70/90 with

antigenic peptides are recognized by the scavenger receptor CD91, expressed in $CD11c^+$ lineage-negative (lin^-) DCs [513,514]. The internalized antigens fuse with vesicles, where they undergo enzymatic processing followed by a presentation on MHC class peptides complexes [511]. MHC I and II molecules present antigens to $CD8^+$ and $CD4^+$ T cells respectively, activating T-cell mediated anti-cancer immunity [515,516].

2.3.2.2. Radiation-induced tumor immunogenicity. Several studies have shown that the efficacy of radiotherapy largely depends on its ability to activate antitumor adaptive immunity and increase tumor cell-specific T-cell infiltration [517]. Activation of the immunogenic responses also extent the local effect of RT outside the treated volume and cause rejection of distant metastatic tumors. These phenomena are commonly referred to as radiation-induced bystander and abscopal effects [518]. Initial observations demonstrated that mice deficient in functional type I IFN receptor showed increased tumor volume and low survival rate, suggesting that type I IFN signaling plays an important role in tumor development [519]. Further studies showed that RT increases antigen-specific T cells via intratumoral production of IFN-β [517], which is released through the activation of the cyclic GMP–AMP synthase (cGAS)-STING cytosolic DNA sensing pathway [520]. cGAS-STING mediated type I IFN production is required for radiation-induced antitumor and abscopal responses [521]. Cytosolic DNA is rapidly degraded by the Trex1 enzyme [522]. Radiation controls Trex1 expression in a dose-dependent manner. A single dose between 12 d 18 Gy was sufficient to induce Trex1 expression and degrade cytosolic DNA, thus inhibit the activation of cGAS-STING pathway-dependent IFN-β production. However, radiation given in repeated doses below 12 Gy resulted in the accumulation of sufficient cytoplasmic DNA to activate the cGAS-STING pathway but not Trex1 [520]. Thus, the level of cytosolic DNA is essential for the induction of type I INF-dependent antitumor immunity.

Therapeutic effects of radiation therapy largely depend on the infiltration of anti-tumor T lymphocytes [523]. For instance, in murine experimental model of melanoma, the reduction of tumor or distant metastasis after ablative radiation therapy was dependent on the presence of $CD8^+$ T cell [524]. Radiation can directly or indirectly impact $CD8^+$ T cell infiltration. One of the direct ways include the genetic reprogramming of preexistent intratumoral immunosuppressive T cells into effector T cells that controls tumor growth [525]. While indirect ways include radiation-induced release of chemokines such as CXCL16 by cancer cells, which binds to CXCR6 on activated CD8 effector T cells and increase their

migration into the TME [526]. Irradiation can also facilitate the cytotoxic T lymphocyte recognition of irradiated cells by up regulating the expression of MHC class I molecules [527] and enhance their cytolytic capacities via Fas/Fas ligand pathway [528].

2.3.2.3. Endothelial damage. Blood vessels are made of three layers the tunica intima, media, and adventitia, while capillaries are made of single-layer endothelial cells, the tunica intima, which is particularly sensitive to radiotherapy [529]. Ionizing radiation induces endothelial damage by increasing ROS production, which leads to severe DNA and mitochondrial damage and apoptosis [530]. Endothelial cell apoptosis was studied on apoptosis-resistant *acid sphingomyelinase* (*asmase*)–deficient or *Bax*-deficient mice showed that microvascular damage is an important factor in the overall tumor response to radiation therapy [531]. Moreover, ionizing radiation induces apoptosis in a dose-dependent manner, which happens in a discrete wave after 6-10 h of irradiation [532]. The molecular pathway of endothelial cell apoptosis at higher radiation doses (> 5Gy) can be either p53- or sphingomyelin /ceramide pathways-dependent [530,533]. However, it was demonstrated that both single and fractionated (24 h interfraction interval) low doses (< 0.5 Gy) of X-ray irradiation do not affect viability and apoptosis of endothelial cells, instead, it changes cells phenotype and promotes endothelial cell activation [534,535].

Endothelial activation is defined by a pro-inflammatory phenotype, which is characterized by expression of chemokines, such CCL2, cytokines, including TNF-α, IL-8, and IL-1, and adhesion molecules, like VCAM-1, ICAM-1, PECAM-1, E-selectin, and P-selectin [535,536]. Endothelial activation is essential for the recruitment of circulating cells, which contribute to the inflammation process [535]. Radiation changes endothelial cell phenotypes by activating the stress-induced NF-κB signaling pathway via DSB and ATM signaling, oxidative stress, and the release of DAMPs [536,537]. Whereas, oxidative stress directly activates redox-sensitive transcription factors, including activator protein 1 (AP-1), NF-E2 related factor 2 (Nrf2), and NF-κB [536,538]. DAMPs released from stressed and dying cells stimulate the receptors of endothelial cells and activate pro-inflammatory signaling pathways, such as NF-κB, MAPK, and IRF3 [536,539]. Inhibition of NF-κB signaling pathway specifically in mice endothelial cells resulted in reduction of adhesion molecules, pro-inflammatory cytokines, and chemokines [540].

2.3.3. Impact of ionizing radiation on immune cells

Radiation therapy can have both direct and indirect impacts on the immune cells. Direct exposure of immune cells to ionizing radiation results in DNA damage [541], cytokine production [542], various surface markers expression [543], apoptosis, and necrosis [544]. Whereas indirect effect arises from the death of tumor cells that release DAMPs, which can both stimulate or suppress the anti-tumor function of immune cells (Figure 19) [545]. DAMPs elicit immunostimulatory effects by recruiting and activating APCs, which subsequently cross-present tumor-derived antigens to T cells, resulting in the establishment of immunological memory [546,547]. In contrast, some DAMPs, such as adenosine [548] and S100 proteins [549] promote tumor growth and resistance to radiotherapy. In this section, we highlight the impact of radiation therapy on the cells of the innate immune system, which are the first line of defense against pathogens and play an essential role in activating the adaptive immune system.

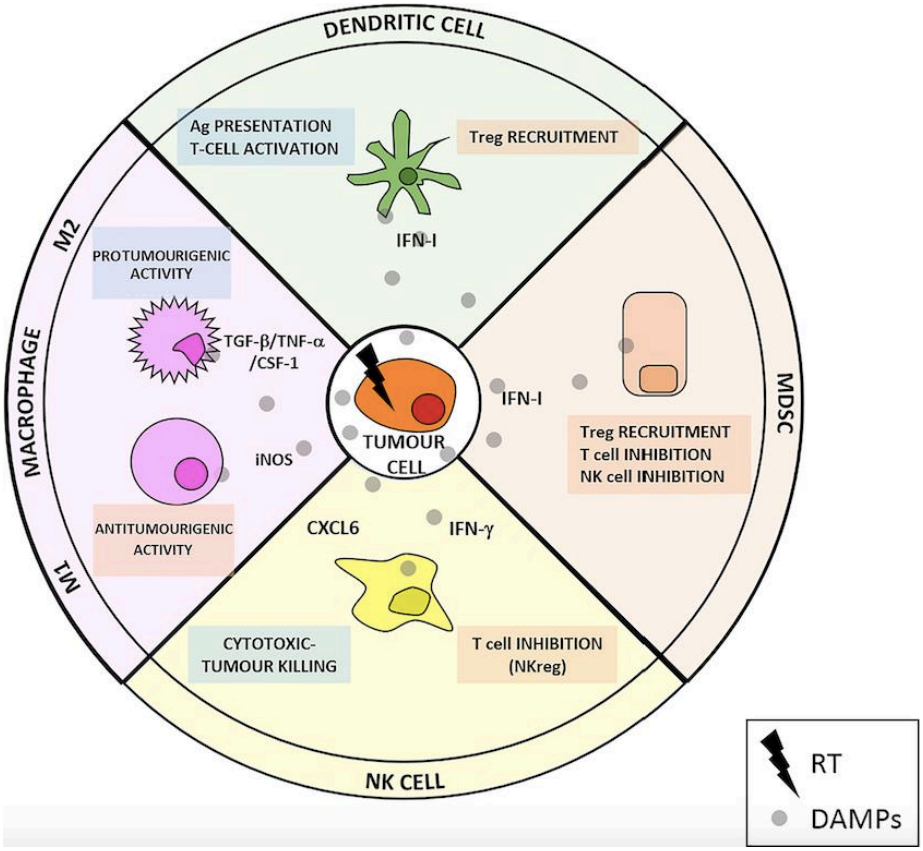

Figure 19. Effect of radiation therapy over the innate immune system.

Radiation therapy causes cancer-cell death which results in DAMPs release that can trigger both anti-tumorigenic (blue boxes) and pro-tumorigenic (red boxes) effects in the various components of the innate immune system. Adapted from *Gómez et al. (2020)* [545].

2.3.3.1. Myeloid-derived suppressor cells (MDSCs). MDSCs are a heterogeneous population of cells of myeloid origin and consist of myeloid progenitor cells and immature myeloid cells (IMCs), such as immature macrophages, immature granulocytes, and immature dendritic cells [550]. In healthy individuals there are few MDSCs, which accumulate in bone marrow, but not in secondary lymphoid organs [550,551] . Under the steady-state condition, MDSCs in bone marrow differentiate into macrophages, granulocytes, and dendritic cells [550,552]. However, under pathological conditions, such as cancer, autoimmune diseases, and infection, the number of MDSCs in bone marrow increases significantly and remains undifferentiated [552,553]. After recruitment to TME, MDSCs protect tumor cells by creating an immunosuppressive environment. Particularly, MDSCs produce high amounts of arginase and iNOS enzymes, and ROS, including superoxide, myeloperoxidase, hydroxyl peroxide, and peroxynitrite, which are mainly involved in the suppression of T-cells function [550,554]. Within TME, MDSCs can also differentiate into TAMs [552]. Radiation therapy can both facilitate and inhibit the development of MDSCs [555]. *In vivo* studies demonstrated that ablative hypofractionated radiation therapy (AHFRT) promotes antitumor immunity by decreasing hypoxia in TME and inhibiting VEGF/VEGFR signaling pathway, which leads to decreased MDSCs recruitment and reduced PD-L1 expression on those cells [556]. On the contrary, conventional fractionated radiation therapy (CFRT) increases MDSCs infiltration by increasing CSF1 accumulation via DNA damage-induced kinase ABL1, which binds to CSF1 promoter and initiates the gene transcription [557]. Radiotherapy can also activate the STING/type I interferon pathway, which promotes MDSCs infiltration and consequent tumor radioresistance [553,558].

2.3.3.2. Natural Killer (NK) cells. NK cells are part of the innate lymphoid cell family [559,560]. In humans, they differentiate from multipotent $CD34^+$ hematopoietic progenitors in the bone marrow [561]. Anti-tumor response of NK cells involves recognizing and killing tumor cells, through the tumor-ligand specific activating receptors, such including NKp46, NKp30, NKp44, natural killer group 2 member D (NKG2D), DNAX accessory molecule-1, and CD244 [560,562]. They are also capable of directly killing the tumor cells by secreting cytotoxic granules, containing perforin and granzymes, and cytokines, such as IFN-γ and TNF-α [560,563]. However, tumor progression and chronic diseases cause the exhaustion of NK cells, leading to their impaired effector functions and altered phenotype [564].

The impact of ionizing radiation on NK cells is largely dose-dependent [560]. In mice, irradiation with single low doses of 0.1 Gy or 0.2 Gy X-rays stimulated cytotoxic NK cells function and prevented tumor metastasis [565]. Similarly, NK cells exposed to single low doses of 25, 75, 150, or 500 mGy X-rays secreted a higher amount of IFN-γ and TNF-α cytokines, possibly through the activation of the P38-MAPK signaling pathway [566]. However, exposure of mice inoculated with Lewis lung cancer cells to higher doses of irradiation (1 Gy) impaired the accumulation of $CD69^+$ NK cells [567]. Thus, low doses of irradiation tend to activate the anti-tumor function of NK cells, while high dose radiations seem to undermine this function.

2.3.3.3. Dendritic cells (DCs). Among antigen-presenting cells, DCs are more efficient in migration and antigen presentation through MHC class I molecules, this process is also known as cross-presentation [568,569]. DCs can be further categorized into three distinct subpopulations: conventional DCs (cDCs), plasmacytoid DCs (pDCs), and monocyte-derived DCs (moDCs) [569,570]. cDCs can be further divided into cDC1 and cDC2 [570,571]. DCs originate from the HSCs in the bone marrow, and their subsequent differentiation largely depends on the activity of IRF4 and IRF8 transcription factors [571]. DCs promote a strong anti-tumor response in several ways. For instance, cDC1 has a strong capacity for cross-antigen presentation to $CD8^+$ T cells, and for inducing T_H1 cell polarization of $CD4^+$ T cells [572]. cDC2 can also present antigens to $CD4^+$ T cells [573]. While, pDCs are mostly described as IFN type I-producing cells, through the induction of TLR7 and 9 [574]. Inflammation induces a high accumulation of moDCs, which release NO, IFN-γ, IL-17A, and promote Th1 and 17 differentiation [575]. Immunosuppressive mechanisms of TME impair the anti-tumor function of DCs [576]. Particularly, tumor cells release cytokines and growth factors, such as GM-CSF, M-CSF, IL-6, and VEGF, that impair DC recruitment, differentiation, maturation, and survival [577,578].

Radiation therapy is known to activate DCs in various ways. After exposure to a single low dose of 2, 5, 10, 15, and 20 Gy X-rays, DCs upregulated level of CD40, CD80, CD86, CXCR4, and CCR7, however, only DCs that received ≥ 5 Gy had higher abilities in homing to lymph nodes and in cross-priming T cells. This process was associated with cytoskeletal reorganization, triggered through the ROS-induced RhoA/ROCK1 signaling pathway [543,579]. Interestingly, in another study low doses of irradiation from 0.02 to 1.0 Gy by ^{137}Cs source increased DCs mediated T cell-activation, through the induction of cytokines, such as IL-2,

IL-12, and IFN-γ [542]. In contrast, DCs irradiated with 30 Gy ^{137}Cs source showed fewer changes in surface phenotype and decreased IL-12 production, while the level of IL-10 remained unchanged [580]. *In vivo* studies in tumor-bearing mice showed that single exposure to 12 Gy alone is not sufficient to induce cDC1-mediated $CD8^+$ T cell activation, which is essential for durable tumor cures [581]. Moreover, it was shown that Langerhans cells promote resistance to RT by overexpressing p21 and generation of Treg cells [582].

2.3.3.4. Macrophages. The impact of radiation therapy on macrophages largely depends on irradiation doses and experimental settings [583,584]. Several *in vitro* studies demonstrated that low doses of radiation can promote both anti-inflammatory and pro-inflammatory macrophage activation [585,586]. For instance, LPS-pretreated human THP1 macrophages exposed to low dose X-ray radiation (0.5 and 0.7 Gy) decreased the secretion of the pro-inflammatory cytokine, IL-1β, in an NF-κB dependent manner [585]. In contrast, IFN-γ or LPS-treated J774.1 and RAW264.7 murine macrophages exposed to a range of irradiation doses (0.5–5 Gy) increased the production of NO, which is a marker of pro-inflammatory macrophage activation, in a dose-dependent manner [587,588].

Monocytes and macrophages isolated from healthy donors responded differently to high doses of ionizing radiation as well. In a study involved seven donors, human macrophages irradiated with 10 Gy γ-rays (^{60}Co source) revealed no significant accumulation of IL-1β and TNF-α, but in two donors the level of IL-6 increased significantly after the irradiation [589]. Similarly, in another study where 10 Gy was delivered in the fractionated scheme (2Gy/fraction/day), human macrophages failed to express IL-1β, TNF-α, and CCR7, but significantly increased the expression of other pro-inflammatory markers, such as CD80, CD86, and HLA-DR [586]. Another study on human macrophages showed that X-ray irradiation (20 Gy) induces expression of CD36 scavenger receptors through activation of the JNK signaling pathway [590].

In vivo studies on tumor-free animals also demonstrated that radiation therapy impacts macrophages in various ways. For example, healthy mice exposed to chronic low-dose total body radiation (0.2 or 2 Gy) increased the levels of IL-3, IL-4, leptin, MCP-1, MCP-5, MIP-1a, thrombopoietin, and VEGF, and reduced the levels of IL12p70, IL-13, IL-17, and IFN-γ, suggesting that systemic low dose irradiation suppresses pro-inflammatory macrophage phenotype [591]. Similarly, fractionated low dose irradiation (5x1.0 Gy or 5x0.5Gy) in

adjuvant-induced arthritis rat model reduced iNOS accumulation, and increased HO-1 expression in macrophages, which was associated with the disease suppression [592]. Although many studies have demonstrated that low doses irradiation promotes anti-inflammatory macrophage activation, some studies have shown the opposite effect can be observed as well. For instance, macrophages isolated from healthy C57BL/6 mice that were exposed to fractionated radiation (0.04 Gy per day, 5 days, total dose 0.2 Gy, γ-rays from ^{60}Co source) had a high level of nitric oxide, increased phagocytic activity, and $CD8^+$ T cell response, thus under these conditions pro-inflammatory macrophage activation was favored [593].

Radiation therapy can promote both anti-inflammatory or pro-inflammatory macrophage activation in tumor-bearing mice, leading to either radioresistance or radiosensitization respectively [584]. In a xerographed mouse model, implanted with OSC-19 tongue squamous cell carcinoma cells, a single local high dose of irradiation (12 Gy, X-rays) promoted $CD11b^+$ M2-like macrophage infiltration in the TME and this was associated with tumor progression and relapse after the irradiation [594]. Analogously, in mice inoculated with B16 melanoma cells that received either a single dose of 20 Gy or fractionated doses of 2 Gy per 10 days, upregulated VEGF release by macrophages via activation of TNFα/TNFR signaling pathway [595]. VEGF promotes radioresistance by suppressing DCs activation and maturation, as well as by recruiting immunosuppressive Tregs and MDSC [596]. On the other hand, in tumor-bearing Rip1-Tag5 mice exposed to the fractionated low dose irradiation (2 Gy per irradiation, 1 time per week for 2 consecutive weeks, γ-rays from ^{60}Co source) resulted in a shift from anti-inflammatory to pro-inflammatory activated macrophages in tumor micromilieu [597]. Similarly, in another study single low dose of irradiation (2 Gy) delivered in a single dose promoted the accumulation of iNOS positive pro-inflammatory macrophages, that expressed T_H1 chemokines and recruited CTL [598].

In our recently published work, we have also demonstrated that low doses of irradiation promote pro-inflammatory macrophage activation via induction of DDR [541]. In a preclinical mouse tumor model, a local single dose of X-ray irradiation (20 Gy) induced infiltration of $iNOS^+CD11b^+$ pro-inflammatory macrophages, which accumulated γ-H2AX foci. Further *in vitro* analysis revealed that macrophages exposed to 2 Gy or 4 Gy of X-ray radiation upregulate pro-inflammatory marker IRF-5 and produce cytokines, such as IL-1β, IL-8, and IL-6. The upregulation of IRF5 was controlled by phosphorylation of ATM at serine 1981, which was regulated by NOX2-induced ROS production. Interestingly, the

NOX2/ATM/IRF5 molecular pathway was also activated in macrophages exposed to IFN-γ, LPS, and CDDP (Figure 20). Finally, we have demonstrated that the alteration of the NOX2/ATM pathway in macrophages was associated with poor tumor response in patients treated with chemoradiotherapy [541].

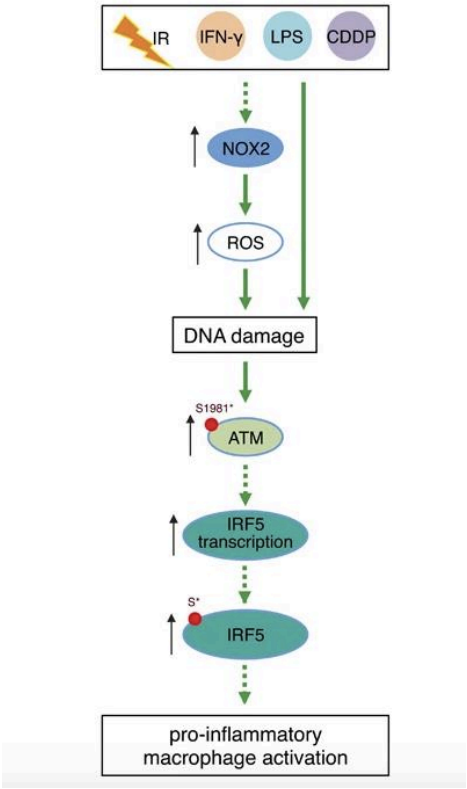

Figure 20. Molecular mechanism of pro-inflammatory macrophage activation.

Adapted from *Q. Wu, Allouch, Paoletti, et al. (2017)* [541].

2.4. Combination of nanomedicine and radiotherapy

In clinic, radiation therapy is often combined with chemotherapy and surgery, however, outcomes on overall 5-year survival rates of these combinations are still limited [599,600]. Even though the combination of radiation therapy and chemotherapy has been shown remarkable results in the reduction of mortality, these treatments cause significant toxicities [601,602]. The ultimate challenge in delivering the radiation therapy is to reduce the toxicity to normal tissue while preserving the therapeutic outcome, this can be accomplished by improving the dose-deposition curve [599,603].

NPs containing high atomic number (high-Z) elements have a high enhanced photo-absorption capacity and when exposed to ionizing radiation are capable of deposing higher

energy at their vicinity [604]. The tumor has an abnormal vasculature, namely poorly aligned endothelial cells and lack of smooth muscles, which creates a wide lumen and allows NPs to travel selectively into the tumor region and avoid healthy tissue [605]. Lack of functional lymphatic drain in TME contributes to NPs retainment over a prolonged time. This phenomenon of NPs accumulation predominantly in the tumor region is commonly known as the EPR effect, and it is widely exploited to enhance the impact of radiation therapy [606,607].

Apart from the radiation-enhancing effects, metal-based NPs can indirectly improve radiation therapy by targeting components of TME, such as DCs, CAF, and TAMs [608]. For instance, liposomes-coated gold nanocages (Lipos-AuNCs) modified with DCs specific antibody directed against aCD11c and loaded with adjuvant monophosphoryl lipid A and melanoma antigen peptide TRP2 were able to promote the activation and maturation of DCs and induce $CD8^+$ T cell-based antitumor immune responses in B16-F10 prophylactic and lung metastasis models [609]. While in the pancreatic tumor xenograft model injection of SPION NPs conjugated to relaxin-2, an endogenous hormone, inhibited CAF differentiation from pancreatic stellate cells (PSCs) and reduced tumor growth [610]. Intravenously injected SPIO NPs followed by MRI imaging demonstrated that these NPs are preferentially internalized by TAMs within the TME [611]. Further investigations revealed that iron oxide NPs reduce tumor growth by attracting macrophages and reprogramming them from anti-inflammatory to pro-inflammatory phenotype [612].

Despite the decades of *in vitro* and *in vivo* research demonstrating the efficient anti-tumor effect of the nanomedicine and radiotherapy combination, only two radio-enhancement NPs, Hafnium oxide known as NBTXR3 and gadolinium-based NPs or AGuIX, are currently studied in clinical trials [384]. NBTXR3 was tested in Phase II/III clinical trial involving 176 patients (87 in the NBTXR3 group and 89 in the radiotherapy alone group) with soft tissue sarcoma. The treatment plan involved a single intravenous injection of NPs, followed by fractionated external beam radiation therapy (EBRT), 50 Gy over 5 weeks (NCT02379845). This study showed that the combination of radiation therapy with NBTXR3 doubled the pathological complete response and had acceptable toxicity [613]. Currently, NBTXR3 efficiency is evaluated in other cancer types, including head and neck cancer in patients not eligible for chemotherapy (NCT01946867) and in combination with chemotherapy (NCT02901483), in prostate adenocarcinoma (NCT02805894), in hepatocellular carcinoma and liver metastasis (NCT027721056). Nanobiotix is currently

recruiting patients with recurrent head and neck squamous cell carcinoma, lung or liver metastasis for Phase I clinical trial, to evaluate the safety of intratumoral injection of NBTXR3 in combination with stereotactic ablative radiotherapy (SABR) and anti-PD-1 therapy (NCT03589339) [614]. Clinical trials involving AGuIX NPs have been explained in previous sections.

AIMS AND OBJECTIVES

TAMs that are detected in the TME and mainly exhibit anti-inflammatory functions that promote tissue repair, angiogenesis, tumor invasion and metastasis. TAMs also contribute to immunosuppression in the TME by releasing cytokines, chemokines, and by expressing specific receptors that modulate functions of multiple immune cells, including CD8+ and CD4+ T cells, Tregs, DCs, NK, and MDSCs. However, TAMs are highly plastic cells and can be functionally reprogrammed into a pro-inflammatory phenotype that favors anti-tumor immune responses. The increasing studies have demonstrated that radiation therapy modulates TAMs phenotype. The effect of IR on immune cells depends on various parameters, including the source of irradiation, dose, and fractionation schedule. Our previous research demonstrated that low doses of X-rays triggers the macrophage phenotypic conversion from anti-inflammatory to pro-inflammatory phenotype by inducing severe DNA damage that triggers DDR directed by ATM kinase. Further experiments revealed that ATM activation is required for mRNA expression and post-translational modifications of IRF5. Thus, our results showed that induction of DNA damage favors pro-inflammatory macrophage activation.

Metallic NPs containing high-Z atoms can be used to amplify the dose deposition of IR and improve the effect of radiotherapy. Several metal-based NPs, including gadolinium-based metallic NPs AGuIX (activation and guiding of irradiation by X-ray), have been widely used as MRI contrast agents in the clinic and have been shown to concentrate predominantly at tumor sites due to the enhanced permeability and retention effect. Upon exposure to IR, AGuIX produces photoelectrons, Auger electrons, and free radicals that cause widespread biomolecular damages, including DNA double-stranded breaks. Although the AGuIX has been proven to act as an efficient radiosensitizer and shown to induce strong anti-tumor responses in combination with radiation therapies, the impact of their combination on immune cells is poorly understood. Thus, ultimate goals of this Ph.D. thesis are to evaluate whether AGuIX NPs in combination with IR can activate DDR in TAMs and enhance radiation-induced macrophage activation. We are also aimed to identify key molecular players that control DDR in macrophages and broaden our knowledge in new therapeutic strategies that can be used to re-educate TAMs.

RESULTS

Article:

Gadolinium-based NPs AGuIX and their combination with ionizing radiation trigger AMPK-dependent pro-inflammatory reprogramming of tumor-associated macrophages

Gadolinium-based nanoparticles AGuIX and their combination with ionizing radiation trigger AMPK-dependent pro-inflammatory reprogramming of tumor-associated macrophages

Zeinaf Muradova[1,2], Désirée Tannous[1-3], Déborah Lecuyer[1,2], Aurelia Deva-Nathan[1,2], Emie Gutierrez-Mateyron[1,2], Ali Mostefa-Kara[1,2], Constance Lamy[1,2], Sophie Broutin[1,2], Angelo Paci[1,2,4], Sandrine Dufort[3], Géraldine Leduc[3], François Lux[5], Olivier Tillement[5], Awatef Allouch[1-3*] and Jean-Luc Perfettini[1,2* ψ]

[1] Université Paris-Saclay, Inserm UMR1030, Laboratory of Molecular Radiotherapy and Therapeutic Innovation, Villejuif, F-94805, France;
[2] Gustave Roussy Cancer Center, F-94805 Villejuif, France;
[3] NH TherAguix, Meylan, F-38240, France;
[4] Département de Biologie et Pathologie médicales, Gustave Roussy, Université Paris-Saclay, Villejuif, France;
[5] Institute Light and Matter, UMR5306, Lyon1 University-CNRS, Lyon University, Villeurbanne, France..

* Coauthorship
ψ Corresponding author.

Contact:

Dr. Jean-Luc PERFETTINI
Laboratory of Molecular Radiotherapy and Therapeutic Innovation,
INSERM UMR1030
Université Paris-Saclay, Institut Gustave Roussy,
114 rue Edouard Vaillant
F-94805 Villejuif, France
Tel. 33-1-42 11 54 24
Fax 33-1-42 11 52 36
e-mail : jean-luc.perfettini@gustaveroussy.fr

Abstract

Tumor-associated macrophages (TAMs) are essential components of the inflammatory microenvironment of tumors and are associated with poor clinical outcomes in the majority of cancers. TAMs mainly exhibit anti-inflammatory functions that promote and support the tissue remodeling, the immune suppression and the tumor growth. Regarding their plasticity, the functional reprogramming of anti-inflammatory TAMs into pro-inflammatory phenotype recently emerged as a therapeutic opportunity to improve the effectiveness of anticancer treatments such as radiotherapy. Here we show that gadolinium-based nanoparticles AGuIX alone and in combination with ionizing radiation (IR) induce in a dose-dependent manner, the accumulation of DNA double strand breaks, an Ataxia telangiectasia mutated (ATM)-dependent DNA-damage response, an increased expression of the Interferon regulatory factor 5 (IRF5) and the release of pro-inflammatory cytokines from targeted macrophages, thus directing their pro-inflammatory reprogramming. This process is associated with the activating phosphorylation of the Adenosine Monophosphate (AMP) activated protein kinase on threonine 172 (AMPKT172*) and the fragmentation of mitochondria. Furthermore, we demonstrate that the inactivation of AMPK reduces the mitochondrial fragmentation and the pro-inflammatory reprogramming of macrophages detected in response to AGuIX and their combination with IR. These results reveal that the AMPK-dependent regulation of mitochondrial fragmentation plays a central role during the pro-inflammatory reprogramming of macrophages. Altogether, our results identify a novel signaling pathway elicited by AGuIX and their combined treatment with IR, that targets macrophage polarization, skews macrophage functions toward the pro-inflammatory phenotype and may enhance the effectiveness of radiotherapy.

Introduction

The tumor microenvironment (TME) is an immunosuppressive niche supporting the cancer progression and the immune escape that recently emerged as promising therapeutic target for cancer treatment (1). Tumor-associated macrophages (TAMs) account for the most abundant myeloid cells in the TME (2) and support both cancer progression and immune evasion (3, 4). One main feature of TAMs is their high plasticity and ability to adapt and reprogram their biological functions to environmental signals (5). TAMs demonstrate anti-inflammatory properties that stimulate angiogenesis, cancer cell invasion, and metastatic dissemination. TAMs also contribute to immunosuppression in the TME by recruiting regulatory T cells and myeloid-derived suppressor cells (MDSCs), inhibiting dendritic cell maturation and/or expressing inhibitory innate and immune adaptive checkpoint proteins (such as SIRPα, PD1 or PDL1) (6, 7). Histological detection of TAMs predicts treatment response and is associated with poor clinical outcomes in the majority of solid cancers and hematological malignancies (8, 9). Targeting the functional reprogramming of TAMs has been proposed to improve the efficacy of anticancer treatments including radiotherapy (6, 10). Highly plastic, anti-inflammatory TAMs can thus be functionally reprogrammed into pro-inflammatory phenotype to establish a tumoricidal microenvironment and to support the development of long-lasting specific anti-tumor immune response. Recently, we demonstrated that ionizing radiation (IR) reprograms pro-tumorigenic macrophages toward a pro-inflammatory phenotype. The IR-mediated macrophage reprograming that we identified requires the activation of the NADPH oxidase 2 (NOX2), the production of reactive oxygen species (ROS), the activating phosphorylation of the Ataxia telangiectasia mutated (ATM) kinase on serine 1981 (ATMS1981*) and the transcriptional activity of the Interferon regulatory factor 5 (IRF5) (11). Briefly, IR triggered DNA damage into the nuclei of targeted macrophages, leading to a DNA damage response that is directed by the ATM kinase. In response to IR, the ATM kinase, which is activated and phosphorylated on serine 1981 (ATMS1981*), controls the macrophage phenotypic conversion from anti-inflammatory to pro-inflammatory phenotype by regulating mRNA expression of IRF5. To further characterize this process, we deciphered upstream signaling pathways and detected that ROS are produced in response to IR. Interestingly, we revealed that NOX2, whose expression is also increased after IR, is involved in ROS production and directed the IR-mediated pro-inflammatory macrophage reprogramming. Moreover, the detection of this signaling pathway on patient's biopsies predicts a good tumor response to preoperative radiotherapy in locally advanced rectal cancer (11). Altogether, these

results convinced us that the identification of novel therapeutic strategy that may enhance the ability of IR to stimulate this signaling pathway and to reprogram TAMs would improve radiotherapy efficacy.

Several applications of nanomedecine (such as radioisotope-labeled or metallic nanoparticles) have been developed to improve the therapeutic index of radiation therapy. Nanomaterials were initially used as contrast agents, to enhance the magnetic resonance imaging (MRI) contrast of tumors and to develop MRI-guided radiotherapy, but also as radiosensitizers, to improve the delivery and the deposition of radiation doses into tumor sites (12-16). Considering the ability of metallic nanoparticles containing high-Z atoms to increase proportionally to their atomic number, the radiation dose absorbed by tissue, gadolinium-based nanoparticles AGuIX have been extensively investigated for their potential to improve radiotherapy. Under exposure to IR, AGuIX produce photons and Auger electrons that improve the total dose rate deposition into the tumors, enhance the DNA double-strand break damage and the production of ROS, and lead to the destruction of numerous tumors (e.g. melanoma, glioblastoma, breast and lung carcinomas)(17-19). Nanomedicine has been recently proposed to amplify antitumor immune response and to sensitize tumors to RT and/or immunotherapies (20, 21). Although the combination of AGuIX with IR (AGuIX+IR) stimulated a growing interest for cancer treatment (NCT02820454, NCT03818386, NCT04899908, NCT04789486, NCT03308604), the immune response induced by AGuIX+IR combination is poorly understood. Here, we revealed that AGuIX alone and their combination with IR induced DNA double-strand break damage into the nuclei of treated macrophages and triggered the pro-inflammatory reprogramming of TAMs in an adenosine monophosphate (AMP) activated protein kinase (AMPK)-dependent manner. Altogether, these results demonstrated that AGuIX alone and AGuIX+IR combination could be used to convert anti-inflammatory macrophages into pro-inflammatory macrophages and to improve the efficacy of radiotherapy.

Results

Gadolinium-based nanoparticles AGuIX and their combination with ionizing radiation trigger DNA double-strand breaks and an ATM-dependent DNA damage response in human and murine macrophages.

We initially demonstrated that DNA damage plays a central role during pro-inflammatory macrophage activation (11). Considering the ability of the combination of AGuIX with IR to increase dose deposition and consequently enhance the accumulation of DNA damage in treated cancer cells (22), we hypothesized that AGuIX+IR combination may also induce DNA damage in TAMs and strengthen their ability to be converted into pro-inflammatory macrophages in response to IR. Using fluorescent microscopy, we first studied the induction of DNA double-strand breaks in phorbol-12-myristate13-acetate (PMA)-differentiated human THP1 macrophages that were exposed to a single dose of 0.2 Gy in presence of different concentrations of AGuIX. As expected, thirty minutes after IR, nuclear foci containing the phosphorylated form of the histone variant H2AX on serine 139 (H2AXS139*) (also known as γ-H2AX$^+$ foci) are detected in treated macrophages (Figures 1A-1C). Moreover, the combination of IR with 200 nM AGuIX significantly enhanced the frequency of macrophages showing the nuclear accumulation of γ-H2AX$^+$ foci, as compared to control or irradiated macrophages (Figures 1B and 1C). We noticed that these nuclear γ-H2AX$^+$ foci persisted until 48 hours after the combined treatment of IR with 200 nM AGuIX (Figure 1C). Interestingly, we observed that higher concentrations of AGuIX (0.6 mM and 1.2 mM) allowed after 1 hour of treatment, the nuclear accumulation of γ-H2AX$^+$ foci in treated macrophages (Figure 1F). The frequency of PMA-differentiated human THP1 macrophages showing nuclear γ-H2AX$^+$ foci and the size of these nuclear foci increased when macrophages were irradiated with a single dose of 0.2 Gy in presence of 0.6 mM AGuIX or 1.2 mM AGuIX (Figures 1A-1F). These results were confirmed on murine RAW264.7 macrophages exposed to a single dose of 0.2 Gy in presence of 0.6 mM AGuIX or 1.2 mM AGuIX (Figure 1G), thus revealing the ability of AGuIX+IR combination to increase the dose deposition and the accumulation of DNA double-strand breaks in treated macrophages. We then analyzed the DNA damage response (DDR) elicited by these genomic alterations and determined whether the DDR is dependent of the Ataxia telangiectasia mutated (ATM) kinase, as we previously described (11). We thus studied the activating phosphorylation of the kinase ATM on serine 1981 (ATMS1981*) in PMA-differentiated human THP1 macrophages (Figure 1H) that were exposed to a single dose of 0.2 Gy in presence of different concentrations of AGuIX. Thirty minutes after treatments, we

detected that 100 nM and 200 nM AGuIX induced ATMS1981* (Figure 1H) and that the level of ATMS1981* phosphorylation is significantly increased after the treatment of PMA-differentiated human THP1 macrophages with AGuIX+IR combination, as compared to control cells (Figure 1H). Murine RAW264.7 macrophages irradiated with a single dose of 0.2 Gy in presence of 0.6 mM AGuIX or 1.2 mM AGuIX also accumulated ATMS1981* in their nuclei and showed a significant increase in the frequency of macrophages showing nuclear ATMS1981* after 1 hour-treatment with AGuIX alone (0.6 mM AGuIX or 1.2 mM AGuIX) or with AGuIX+IR combination (Figure 1I). Altogether, these results revealed the ability of AGuIX to direct DNA damage in macrophages and to enhance the amount of DNA damage and the induction of DDR in anti-inflammatory macrophages that were irradiated in their presence.

Gadolinium-based nanoparticles AGuIX and their combination with ionizing radiation favor the pro-inflammatory reprogramming of macrophages.

Considering that we previously revealed that DDR and ATM dictate pro-inflammatory macrophage phenotype (11), we then studied the impact of AGuIX and their combination with IR on macrophage functional reprogramming. Using fluorescent microscopy, we first determined the expression level of a pro-inflammatory marker of macrophage activation, the inducible nitric oxide synthase (iNOS) on PMA-differentiated human THP1 macrophages that were irradiated with 0.2 Gy in combination with different concentrations of AGuIX. Although PMA-treated human THP1 macrophages that were treated with 100 nM or 200 nM of AGuIX and/or irradiated with 0.2 Gy did not exhibit an increased expression of iNOS at 2 hours after irradiation, the frequency of $iNOS^+$ macrophages significantly increased after 48 hours in presence of 100 nM or 200 nM AGuIX alone, 0.2 Gy irradiation or the combination of 200 nM AGuIX with 0.2 Gy irradiation (Figures 2A-2C). Interestingly, we observed that PMA-differentiated human THP1 macrophages that were treated with 0.6 mM or 1.2 mM AGuIX also revealed a significant increase of iNOS expression levels, as compared to control macrophages (Figures 2D-2F), thus revealing that the potential of AGuIX to trigger the pro-inflammatory phenotype of macrophages in absence of IR. To confirm these results, we determined by immunoblot analysis the cellular expression of IRF5 and the release into the supernatant of two pro-inflammatory cytokines, interleukins 1β (IL-1β) and 6 (IL-6) that we previously detected during IR-mediated pro-inflammatory macrophage reprogramming (11). We observed that after 48 hours of IR and combined treatments with 100 nM, 200 nM, 0.6 mM

or 1.2 mM of AGuIX enhanced the expression of IRF5 in treated macrophages (Figures 2G and 2H). Interestingly, we detected that the combination of IR with 200 nM AGuIX was associated with the release of IL-1β and IL-6 in the supernatant of treated macrophages (Figure 2I). We detected that AGuIX alone (100 nM AGuIX or 200 nM AGuIX) increased the expression of IRF5 in PMA-treated human THP1 monocytes (Figures 2G and 2H) and the secretion of pro-inflammatory cytokine IL-6 in absence of IR (Figure 2I). Altogether, these results indicate that AGuIX prime anti-inflammatory macrophages for pro-inflammatory reprogramming and as a consequence, their combination with IR enhance the ability of irradiated macrophages to acquire a pro-inflammatory phenotype.

Ionizing radiation, gadolinium-based nanoparticles AGuIX and combined treatments induce AMPK activation and macrophage mitochondrial fragmentation.

Considering that mitochondrial dynamics may influence the functional reprogramming of TAMs (23), we analyzed the shape of mitochondria in PMA-differentiated THP1 macrophages that were treated with single dose of 0.2 Gy and with indicated concentrations of AGuIX. After 1 hour treatment, we detected the expression of the translocase of the outer mitochondrial membrane 20 (TOM20) by confocal microscopy and observed that single dose 0.2 Gy and treatments with 100 nM, 200 nM, 0.6 mM or 1.2 mM AGuIX led to the accumulation of shortened, rounded, fragmented mitochondria in treated PMA-differentiated THP1 macrophages (Figures 3A-3E), as compared to control PMA-differentiated THP1 macrophages. We demonstrated that the frequency of PMA-differentiated THP1 macrophages showing mitochondrial fragmentation increases in dose-dependent manner with AGuIX concentrations (Figures 3F and 3G). Beside, treatments of PMA-differentiated THP1 macrophages with 0.6 mM or 1.2 mM AGuIX respectively triggered the accumulation of fragmented mitochondria in more than 75% to 80% of treated macrophages (Figure 3H) as compared to control PMA-differentiated THP1 macrophages. These results thus revealed that IR and treatments with AGuIX altered mitochondrial dynamics and let to the accumulation of fragmented mitochondria in treated macrophages. Interestingly, we showed that the accumulation of fragmented mitochondria on treated PMA-differentiated THP1 macrophages was increased when macrophages were irradiated in presence of 100 nM or 200 nM AGuIX (Figures 3A, 3B and 3F). Considering the strong effects of 0.6 mM or 1.2 mM AGuIX on the

frequency of macrophages showing mitochondrial fragmentation (Figure 3G), we also found that the combination of single dose 0.2 Gy with 0.6 mM or 1.2 mM AGuIX failed to show a significant enhancement of mitochondrial fragmentation in treated PMA-differentiated THP1 macrophages (Figure 3G), as compared to irradiated PMA-differentiated THP1 macrophages. Altogether, these results demonstrate that single dose 0.2 Gy, treatment with different concentrations of AGuIX and combined treatments affect the mitochondrial dynamics of treated PMA-differentiated THP1 macrophages. To identify signaling pathways associated with deregulated mitochondrial dynamics, we determined whether the adenosine monophosphate (AMP) activated protein kinase (AMPK), which was recently involved in the regulation of mitochondrial dynamics (24), is phosphorylated and activated in response to these treatments. The activating phosphorylation of AMPK on threonine 172 (AMPKT172*) was then determined on control and treated PMA-differentiated THP1 macrophages (Figures 3H and 3I). Interestingly, we observed that AMPKT172* phosphorylation is strongly increased when PMA-differentiated THP1 macrophages were irradiated with all tested concentrations of AGuIX (Figures 3H and 3I). All these processes are detected after 1 hour of treatment (Figure 3) and before the induction of the pro-inflammatory activation of macrophages (Figure 2), thus highlighting an unsuspected link between treatments with IR and/or AGuIX, the activation of AMPK, the mitochondrial fragmentation and the pro-inflammatory reprogramming of macrophages.

AMPK activation controls the mitochondrial dynamics and the pro-inflammatory reprogramming of macrophages treated with IR, AGuIX and IR+AGuIX combination.

We then investigated the effects of the AMPK activation on the pro-inflammatory reprogramming of macrophages induced by IR, AGuIX and combined treatment. PMA-differentiated THP1 macrophages were treated with 0.2 Gy single dose irradiation and 200 nM AGuIX in presence of 10 μM AMPK inhibitor Dorsomorphin (DRS) and analyzed for AMPKT172* after 1 hour treatment. As previously shown (Figure 3H), IR and AGuIX induced AMPKT172* phosphorylation and IR+AGuIX combination strongly enhanced AMPKT172* phosphorylation (Figure 4A). The pharmacological inhibition of AMPK with Dorsomorphin strongly impaired AMPKT172* phosphorylation (Figure 4A) and the upregulation of IRF5 expression (Figure 4B) that were detected respectively 1 and 48 hours after 0.2 Gy single dose irradiation of PMA-differentiated THP1 macrophages in presence of 200 nM AGuIX. These results suggested that AMPK activation plays a central role during IR-, AGuIX-, IR+AGuIX-

mediated activation of anti-inflammatory macrophages toward a pro-inflammatory phenotype. To further characterize effects of AMPK on the pro-inflammatory reprogramming of macrophages in response to IR alone, AGuIX alone or AGuIX+IR combination, we then analyzed effects of the genetic depletion of AMPKα2, which is a catalytic subunit isoform of the serine/threonine kinase AMPK (25), on the mitochondrial fragmentation, the induction of ATMS1981* phosphorylation and the upregulation of IRF5 that were detected 1 hour (for mitochondrial fragmentation) and 48 hours (for ATMS1981* and IRF5) after 0.2 Gy single dose irradiation of PMA-differentiated THP1 macrophages in presence of 1.2 mM AGuIX. The specific depletion of AMPKα2 by means of small interfering RNA (Figure 4C) significantly reduced the frequency of treated macrophages showing fragmented mitochondria (Figures 4D and 4E), inhibited ATMS1981* phosphorylation (Figure 4F) and impaired IRF5 upregulation (Figure 4F). Altogether, these results confirmed the essential role of AMPK during the functional reprogramming of anti-inflammatory macrophages into pro-inflammatory macrophages and identified signaling events (Mitochondrial fragmentation → ATMS1981* → IRF5) that are induced by AMPK activation and are required for the pro-inflammatory reprogramming of macrophages in response to IR, AGuIX and IR+AGuIX combination.

Discussion

Resistance to cancer treatments is a major obstacle to overcome for cancer cure. The therapeutic targeting of tumor microenvironment has recently emerged as a promising approach to reduce refractoriness to cancer treatments and to enhance cancer treatment efficacy (1). TAMs, which are major cellular components of TME, have gained attention as novel cellular targets for anticancer therapy. In the vast majority of cancers, TAMs are associated with poor prognosis and therapeutic resistances (3, 26, 27). Several therapeutic approaches targeting TAMs for depletion, repression of migration and/or functional reprogramming have been approved or are still under consideration for clinical use (27). These strategies include neutralizing antibodies or small molecules inhibitors of colony-stimulating factor 1 receptor (CSF1R) (28, 29), CC-motif chemokine ligand 2 (CCL2) (30), CC-chemokine receptor 2 (CCR2) (31), surface receptor TREM2 (32), and PI3Kγ (33). We previously demonstrated that radiotherapy also triggers the pro-inflammatory reprogramming of TAMs through the induction of a molecular cascade that requires the increased expression of NOX2, the production of ROS, the promotion of double strand breaks, the activation and the phosphorylation ATMS1981*, the induction of IRF5, the expression of iNOS and the secretion of pro-inflammatory cytokines IL-1β, IL-6, IL-8, IFN-γ, and TNF-α (11). In addition, we revealed that other cancer treatments such as cisplatinium and the poly(ADP-ribose)polymerase (PARP) inhibitor olaparib also induced the pro-inflammatory activation of macrophages by stimulating this signaling pathway (11), thus revealing that combining radiotherapy with other modalities of cancer treatments might enhance the efficacy of radiotherapy through the reprogramming of TAMs.

In this study, we demonstrated that the combination of radiotherapy with gadolinium-based nanoparticles AGuIX enhances the ability of macrophages to undergo a pro-inflammatory activation in response to IR (Figure 5). Consistent with several *in vitro* and *in vivo* studies showing that IR+AGuIX combination increases the dose deposition in several cancer cells (34, 35), our results revealed that the *in vitro* treatment of macrophages with IR+AGuIX combination is associated with an increased dose deposition in treated macrophages, as compared to irradiated macrophages, thus providing the first evidence that IR+AGuIX combination is able to target and potentially control the fate of TAMs cells in the TME. Moreover, our results showed that the kinase ATM is phosphorylated on serine 1981 and activated in response to IR+AGuIX combination (Figure 1), thus suggesting that the kinase

ATM may potentially play a central role during IR+AGuIX-mediated pro-inflammatory macrophage reprogramming, as we previously shown for IR alone (11). Our results also revealed that the transcription factor IRF5, which is the major transcriptional regulator of IR-mediated pro-inflammatory macrophage activation (11), exhibited an increased expression in response to IR+AGuIX combination. The increased secretion of IL-1β and IL-6, and an augmented production of iNOS were also detected in response to IR+AGuIX combination, as compared to treatments with IR or AGuIX alone, demonstrating that IR+AGuIX combination enhanced the ability of macrophages to be reprogrammed into pro-inflammatory macrophages. These results are consistent with previous publications revealing the functional switch of macrophages from anti-inflammatory to pro-inflammatory phenotype in response to other metallic nanoparticles alone (such as gold-based nanoparticles (36), iron oxide nanoparticles (37) and titanium dioxide nanoparticles (38)) or combined treatments with IR (39). From theoretical point of view, these results suggested that AGuIX should be used alone (without radiotherapy) to re-educate TAMs and to enhance antitumor immune response. Further in vivo investigations are needed to demonstrate the ability of AGuIX to overcome anti-inflammatory programming of TAMs and to remodel immunosuppressive TME in absence of IR.

In this study, we also demonstrated that all treatments used (IR, AGuIX and IR+AGuIX combination) induced the phosphorylation and the activation of the AMPK, which is a central metabolic sensor that regulates cellular energy homeostasis through the modulation of numerous cellular processes such as autophagy (40), oxidative phosphorylation (41), mitochondrial dynamics and integrity (42). We showed that AMPKT172* is rapidly detected in response to treatments and positively correlated with the accumulation of fragmented "stressed" mitochondria in the cytosol of treated macrophages. Interestingly, we demonstrated that pharmacological inhibition (with Dorsomorphin) or genetic depletion of AMPKα2 abolished mitochondrial fragmentation and impaired the pro-inflammatory reprogramming of treated macrophages, thus revealing a counterintuitive link between the AMPK activation, the mitochondrial fragmentation and the pro-inflammatory reprogramming of macrophages. In one hand, the activation of AMPK was previously involved in the promotion of the anti-inflammatory reprogramming of macrophages (43) and the repression of LPS-induced pro-inflammatory reprogramming of astrocytes, microglia and peritoneal macrophages (44). The activation of AMPK was also shown to increase fatty acid oxidation (45). In other hand, the activation of AMPK is required for the fragmentation of mitochondria through the modulation of the dynamin-related protein 1 (DRP1) activity (42) and the mitochondrial fragmentation was

associated metabolic regulation of several immune cells such as lymphocytes, regulatory T cells (46) and NK cells (47). Our results provide the first evidence that the activation of AMPK by IR modulates mitochondrial dynamics and activate ATM for the pro-inflammatory reprogramming of macrophages. Further molecular characterizations are needed to precise the contribution of AMPKT172* and mitochondrial fragmentation to the pro-inflammatory signaling pathway elicited by IR that we previously described (11). Altogether, these results demonstrated that the combination of IR with AGuIX enhanced the ability of anti-inflammatory macrophages to undergo a pro-inflammatory activation in response to IR and might be useful to improve patient's response to radiotherapy through an AMPK-dependent pro-inflammatory reprogramming of TAMs.

Materials and Methods

Cells and Reagents.

The human monocyte cell line THP1 cells and murine RAW264.7 macrophages were maintained in RMPI-1640-Glutamax medium and DMEM-Glutamax medium, respectively, (Life Technologies, Carlsbad, CA, USA) supplemented with 10% heat-inactivated fetal bovine serum (FBS) (Hycultec GmbH, Beutelsbach, Germany) and 100 IU/ml penicillin–streptomycin (Life Technologies). To obtain THP1 macrophages, THP1 monocytes were differentiated with 320 nM of PMA (#tlrl-PMA, Invivogen, San Diego, CA, USA) during 24 hours. Then, cells were washed three times to remove PMA and were rested for additional 24 hours. All cells were maintained under 5% CO2 humidified atmosphere at 37 °C. Dorsomorphin (#3093/10) was from Tocris Bioscience (Bristol, UK). PMA (#tlrl-PMA) was from Invivogen. Gadolinium (Gd)-based AGuIX NPs were synthesized and provided by NH TherAguix company (Lyon, France).

Antibodies.

Antibodies used for immunofluorescence were anti-phospho-H2AX (Ser139) (#05-636) antibody from EMD Millipore (Billerica, MA, USA), anti-phospho-ATM (Ser1981*) (#GTX132146) from Genetex (Irvine, USA), anti-iNOS (#3523) antibody from Abcam (Cambridge, UK), anti-Tom20 (F-10) (#sc-17764) antibody from Santa Cruz Biotechnology (Oregon, USA). Antibodies used for immunoblots were anti-phospho-ATM (Ser1981) (10H1.E12) (#4526), anti-ATM (D2E2) (#2873), anti-phospho-AMPKα (Thr172) (40H9) (#2535), anti-AMPKα (#2532) antibodies from Cell Signaling Technology, anti-IRF5 (#ab21689), anti-beta Actin HRP [AC-15] (#ab49900), anti-IL 1 Beta (#ab2105) antibodies from Abcam, anti-AMPKα2 (#AF2850), anti-IL6 (RD#AB-206-NA) antibodies from R&D Systems (Minneapolis, MN, USA).

Irradiation and treatment with gadolinium-nanoparticle AGuIX.

THP1 macrophages were differentiated in 12-well plates (10^6 cells per well), 24-well plates ($5x10^5$ cells per well) or 48-well plates ($2.5x10^5$ cells per well) as described above. RAW264.7 macrophages were seeded in 24-well plates ($5x10^4$ per well) 24 hours before treatments. The cells were then treated with different concentrations of AGuIX diluted in HBSS (#14025092, Thermo Fisher Scientific) at 37 °C for 1 hour. Afterwards, nanoparticles suspension was replaced with fresh macrophage medium supplemented with 10% FBS, incubated for 1hour at 37 °C and then cells were irradiated at the indicated dose with X-ray irradiator (1 Gy/min, X-RAD 320, Precision X-Ray). Cells were then harvested at 30 min, 1 hour, 24 hours, and 48 hours after irradiation for cell lysates and for immunofluorescence for subsequent experiments. Supernatants (SN) were harvested 48 hours after treatments.

RNA-mediated interference.

The SMARTpool siGENOME Human PRKAA2 (5563) siRNA (M-005361-02-0005) against AMPK alpha-2 and siGENOME non-targeting siRNA Pool #1 (D-001206-13-05) as control were purchased from Dharmacon (Lafayette, CO, USA). Sequences of SMARTpool siGENOME Human PRKAA2 (5563) siRNA are as follows: siRNA-1: 5'-GUACCUACGUUAUUUAAGA-3'; siRNA-2: 5'-GGAAGGUAGUGAAUGCAUA-3'; siRNA-3: 5'-GACAGAAGAUUCGCAGUUU-3'; siRNA-4 :5'-ACAGAAGAUUCGCAGUUUA-3'. The siRNAs used as a control were siGENOME made of a pool of four on-target plus non-targeting siRNAs. PMA-differentiated THP1 macrophages were transfected by double-shot transfection method with Lipofectamine RNAi max (#13778150, Life Technologies, Illkrich, France) according to the manufacturer's instructions. Briefly, THP1 monocytes were differentiated as described above (10^6 cells per ml per well in 12-well plate). The Lipofectamine and siRNA were mixed in Opti-MEM reduced serum medium (Thermo Fisher Scientific) was let to incubate at room temperature for 5 minutes. The transfection mix was then added to the cells to the final concentration of 12 nM siRNAs and cells were incubated at 37 °C for 24 hours. After 24 hours, the medium was replaced by fresh macrophage medium supplemented with 10% FBS and new transfection mix was added. Cells were then incubated for additional 24 hours and used further in subsequent experiments.

Immunofluorescence microscopy.

THP1 macrophages were treated and incubated as described above on 10 mm coverslips (Deckglaser#41001110, Germany) at a concentration of $2.5x10^5$ cells per well in 48-well plates. RAW264.7 macrophages were seeded 24 hours before treatments on 13 mm coverslips (VWR#ECN 631-1578, Germany) in 24-well plates ($5x10^4$ per well). Afterwards, cells were rinsed once with PBS, fixed with 4% (w/v) paraformaldehyde (Sigma-Aldrich, Germany) for 10 minutes and then permeabilized with 0.3% Triton X-100 (Sigma-Aldrich, Germany) in PBS for 20 minutes. After two times rinsing with DPBS 1X (Gibco), the cells were blocked with 10% FBS in PBS for 1 hour, followed by incubation with primary antibodies in 10% FBS in PBS (at a dilution 1:100, except for anti-iNOS antibody (1:500) and anti-ATMS1981 (1:50)) for 1 hour and 30 minutes at room temperature. Subsequently, cells were washed with PBS three times and were incubated with the secondary antibodies Alexa Fluor-488 green or Alexa Fluor-546 red (Life Technologies, Illkrich, France) (at a dilution 1:500) and Hoechst 33342 for nuclei (Thermo Fisher Scientific) (at a dilution 1:1000) diluted in 10% FBS in DPBS 1X (Gibco) for 30 min at room temperature. The samples were then washed three times and mounted with Fluoromount-G (SouthernBiotech, Birmingham, AL, USA) on microscope slides (Thermo Fisher Scientific). The quantification of cells (from minimum 300 cells from at least independent 5 fields for each condition) were performed with Leica DMI8 fluorescent microscopy (Leica Microsystems, Nanterre, France) using a 63X oil objective. For representative images illustration in the figures, cells from different conditions were acquired by confocal microscopy (SP8, Leica) by hybrid detectors (pinhole airy: 0.6; pixel size: 180 nm) with optimal optical sectioning (OOS) of 0.8 μm from the top to the botom of each cell and then cells were constructed on max-intensity of z projection images using Image J software.

Western blot analysis.

Cells were washed once with cold PBS and total cellular proteins were extracted in Chaps buffer (10 mM TRIS (pH = 7.4), 850 mM NaCl, and 0.1% (3cholamidopropyl) dimethylamonio]-1-propanesulfonate (Chaps)) complemented with protease and phosphatase inhibitors (Roche, Basel, Switzerland) for 20 minutes. About 3-30 μg of protein extract were run on 4-12%, 10% or 12% NuPAGE gels (Invitrogen, Illkrich, France) and then were

transferred onto a nitrocellulose membrane (0.2 µm Bio-Rad, Marnes-la-coquette, France) at room temperature. After incubation with 5% bovine serum albumin (BSA) in Tris-buffered saline and 0.1% Tween 20 (TBS-T) at room temperature for 1 hour, membranes were then subsequently incubated with primary antibodies overnight at 4 °C. Afterwards, membranes were incubated with appropriate horseradish peroxidase-conjugated anti-rabbit or anti-mouse IgG (SouthernBiotech, Birmingham, AL, USA) for 2 hours at room temperature. Then, membranes were washed three times with TBS-T and were revealed using G:BOX Chemi XL1.4 Fluorescent & Chemiluminescent Imaging System (Syngene, Cambridge, UK).

Statistical analysis.

Statistical analysis of data was performed by using two-way ANOVA test (for Figures 1C, 1F, 2C, 2F), one-way ANOVA test (for Figures 1G, 1I, 3F, 3G, 4E) or Student's t-test (for Figure 4C). Statistical parameters including precisions measures (mean±SEM) and statistical significances for each analysis are shown in the Figures and the Figures legends. All values were expressed as the mean±SEM of at least three independent experiments. GraphPad Prism version 6.0b (GraphPad Software, La Jolla, CA, USA) was used to perform statistical analysis.

Acknowledgements

This work has benefited from the facilities and expertise of the Imaging and Cytometry Platform UMS 3655 CNRS / US 23 INSERM, Gustave Roussy Cancer Campus Villejuif, France. This work has been supported by funds from Agence Nationale de la Recherche (ANR-10-IBHU-0001, ANR-10-LABX33, ANR-11-IDEX-003-01 and ANR Flash COVID-19 "MAcCOV"), Fondation Gustave Roussy, Institut National du Cancer (INCa 9414 and INCa 16087), The SIRIC Stratified Oncology Cell DNA Repair and Tumor Immune Elimination (SOCRATE), FHU Cancer and Autoimmune / inflammatory diseases Relationships (CARE) (directed by X. Mariette, Kremlin Bicêtre AP-HP), Université Paris-Saclay and by the Fondation ARC pour la recherche sur le cancer www.fondation-arc.org (to J.-L. P.) and The SIRIC Stratified Oncology Cell DNA Repair and Tumor Immune Elimination 2.0 (SOCRATE 2.0, INCA-DGOS-INSERM 12551) (to A. A.). D. T. is recipient of PhD fellowship from CIFRE with NH TherAguix and ANRT. D. L. is supported by the Laboratory of Excellence LERMIT with a grant from ANR (ANR-10-LABX-33) under the program "Investissements d'Avenir" ANR-11-IDEX-0003-01. Z. M., A. D.-N., E. G.-M. and C. M. are recipients of PhD fellowships from Université Paris-Saclay and A. M.-K. is recipient of PhD fellowship from "Ecole et Loisirs".

Author Contributions

Z. M., D. T. and A. A. performed experiments. J-L. P. designed the study. Z. M., D. T., A. A. and J-L. P. analyzed the results, assembled the figures and wrote the paper. Z. M. and A. A. performed statistical analysis. D.L., A. D.-N., E. G.-M., A. M.-K., C. L., S. B., A. P., S. D., G. L., F. L. and O.T. provided advices and edited the paper.

Competing Financial Interests

J.-L. P. reports research grants from NH TherAguix and Wonna Therapeutics and is founder of Findimmune, a biotech company devoted to develop novel anticancer treatments including therapeutic strategies for TAMs reprogramming. A. A., S. D., G. L. are currently employees of NH TherAguix. D. T. is recipient of a CIFRE contract in partnership with NH TherAguix. J.-L. P. and A. A. are co-inventors on patents (WO2016185026;WO2018050928), relating to macrophage reprogramming. J.-L. P., A. A., F. L. and O.T are co-inventors on patents (WO21019/008040A1; WO2021/053173A1), relating to AGuIX and relevant to the current work. G.L., F. L. and O.T are co-inventors on patent (WO2011135101), relating to AGuIX. The remaining authors declare no competing interests.

References

1. Bejarano L, Jordao MJC, Joyce JA. Therapeutic Targeting of the Tumor Microenvironment. Cancer Discov. 2021;11(4):933-59.

2. Guerriero JL. Macrophages: The Road Less Traveled, Changing Anticancer Therapy. Trends Mol Med. 2018;24(5):472-89.

3. Mantovani A, Marchesi F, Malesci A, Laghi L, Allavena P. Tumour-associated macrophages as treatment targets in oncology. Nat Rev Clin Oncol. 2017;14(7):399-416.

4. Qiu Y, Chen T, Hu R, Zhu R, Li C, Ruan Y, et al. Next frontier in tumor immunotherapy: macrophage-mediated immune evasion. Biomark Res. 2021;9(1):72.

5. Biswas SK, Mantovani A. Macrophage plasticity and interaction with lymphocyte subsets: cancer as a paradigm. Nat Immunol. 2010;11(10):889-96.

6. Pathria P, Louis TL, Varner JA. Targeting Tumor-Associated Macrophages in Cancer. Trends Immunol. 2019;40(4):310-27.

7. Feng M, Jiang W, Kim BYS, Zhang CC, Fu YX, Weissman IL. Phagocytosis checkpoints as new targets for cancer immunotherapy. Nat Rev Cancer. 2019;19(10):568-86.

8. Bruni D, Angell HK, Galon J. The immune contexture and Immunoscore in cancer prognosis and therapeutic efficacy. Nat Rev Cancer. 2020;20(11):662-80.

9. Noy R, Pollard JW. Tumor-associated macrophages: from mechanisms to therapy. Immunity. 2014;41(1):49-61.

10. Wu Q, Allouch A, Martins I, Brenner C, Modjtahedi N, Deutsch E, et al. Modulating Both Tumor Cell Death and Innate Immunity Is Essential for Improving Radiation Therapy Effectiveness. Front Immunol. 2017;8:613.

11. Wu Q, Allouch A, Paoletti A, Leteur C, Mirjolet C, Martins I, et al. NOX2-dependent ATM kinase activation dictates pro-inflammatory macrophage phenotype and improves effectiveness to radiation therapy. Cell Death Differ. 2017;24(9):1632-44.

12. Hainfeld JF, Slatkin DN, Focella TM, Smilowitz HM. Gold nanoparticles: a new X-ray contrast agent. Br J Radiol. 2006;79(939):248-53.

13. Dorsey JF, Sun L, Joh DY, Witztum A, Kao GD, Alonso-Basanta M, et al. Gold nanoparticles in radiation research: potential applications for imaging and radiosensitization. Transl Cancer Res. 2013;2(4):280-91.

14. Taupin F, Flaender M, Delorme R, Brochard T, Mayol JF, Arnaud J, et al. Gadolinium nanoparticles and contrast agent as radiation sensitizers. Phys Med Biol. 2015;60(11):4449-64.

15. McQuaid HN, Muir MF, Taggart LE, McMahon SJ, Coulter JA, Hyland WB, et al. Imaging and radiation effects of gold nanoparticles in tumour cells. Sci Rep. 2016;6:19442.

16.

Wang H, Mu X, He H, Zhang XD. Cancer Radiosensitizers. Trends Pharmacol Sci. 2018;39(1):24-48.

17. Le Duc G, Miladi I, Alric C, Mowat P, Brauer-Krisch E, Bouchet A, et al. Toward an image-guided microbeam radiation therapy using gadolinium-based nanoparticles. ACS Nano. 2011;5(12):9566-74.

18. Dufort S, Bianchi A, Henry M, Lux F, Le Duc G, Josserand V, et al. Nebulized gadolinium-based nanoparticles: a theranostic approach for lung tumor imaging and radiosensitization. Small. 2015;11(2):215-21.

19. Hainfeld JF, Slatkin DN, Smilowitz HM. The use of gold nanoparticles to enhance radiotherapy in mice. Phys Med Biol. 2004;49(18):N309-15.

20. Lakshmanan VK, Jindal S, Packirisamy G, Ojha S, Lian S, Kaushik A, et al. Nanomedicine-based cancer immunotherapy: recent trends and future perspectives. Cancer Gene Ther. 2021.

21. Irvine DJ, Dane EL. Enhancing cancer immunotherapy with nanomedicine. Nat Rev Immunol. 2020;20(5):321-34.

22. Du Y, Sun H, Lux F, Xie Y, Du L, Xu C, et al. Radiosensitization Effect of AGuIX, a Gadolinium-Based Nanoparticle, in Nonsmall Cell Lung Cancer. ACS Appl Mater Interfaces. 2020;12(51):56874-85.

23. Gao Z, Li Y, Wang F, Huang T, Fan K, Zhang Y, et al. Mitochondrial dynamics controls anti-tumour innate immunity by regulating CHIP-IRF1 axis stability. Nat Commun. 2017;8(1):1805.

24. Herzig S, Shaw RJ. AMPK: guardian of metabolism and mitochondrial homeostasis. Nat Rev Mol Cell Biol. 2018;19(2):121-35.

25. Hawley SA, Davison M, Woods A, Davies SP, Beri RK, Carling D, et al. Characterization of the AMP-activated protein kinase kinase from rat liver and identification of threonine 172 as the major site at which it phosphorylates AMP-activated protein kinase. J Biol Chem. 1996;271(44):27879-87.

26. DeNardo DG, Ruffell B. Macrophages as regulators of tumour immunity and immunotherapy. Nat Rev Immunol. 2019;19(6):369-82.

27. Cassetta L, Pollard JW. Targeting macrophages: therapeutic approaches in cancer. Nat Rev Drug Discov. 2018;17(12):887-904.

28. Tap WD, Wainberg ZA, Anthony SP, Ibrahim PN, Zhang C, Healey JH, et al. Structure-Guided Blockade of CSF1R Kinase in Tenosynovial Giant-Cell Tumor. N Engl J Med. 2015;373(5):428-37.

29. Moughon DL, He H, Schokrpur S, Jiang ZK, Yaqoob M, David J, et al. Macrophage Blockade Using CSF1R Inhibitors Reverses the Vascular Leakage Underlying Malignant Ascites in Late-Stage Epithelial Ovarian Cancer. Cancer Res. 2015;75(22):4742-52.

30. Loberg RD, Ying C, Craig M, Day LL, Sargent E, Neeley C, et al. Targeting CCL2 with systemic delivery of neutralizing antibodies induces prostate cancer tumor regression in vivo. Cancer Res. 2007;67(19):9417-24.

31. Yang Z, Li H, Wang W, Zhang J, Jia S, Wang J, et al. CCL2/CCR2 Axis Promotes the Progression of Salivary Adenoid Cystic Carcinoma via Recruiting and Reprogramming the Tumor-Associated Macrophages. Front Oncol. 2019;9:231.

32. Molgora M, Esaulova E, Vermi W, Hou J, Chen Y, Luo J, et al. TREM2 Modulation Remodels the Tumor Myeloid Landscape Enhancing Anti-PD-1 Immunotherapy. Cell. 2020;182(4):886-900 e17.

33. Kaneda MM, Cappello P, Nguyen AV, Ralainirina N, Hardamon CR, Foubert P, et al. Macrophage PI3Kgamma Drives Pancreatic Ductal Adenocarcinoma Progression. Cancer Discov. 2016;6(8):870-85.

34. Hu P, Fu Z, Liu G, Tan H, Xiao J, Shi H, et al. Gadolinium-Based Nanoparticles for Theranostic MRI-Guided Radiosensitization in Hepatocellular Carcinoma. Front Bioeng Biotechnol. 2019;7:368.

35. Sancey L, Lux F, Kotb S, Roux S, Dufort S, Bianchi A, et al. The use of theranostic gadolinium-based nanoprobes to improve radiotherapy efficacy. Br J Radiol. 2014;87(1041):20140134.

36. Yen HJ, Hsu SH, Tsai CL. Cytotoxicity and immunological response of gold and silver nanoparticles of different sizes. Small. 2009;5(13):1553-61.

37. Zanganeh S, Hutter G, Spitler R, Lenkov O, Mahmoudi M, Shaw A, et al. Iron oxide nanoparticles inhibit tumour growth by inducing pro-inflammatory macrophage polarization in tumour tissues. Nat Nanotechnol. 2016;11(11):986-94.

38. Zhao F, Wang C, Yang Q, Han S, Hu Q, Fu Z. Titanium dioxide nanoparticle stimulating pro-inflammatory responses in vitro and in vivo for inhibited cancer metastasis. Life Sci. 2018;202:44-51.

39. Jin JZ, Q. Engineering nanoparticles to reprogram radiotherapy and immunotherapy: recent advances and future challenges J Nanobiotechnology. 2020;18(1):75.

40. Kim J, Kundu M, Viollet B, Guan KL. AMPK and mTOR regulate autophagy through direct phosphorylation of Ulk1. Nat Cell Biol. 2011;13(2):132-41.

41. Tailor D, Going CC, Resendez A, Kumar V, Nambiar DK, Li Y, et al. Novel Aza-podophyllotoxin derivative induces oxidative phosphorylation and cell death via AMPK activation in triple-negative breast cancer. Br J Cancer. 2021;124(3):604-15.

42. Toyama EQ, Herzig S, Courchet J, Lewis TL, Jr., Loson OC, Hellberg K, et al. Metabolism. AMP-activated protein kinase mediates mitochondrial fission in response to energy stress. Science. 2016;351(6270):275-81.

43. Sag D, Carling D, Stout RD, Suttles J. Adenosine 5'-monophosphate-activated protein kinase promotes macrophage polarization to an anti-inflammatory functional phenotype. J Immunol. 2008;181(12):8633-41.

44. Giri S, Nath N, Smith B, Viollet B, Singh AK, Singh I. 5-aminoimidazole-4-carboxamide-1-beta-4-ribofuranoside inhibits proinflammatory response in glial cells: a possible role of AMP-activated protein kinase. J Neurosci. 2004;24(2):479-87.

45. Pilon G, Dallaire P, Marette A. Inhibition of inducible nitric-oxide synthase by activators of AMP-activated protein kinase: a new mechanism of action of insulin-sensitizing drugs. J Biol Chem. 2004;279(20):20767-74.

46. Field CS, Baixauli F, Kyle RL, Puleston DJ, Cameron AM, Sanin DE, et al. Mitochondrial Integrity Regulated by Lipid Metabolism Is a Cell-Intrinsic Checkpoint for Treg Suppressive Function. Cell Metab. 2020;31(2):422-37 e5.

47. Zheng X, Qian Y, Fu B, Jiao D, Jiang Y, Chen P, et al. Mitochondrial fragmentation limits NK cell-based tumor immunosurveillance. Nat Immunol. 2019;20(12):1656-67.

Figure legends

Figure 1. AGuIX alone and combined treatment with ionizing radiation induces DNA damage and DNA damage response in macrophages. (A, B) Confocal microscopy images of not activated phorbol-12-myristate-13-acetate (PMA)-differentiated human THP1 macrophages showing γ-H2AX$^+$ foci detected after 30 minutes of treatment with control, 100 nM AGuIX, 0.2 Gy single-dose irradiation, 100 nM AGuIX combined with 0.2 Gy single-dose irradiation (A) or (B) control, 200 nM AGuIX, 0.2 Gy single-dose irradiation, 200 nM AGuIX combined with 0.2 Gy single-dose irradiation are shown (scale bar, 5 μm). Images are representative from 3 independent experiments. (C) Percentage of γ-H2AX$^+$ foci detected on PMA-differentiated human THP1 macrophages after 30 minutes, 1 hour, 2 hours or 48 hours of treatment with control, 100 nM AGuIX, 200 nM AGuIX, 0.2 Gy single-dose irradiation, 100 nM AGuIX combined with 0.2 Gy single-dose irradiation, or 200 nM AGuIX combined with 0.2 Gy single-dose irradiation at corresponding time points are shown. (D, E) Representative confocal microscopy images of PMA-differentiated human THP1 macrophages from three independent experiments showing γ-H2AX$^+$ foci detected 1 hour after treatment with (D) control, 0.6 mM AGuIX, 0.2 Gy single-dose irradiation, 0.6 mM AGuIX combined with 0.2 Gy single-dose irradiation or (E) control, 1.2 mM AGuIX, 0.2 Gy single-dose irradiation, 1.2 mM AGuIX combined with 0.2 Gy single-dose irradiation are illustrated (scale bar, 5 μm). (F, G) Percentage of γ-H2AX$^+$ foci cells detected on PMA-differentiated human THP1 macrophages at 1 hour, 2 hours or 24 hours (F) or detected on murine RAW264.7 macrophages at 1 hour (G) after treatments with control, 0.6 mM AGuIX, 1.2 mM AGuIX, 0.2 Gy single-dose irradiation, 0.6 mM AGuIX combined with 0.2 Gy single-dose irradiation, or 1.2 mM AGuIX combined with 0.2 Gy single-dose irradiation. (H) ATMS1981* and ATM expressions that have been detected in PMA-differentiated human THP1 macrophages after 30 minutes treatment with control, 100 nM AGuIX, 200 nM AGuIX, 0.2 Gy single-dose irradiation, 100 nM AGuIX combined with 0.2 Gy single-dose irradiation, or 200 nM AGuIX combined with 0.2 Gy single-dose irradiation. Representative immunoblot is shown. Actin is used as loading control. (I) Percentage of ATMS1981*$^+$ cells detected on murine RAW264.7 macrophages treated as in (G). Data are means ± S.E.M from three independent experiments. P-values (****P< 0.0001, ***P< 0.001 and *P<0.05) were calculated by using two-way ANOVA test (for C and F) and one-way ANOVA test (for G and I).

Figure 2. AGuIX alone and combined treatment with ionizing radiation activates macrophages toward a pro-inflammatory phenotype. (A, B) Confocal microscopy images of not activated PMA-differentiated human THP1 macrophages expressing iNOS detected after 48 hours of treatment with (A) control, 100 nM AGuIX, 0.2 Gy single-dose irradiation, 100 nM AGuIX combined with 0.2 Gy single-dose irradiation or (B) control, 200 nM AGuIX, 0.2 Gy single-dose irradiation, 200 nM AGuIX combined with 0.2 Gy single-dose irradiation are shown (scale bar, 5 μm). Images are representative from 3 independent experiments. (C) Percentage of $iNOS^+$ cells detected on PMA-differentiated human THP1 macrophages after 30 minutes, 1 hour, 2 hours or 48 hours of treatment with control, 100 nM AGuIX, 200 nM AGuIX, 0.2 Gy single-dose irradiation, 100 nM AGuIX combined with 0.2 Gy single-dose irradiation, or 200 nM AGuIX combined with 0.2 Gy single-dose irradiation at corresponding time points are shown. (D, E) Representative confocal microscopy images of PMA-differentiated human THP1 macrophages from three independent experiments showing $iNOS^+$ cells detected 24 hours after treatment with (D) control, 0.6 mM AGuIX, 0.2 Gy single-dose irradiation, 0.6 mM AGuIX combined with 0.2 Gy single-dose irradiation or (E) control, 1.2mM AGuIX, 0.2 Gy single-dose irradiation, 1.2 mM AGuIX combined with 0.2 Gy single-dose irradiation are illustrated (scale bar, 5 μm). (F) Percentage of $iNOS^+$ cells detected on PMA-differentiated human THP1 macrophages after 1 hour, 2 hours or 24 hours treatment with control, 0.6 mM AGuIX, 1.2 mM AGuIX, 0.2 Gy single-dose irradiation, 0.6 mM AGuIX combined with 0.2 Gy single-dose irradiation, or 1.2 mM AGuIX combined with 0.2 Gy single-dose irradiation. (G-I) IRF5 expression (G, H) and secretion of IL-1β and IL6 (I) detected after 48 hours treatment of PMA-differentiated human THP1 macrophages with control, 100 nM AGuIX, 200 nM AGuIX, 0.2 Gy single-dose irradiation, 100 nM AGuIX combined with 0.2 Gy single-dose irradiation, or 200 nM AGuIX combined with 0.2 Gy single-dose irradiation (G, I) or with control, 0.6 mM AGuIX, 1.2 mM AGuIX, 0.2 Gy single-dose irradiation, 0.6 mM AGuIX combined with 0.2 Gy single-dose irradiation, or 1.2 mM AGuIX combined with 0.2 Gy single-dose irradiation (H). Representative immunoblots are shown. Actin is used as loading control. Data are means ± S.E.M from three independent experiments. P-values (****$P< 0.0001$, ***$P< 0.001$,**$P< 0.01$ *$P<0.05$) were calculated by using two-way ANOVA test.

Figure 3. AGuIX alone and combined treatment with ionizing radiation alters macrophage mitochondrial dynamics and activates AMPK. (A-D) Confocal microscopy images of 3D reconstructions of the mitochondrial networks on not activated PMA-differentiated human THP1 macrophages stained for TOM20 after 1 hour of treatment with control, 100 nM AGuIX, 0.2 Gy single-dose irradiation, 100 nM AGuIX combined with 0.2 Gy single-dose irradiation (A), or control, 200 nM AGuIX, 0.2 Gy single-dose irradiation, 200 nM AGuIX combined with 0.2 Gy single-dose irradiation (B) or control, 0.6 mM AGuIX, 0.2 Gy single-dose irradiation, 0.6 mM AGuIX combined with 0.2 Gy single-dose irradiation (C), or control, 1.2 mM AGuIX, 0.2 Gy single-dose irradiation, 1.2 mM AGuIX combined with 0.2 Gy single-dose irradiation (D) are shown (scale bar, 5 μm). Images are representative from 3 independent experiments. (E) Higher magnification details of the mitochondrial networks in A, B, C and D are shown respectively (scale bar, 1 μm). (F, G) Frequency of PMA-differentiated human THP1 macrophages showing mitochondrial fragmentation after 1 hour treatment with control, 100 nM AGuIX, 200 nM AGuIX, 0.2 Gy single-dose irradiation, 100 nM AGuIX combined with 0.2 Gy single-dose irradiation, 200 nM AGuIX combined with 0.2 Gy single-dose irradiation (F) or control, 0.6 mM AGuIX, 1.2 mM AGuIX, 0.2 Gy single-dose irradiation, 0.6 mM AGuIX combined with 0.2 Gy single-dose irradiation, or 1.2 mM AGuIX combined with 0.2 Gy single-dose irradiation (G). (H, I) AMPK and the phosphorylation of the AMPK on threonine 172 (AMPK172*) expressions detected on PMA-differentiated human THP1 macrophages after 1 hour treatment with control, 100 nM AGuIX, 200 nM AGuIX, 0.2 Gy single-dose irradiation, 100 nM AGuIX combined with 0.2 Gy single-dose irradiation, 200 nM AGuIX combined with 0.2 Gy single-dose irradiation (H) or control, 0.6 mM AGuIX, 1.2 mM AGuIX, 0.2 Gy single-dose irradiation, 0.6 mM AGuIX combined with 0.2 Gy single-dose irradiation, or 1.2 mM AGuIX combined with 0.2 Gy single-dose irradiation (I). Representative immunoblots are shown. Actin is used as loading control. Data are means ± S.E.M from three independent experiments. P-values (****P< 0.0001,**P< 0.01) were calculated by using one-way ANOVA test.

Figure 4. AMPK is required for mitochondrial fragmentation and pro-inflammatory reprogramming of macrophages induced by AGuIX alone and their combination with ionizing radiation. (A, B) AMPK172* (A), AMPK (A) and IFR5 (B) expressions after, respectively, 1 hour and 48 hours of culture of not activated PMA-differentiated human THP1

macrophages that have been incubated with 10 μM of dorsomorphin (DRS) and treated with control, 200 nM AGuIX, 0.2 Gy single-dose irradiation, or 200 nM AGuIX combined with 0.2 Gy single-dose irradiation. Representative immunoblots are shown. Actin is used as loading control. (C) Western blot analysis and its quantification to measure AMPKα2 expression in siAMPKα2 treated PMA-differentiated human THP1 macrophages at 48 hours after transfection. Representative immunoblot is shown. Actin is used as loading control. (D, E) Confocal micrographs (D) and frequency (E) of PMA-THP1 macrophages showing mitochondrial fragmentation after 1 hour culture of PMA-THP1 macrophages depleted for AMPKα2 and treated with control, 1.2 mM AGuIX, 0.2 Gy single-dose irradiation, or 1.2 mM AGuIX combined with 0.2 Gy single-dose irradiation. Magnifications are shown in a-h. (F) ATMS1981*, ATM, AMPKα2 and IRF5 expressions after 24 hours of culture of PMA-differentiated human THP1 macrophages depleted for AMPKα2 and treated with control, 1.2mM AGuIX, 0.2 Gy single-dose irradiation, or 1.2mM AGuIX combined with 0.2 Gy single-dose irradiation. Representative immunoblot is shown. Actin is used as loading control. Data are means ± S.E.M from three independent experiments. P-values (*P< 0.05, ****P< 0.0001 and ***P< 0.001) were calculated by using unpaired Student's t-test (C) or one-way ANOVA test (E).

Figure 5. Proposed model for the roles of AMPK and mitochondrial fragmentation in the pro-inflammatory macrophage reprogramming detected in response to IR, AGuIX alone and AGuIX+ IR combination.

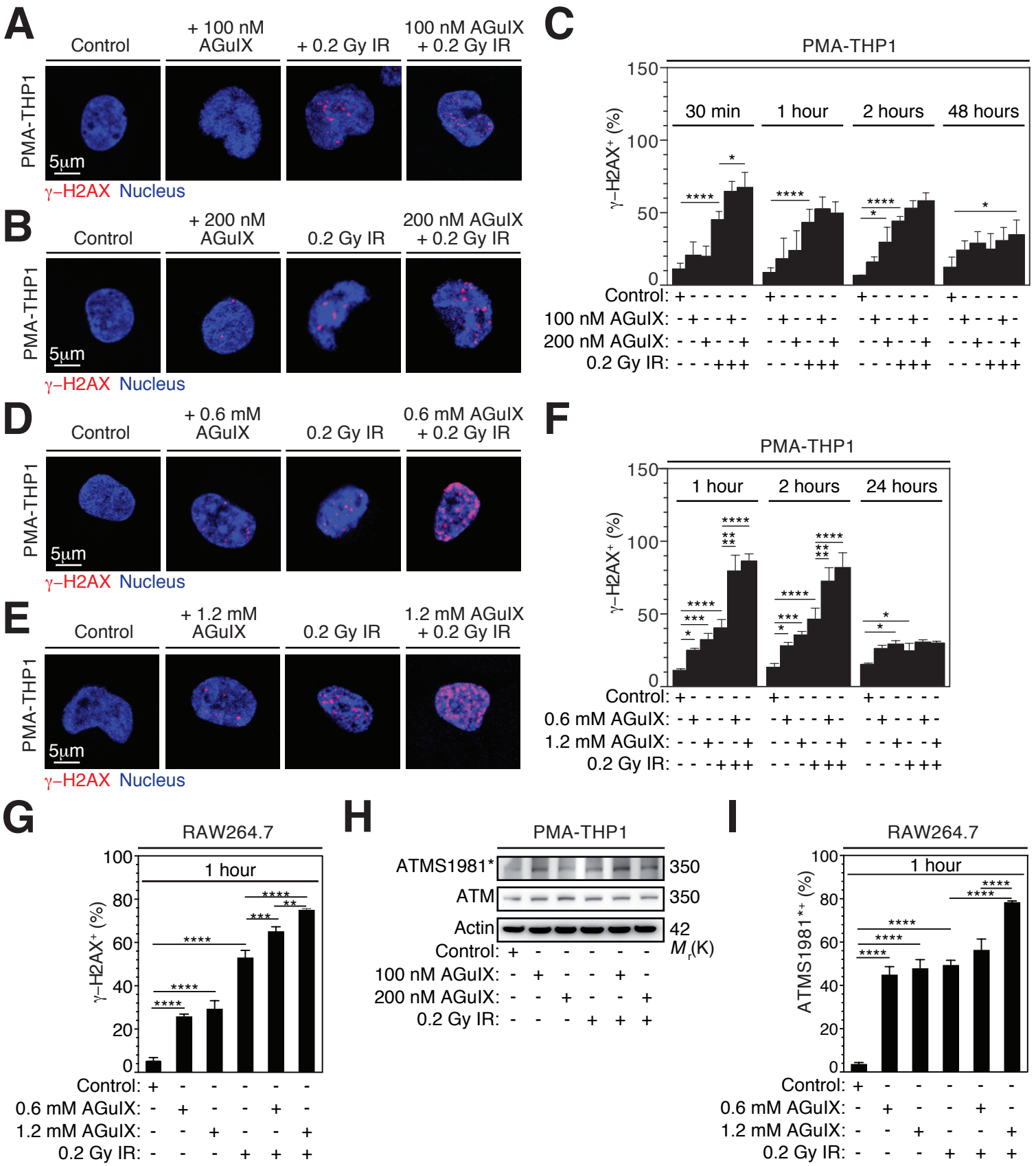
A
Control
+ 100 nM AGuIX
+ 0.2 Gy IR
100 nM AGuIX + 0.2 Gy IR
PMA-THP1
5μm
γ–H2AX Nucleus
B
Control
+ 200 nM AGuIX
0.2 Gy IR
200 nM AGuIX + 0.2 Gy IR
PMA-THP1
5μm
γ–H2AX Nucleus
C
PMA-THP1
30 min
1 hour
2 hours
48 hours
γ–H2AX+ (%)
150
100
50
0
Control: + - - - - - + - - - - - + - - - - - + - - - - -
100 nM AGuIX: - + - - + - - + - - + - - + - - + - - + - - +
200 nM AGuIX: - - + - - + - - + - - + - - + - - + - - + - -
0.2 Gy IR: - - - + + + - - - + + + - - - + + + - - - + + +
D
Control
+ 0.6 mM AGuIX
0.2 Gy IR
0.6 mM AGuIX + 0.2 Gy IR
PMA-THP1
5μm
γ–H2AX Nucleus
E
Control
+ 1.2 mM AGuIX
0.2 Gy IR
1.2 mM AGuIX + 0.2 Gy IR
PMA-THP1
5μm
γ–H2AX Nucleus
F
PMA-THP1
1 hour
2 hours
24 hours
γ–H2AX+ (%)
150
100
50
0
Control: + - - - - - + - - - - - + - - - - -
0.6 mM AGuIX: - + - - + - - + - - + - - + - - + - - + - - +
1.2 mM AGuIX: - - + - - + - - + - - + - - + - - + - - + - -
0.2 Gy IR: - - - + + + - - - + + + - - - + + + - - - + + +
G
RAW264.7
1 hour
γ–H2AX+ (%)
100
80
60
40
20
0
Control: + - - - - -
0.6 mM AGuIX: - + - - + -
1.2 mM AGuIX: - - + - - +
0.2 Gy IR: - - - + + +
H
PMA-THP1
ATMS1981*
ATM
Actin
350
350
42
Mr(K)
Control: + - - - - -
100 nM AGuIX: - + - - + -
200 nM AGuIX: - - + - - +
0.2 Gy IR: - - - + + +
I
RAW264.7
1 hour
ATMS1981**+ (%)
100
80
60
40
20
0
Control: + - - - - -
0.6 mM AGuIX: - + - - + -
1.2 mM AGuIX: - - + - - +
0.2 Gy IR: - - - + + +

MURADOVA#1

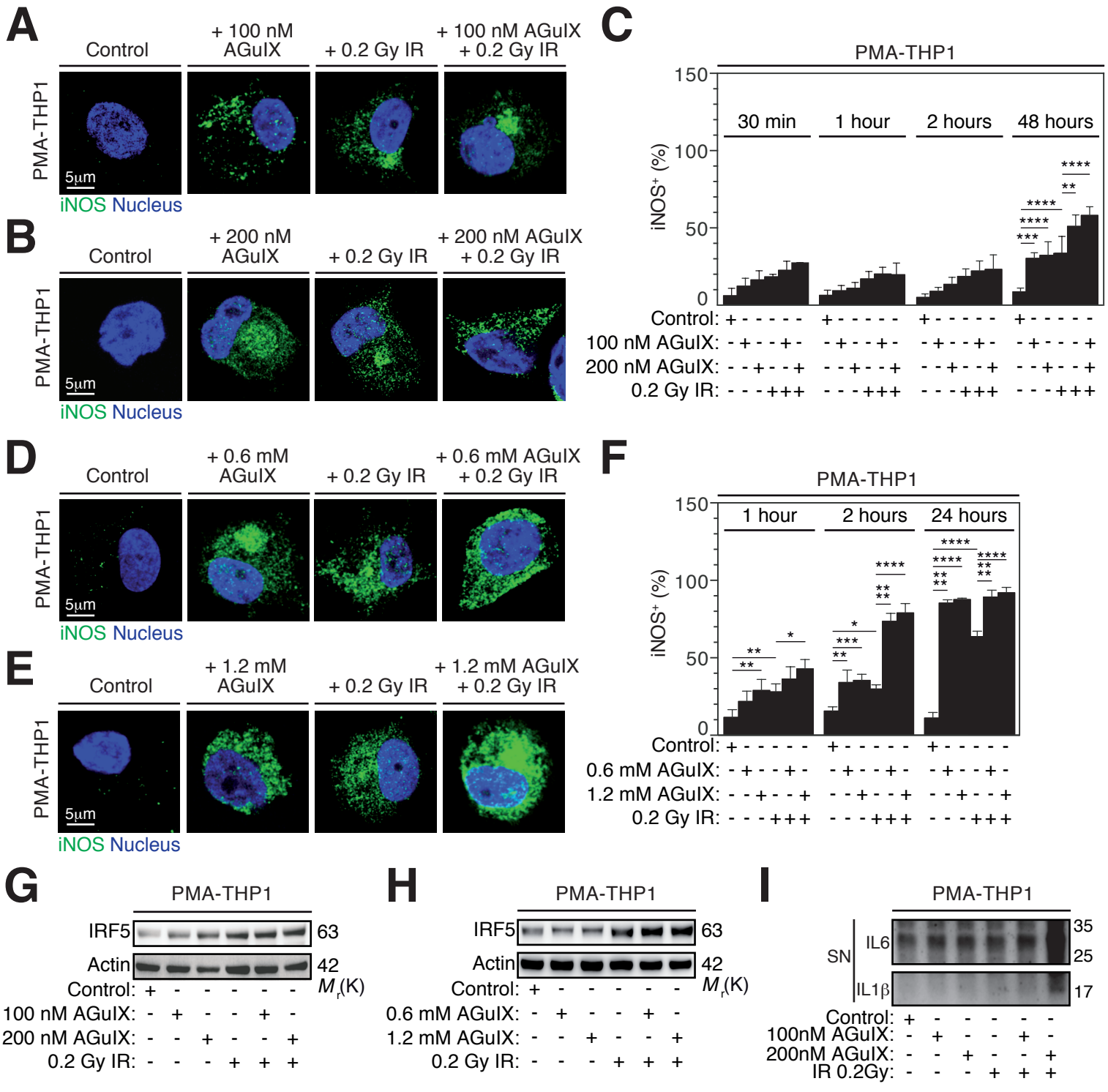
A
Control
+ 100 nM AGuIX
+ 0.2 Gy IR
+ 100 nM AGuIX + 0.2 Gy IR
PMA-THP1
5μm
iNOS Nucleus
B
Control
+ 200 nM AGuIX
+ 0.2 Gy IR
+ 200 nM AGuIX + 0.2 Gy IR
PMA-THP1
5μm
iNOS Nucleus
C
PMA-THP1
30 min
1 hour
2 hours
48 hours
iNOS+ (%)
150
100
50
0
Control: + - - - - - + - - - - - + - - - - - + - - - - -
100 nM AGuIX: - + - - + - - + - - + - - + - - + - - + - -
200 nM AGuIX: - - + - - + - - + - - + - - + - - + - - + -
0.2 Gy IR: - - - + + + - - - + + + - - - + + + - - - + + +
D
Control
+ 0.6 mM AGuIX
+ 0.2 Gy IR
+ 0.6 mM AGuIX + 0.2 Gy IR
PMA-THP1
5μm
iNOS Nucleus
E
Control
+ 1.2 mM AGuIX
+ 0.2 Gy IR
+ 1.2 mM AGuIX + 0.2 Gy IR
PMA-THP1
5μm
iNOS Nucleus
F
PMA-THP1
1 hour
2 hours
24 hours
iNOS+ (%)
150
100
50
0
Control: + - - - - - + - - - - - + - - - - -
0.6 mM AGuIX: - + - - + - - + - - + - - + - - + - - + - -
1.2 mM AGuIX: - - + - - + - - + - - + - - + - - + - - + -
0.2 Gy IR: - - - + + + - - - + + + - - - + + + - - - + + +
G
PMA-THP1
IRF5
63
Actin
42
Mr(K)
Control: + - - - - -
100 nM AGuIX: - + - - + -
200 nM AGuIX: - - + - - +
0.2 Gy IR: - - - + + +
H
PMA-THP1
IRF5
63
Actin
42
Mr(K)
Control: + - - - - -
0.6 mM AGuIX: - + - - + -
1.2 mM AGuIX: - - + - - +
0.2 Gy IR: - - - + + +
I
PMA-THP1
SN
IL6
IL1β
35
25
17
Control: + - - - - -
100nM AGuIX: - + - - + -
200nM AGuIX: - - + - - +
IR 0.2Gy: - - - + + +

MURADOVA#2

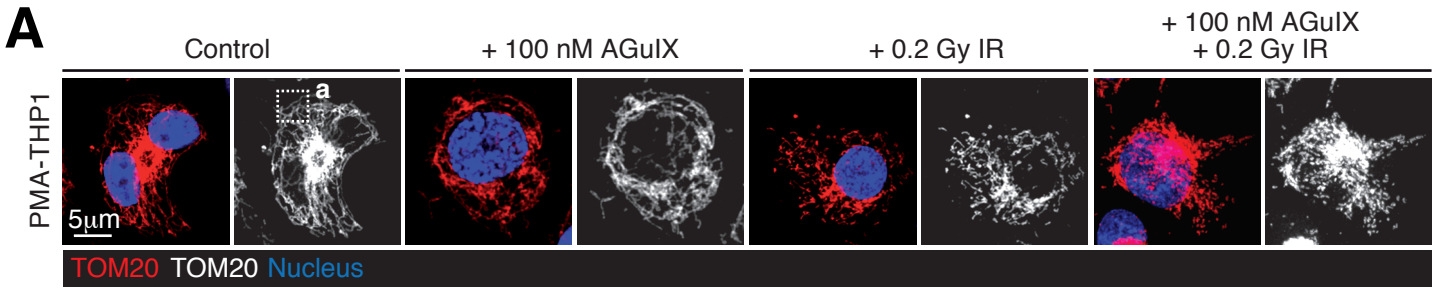
A
Control
+ 100 nM AGuIX
+ 0.2 Gy IR
+ 100 nM AGuIX
+ 0.2 Gy IR
PMA-THP1
a
5μm
TOM20 TOM20 Nucleus

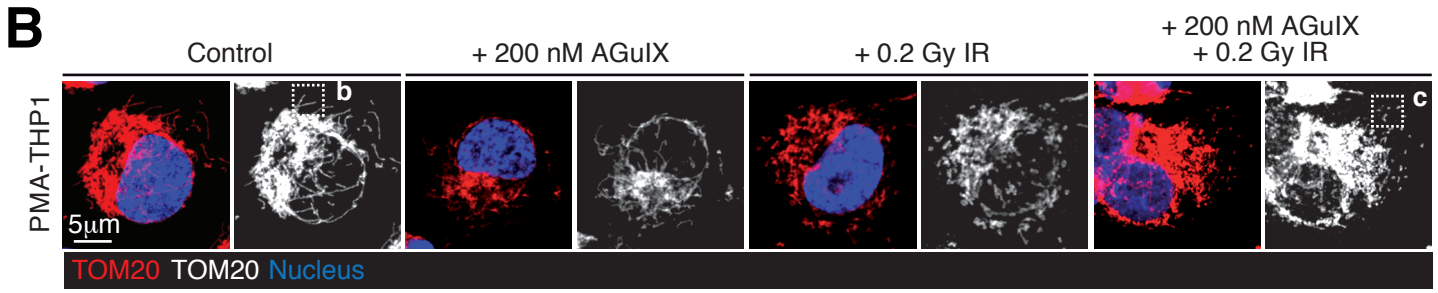
B
Control
+ 200 nM AGuIX
+ 0.2 Gy IR
+ 200 nM AGuIX
+ 0.2 Gy IR
PMA-THP1
b
c
5μm
TOM20 TOM20 Nucleus

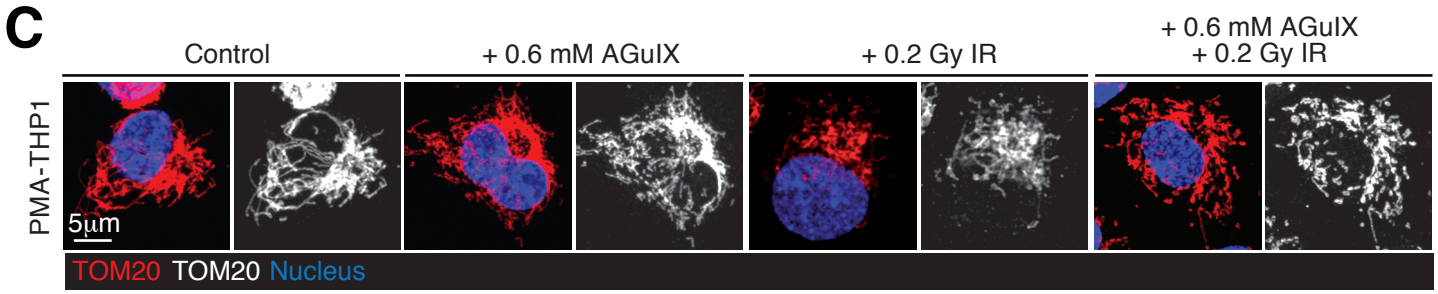
C
Control
+ 0.6 mM AGuIX
+ 0.2 Gy IR
+ 0.6 mM AGuIX
+ 0.2 Gy IR
PMA-THP1
5μm
TOM20 TOM20 Nucleus

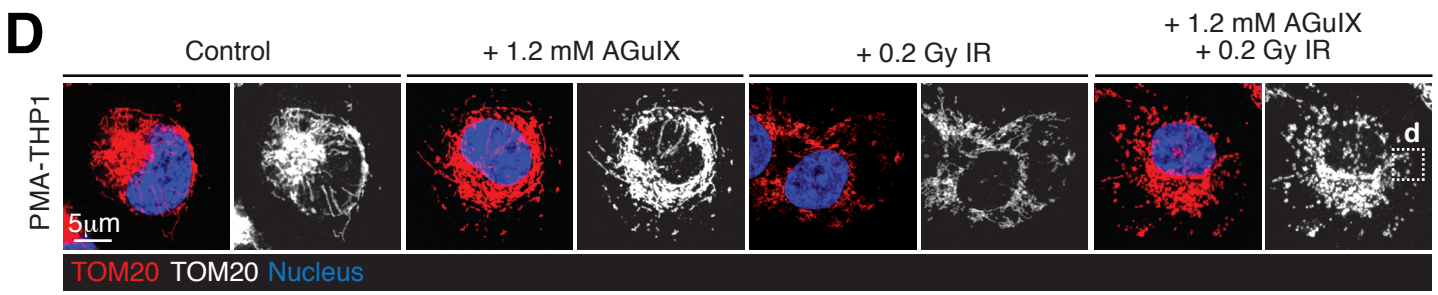
D
Control
+ 1.2 mM AGuIX
+ 0.2 Gy IR
+ 1.2 mM AGuIX
+ 0.2 Gy IR
PMA-THP1
d
5μm
TOM20 TOM20 Nucleus

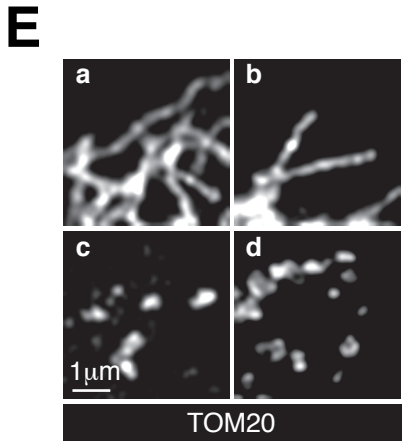
E
a
b
c
d
1μm
TOM20

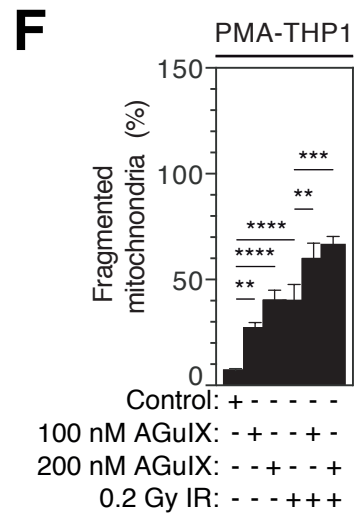
F
PMA-THP1
Fragmented mitochondria (%)
150
100
50
0
Control: + - - - - -
100 nM AGuIX: - + - - + -
200 nM AGuIX: - - + - - +
0.2 Gy IR: - - - + + +

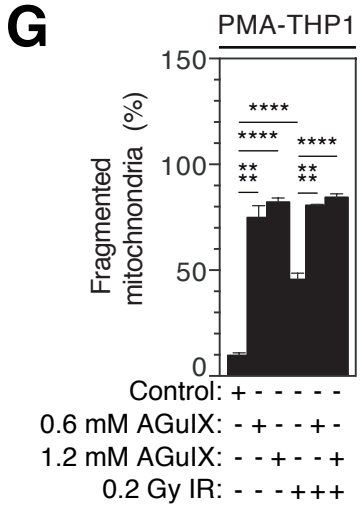
G
PMA-THP1
Fragmented mitochondria (%)
150
100
50
0
Control: + - - - - -
0.6 mM AGuIX: - + - - + -
1.2 mM AGuIX: - - + - - +
0.2 Gy IR: - - - + + +

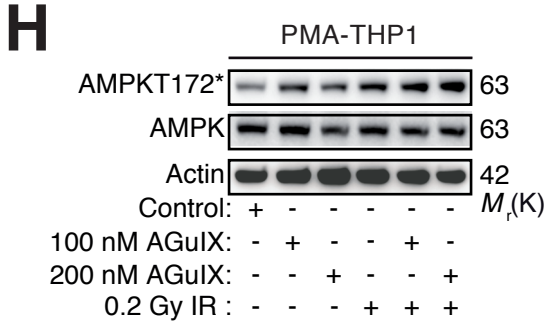
H
PMA-THP1
AMPKT172*
AMPK
Actin
63
63
42
Mr(K)
Control: + - - - - -
100 nM AGuIX: - + - - + -
200 nM AGuIX: - - + - - +
0.2 Gy IR : - - - + + +

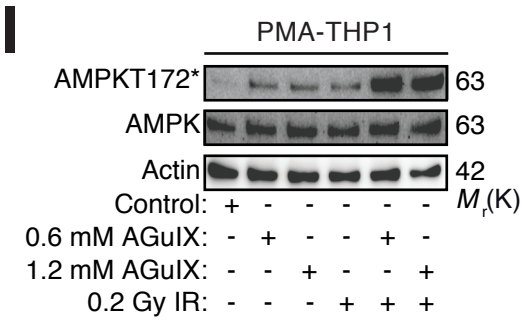
I
PMA-THP1
AMPKT172*
AMPK
Actin
63
63
42
Mr(K)
Control: + - - - - -
0.6 mM AGuIX: - + - - + -
1.2 mM AGuIX: - - + - - +
0.2 Gy IR: - - - + + +

MURADOVA#3

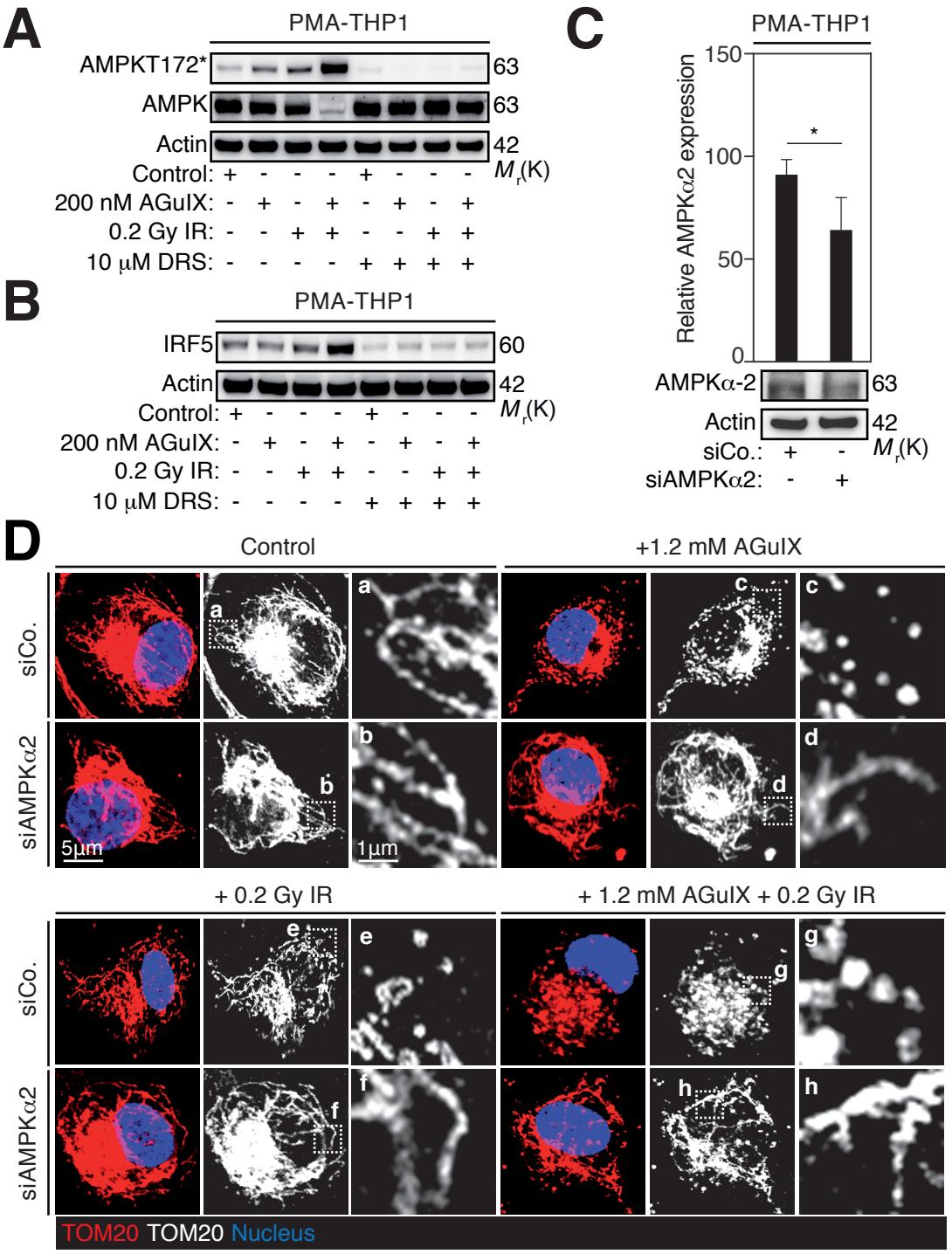
A
PMA-THP1
AMPKT172*
AMPK
Actin
63
63
42
Control: + - - - + - - -
200 nM AGuIX: - + - + - + - +
0.2 Gy IR: - - + + - - + +
10 μM DRS: - - - - + + + +
M r(K)
B
PMA-THP1
IRF5
Actin
60
42
Control: + - - - + - - -
200 nM AGuIX: - + - + - + - +
0.2 Gy IR: - - + + - - + +
10 μM DRS: - - - - + + + +
M r(K)
C
PMA-THP1
Relative AMPKα2 expression
150
100
50
0
*
AMPKα-2
Actin
63
42
siCo.: + -
siAMPKα2: - +
M r(K)
D
Control
+1.2 mM AGuIX
siCo.
siAMPKα2
a
b
c
d
5μm
1μm
+ 0.2 Gy IR
+ 1.2 mM AGuIX + 0.2 Gy IR
e
f
g
h
TOM20 TOM20 Nucleus
E
PMA-THP1
Fragmented mitochondria (%)
150
100
50
0
****
**
***
Control: + - - - + - - -
1.2 mM AGuIX: - + - + - + - +
0.2 Gy IR: - - + + - - + +
siCo.: + + + + - - - -
siAMPKα2: - - - - + + + +
F
PMA-THP1
ATMS1981*
ATM
IRF5
Actin
350
350
60
42
Control: + - - - + - - -
1.2 mM AGuIX: - + - + - + - +
0.2 GyIR : - - + + - - + +
siCo.: + + + + - - - -
siAMPKα2: - - - - + + + +
M r(K)

MURADOVA#4

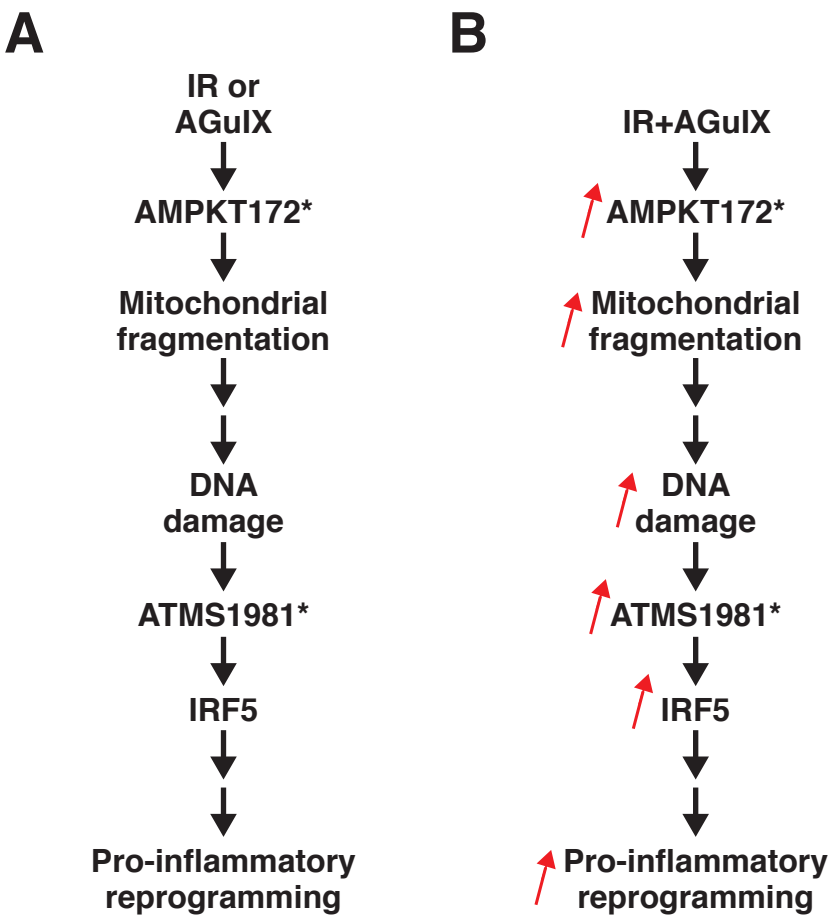
A
IR or AGuIX
AMPKT172*
Mitochondrial fragmentation
DNA damage
ATMS1981*
IRF5
Pro-inflammatory reprogramming
B
IR+AGuIX
AMPKT172*
Mitochondrial fragmentation
DNA damage
ATMS1981*
IRF5
Pro-inflammatory reprogramming

MURADOVA#5

DISCUSSIONS AND PERSPECTIVES

5. Discussion

5.1. Impacts of Gadolinium-based NPs AGuIX and their combination with ionizing radiation on DNA damage responses in anti-inflammatory human macrophages.

Ionizing radiation may induce indirect DNA damage by the generation of reactive ions and ROS, which creates a variety of lesions, or direct DNA damage, such as DNA double-strand breaks (DSBs) [615,616]. In response to DSBs, eukaryotic cells activate ATM (ataxia telangiectasia mutated) protein kinase, which phosphorylates the histone H2A variant, H2AX, at Serine 139, known as γ-H2AX foci [444]. ATM plays a vital role in activating DDR pathways that control DNA repair, cell-cycle arrest, apoptosis, and senescence [617]. In cancer, ATM promotes tumor-suppressive effects mainly via inducing SIRT1 and p53-dependent cellular apoptosis [463] and Chk1-dependent cell cycle arrest [618,619]. Thus, mutations in the *ATM* gene are associated with immunodeficiency, cancer predisposition, radiation sensitivity, and cell cycle abnormalities [620].

Several studies have demonstrated that Gd-based NPs, AGuIX, can be activated by ionizing radiation and induce severe DNA damage [410]. For instance, a significant amount of γ-H2AX foci accumulation was detected in B16F10 mouse melanoma cells exposed to 0.6 mM of AGuIX in combination with 2 Gy [400], in A549-GFP human lung tumor cells exposed to 10 mM of AGuIX and irradiated with 4 Gy [409], and in H1299 human non-small cell lung carcinoma cells incubated with 1 mM of AGuIX and irradiated with 4 Gy [621]. In all the above-mentioned studies, γ-H2AX foci formation was higher in the condition where AGuIX were combined with ionizing radiation, however, AGuIX alone were not able to induce a significant number of γ-H2AX foci accumulation. Moreover, in H1299 cells, the combination of 1 mM of AGuIX with 8 Gy of irradiation increased phosphorylation of ATM at serine 1981 (ATMS1981*) and Chk1 at serine 345 (Chk1S345*) [621].

Previously, we have demonstrated that irradiation (2 Gy), induces γ-H2AX foci formation and ATMS1981* in murine RAW264.7 and in PMA-differentiated human THP1 macrophages. Moreover, in biopsies of mice inoculated with colorectal HCT116 cells and exposed to single-dose irradiation (20 Gy), we were able to detect a significant amount of γ-H2AX positive $CD11b^{+}$ macrophages, that was positively correlated with tumor regression [541]. In this study, for the first time it was shown that AGuIX NPs alone and in combination with low dose X-ray radiation (0.2 Gy) can induce γ-H2AX accumulation and

ATMS1981* in PMA-differentiated human THP1 macrophages. These results have demonstrated that the presence of AGuIX NPs in nanomolar and micromolar ranges was able to induce DDR in macrophages, and after AGuIX combination with irradiation, the impact was significantly boosted. The dose enhancement effect after the combinational treatments is attributed to a strong photoelectric effect and increased production of Auger electrons [390,622].

5.2. Impacts of gadolinium-based nanoparticles AGuIX and their combination with ionizing radiation in the functional reprogramming of anti-inflammatory macrophages

Depending on the irradiation doses and experimental settings, radiation therapy can activate macrophages toward either anti-inflammatory or pro-inflammatory phenotypes [584]. THP1 macrophages exposed to doses below 1 Gy (0.5 Gy and 0.7 Gy) decreased the secretion of the pro-inflammatory cytokine, IL-1β [585], while J774.1 and RAW264.7 murine macrophages exposed to 0.5 Gy increased NO accumulation [587], the metabolic product of inducible nitric oxide synthase (iNOS) activity [53]. Similarly, high irradiation doses (10 Gy) in human macrophages induced no significant accumulation of IL-1β and TNF-α [589], but when delivered in fractionated scheme (2Gy/fraction/day) macrophages expressed pro-inflammatory markers, including CD80, CD86, and HLA-DR [586]. We have also demonstrated that single irradiation with 2 and 4 Gy X-ray upregulates IRF5 expression, and increases iNOS accumulation in RAW264.7, THP1, and human monocyte-derived macrophages (hMDM) [541]. IRF5 expression determines pro-inflammatory macrophage polarization both *in vivo* and *in vitro* by inducing the transcription of the proinflammatory genes, such as IL-12 subunit p40 (IL-12p40), IL-12p35, and IL-23p19, and by inhibiting the anti-inflammatory genes, like IL-10 [86,623].

Several studies demonstrated that NPs could target and reprogram TAMs as well [608,624]. Among metal NPs, gold (AuNPs), but not silver (AgNPs) was able to induce pro-inflammatory macrophage polarization in J774 A1 murine macrophages [625]. AuNPs of different sizes small (3 nM), medium (6 nM), and large (38 nM) induced the expression of pro-inflammatory cytokines in a size-dependent manner; smaller NPs had a higher capacity to upregulate the expressions of IL-1, IL-6, and TNF-α and induce pro-inflammatory responses. It was hypothesized that the internalization pathway may play a decisive role, as

AuNPs were mainly internalized via receptor-mediated endocytosis, and AgNPs via pinocytosis [625]. Similarly, in another study AgNPs dispersed in water showed higher cytotoxicity in RAW24.7 macrophages than AuNPs diluted in the same media [626]. However, AgNPs at ultralow concentrations were able to increase the expression of pro-inflammatory genes Nf-κB, IL-1β, and IL-6 in RAW24.7 macrophages [627]. In addition, several studies showed that iron-based NPs can activate macrophages toward the pro-inflammatory phenotype. For instance, systematic delivery of (FDA)-approved iron supplement ferumoxytol were able to significantly reduce the growth of subcutaneous adenocarcinomas and liver metastasis in FVB/N mice by re-programming TAMs toward pro-inflammatory phenotype in the tumor tissues. Further studies on co-culture of RAW264.7 murine macrophages with MMTV-PyMT cancer cells in the presence of ferumoxytol revealed that ferumoxytol stimulates ROS release, TNF- a secretion, and inhibits IL-10 production in macrophages [612].

Our study demonstrated that AGuIX NPs alone and in combination with 0.2 Gy are also able to activate macrophages toward the pro-inflammatory antitumor phenotype. Particularly, we showed that exposure of anti-inflammatory macrophages to low concentrations (100 nM and 200 nM) and high concentrations (0.6 mM and 1.2 mM) of AGuIX NPs induce IRF5 expression and iNOS accumulation in PMA-treated human THP1 macrophages. Interestingly, high doses of AGuIX re-programmed anti-inflammatory macrophages faster (1-2 h post-exposure), compared to low doses (48 h post-exposure). The combination of AGuIX NPs with low doses of irradiation (0.2 Gy) produced synergetic effects. Thus, our results confirmed that a low dose of irradiation and ultrasmall metal-based NPs can reprogram macrophages toward a pro-inflammatory phenotype.

5.3. Impacts of ionizing radiation, gadolinium-based nanoparticles AGuIX and combined treatments on mitochondrial dynamics in anti-inflammatory macrophages

Mitochondria is a highly dynamic organelle, and its shape changes by fusion and fission processes [132,628]. The mechanism of mitochondrial fusion is controlled by dynamin-related GTPases, including mitofusin 1 (MFN1), MFN2, optic atrophy 1 (OPA1), and two mitochondrial outer membrane proteins, FAM73a and FAM73b, also known as mitoguardin 1 and 2, respectively [135,136]. While the fission process is mediated by dynamin-related

protein 1 (Drp1), mitochondrial fission 1 (Fis1), and mitochondrial fission factors (MFF) [137,629].

Mitochondrial fission is tightly regulated by adenosine monophosphate (AMP)–activated protein kinase (AMPK) [630]. AMPK is a highly conservative energy sensor inside the cell, which becomes activated when the ATP level decreases [631]. It is a heterotrimeric complex comprised of a catalytic α subunit and regulatory β and γ subunits [153]. The activity of AMPK is dependent on the phosphorylation of threonine (T172) within the activation loop of a catalytic α subunit, which is highly conserved between the two α1 and α2 isoforms [153,632]. Activated AMPK targets numerous downstream targets, including mitochondrial fission factors, which is a mitochondrial outer membrane receptor for DRP1 that mediates mitochondrial fission [630].

Previous studies in epithelial cells have demonstrated that ionizing radiation can modulate mitochondrial fusion and fission dynamics [633,634]. For instance, studies on Hela cells demonstrated that low X-ray irradiation (< 1 Gy) promoted mitochondrial fusion, while high dose (> 1 Gy) triggered mitochondrial fission via ERK1/2-mediated phosphorylation of Drp1 [633]. Similarly, cytoplasmic irradiation with ^{4}He ions induced mitochondrial fragmentation in human small airway epithelial cells by activating the fission gene *DRP1* expression and by suppressing the fusion genes *MFN1*, *MFN2*, and *OPA1* [634]. UVB irradiation also triggered the mitochondrial fission in normal human epidermal keratinocytes (NHEK) isolated from healthy donors, but the observed fragmentation was partially associated with Drp1 activation, suggesting the existence of other fission mechanisms in this cell type [635].

In the present study, we have shown that a low dose of X-ray irradiation, AGuIX, and their combination induced a high level of mitochondrial fragmentation and activate AMPK at T172 in anti-inflammatory macrophages. Particularly, we have quantified mitochondrial fragmentation in PMA-differentiated THP1 cells after treatments with 0.2 Gy alone and in combination with low and high doses of AGuIX and revealed extensive accumulation of fragmented mitochondria in the anti-inflammatory macrophages. The mitochondrial fragmentation was especially severe after treatment with high doses of AGuIX NPs alone and in the presence of irradiation. The synergetic effect on fragmentation was detected only after treatment with low doses of AGuIX and 0.2Gy of irradiation. However, the synergy phenomenon has been observed in phosphorylation of AMPK at T172 after exposure to

both high doses and low doses of AGuIX in combination with 0.2Gy. The difference between these two observations can be explained with the time-dependent effect, where mitochondrial fragmentation after treatment with high doses of AGuIX occurs rapidly and the synergy effect could be detected only at early time points after the treatments, while once phosphorylated AMPK remains activated for a longer period.

Indeed, in accordance with our results, *in vitro* studies in lung, prostate, and breast cancer cells have previously shown that a high dose of ionizing radiation (2-8Gy) activates AMPK in an LKB1-independent manner [636]. Likewise, several types of NPs were reported to induce mitochondrial fragmentation [637]. For instance, titanium dioxide NPs caused mitochondrial fragmentation and fission/fusion imbalance through upregulating Drp1 and downregulated Opa1 expressions in HT22 cells [637]. Treatment with iron NPs [638] and silver NPs [639] was able to alter AMPK signaling pathway in SH-SY5Y cells. AMPK prevented nanoparticle-induced neurotoxicity [638] and cellular apoptosis [639]. In our current study, we have not yet explored the impact of AMPK activation on Drp1 expression and cell fate of anti-inflammatory macrophages exposed to the low dose of irradiation and AGuIX NPs, but this will be addressed in the following studies.

5.4. Roles of mitochondrial dynamics and AMPK activation in macrophage proinflammatory activation

Previous studies have demonstrated that mitochondrial fusion and fission processes are essential for macrophage activation. For instance, it is shown that fusion protein MFN2 controls ROS accumulation in macrophages and its deficiency impairs pro-inflammatory cytokine production, autophagy, apoptosis, phagocytosis, and antigen processing in LPS-stimulated macrophages [140,141]. Similarly, genetic ablation of the fusion protein FAM73b in BMDMs activated IL-12 expression but severely inhibited IL-10, IL-23, and arginase expression after LPS treatment. FAM73b deficient cells exhibited reduced ROS production and OXPHOS activity. Moreover, in myeloid cell specific FAM73b KO mice inoculated with B16 melanoma cells the tumor growth was suppressed due to the high infiltration of $CD8^+$ T cells, reduced the accumulation of TAMs, and MDSCs in the TME [136].

Activation of mitochondrial fission protein Drp1 has been also associated with proinflammatory macrophage polarization [145,146]. LPS treatment in mouse BMDMs phosphorylated Drp1 protein at S635 through activation of TLR4 and promoted

mitochondrial fission. Activation of Drp1 was essential for the expression of pro-inflammatory genes, such as IL-6, IL-1β, and IL-12b [145]. Similarly, LPS induced STAT2-dependent phosphorylation of Drp1 at S616, which resulted in mitochondrial mass increase and release of proinflammatory cytokines, like IL-6 and TNF-α [146]. Interestingly, it was shown that in LPS-treated macrophages Drp1 upregulates TNF-α production by controlling post-transcriptional modifications [640] .

In this study, we illustrated that mitochondrial fragmentation induced by IR, AGuIX, and their combination played a central role in proinflammatory macrophage polarization triggered by the treatments. Our results showed that genetic inhibition of AMPKα2 isoform impaired both mitochondrial fragmentation and IRF5 expression in human macrophages, suggesting the link between AMPK activation, mitochondrial dynamics, and macrophage proinflammatory polarization. Previous studies on AMPKα2 knockout mice bearing liver metastasis showed that inhibition of AMPKα2 results in increased tumor size and high infiltration of anti-inflammatory macrophages in TME [641]. Meanwhile, there are studies demonstrating that AMPKα1 isoform control anti-inflammatory macrophage activation [157,161]. The activation of AMPKα1 isoform at T172 was shown to induce IL-10-dependent anti-inflammatory pathways [161] and to diminish TNF-α and IL-6 production [157]. Likewise, AMPKα1 knockout macrophages were unable to acquire anti-inflammatory phenotype [642]. It is known that mouse and human macrophages express predominantly the AMPKα1 isoform [157], however, the single dose of 8Gy IR enhanced AMPKα subunits expression in lung cancer cells [643], suggesting that IR can induce α2 isoform expression in macrophages as well. The role of AMPKα1 isoform in mitochondrial fission and fusion processes has not yet been explored. Thus, our results suggest that AMPK controls macrophage polarization in isoform-specific manner and further in-depth studies are required to identify the upstream activators of AMPKα isoforms that regulate macrophage functional polarization.

Another important finding of this study was that the inhibition of AMPKα2 isoform activated after IR, AGuIX and their combination impairs ATM phosphorylation at S198, which was previously shown to regulate IRF5 transcriptional expression and irradiation-induced proinflammatory macrophage polarization [541]. These results are in agreement with previous studies, where AMPKα1/α2 knockout mouse embryo fibroblast exposed to 8Gy of ionizing radiation downregulated ATM activity by decreasing induction of its

downstream substrates γ-H2AX and Chk2 [636]. Although, our results demonstrate the link between AMPK activation, ATM phosphorylation, and IRF5 expression in macrophages, the exact molecular mechanism of their interaction must be explored further.

6. Perspectives

6.1. Deciphering the molecular mechanism of AMPK activation by AGuIX nanoparticles *in vitro*

One of the important questions that remains unanswered in the current study is the mechanism by which AGuIX NPs activate AMPK. In our study, we observed that the treatment with AGuIX NPs alone can phosphorylate AMPK and the ionizing radiation boosts the effect further. However, the exact mechanism of this observed phenomenon remains unclear.

AMPK phosphorylation at T172 within the catalytic α subunit is generally regulated by direct and indirect activators. Among the indirect activators, the most described are two upstream kinases, LKB1 [644] and CaMKK [645]. LKB1 activates AMPK residing on the surface of the late endosome with the help of the initial energy stress sensor lysosomal v-ATPase (vacuolar ATPase)-Ragulator complex and the scaffold protein AXIN [646]. Previous studies showed that after internalization AGuIX NPs localized in the endosomal vacuoles of the cell [399,403]. It could be possible that AGuIX NPs activate AMPK on the surface of endosomes through v-ATPase-Ragulator-AXIN/LKB1 pathway. Whereas CaMKKbetta activates AMPK in the presence of excessive intracellular Ca^{2+} [645], which can be released from the stressed endoplasmic reticulum (ER) [647]. Exposure to several metal-based NPs, including gold [648], silver [649], and zinc [650], have been reported to induce ER stress [651,652]. However, it is not yet known whether AGuIX NPs can induce ER stress and consequently activate CaMKKbetta.

In addition to kinases, AMPK can be indirectly activated by small molecules, which interfere with the mitochondrial electron transport chain leading to an increased AMP to ATP ratio [653]. Among the most known are metformin [654] and thiazolidinediones (TZDs) [655], which are known to activate AMPK through inhibition of complex I of the mitochondrial respiratory chain. Both these drugs are widely used to treat non-insulin-dependent diabetes [655,656]. Several studies showed that metal NPs, such as AgN [657] and cationic Au-NPs [658] can

decrease the activity of mitochondrial respiratory chain complexes. In the current study we observed a significantly high amount of mitochondrial fragmentation triggered by AGuIX treatment, perhaps AGuIX NPs as well can activate AMPK through induction of mitochondrial dysfunction.

Overall, identifying the molecular mechanism of AMPK activation by AGuIX is essential for predicting the physiological outcome of the treatment and for increasing the likelihood of AGuIX success in treating various metabolic diseases, including cancer, diabetes, and obesity.

6.2. Evidence of the role of AMPK in macrophage activation *in vivo* tumor models

In vivo cancer models will be a valuable tool to use to verify the significance of AMPK activation in macrophage polarization and its biological impact on tumor development. AGuIX NPs have been widely tested in different tumor models, including brain [392], lung [659], and colorectal cancer [417], and have shown strong anti-tumor effects in combination with ionizing radiation. The question remains whether or not the activation of AMPK specifically in TAMs is a key contributing factor. To access this question several *in vivo* models can be used, including analysis of tumor biopsies and conditional knockout mice.

Tumor biopsies isolated from mice treated with AGuIX, IR, and its combination can be used to access immune infiltrates within the TME before and after the treatment. The expression of phosphorylated AMPK in TAMs and their total infiltration can be revealed by immunohistochemistry (IHC). Similarly, if TAMs are repolarized into pro-inflammatory phenotype, they release pro-inflammatory cytokines and chemokines [660] which recruit effector immune cells such as activated $CD8^+$ T cells and NK cells [661] that turn "cold" immunosuppressive cancers into "hot" immonoresponsive phenotype [662]. Pro-inflammatory^{hot} TAMs within TME also express CXCL9 chemokine which recruits $CD8^+$ tissue-resident memory T cells (T_{RM}) [663] that can cross-talk with DCs and thereby augment the adaptive antitumor responses [664]. Thus, revealing the immune infiltrates phenotype within TME can give clues about the mechanisms by which AGuIX NPs in combination with IR strengthen antitumor immunity.

To further validate the target, a time-dependent monocyte/macrophage-specific conditional AMPKα2 knockout mouse can be generated. This can be achieved by using the Cre-ERt2

system which has been widely used for deletion of the genes of interest in monocyte/macrophage lineages in mouse models [665]. Inducible Cre system allows to silence gene expression at the precise time and in a specific cell [666], thus the impact of AMPKα2 isoform deletion in macrophages before the treatment with AGuIX NPs and IR can be accurately accessed under these settings. Previous studies on the liver metastasis model of colon cancer involving total AMPKα2 knockout mice demonstrated that its deficiency increased tumor size and enhanced anti-inflammatory macrophage accumulation within the TME [641]. Therefore, the role of AMPKα2 isoform deletion in TAMs should be explored further in future studies.

6.3. Clinical implications of AMPK-induced macrophage proinflammatory activation

Currently, AGuIX NPs in combination with IR are tested in two clinical trials in France. First is NanoCOL and it involves patients with locally advanced cervical cancer (NCT03308604). Another study is NanoRAD and it was designed for patients with multiple brain metastases (NCT02820454). The analysis of resected specimens from these patients may reveal whether AMPK is activated in TAMs and can be correlated to a predictive factor for treatment effectiveness. In case of positive correlation, AMPKα2 can be a useful molecular marker in stratifying patients into responders and non-responders for AGuIX treatments. This may allow to increase the effectiveness of the delivered treatments and minimize morbidity.

CONCLUSION

7. Conclusion

In conclusion, in this study, we demonstrated that AGuIX NPs alone and in combination with X-ray radiation-induced proinflammatory macrophage activation and identified key molecular players involved in this process (Scheme 1). We showed that AMPK activation at T172 mediates mitochondrial dynamics, ATM activation, and IRF5 expression. We envision that future studies will demonstrate the biological impact of this signaling pathway on the antitumor efficacy of radiotherapy in combination with AGuIX NPs.

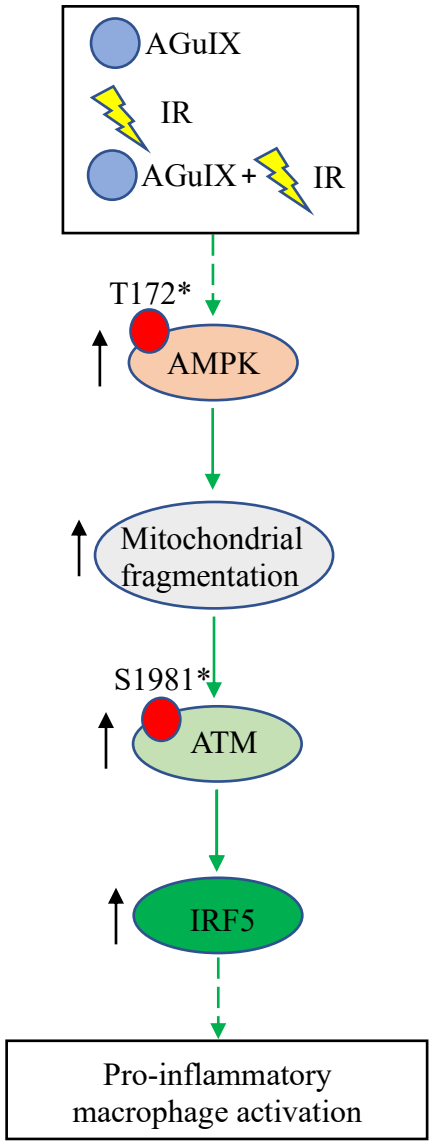

Scheme 1. Proposed mechanism of AGuIX NPs alone and in combination with X-ray radiation-induced proinflammatory macrophage polarization.

APPENDIX

Cell Death and Differentiation (2017) 24, 1632–1644

www.nature.com/cdd

NOX2-dependent ATM kinase activation dictates pro-inflammatory macrophage phenotype and improves effectiveness to radiation therapy

Qiuji Wu[1,2,3,4,5,6], Awatef Allouch[1,2,3,4], Audrey Paoletti[1,2,3,4], Celine Leteur[2,3,4], Celine Mirjolet[7], Isabelle Martins[1,2,3,4], Laurent Voisin[1,2,3,4], Frédéric Law[1,2,3,4], Haithem Dakhli[1,2,3,4], Elodie Mintet[1,2,3,4], Maxime Thoreau[1,2,3,4], Zeinaf Muradova[1,2,3,4], Mélanie Gauthier[7], Olivier Caron[3], Fabien Milliat[8], David M Ojcius[9], Filippo Rosselli[10], Eric Solary[11], Nazanine Modjtahedi[2,3,4], Eric Deutsch[2,3,4,12] and Jean-Luc Perfettini*[,1,2,3,4,12]

Although tumor-associated macrophages have been extensively studied in the control of response to radiotherapy, the molecular mechanisms involved in the ionizing radiation-mediated activation of macrophages remain elusive. Here we show that ionizing radiation induces the expression of interferon regulatory factor 5 (IRF5) promoting thus macrophage activation toward a pro-inflammatory phenotype. We reveal that the activation of the ataxia telangiectasia mutated (ATM) kinase is required for ionizing radiation-elicited macrophage activation, but also for macrophage reprogramming after treatments with γ-interferon, lipopolysaccharide or chemotherapeutic agent (such as cisplatin), underscoring the fact that the kinase ATM plays a central role during macrophage phenotypic switching toward a pro-inflammatory phenotype through the regulation of mRNA level and post-translational modifications of IRF5. We further demonstrate that NADPH oxidase 2 (NOX2)-dependent ROS production is upstream to ATM activation and is essential during this process. We also report that the inhibition of any component of this signaling pathway (NOX2, ROS and ATM) impairs pro-inflammatory activation of macrophages and predicts a poor tumor response to preoperative radiotherapy in locally advanced rectal cancer. Altogether, our results identify a novel signaling pathway involved in macrophage activation that may enhance the effectiveness of radiotherapy through the reprogramming of tumor-infiltrating macrophages.

Cell Death and Differentiation (2017) **24,** 1632–1644; doi:10.1038/cdd.2017.91; published online 2 June 2017

Approximately, half of all cancer patients are treated with radiotherapy alone or in combination with chemotherapy. Although ionizing radiation (IR) directly causes senescence and death of tumor cells through the generation of reactive oxygen species (ROS) and DNA damage,[1] recent studies underscore the fact that IR can also modulate immune cell functions and favor consequently the development of anticancer immunity.[2,3] IR can induce the exposure of 'eat-me' signals (such as calreticulin) and the release of danger signals (such as ATP and HMGB1) by the irradiated dying tumor cells (also referred as immunogenic cell death),[4] thus contributing to specific T-cell response by increasing the tumor antigen cross-presentation to dendritic cells[5] and/or modifying the immunosuppressive microenvironment of tumors.[6,7] IR can also control tumor immune response through the direct modulation of innate immune cell functions. Treatment with IR can modulate Langerhans cell functions and induce the accumulation of regulatory T cells into tumors.[8] In addition, IR controls macrophage plasticity and programs tumor-associated macrophages (TAMs) toward a pro-inflammatory phenotype that orchestrates specific tumor immune response.[9] However, microenvironment factors such as hypoxia may affect this IR-responsive macrophage activation program by favoring a pro-tumorigenic activation phenotype that is associated with tumor resistance.[10] Nevertheless, the molecular mechanisms underlying IR-induced macrophage activation remain elusive.

TAMs represent a major cellular component of the tumor microenvironment.[11] These macrophages derive from blood monocytes that, after their recruitment into tumors, differentiate and are activated in response to different environmental signals. Macrophages can be broadly classified as classically activated pro-inflammatory macrophages and alternatively activated pro-tumorigenic macrophages.[12] The interferon regulatory factor 5

[1]Cell Death and Aging Team, Gustave Roussy, 114 rue Edouard Vaillant, Villejuif F-94805, France; [2]Laboratory of Molecular Radiotherapy, INSERM U1030, Gustave Roussy, 114 rue Edouard Vaillant, Villejuif F-94805, France; [3]Gustave Roussy, 114 rue Edouard Vaillant, Villejuif F-94805, France; [4]Université Paris Sud - Paris Saclay, 114 rue Edouard Vaillant, Villejuif F-94805, France; [5]Department of Radiation and Medical Oncology, Zhongnan Hospital, Wuhan University, 169 Dong Hu Road, Wuhan 430071, China; [6]Hubei Key Laboratory of Tumor Biological Behaviors, Zhongnan Hospital, Wuhan University, 169 Dong Hu Road, Wuhan 430071, China; [7]Centre Georges François Leclerc, 1 rue du Pr Marion, Dijon F-21079, France; [8]Laboratoire de Recherche en Radiobiologie et radiopathologie, Institut de Radioprotection et de Sureté Nucléaire, Fontenay-aux-Roses F-92262, France; [9]Department of Molecular Cell Biology, Health Sciences Research Institute, University of California, Merced, CA 95343, USA; [10]Laboratoire «Stabilité Génétique et Oncogenèse», CNRS - UMR 8200, 114 rue Edouard Vaillant, Villejuif F-94805, France and [11]INSERM U1170, Gustave Roussy, 114 rue Edouard Vaillant, Villejuif F-94805, France

*Corresponding author: J-L Perfettini, Cell death and Aging Team, Gustave Roussy, 114 rue Edouard Vaillant, Villejuif F-94805, France. Tel: +33 1 42115424; Fax: +33 1 42116665; E-mail: perfettini@orange.fr

[12]ED and J-LP share senior coauthorship.

Received 31.8.16; revised 19.4.17; accepted 02.5.17; Edited by M Piacentini; published online 02.6.17

(IRF5) was demonstrated to determine the pro-inflammatory macrophage phenotype[13–15] along with other transcription factors (such as STAT1 and NF-κB), whereas IRF4,[16] STAT6[17] and KLF4[18] are key transcription factors required for the pro-tumorigenic macrophage phenotype. Interferon gamma plus lipopolysaccharide (LPS) or tumor necrosis factor *α* alone are known to induce classical macrophage activation that is characterized by an increased secretion of pro-inflammatory cytokines and chemokines (such as interleukin (IL)-1*β*), an augmented production of inducible nitric oxide synthase (iNOS)[19] and of ROS.[12] Conversely, glucocorticoids, IL-4/IL-13 and IL-10 drive macrophages toward the alternative activation program with a reduced production of pro-inflammatory cytokines but a higher level of anti-inflammatory IL-10, TGF-*β*, arginase, membrane scavenger and mannose receptors. Pro-inflammatory macrophages possess bactericidal and anti-tumoral activities, while pro-tumorigenic macrophages are associated with immune regulatory and tissue repair activities, highlighting the diversity of macrophage functions. In response to tumor microenvironment signals (such as hypoxia and tumor-derived lactate[20,21]), TAMs mainly adopt a pro-tumorigenic phenotype that contributes to tumor progression by promoting tumor growth, metastasis, angiogenesis and by suppressing immune responses.[22–24] In addition, several studies have demonstrated that TAMs are also associated with treatment resistance and poor clinical outcomes in various cancer settings (such as lymphoma, melanoma, sarcomas and lung cancer[25–28]), making them attractive targets for the development of new anticancer strategies.[29,30] In this context, a better understanding of the molecular basis of the IR-mediated macrophage activation is needed for the improvement of the efficacy of radiotherapy. In this study, we explored the molecular mechanisms involved in IR-induced macrophage reprogramming.

Results

Cell-autonomous activation of macrophages after ionizing radiation. Considering that immune cells may influence the functional reprogramming of macrophages,[29] we first analyzed IR-mediated macrophage activation using human colon tumor xenografts in immunodeficient mice. HCT116 cells were subcutaneously inoculated into the right flanks of athymic nude mice. Seven days after inoculation, the irradiation of the palpable tumor mass with a single dose of 20 Gy resulted in significant tumor growth inhibition, as compared to the controls (Figure 1a). After 29 days, the residual irradiated tumors did not show any increase of the density of $CD11b^+$ macrophages (Supplementary Figure 1a), but revealed an increased frequency of $CD11b^+$ macrophages that expressed iNOS ($iNOS^+CD11b^+$) (Figure 1b). We detected a significant accumulation of $iNOS^+CD11b^+$ macrophages in irradiated tumors as compared with non-irradiated ones (Figure 1c). The accumulation of $iNOS^+CD11b^+$ TAMs positively correlated with tumor response to IR, confirming as previously published that the presence of $iNOS^+$/pro-inflammatory phenotype macrophages in irradiated tumors is required for the modification of tumor microenvironment and tumor regression. Of note, previous reports characterized this process in conditions of relatively low-dose IR (2 Gy) exposure.[6,9] Our observation that TAMs exhibited an increased phosphorylation of the histone variant H2AX (also known as *γ*-H2AX) on serine 139 (Figures 1d and e) underlined an unsuspected link between DNA damage response and macrophage activation. To check the possibility whether IR can directly target and activate macrophages, we irradiated human THP1 macrophages with a single dose of 2 Gy and analyzed, by fluorescence microscopy and flow cytometry, the expression levels of iNOS and *γ*-H2AX. The increase in iNOS and *γ*-H2AX expression levels in irradiated THP1 macrophages (Figures 1f–h, Supplementary Figures 1b and 1c) revealed that IR could directly target macrophages to promote their activation toward a pro-inflammatory phenotype. We then analyzed by immunoblot the expression of a central transcription factor involved in macrophage activation, the IRF5[15] and observed that after single radiation doses of 2 and 4 Gy, phorbol-12-myristate-13-acetate (PMA)-differentiated human THP1 macrophages (Figure 1i), human primary monocyte-derived macrophages (hMDM) (Figure 1j) and murine RAW264.7 macrophages (Figure 1k) exhibited an enhanced expression of IRF5 (Figures 1i–k). In addition, through immunoprecipitation experiments, we observed that after 2 Gy irradiation of RAW264.7 macrophages the pro-inflammatory transcription factor IRF5 was phosphorylated on serine (Figure 1l). We also demonstrated that after, respectively, 96 and 12 h of irradiation, hMDM (Figure 1m) and murine RAW264.7 macrophages (Figure 1n) released two pro-inflammatory cytokines IL-1*β* and IL-8. To further complete the cytokine profile analysis, we determined the transcription levels of pro- and anti-inflammatory cytokines and observed increased mRNA expression of pro-inflammatory cytokines (such as TNF-*α*, IFN-*γ*, IL-6 or IL-23) in 2 Gy-irradiated PMA-differentiated human THP1 macrophages (Figures 1o–r) and detected an increased secretion of pro-inflammatory cytokines by 4 Gy-irradiated hMDM (including TNF-*α*, IFN-*γ*, IL-6 and IL-8) as compared with controls (Figures 1s, t and Supplementary Figures 1d–1g). Altogether, these results indicate that IR can promote a cell-autonomous activation of macrophages toward a pro-inflammatory phenotype.

ATM-mediated DNA damage response regulates the transcription of IRF5 in response to ionizing radiation. To further characterize the molecular mechanisms involved in IR-elicited macrophage activation, we first studied the induction of DNA damage-associated signaling pathways. Fifteen minutes after single radiation dose of 2 Gy, PMA-differentiated human THP1 macrophages (Figures 2a–c) exhibited a strong nuclear accumulation of *γ*-$H2AX^+$ foci (Figures 2a and b) and of $53BP1^+$ foci (Figures 2a and c) that could still be detected 6 h after exposure (Figures 2b and c), revealing the fact that DNA double-strand breaks are produced in response to IR. One hour after single radiation dose of 2 Gy, murine RAW264.7 macrophages also displayed increased *γ*-$H2AX^+$ foci (Figures 2d and e). Considering that the kinase ATM (mutated in the inherited recessive autosomal disease ataxia telangiectasia) is the major kinase involved in the phosphorylation of H2AX (on serine 139),[31] we evaluated the role of ATM in the activation of macrophages in response

to IR. We observed that the vast majority of 2 Gy-irradiated murine RAW264.7 macrophages exhibited the activating auto-phosphorylation of ATM on serine 1981 (ATMS1918*) 1-h post irradiation (Figures 2d and f). These results that were confirmed by immunoblots (Figures 2g and h) and flow cytometry (Supplementary Figure 2a) revealed also the positive correlation between ATMS1981* and IRF5 expression when hMDM (Figure 2g) or murine RAW264.7 macrophages (Figure 2h) were irradiated with single doses of 2, 4 and 8 Gy. In addition, we detected an increase of ATMS1981* in $CD68^+$ macrophages that were found in tumor samples after radiotherapy of rectal cancer patients (Figures 2i and j), as compared to unirradiated patients. The ATMS1918* phosphorylation was positively correlated with the increased frequencies of tumor-associated $iNOS^+CD68^+$ macrophages that have been detected 6 weeks after radiotherapy

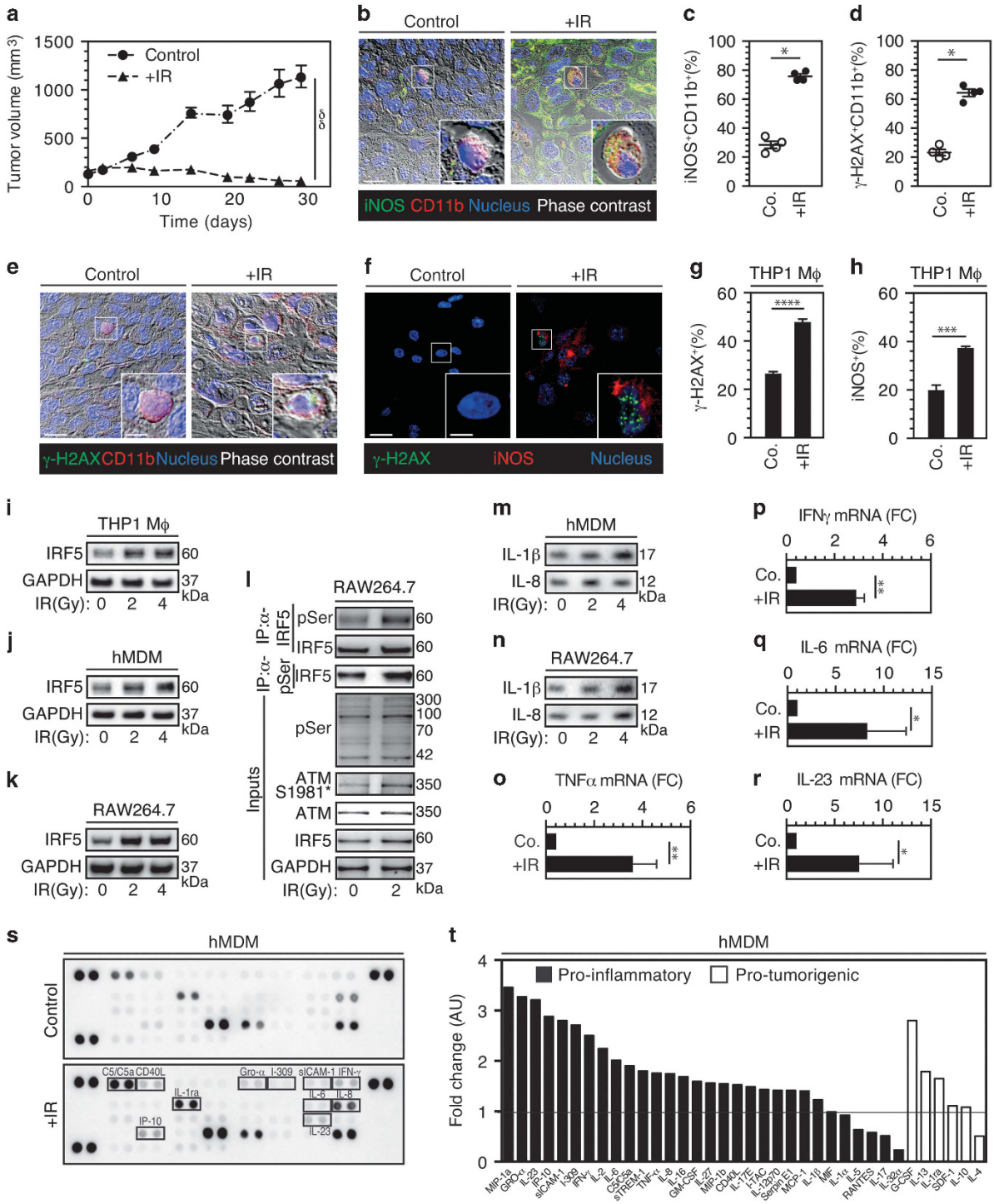

(Figures 2k and l), demonstrating that the kinase ATM was sustainably activated in macrophages after radiotherapy. We next investigated the impact of ATM inactivation on IR-induced macrophage activation. The depletion of ATM by means of specific small interfering RNA (Figure 2m) or pharmacological inhibition with KU55933 (Figure 2n, Supplementary Figures 2b–2d and 2i) impaired γ-H2AX and ATMS1981* phosphorylation and the upregulation of IRF5 expression that was detected, respectively, 6 and 96 h after 2 and 4 Gy single-dose irradiation of murine RAW264.7 macrophages (Figure 2m, Supplementary Figures 2b–2d and 2i) or hMDM (Figure 2n) without altering macrophage viability (Supplementary Figures 2e–2h). We also observed that an enhancement of ATM activation through the pharmacological inhibition of poly(ADP-ribose)polymerase (PARP) with Olaparib further enhanced the inflammatory macrophage activation elicited by IR (as revealed by the increased expression of IRF5 (Figure 2o)). Finally, we demonstrated that ATM regulated the expression of IRF5 at transcriptional level (as shown by quantitative real-time (RT) PCR (Figure 2p and Supplementary Figure 2j)), confirming thus the central role of the kinase ATM during IR-mediated activation of macrophages toward a pro-inflammatory phenotype.

The kinase ATM dictates classical macrophage activation. In order to check whether the activation of ATM was a common feature of various pro-inflammatory macrophage activation programs, we analyzed the presence of DNA damage-associated nuclear foci in response to classical macrophage activators.[32] Using confocal microscopy, we detected an accumulation of ATMS1981^{*+} and γ-H2AX^{+} foci in the nuclei of murine RAW264.7 macrophages that were treated for 24 h with recombinant murine IFN-γ (mIFN-γ) or LPS (Figures 3a–c). Using immunoblots, we also observed that the activation of ATM was concomitant with an increased expression of IRF5 in the PMA-differentiated THP1 macrophages (Figures 3d and f) or murine RAW264.7 macrophages (Figure 3e) stimulated with human or murine IFN-γ (Figures 3d and e) or LPS (Figure 3f). As expected, treatments of these macrophages with some other DNA strand break inducers (such as Cisplatin (Figures 3a–c, g and h) or neocarzinostatin (NCZ) (Figure 3i)) or modulators of DNA repair (such as Olaparib (Figure 3j)), not only activated ATM but also increased IRF5 expression (Figures 3g–j). The results that are observed in absence of macrophage cytotoxicity (Supplementary Figure 3a) suggest that the DNA damage response signaling pathway might be a common pathway involved in classical macrophage activation. Moreover, we demonstrated that the pharmacological inhibition (Figures 3k and l) and the specific depletion (Figures 3m and n) of ATM inhibited the increase of IRF5 expression that we previously detected after the treatment of PMA-differentiated THP1 macrophages (Figure 3k), murine RAW264.7 macrophages (Figures 3l and m) or hMDM (Figure 3n) with human or murine IFN-γ (Figures 3k–n) without impacting macrophage viability (Supplementary Figure 3b), confirming the essential role of the kinase ATM in classical macrophage activation.

ROS production induces ATMS1981* phosphorylation and IRF5 expression during macrophage activation. Considering that ROS have been involved in both ATM activation and macrophage differentiation,[33,34] we investigated the role of ROS production during macrophage activation. Using flow cytometry to detect the conversion of the 2,7-dichlorohydro fluorescein diacetate (H_2DCFDA) into 2,7-dichlorohydro fluorescein (DCF) when ROS are produced, we evaluated the ability of murine RAW264.7 macrophages to generate ROS following IR or mIFN-γ treatment and revealed that both these treatments induced ROS production (Figures 4a–d). Importantly, we demonstrated that the N-acetyl cysteine (NAC) and the superoxide dismutase (SOD) mimetic Mn(III)tetrakis (4-benzoic acid) (MnTBAP) that blunted the ROS production (Figures 4a–d), inhibited also ATMS1981* (Figures 4e–g) and reduced the increased expression of IRF5 (Figures 4e–g) that we observed after treatment with IR (Figures 4e and g) or mIFN-γ (Figure 4f) of RAW264.7 macrophages (Figures 4e and f) or treatment with IR of PMA-differentiated THP1 macrophages (Figure 4g) without impacting macrophage

Figure 1 Irradiation activates macrophages toward pro-inflammatory phenotype.(**a**) Colorectal HCT116 cells were injected subcutaneously (4×10^6 cells per mouse) into immunodeficient mice and tumor growth was monitored. Results are expressed as mean value $\pm$ S.E.M. *P*-value ($^{\delta\delta}P < 0.01$) was calculated by means of two-way ANOVA test. (**b**–**e**) Representative confocal micrographs and frequencies of iNOS$^+$CD11b$^+$ (**b**, **c**) or γ-H2AX$^+$CD11b$^+$ (**d**, **e**) tumor-associated macrophages detected in absence or after 20 Gy single-dose irradiation are shown (scale bar, 20 μm). Representative iNOS$^+$CD11b$^+$ or γ-H2AX$^+$CD11b$^+$ macrophages are shown in inserts (scale bar, 5 μm). Results are expressed as mean value $\pm$ S.E.M. *P*-value ($^*P < 0.05$) was calculated using Mann–Whitney *U*-test. (**f**–**h**) Representative confocal micrographs and frequencies of phorbol-12-myristate-13-acetate (PMA)-differentiated human THP1 macrophages showing γ-H2AX$^+$ nuclear foci (**f**, **g**) or expressing iNOS (iNOS$^+$) (**f**, **h**) in control cells or 24 h after 2 Gy irradiation are shown (scale bar, 20 μm). Representative γ-H2AX$^+$ nuclear foci or iNOS expressing macrophages are shown in inserts (scale bar, 5 μm). Results are expressed as mean value $\pm$ S.E.M. *P*-values ($^{***}P < 0.001$, $^{****}P < 0.0001$) were calculated using unpaired Student's *t*-test. (**i**–**k**) IRF5 expression after, respectively, 96, 96 and 6 h culture of PMA-differentiated human THP1 macrophages (**i**), hMDM (**j**) or murine RAW264.7 macrophages (**k**) that have been irradiated (or not) with indicated doses. Representative immunoblots are shown. GAPDH is used as loading control. (**l**) Murine RAW264.7 macrophages that have been irradiated (or not) with 2 Gy were immunoprecipitated 6 h post irradiation for IRF5 and phopsho-serine (pSer), and analyzed for IRF5 and pSer expressions. Inputs were analyzed for IRF5, pSer, ATMS1981*, ATM and GAPDH. (**m**, **n**) Detection of IL-1β and IL-8 release in the supernatants of hMDM (**m**) or murine RAW264.7 macrophages (**n**) that have been irradiated (or not) with indicated doses. Representative immunoblots are shown. (**o**–**r**) TNFα, IFNγ, IL-6 and IL-23 mRNA expressions on PMA-differentiated THP1 macrophages that have been irradiated (or not) with 2 Gy were determined by quantitative real-time PCR. Results are expressed as mean value $\pm$ S.E.M. and represented as fold change as compared to controls. *P*-values ($^*P < 0.05$, $^{**}P < 0.01$) were calculated using unpaired Student's *t*-test. (**s**, **t**) Detection of cytokine secretion in the supernatants of hMDMs that have been treated (or not) with 4 Gy irradiation. Array images were captured following 1–10 min exposures to peroxidase substrate (**s**). Relative levels of cytokines detected in the supernatants of irradiated macrophages as compared to those detected in non-irradiated macrophages are revealed as fold change of arbitrary units. Pro-inflammatory and pro-tumorigenic cytokines and chemokines are indicated (**t**). Data are representative of three independent experiments performed with primary human macrophages obtained from three healthy representative donors

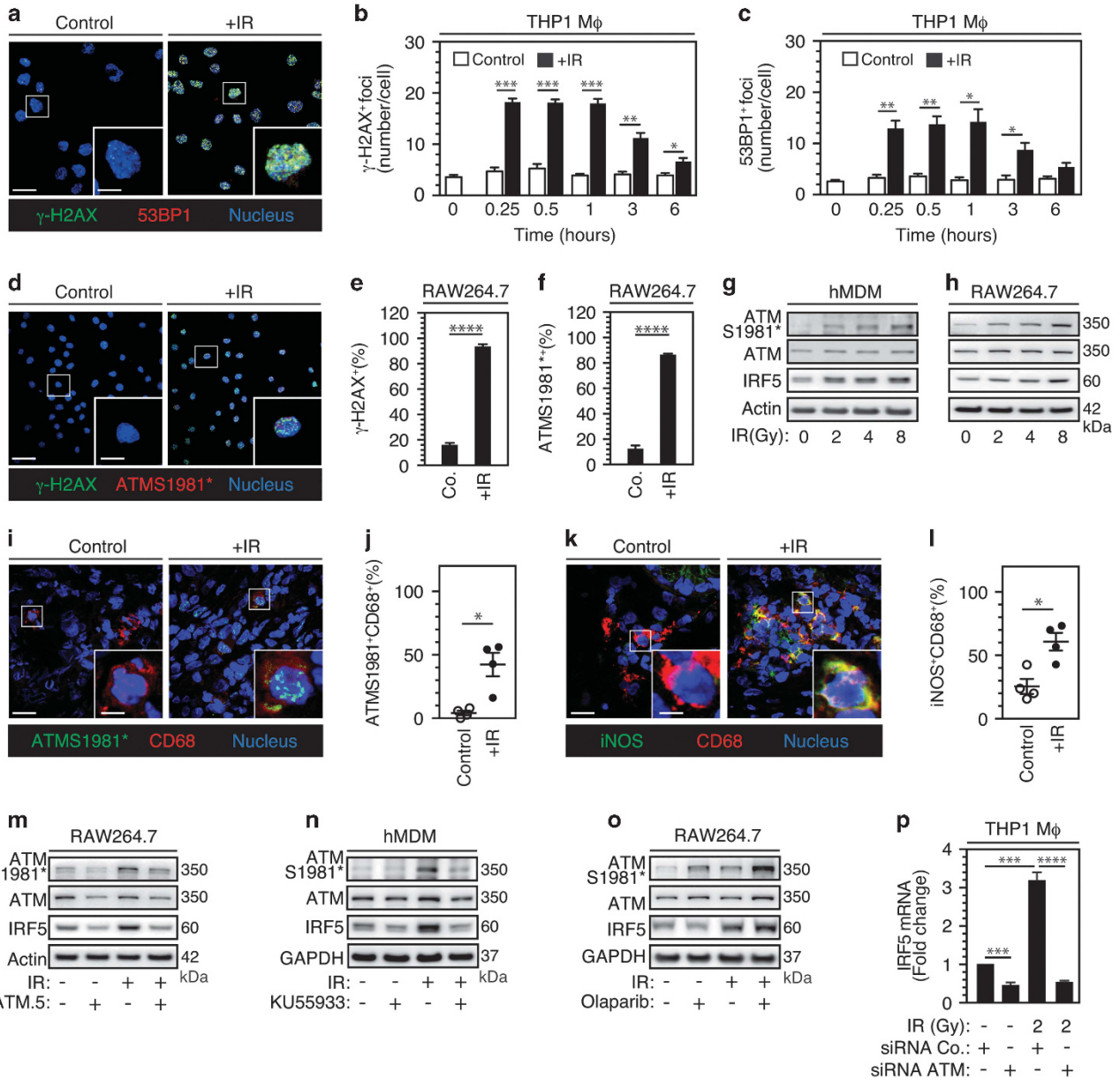

Figure 2 ATM activation controls IRF5 transcriptional expression and IR-induced pro-inflammatory macrophage phenotype.(**a**) Representative confocal micrographs of phorbol-12-myristate-13-acetate (PMA)- differentiated human THP1 macrophages showing γ-H2AX$^+$ or 53BP$^+$ foci following 2 Gy single-dose irradiation are shown (scale bar, 20 μm). Scale bar of inserts is 5 μm. (**b**, **c**) Frequencies of γ-H2AX$^+$ (**b**) or 53BP$^+$ (**c**) nuclear foci in PMA-differentiated human THP1 macrophages after 2 Gy single-dose irradiation are shown at indicated times. (**d**–**f**) Representative confocal micrographs and frequencies of murine RAW264.7 macrophages showing γ-H2AX$^+$ nuclear foci (**d**, **e**) or AMTS1981* phosphorylation (ATMS1981^{*+}) (**d**, **f**), in control cells or 1 h after 2 Gy single-dose irradiation are shown (scale bar, 20 μm). Representative γ-H2AX$^+$ nuclear foci and ATMS1981^{*+} macrophages are shown in inserts (scale bar, 5 μm). Results are expressed as mean value ± S.E.M. *P*-values (*$P<0.05$, **$P<0.01$, ***$P<0.001$, ****$P<0.0001$) were calculated using unpaired Student's *t*-test. (**g**, **h**) ATMS1981*, ATM and IRF5 expression after, respectively, 96 and 6 h culture of hMDM (**g**) or murine RAW264.7 macrophages (**h**) that have been irradiated (or not) with indicated doses are determined. Representative immunoblots are shown. Actin is used as loading control. (**i**–**l**) Representative confocal micrographs and frequencies of ATMS1981^{*+}CD68$^+$ (**i**, **j**) or iNOS$^+$CD68$^+$ (k, l) macrophages that have been detected in absence or after 45 Gy total dose of fractionated irradiation on tumor samples obtained from locally advanced rectal cancer patients are shown (scale bar, 20 μm; scale bar of insert, 5 μm). Results are expressed as mean value ± S.E.M. *P*-value (*$P<0.05$) was calculated using Mann–Whitney *U*-test. (**m**, **n**) ATMS1981*, ATM and IRF5 expression after, respectively, 6 and 96 h culture of murine RAW264.7 macrophages that have been depleted for ATM (**m**) or hMDM that have been treated with 20 μM of KU55933 (**n**) and irradiated (or not) with 2 Gy (**m**) or 4 Gy (**n**) are shown. Representative immunoblots are shown. GAPDH (or actin) is used as loading control. (**o**) ATMS1981*, ATM and IRF5 expression after 6 h culture of murine RAW264.7 macrophages that have been treated with 10 μM of Olaparib and irradiated (or not) with 2 Gy are shown. Representative immunoblots are shown. GAPDH is used as loading control. (**p**) IRF5 mRNA expression on PMA-differentiated human THP1 macrophages that have been depleted for ATM and irradiated (or not) with 2 Gy was determined by quantitative real-time PCR. Results are expressed as mean value ± S.E.M. and represented as fold change as compared to controls. *P*-values (***$P<0.001$ and ****$P<0.0001$) were calculated using one-way ANOVA test. Quantification of western blot bands are shown in Supplementary Figure 4

viability (Supplementary Figures 3c and 3d). Altogether, these results indicate that by controlling the phosphorylation of ATM and the induction of the IRF5, ROS produced in the stimulated macrophages play a key role in the activation process.

The NADPH oxidase 2 is responsible for ROS production and ATM phosphorylation during macrophage activation. The NADPH oxidases are major regulated sources of ROS generation.[35,36] To characterize mechanisms that are involved in ROS generation during macrophage activation,

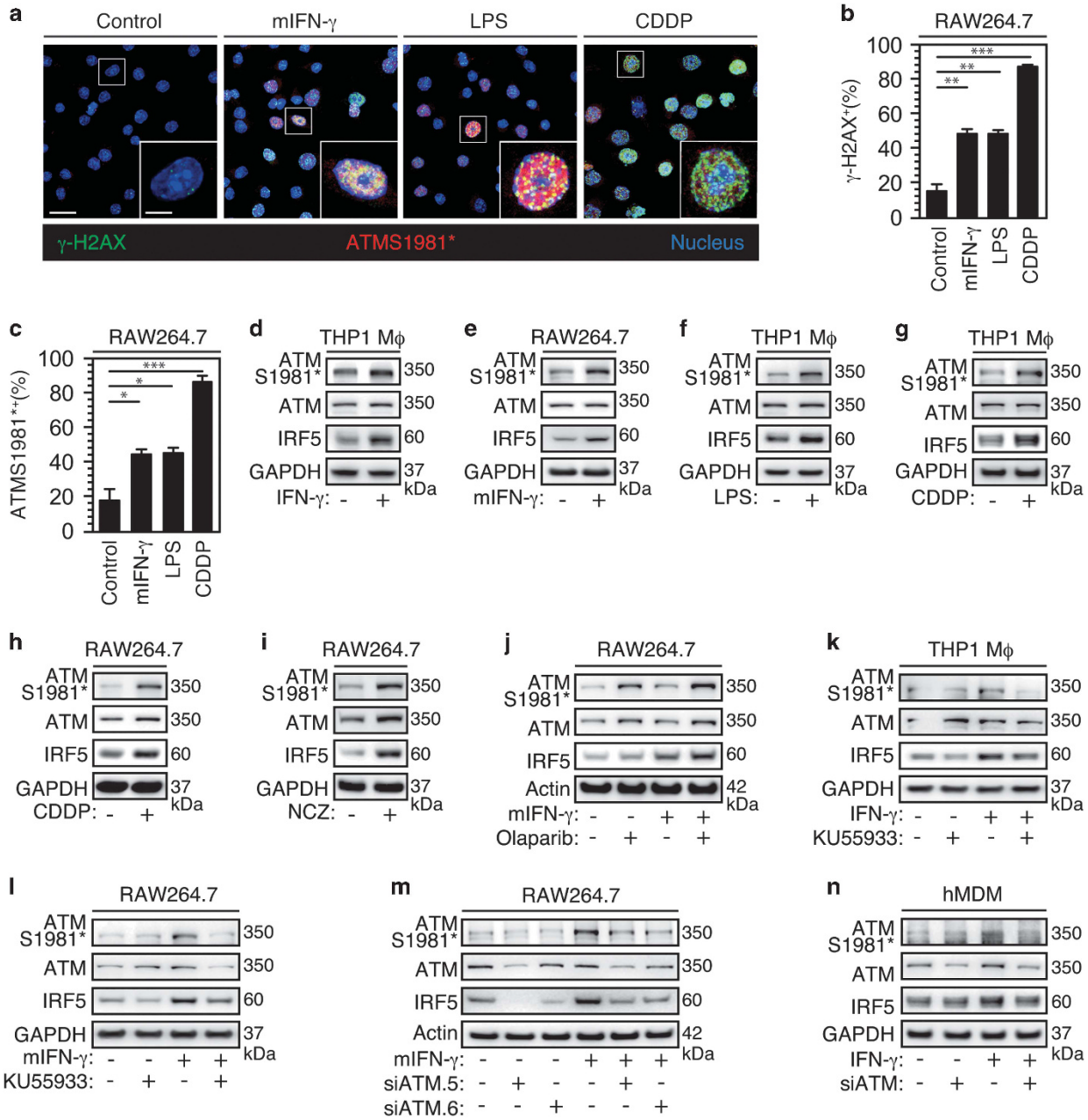

Figure 3 Classical macrophage activation is dependent on ATM. (**a**–**c**) Representative confocal micrographs and frequencies of murine RAW264.7 macrophages showing γ-H2AX$^+$ nuclear foci (**a**, **b**) or ATMS1981* phosphorylation (ATMS1981^{*+}) (**a**, **c**) in control cells or after 24 h treatments with 20 ng/ml of recombinant murine IFN-γ (mIFN-γ), 100 ng/ml of lipopolysaccharide (LPS) or 10 μM of cisplatinium (CDDP) are shown (scale bar, 20 μm). Representative macrophages with ATMS1981^{*+} and γ-H2AX$^+$ nuclear foci are shown in inserts (scale bar, 5 μm). Results are expressed as mean value ± S.E.M. *P*-values (*$P<0.05$, **$P<0.01$, ***$P<0.001$) were calculated using unpaired Student's *t*-test. (**d**–**i**) ATMS1981*, ATM and IRF5 expressions after 24 h culture of PMA-differentiated human THP1 macrophages (**d**, **f**, **g**) or murine RAW264.7 macrophages (**e**, **h**, **i**) that have been treated (or not) with 20 ng/ml of recombinant human IFN-γ (IFN-γ) (**d**), 20 ng/ml of recombinant murine IFN-γ (mIFN-γ) (**e**), 100 ng/ml of LPS (**f**), 10 μM of CDDP (**g**, **h**) or 200 ng/ml of neocarzinostatin (NCZ) (**i**) are determined. Representative immunoblots are shown. GAPDH is used as loading control. (**j**–**n**) ATMS1981*, ATM and IRF5 expressions after, respectively, 24 h culture of murine RAW264.7 macrophages (**j**, **l**, **m**), PMA-differentiated human THP1 macrophages (κ) or hMDMs (**n**) that have been incubated with 10 μM of Olaparib (**j**), with 20 μM of KU55933 (**k**, **l**) or depleted for ATM (**m**, **n**) and treated (or not) with 20 ng/ml mIFN-γ (for RAW264.7 macrophages) (**j**, **l**, **m**), 20 ng/ml human IFN-γ (for PMA-differentiated human THP1 macrophages) (κ) or 4 μg/ml of human IFN-γ (for hMDM) (**n**) are evaluated. Representative immunoblots are shown. Actin (or GAPDH) is used as loading control. Quantification of western blot bands is shown in Supplementary Figure 4

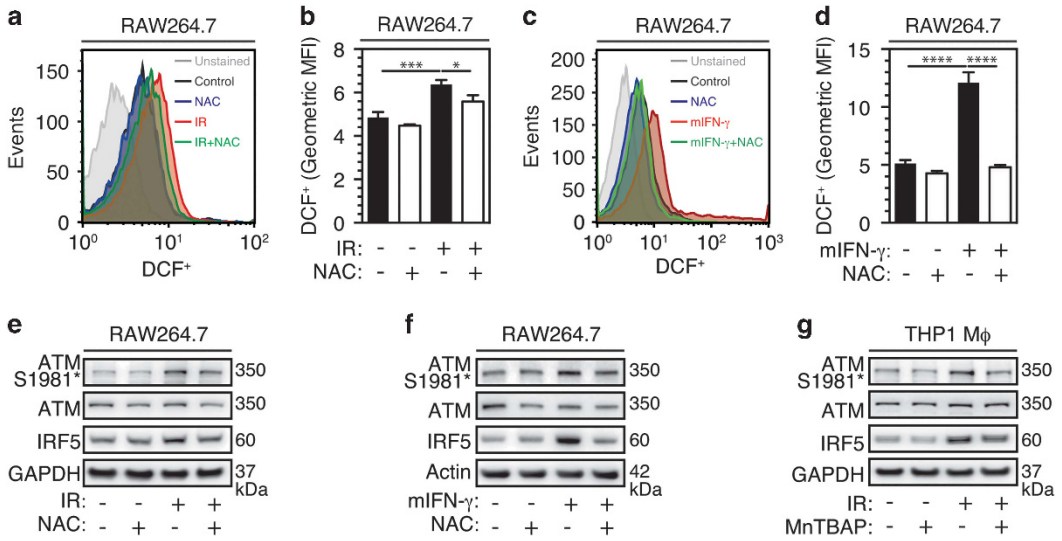

Figure 4 Reactive oxygen species are involved in IR-induced pro-inflammatory macrophage activation.(**a**–**d**) Murine RAW264.7 macrophages treated with 1 μg/ml of NAC were stimulated with 2 Gy single-dose irradiation (**a**, **b**) or 20 ng/ml mIFN-γ (**c**, **d**), stained with H_2DCFDA and analyzed by flow cytometry. Representative flow cytometry analysis and quantifications of geometric mean fluorescence intensity (MFI) are shown. Data are presented as means ± S.E.M. in **b** and **d** panels. Significances are $^*P<0.05$, $^{***}P<0.001$ and $^{****}P<0.0001$, and were obtained using one-way ANOVA test. (**e**, **f**) ATMS1981*, ATM and IRF5 expressions after, respectively, 6 and 24 h culture of murine RAW264.7 macrophages that have been incubated with 1 μg/ml of NAC and irradiated with 2 Gy single dose (**e**) or treated with 20 ng/ml mIFN-γ (**f**) were determined. Representative immunoblots are shown. GAPDH (or actin) is used as loading control. (**g**) ATMS1981*, ATM and IRF5 expressions after 48 h culture of PMA-differentiated human THP1 macrophages that have been incubated with 10 μM of MnTBAP and irradiated with 8 Gy single dose were determined. Representative immunoblots are shown. GAPDH is used as loading control. Quantification of western blot bands are shown in Supplementary Figure 5

we examined the role of NADPH oxidase 2 (NOX2), which is mainly expressed in macrophages and neutrophils.[35,36] First, using immunoblots, we observed that NOX2 was upregulated after irradiation of PMA-differentiated THP1 macrophages (Figure 5a) with single doses of 2 and 4 Gy. These results were confirmed with the treatments of hMDM (Figure 5b), PMA-differentiated THP1 macrophages (Figure 5c) and RAW264.7 macrophages (Figures 5d and e) with human or murine IFN-γ (Figures 5b, c and e) or IR (Figure 5d). NOX2 expression was also found increased in $CD68^+$ macrophages that were detected in tumor samples obtained 6 weeks after radiotherapy of rectal cancer patients (Figures 5f and g), as compared to biopsies obtained from the same patients before radiotherapy. Then, we evaluated the effect of the pharmacological NADPH oxidase inhibitor, diphenylene iodonium (DPI) on ROS production, ATMS1981* and IRF5 upregulation detected after the treatment of RAW264.7 macrophages with IR (Figures 5h, i and l) or mIFN-γ (Figures 5j, k and m). We demonstrated that DPI impaired all events of the above-described signaling cascade (Figures 5h–m) without modifying macrophage viability (Supplementary Figures 3e and 3f). In addition, as revealed by immunoblots, the depletion of NOX2 with specific small interfering RNA in irradiated (Figure 5n and Supplementary Figure 3g) or mIFN-γ-treated (Figure 5o and Supplementary Figure 3h) RAW264.7 macrophages reduced also ATMS1981* and IRF5 upregulation, in comparison to control cells. These results demonstrate that the induction of NOX2-dependent ATM activation is required for tuning macrophages toward a pro-inflammatory phenotype.

The alteration of NOX2-dependent tumor macrophage activation is associated with poor prognosis after radiotherapy. Despite the fact that neoadjuvant chemoradiotherapy for locally advanced rectal cancer patients improve the local control of the tumors, only 15% of patients exhibit a complete response to treatment.[37] In this context, we determined whether the perturbation of the signaling pathway that we involved in the macrophage activation toward a pro-inflammatory phenotype might be associated with the absence of local response to radiotherapy. We analyzed resected specimens of rectal cancer patients obtained after neoadjuvant radiotherapy performed before radical tumor resection. According to the tumor regression grade (TRG) criteria, these patients were classified into 'good responders' (TRG $\leqslant 2$, $n=29$) and 'bad responders' (TRG $\geqslant 3$, $n=27$) (Supplementary Table 1). We analyzed the total number of $CD68^+$ TAM in both groups of irradiated tumors, and did not detect a significant difference in the $CD68^+$ TAMs infiltration (Figure 6a). In addition, we also detected the autophosphorylation ATMS1981* in ~20% of TAMs (Figure 6b), but we did not observe a significant difference for the frequencies of TAMs exhibiting ATMS1981* ($ATMS1981^{*+}$ $CD68^+$) between the two groups of tumors (Figure 6c). Interestingly, we detected a significant increase in the frequency of TAMs revealing an enhanced expression of iNOS ($iNOS^+CD68^+$) in tumor samples obtained from 'good responders' as compared to those obtained from 'bad responders' (Figures 6d and e), confirming that macrophage activation toward a pro-inflammatory phenotype is associated with the local tumor control. Finally, we found a higher frequency of TAMs showing an upregulation of

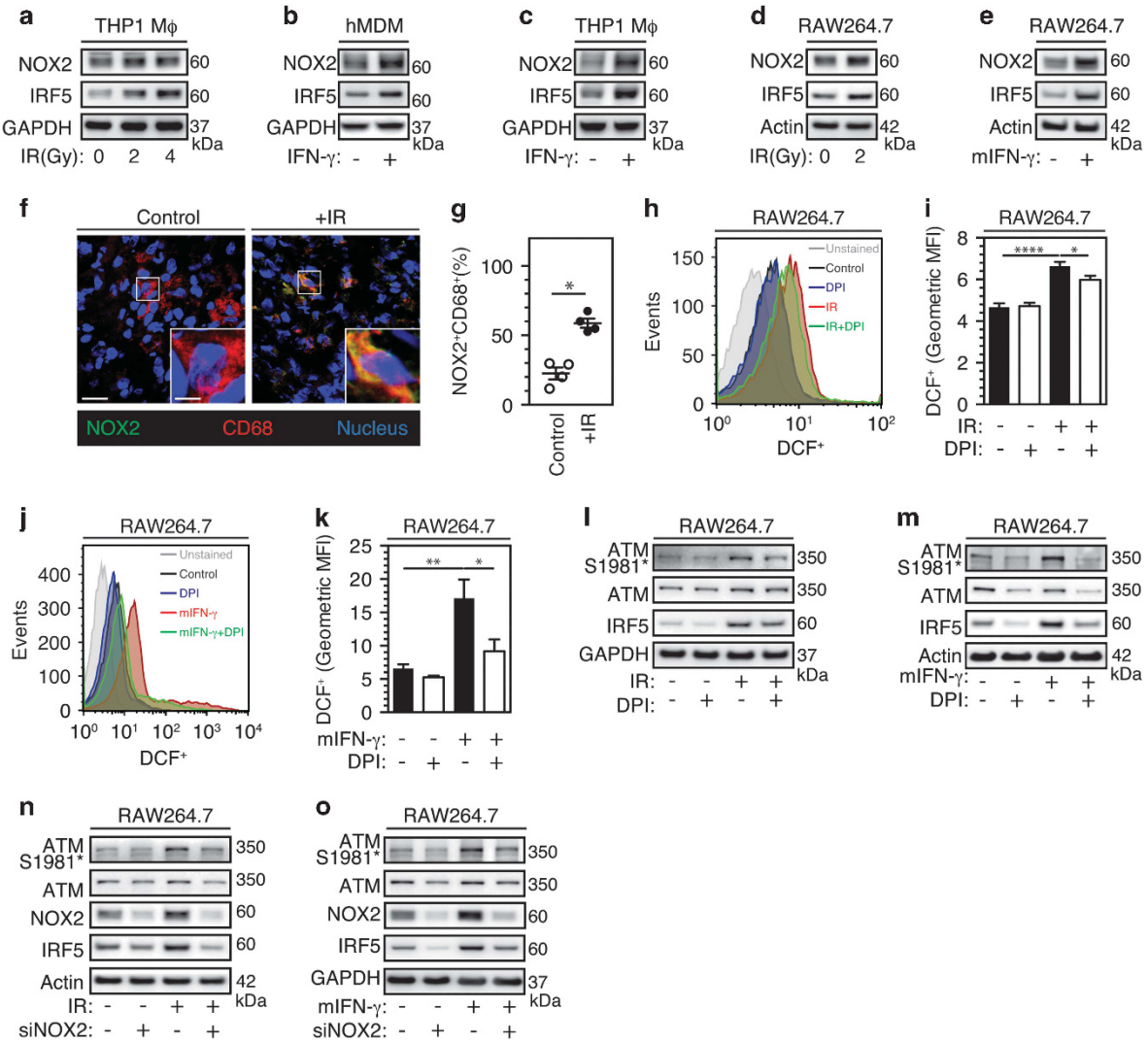

Figure 5 NOX2-dependent ROS production is involved in the pro-inflammatory macrophage activation. (**a**–**e**) NOX2 and IRF5 expressions after, respectively, 96 and 6 h culture of PMA-differentiated human THP1 macrophages (**a**) or murine RAW264.7 macrophages (**d**) that have been irradiated (or not) with indicated doses (**a** and **d**); or 24 h culture of hMDM with 4 μg/ml of human IFN-γ (**b**), PMA-differentiated human THP1 macrophages with 20 ng/ml of human IFN-γ (**c**) or murine RAW264.7 macrophages with 20 ng/ml of mIFN-γ (**e**) were determined. Representative immunoblots are shown. GAPDH and actin were used as loading control. (**f**, **g**) Representative confocal micrographs and frequencies of $NOX2^+CD68^+$ tumor-associated macrophages detected in absence or after 45 Gy total dose of fractionated irradiation on tumor samples obtained from locally advanced rectal cancer patients are shown (scale bar, 20 μm; scale bar of insert, 5 μm). Results are expressed as mean value ± S.E.M. *P*-value (*$P<0.05$) was calculated using Mann–Whitney *U*-test. (**h**–**k**) Murine RAW264.7 macrophages treated with 200 nM of DPI and irradiated with 2 Gy single dose (**h**, **i**) or stimulated with 20 ng/ml mIFN-γ (**j**, **k**) stained with H_2DCFDA and analyzed by flow cytometry. Representative flow cytometry analysis and quantifications of geometric MFI are shown. Data are presented as means ± S.E.M. in **i** and **k** panels. Significances are *$P<0.05$, **$P<0.01$ and ****$P<0.0001$, and were obtained using one-way ANOVA test. (**l**–**o**) ATMS1981*, ATM and IRF5 expressions after, respectively, 6 and 24 h culture of murine RAW264.7 macrophages that have been incubated with 200 nM of DPI (**l**, **m**) or depleted for NOX2 (**n**, **o**) and irradiated with 2 Gy single dose (**l**, **n**) or treated with 20 ng/ml mIFN-γ (**m**, **o**) were determined. Representative immunoblots are shown. GAPDH and actin were used as loading control. Quantification of western blot bands are shown in Supplementary Figure 6

$NOX2^+CD68^+$) in resected specimens obtained from 'good responders', as compared to those obtained from 'bad responders' (Figures 6f and g), revealing that the detection of NOX2 expression on TAMs may serve as a predictive factor for radiotherapy effectiveness. Multivariate statistical analysis confirmed these results (Table 1). Altogether, these results confirm that the NOX2 → ROS → ATMS1981* cascade may contribute to an efficient macrophage activation in response to radiotherapy.

Discussion

Phenotypic and functional plasticity are key features of immune cells.[38] TAMs display a mixed functional phenotype with a majority of alternative features[39] that have been associated with tumor growth and resistance to anticancer therapies. Although reprogramming TAMs represents a promising approach to enhance cancer therapies,[40–44] molecular mechanisms underlying IR-elicited macrophage activation have been poorly characterized.

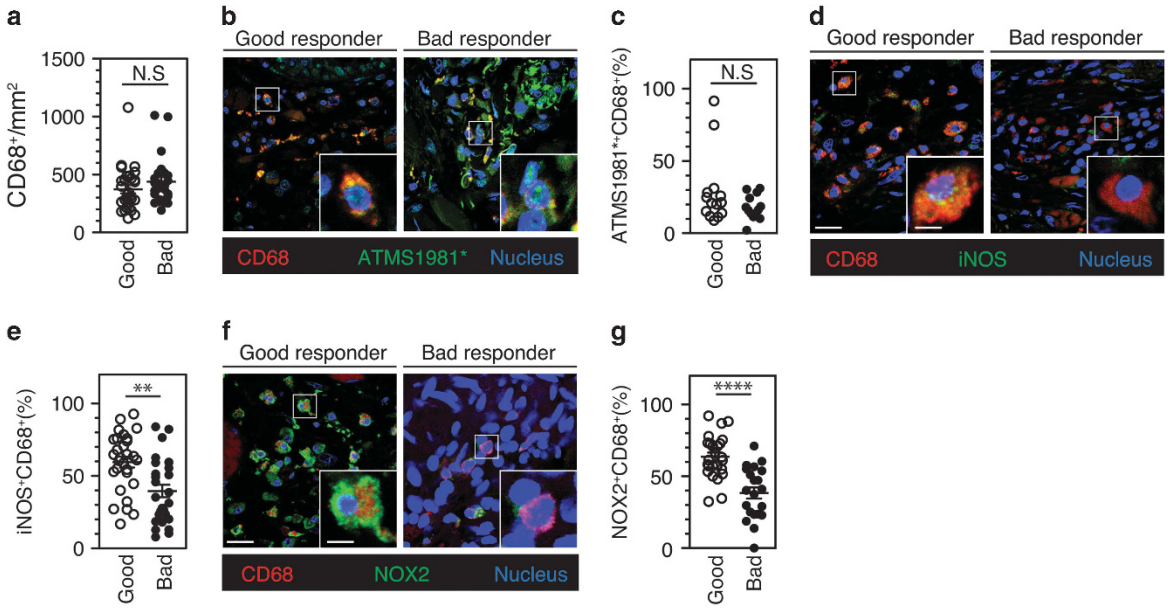

Figure 6 The perturbation of NOX2/ATM-dependent signaling pathway is associated with poor tumor response to radiation therapy.(**a**) Densities of $CD68^+$ tumor-infiltrating macrophages detected on biopsies of human rectal tumor samples from good responders ($n=29$) and bad responders ($n=27$) to neoadjuvant radiation therapy were analyzed. Data are presented as means ± S.E.M. (**b**) Representative confocal micrographs and frequencies of $ATMS1981^{*+}CD68^+$ (**b**, **c**), $iNOS^+CD68^+$ (**d**, **e**) or $NOX2^+CD68^+$ (**f**, **g**) tumor-associated macrophages detected in good responders ($n=29$) and bad responders ($n=27$) to neoadjuvant radiation therapy are shown (scale bar, 20 μm). Representative $ATMS1981^{*+}CD68^+$, $iNOS^+CD68^+$ or $NOX2^+CD68^+$ macrophages are shown in inserts (scale bar, 5 μm). Results are expressed as mean value ± S.E.M. *P*-values (**$P<0.01$ and ***$P<0.001$) were calculated using Mann–Whitney *U*-test

Table 1 Multivariate analysis of macrophage histological markers in rectal cancer response to neoadjuvant radiotherapy

	OR TRG (3–4–5) *versus* (1–2)	95% CI	*P*-value
$CD68^+/mm^2$			
Median cutoff			0.635
<376.23	1		
$\geqslant 376.23$	1.369	(0.374–5.010)	
$iNOS^+/CD68^+$ (%)			
Median cutoff			**0.003**
<53.72	1		
$\geqslant 53.72$	0.089	(0.018–0.431)	
$NOX2^+/CD68^+$ (%)			
Median cutoff			**0.006**
<55.07	1		
$\geqslant 55.07$	0.077	(0.013–0.472)	
$ATMS1981^{*+}/CD68^+$ (%)			
Median cutoff			0.339
<14.93	1		
$\geqslant 14.93$	0.513	(0.131–2.013)	

Abbreviations: CI, confidence interval; OR, odds ratios.
The statistical comparisons of indicated histological markers between 'good responders' (TRG $\leqslant 2$, $n=29$) and 'bad responders' (TRG $\geqslant 3$, $n=27$) have been adjusted on TNM stages, time interval between radiotherapy and surgery, and concomitance with chemotherapy. Median cutoff, OR and 95% CI are indicated. *P*-values were calculated using Wald test and significant *P* values are indicated in bold

In this paper, we showed that the *in vitro* treatment of macrophages with various doses of IR led to their activation toward a pro-inflammatory phenotype. Our observations were confirmed using xenograft tumor models and human rectal cancer specimens obtained from patients that have been treated with chemoradiotherapy. Consistent with other *in vitro* and *in vivo* studies,[13,15,45,46] our results revealed that the transcription factor IRF5, which is the major regulator of pro-inflammatory macrophage phenotype,[15] is activated in response to IR (as revealed by the upregulated expressions of IRF5- and IRF5-dependent target genes (such as IL-6, TNF-α or IFN-γ)). IRF5, which is involved in the regulation of the expression of pro-inflammatory cytokine genes and in the repression of anti-inflammatory cytokine genes (such as IL-10),[15,47] plays also a central role in hematopoietic cell development[48] and in the susceptibility to inflammatory autoimmune diseases (such as systematic lupus erythematosus, rheumatoid arthritis and multiple sclerosis),[49–51] demonstrating that the expression of IRF5 is tightly regulated during macrophage homeostasis.

Considering that IR mainly acts through the induction of DNA damages and the production of ROS,[52,53] we then investigated the role of DNA damage response and ROS production during this process. In this paper, we initially reported that the DNA damage/repair kinase ATM is activated by IR and by classical macrophage activators (such as LPS and IFN-γ), and that DNA damage/repair ATM kinase is required for macrophage activation. Despite the fact that the ATM kinase may contribute to the development of T cells[54] and of professional antigen-presenting cells (such as macrophage and dendritic cells)[55,56] and modulate functions of immune cells (such as STING-dependent macrophage production of type I IFNs[57]), the contribution of ATM to macrophage activation was never investigated. Here, we found that IR induced the phosphorylation of ATM (on serine 1981) and of

the histone H2AX (on serine 139) in a time- and dose-dependent manner in macrophages, indicating that DNA double-strand breaks and DNA damage response are elicited during macrophage activation. Moreover, our results also demonstrated that ATM inhibition reduces IRF5 mRNA level, highlighting that the biological activity of the kinase ATM controls macrophage activation through the regulation of IRF5 transcription. Despite the fact that several molecular components of DNA damage response pathways (such as Nijmegen breakage syndrome 1 (NBS1) protein[58]) have already been involved in monocyte/macrophage development and functions, the cellular events and signaling pathways that lead to ATM activation and control IRF5 expression during macrophage activation were until now never characterized.

In this study, we also identified the NOX2-dependent ROS production as an upstream second messenger required for ATM phosphorylation and macrophage activation. We found that the expression of NOX2 was increased after IR or IFN-γ treatment. The increased NOX2 expression that we detected both *in vitro* and in 'good responders' to radiotherapy might be regulated at transcriptional level (through the activation of PU.1 or NF-κB transcription factors[35]) or at post-transcriptional level.[35] Increased expression of NOX2 then led to the generation of ROS that contributes to double-strand breaks formation, induces the activation of ATM and IRF5, and favors the functional switch of macrophages from anti-inflammatory to pro-inflammatory phenotype (Figure 7). Although we demonstrated that NOX2 expression controlled macrophage activation after IR or IFN-γ stimulation, the precise mechanisms involved in NOX2 expression or linking DNA double-stand breaks formation, phosphorylation of ATM (ATMS1981*) and IRF5 expression are under active investigations. In this study, we also demonstrated that the histological detection of any components of the molecular cascade that we described in macrophages (NOX2 → ROS → ATMS1981* → IRF5) predicted the effectiveness of radiotherapy and might also help for the prediction of other anticancer treatments.

We also showed that the modulation of these components impacts the reprogramming of macrophages elicited by IR or IFN-γ. We found that ROS scavenging or inhibition of NOX2 or ATM activity interrupts this molecular cascade *in vitro*. Moreover, we did not detect the induction of this signaling pathway on tumor samples obtained from 'bad responders' as compared to those obtained from 'good responders'. More importantly, we demonstrated that modulators of DNA repair (such as Olaparib) that are currently evaluated in combination with radiotherapy triggered this signaling pathway and resulted in macrophage activation toward a pro-inflammatory phenotype. In this context, the stimulation of NOX2 activity, the enhanced generation of ROS, the inhibition of DNA repair, the activation of ATM or the transactivation of IRF5 could constitute effective strategies to enhance radiotherapy efficacy in clinic. Therefore, our results suggested that macrophage activation toward NOX2-/ATM-dependent pro-inflammatory phenotype was involved in the tumor response to chemoradiotherapy (with no impact on the overall survival and disease-free survival of patients). We propose that by combining radiotherapy with other modalities of cancer treatments (such as PARP inhibitors) might enhance the tumor response to radiotherapy and lead to a long-term benefit to rectal patients.

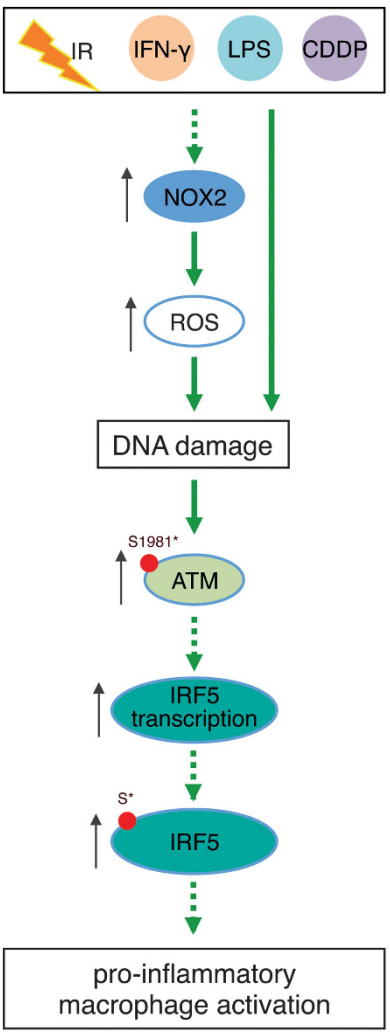

Figure 7 Proposed model for the roles of NOX2 and ATM activations in pro-inflammatory macrophage activation

Materials and Methods

Cells and reagents. The human monocyte cell line THP1 cells and the murine macrophage-like RAW264.7 cells were maintained in RMPI-1640-Glutamax medium (Life Technologies, Carlsbad, CA, USA) supplemented with 10% heat-inactivated fetal bovine serum (FBS) (Hycultec GmbH, Beutelsbach, Germany) and 100 IU/ml penicillin–streptomycin (Life Technologies). To obtain THP1 macrophages, THP1 monocytes were differentiated with 320 nM of PMA (#tlrl-PMA, Invivogen, San Diego, CA, USA) during 24 h. Then, cells were washed three times to remove PMA and non-adherent cells. For the generation of hMDM, buffy coats from healthy donor blood were obtained from the French blood bank (Etablissement Français du Sang) under the control of convention with the INSERM. In accordance with French law, written informed consent for the use of cells for clinical research was obtained from each donor. Monocytes were obtained from buffy coats and were differentiated into macrophages by using human AB serum in macrophage medium, as previously described.[59] After 7-day differentiation, hMDM were harvested and suspended in macrophage medium containing 10% (vol/vol) heat-inactivated FBS, yielding from 91 to 96% of CD14-positive cells that expressed macrophage differentiation markers (C11b and CD71), and macrophage alternative activation markers (CD163). All cells were maintained under 5% CO_2 humidified atmosphere at 37 °C. Dimethyl sulfoxide

(DMSO, #D2650), LPS (#L2880), N-acetyl-L-cysteine (NAC, #A7250), diphenyleneiodonium chloride (DPI, D2926), NCZ (#N9162), *cis*-diammineplatinum(II) dichloride (cisplatin) (CDDP, #P4394) were purchased from Sigma-Aldrich (St. Louis, MO, USA). Recombinant murine IFN-γ (mIFN-γ, ♯315 – 05) was obtained from PeproTech (Neuilly-sur-seine, France). Recombinant Human IFN-γ (IFN-γ, #285-IF/CF) was from R&D Systems (Minneapolis, MN, USA). KU55933 (#3544/10) was from Tocris Bioscience (Bristol, UK). Mn(III)tetrakis (Fontenay-sous-bois, France) (4-benzoic acid) porphyrin chloride (MnTBAP, #475870) was from Calbiochem (San Diego, CA, USA). Olaparib (#S1060) was from Selleckchem (Houston, TX, USA). PMA (#tlrl-PMA) was from Invivogen.

Antibodies. Antibodies used for immunofluorescence were anti-phospho-ATM (Ser1981) (#ab36810), anti-iNOS (#3523) antibodies from Abcam (Cambridge, UK), anti-53BP1 (#4937) antibody from Cell Signaling Technology (Danvers, MA, USA), anti-phospho-H2AX (Ser139) (#05-636) antibody from EMD Millipore (Billerica, MA, USA). Antibodies used for immunoblots were anti-phospho-ATM (Ser1981) (10H11.E12) (#4526) and anti-ATM (D2E2) (#2873) antibodies from Cell Signaling Technology; anti-IRF5 (#ab21689), anti-phospho-serine (#ab9332) and anti-IL-1β (#ab2105) antibodies were from Abcam; anti-gp91-phox (54.1) (NOX2) (#sc-13054) antibody was from Santa Cruz (Dallas, TX, USA). Anti-GAPDH antibody (#MAB374, EMD Millipore) or anti-beta actin antibody (AC-15) (HRP) (#49900, Abcam) was used as a loading control. Phenotypic analyses on primary human MDMs were realized by flow cytometry using anti-CD14 (PE) (#12-1049-42, eBioscience, Illkrich, France), anti-CD11b (APC-Cy7) (#557657, BD Pharmingen, Le pont de Claix, France), anti-CD71 (PE) (#555537, BD Pharmingen, Le pont de Claix, France) and anti-CD163 (Alexa Fluor 647) (#562669, BD Pharmingen) antibodies. For immunohistochemistry staining, anti-mouse CD11b (Clone M1/70, #550282) antibody was purchased from BD Biosciences (Le pont de Claix, France); anti-phospho-ATM (Ser1981) (EP1890Y, #GTX61739) antibody was from GeneTex (Irvine, CA, USA); anti-gp91-phox (54.1) (NOX2) antibody was from Santa Cruz (sc-130534, Dallas, TX, USA); anti-phospho-H2AX (Ser139) (#05-636) was from EMD Millipore, anti-iNOS (#ab3523) was from Abcam and anti-human CD68 antibodies were, respectively, from DAKO (Santa Clara, CA, USA) (#MO876) and Thermo Fischer Scientific (#PA5-32331, Illkrich, France).

Macrophage activation. Human MDM (10^6) were activated by treatment with 4 μg recombinant human IFN-γ for 24 h. THP1 monocytes were differentiated into macrophages by 320 nM PMA for 24 h. Then, macrophages were activated with 20 ng/ml recombinant human IFN-γ or 100 ng/ml LPS during 24 h. RAW264.7 macrophages were activated with 20 ng/ml recombinant murine IFN-γ or 100 ng/ml LPS for 24 h.

Irradiation. Cells were seeded in 6-well plates, 12-well plates or 25 cm^2 flasks and irradiated with gamma-ray irradiator IBL-637 (Cs^{137}, 1 Gy/min, gamma CIS-BioInternational, IBA, Saclay, France) or with X-ray irradiator (1 Gy/min, X-RAD 320, Precision X-Ray). Cells were harvested at indicated time points (hMDMs and THP1 macrophages at 96 h, RAW264.7 macrophages at 6 h for cell lysates and 12 h for supernatants) after irradiation for subsequent experiments.

RNA-mediated interference. The SMARTpool siGENOME ATM siRNA (M-003201-04-0005) against ATM (siRNA ATM), SMARTpool siGENOME CYBB siRNA (M-011021-01-0005) against NOX2 (siRNA NOX2) and siGENOME Non-Targeting siRNA Pool #1 (D-001206-13-05) as control were purchased from Dharmacon (Lafayette, CO, USA). siRNA-5 control, siRNA-4 and siRNA-5 against ATM were from Sigma-Aldrich. Sequences of siRNAs are as follows: SMARTpool siGENOME CYBB siRNAs (containing siRNA-1: 5′-GAAGACAACUGGACAGGAA-3′; siRNA-2: 5′-GGAACUGGGCUGUGAAUGA-3′; siRNA-3: 5′-GUGAAUGCCCGAGUCAAUA-3′ and siRNA-4: 5′-GAAACUACCUAAGAUAGCG-3′); SMARTpool siGENOME ATM siRNAs (containing siRNA-1: 5′-GCAAAGCCCUAGUAACAUA-3′; siRNA-2: 5′-GGGCAUUACGGGUGUUGAA-3′; siRNA-3: 5′-UCGCUUAGCAGGAGGUGUA-3′; siRNA-4: 5′-UGAUGAAGAGAGACGGAAU-3′); ATM siRNA-5 (5′-UGAAGUCCAUUGCUAAUCA-3′); ATM siRNA-6 (5′-AACAUACUACUCAAAGACA-3′) and control siRNA-5 (5′-UUCAAUAAAUUCUUGAGGU-3′). Sequences of ATM siRNA-5, ATM siRNA-6 and SMARTpool siGENOME CYBB siRNA (M-011021-01-0005) that we used are, respectively, perfectly aligned against mouse *ATM* or *NOX2* genes. The control siGENOME Non-Targeting siRNAs were a pool of four on-target plus non-targeting siRNAs. INTERFERin Reagent (#409-10, Polyplus Transfection, Illkrich, France) was used as the siRNA transfection reagent for hMDM and PMA-differentiated THP1 macrophages according to the manufacturer's instructions. Transfection of hMDM was performed as previously described.[59] Briefly, hMDM were seeded (2.5×10^5 hMDM/0.25 ml per well in 24-well plate in macrophages medium+10% FBS) and were allowed to adhere to the substrate by culturing at 37 °C for 2 h prior to siRNAs transfection. siRNAs were pre-diluted in 125 μl of Opti-MEM (Thermo Fisher Scientific) in which 10 μl of INTERFERin were then added. The transfection mix was left to incubate at room temperature for 15 min and was added to hMDM to achieve the final concentration of 100 nM siRNAs. The MDMs were then incubated at 37 °C for 24 h. The medium was replaced by fresh macrophage medium supplemented with 10% FBS before subsequent experiments. Lipofectamine RNAi max (#13778150, Life Technologies, Illkrich, France) was used to transfect RAW264.7 macrophages according to the manufacturer's instructions. Briefly, RAW264.7 cells were seeded (10^5 cells per ml per well in 12-well plate) and were allowed to adhere to the substrate by culturing at 37 °C for 24 h prior to siRNAs transfection. The transfection mix was added to the final concentration of 10 nM siRNAs. The RAW264.7 cells were then incubated at 37 °C for 24 h before subsequent experiments.

Immunofluorescence microscopy and flow cytometry. Cells were grown on coverslips and were treated as indicated. After treatment, cells were rinsed twice, fixed with 10% neutral buffered formalin (Sigma-Aldrich) for 10 min and then permeabilized with 0.3% Triton X-100 in PBS for 15 min. Cells were then washed twice with PBS and were blocked with 10% FBS in PBS for 1 h at room temperature, followed by incubation with primary antibodies in 10% FBS in PBS for 1 h at 30 °C at room temperature. Then, samples were incubated with secondary antibodies using Alexa Fluor 488 green or Alexa Fluor-546 red (Life Technologies, Illkrich, France) and Hoechst 33342 for nuclei (Thermo Fisher Scientific) in 10% FBS in PBS for 30 min at room temperature. Coverslips were mounted with Fluoromount-G (SouthernBiotech, Birmingham, AL, USA) and then visualized with Leica TCS SPE confocal microscope (Leica Microsystems, Nanterre, France) using a $\times$63 objective. In experiments of 53BP1 and γ-H2AX foci visualization in irradiated THP1 cells, Z series of optical sections at 1 μm increments was acquired. In experiments of ATMS1981* and γ-H2AX foci visualization in RAW264.7 cells treated with mIFN-γ, LPS or CDDP, Z series of optical sections at 1.7 μm increments were acquired. In experiments of ATMS1981* and γ-H2AX foci visualization in RAW264.7 cells treated with KU55933 and irradiated, Z series of optical sections at 2.0 μm increments were acquired. For flow cytometry analysis, PMA-differentiated THP1 macrophages were fixed in 4% paraformaldehyde–PBS for 15 min and permeabilized with 0.03% Triton X-100 (Sigma-Aldrich) for 15 min at room temperature. Cells were then blocked with FBS during 1 h at 4 °C and incubated as indicated for 30 min at 4 °C, with anti-phospho-ATM (Ser1981) (EP1890Y) (#GTX61739, GeneTex, Irvine, CA, USA), anti-phospho-H2AX (Ser139) (#05-636, EMD Millipore) or anti-iNOS (#ab3523, Abcam) antibodies. Then, cells were incubated with the secondary antibodies conjugated to Alexa Fluor 488 fluorochrome (Life Technologies) for 30 min at 4 °C and analyzed with Guava flow cytometer (EMD Millipore).

Immunoprecipitation and western blots. Cells were washed twice with cold PBS and lysed with NEHN buffer (0.5% NP40, 20% Glycerol, 300 mM NaCl, 20 mM Hepes, pH 7.5 and 1 mM EDTA) complemented with 2.5 mM DTT, and the protease and phosphatase inhibitor (Roche, Basel, Switzerland) at 4 °C. About 5–20 μg of proteins were separated by NuPAGE 4–12% or 10% SDS-PAGE gel (Invitrogen, Illkrich, France), and then were transferred onto a nitrocellulose membrane (0.2 μ, Bio-Rad, Marnes-la-coquette, France). Membranes were blocked with 5% non-fat milk or 5% bovine serum albumin (BSA) in Tris-buffered saline and 0.1% Tween 20 (TBS-T) at room temperature for 1 h and then subsequently probed with primary antibodies overnight at 4 °C. Then, membranes were incubated with appropriate horseradish peroxidase-conjugated anti-rabbit or anti-mouse IgG (SouthernBiotech, Birmingham, AL, USA) for 1 h at room temperature. After three washes with TBS-T, immunoblots were revealed using G:BOX Chemi XL1.4 Fluorescent & Chemiluminescent Imaging System (Syngene, Cambridge, UK). For immunoprecipitations, 2 Gy-irradiated RAW264.7 cells were harvested and lysed in NEHN buffer. About 2 mg of total lysates were incubated with 2 μg of anti-IRF5 antibodies (#ab21689, Abcam) or with anti-phospho-serine antibodies (#ab9332, Abcam) at 4 °C on the wheel for overnight. Then, the immunocomplexes were precipitated with protein G immobilized on sepharose beads for further 4 h at 4 °C. After three washings in NEHN buffer containing 300 mM NaCl and one in NEHN buffer with 600 mM NaCl, immunoprecipitates and protein inputs were boiled in the Laemmli buffer (Bio-Rad, Marnes-la-coquette, France) for 10 min at 95 °C and analyzed by western blot for the indicated antibodies.

Detection of ROS production. Hydrogen peroxide and anion superoxide production were determined by staining cells with 5 μM of 2,7-dichlorodihydrofluorescein diacetate (H_2DCFDA, #D6883, Sigma-Aldrich) for 40 min at 37 °C. Cells were then washed twice with Hanks' balanced salt solution (HBSS, Thermo Fisher Scientific, Illkrich, France) and suspended in cold HBSS solution containing 1% FBS for FACS analysis.

Determination of LDH release. The release of LDH in the supernatants of cultured cells was detected using Cytotoxicity Detection KitPLUS (LDH, #04744926001) from Roche according to the manufacturer's instructions.

Quantitative RT-PCR. Total RNA of 2 Gy-irradiated PMA-differentiated THP1 macrophages and control cells were purified using RNeasy kit (Qiagen, Hilden, Germany) after 96 h post irradiation according to the manufacturer's instructions. For the detection of cytokine mRNA, the synthesis of cDNA and the quantitative PCR procedure using Syber Green were performed as previously described.[60] The sequences of the primers used are the following: (5′–3′) IL-23 (F:GTTCTGCTT GCAAAGGATCCA, R:TATCCGATCCTAGCAGCTTCTCA), IL-6 (F:GCTGCAGGCAC AGAACCA, R:ACTCCTTAAAGCTGCGCAGAA), TNFα (F:GGAGAAGGGTGACCG ACTCA, R:TGCCCAGACTCGGCAAAG), IFNγ (F:AACTCATCCAAGTGATGGCTG AA, R:CTGACTCCTTTTTCGCTTCCCTG) and HPRT1 (F:GGACAGGACTGAACG TCTTGC, R:CTTGAGCACACAGAGGGCTACA). All samples were normalized with the endogenous hypoxanthine phosphoibosyltransferase 1 (HRPT1) mRNA. For the detection of IRF5 and ATM mRNA, the cDNA synthesis and TaqMan qPCR procedures were performed as previously described.[59] The used probes of IRF5 (Hs 00158114 m1), ATM (Hs01112355 gl) and GAPDH (Hs02758991 gl) were included in the premade TaqMan Gene expression mixes obtained from Applied Biosystems (Foster City, CA, USA). Results were analyzed with the cycle threshold methods (C_T) and each sample was normalized to the quantity of endogenous GAPDH mRNA.

Human cytokine profiling. Human MDMs were irradiated at 4 Gy and were further incubated for 96 h. The supernatants were harvested, centrifuged and stored at − 80 °C until use. Human cytokines in these supernatants were measured using the proteome profiler Human cytokine array panel A (proteome profiler, #ARY005, R&D Systems) according to the manufacturer's instructions. Briefly, membranes were blocked with the blocking buffer at room temperature for 1 h. Supernatants of hMDMs were mixed with a biotinylated detection antibody cocktail and then incubated with the membranes overnight at 4 °C. Membranes were washed three times for 10 min and subsequently incubated with streptavidin–horseradish peroxidase for 30 min at room temperature. Membranes were then washed three times for 10 min and exposed to peroxidase substrate, and revealed with the G:BOX Chemi XL1.4 Fluorescent and Chemiluminescent Imaging System (Syngene). Time of exposure was between 1 and 10 min. The images were then analyzed using GeneTools software gel image analysis (Syngene).

***In vivo* mouse tumor model.** To generate xenograft tumor model, 4×10^6 human colorectal HCT116 cells were inoculated subcutaneously in the flanks of 5-week female nude mice. Two weeks later, the tumors were irradiated at 20 Gy using Variant-NDI-226-n°87262-YO X-Ray Tube. Tumor volume was monitored every 4–5 days. Mice were killed when tumors in the control group exceeded 1000 mm^3.

Immunohistochemistry. Tumors obtained from *in vivo* experiments were resected, fixed and embedded in paraffin. Paraffin-embedded tumor samples from rectal patients undergoing neoadjuvant radiotherapy were kindly offered by Dr. Celine Mirjolet in Centre Georges-François Leclerc, Dijon. Frozen tumor samples from rectal patients before and after radiotherapy were obtained from Gustave Roussy Cancer Center. Tumor sections were then dried, deparaffinized and hydrated, followed by antigen retrieval with 0.01 M sodium citrate buffer, pH 6.0 at 97.6 °C for 20 min. After washing with TBS-T, slides were blocked with 10% FBS in PBS at room temperature for 1 h. Then primary antibodies diluted in 10% FBS in PBS were applied to each section and incubated overnight in humidified chamber at 4 °C. After three washes with TBS-T, Alexa Fluor-conjugated secondary antibodies and Hoechst 33342 diluted in 10% FBS in PBS were applied to each section and incubated for 30 min at room temperature. Then, the slides were washed three times with TBS-T and once with water. Coverslips were mounted on slides using Fluoromount-G medium (SouthernBiotech) before visualization with Leica TCS SPE confocal microscope (Leica Microsystems) using a ×63 objective.

Human samples. Human tissue samples of locally advanced rectal tumors that were resected 42 days after receiving 45 Gy (1.8 Gy/sessions) concomitantly to chemotherapy (5-FU) ($n=4$) or left unirradiated ($n=4$) were obtained from Gustave Roussy Cancer Campus (Villejuif, France). All tumor samples from responders and non-responders to chemoradiotherapy were obtained from Centre Georges François Leclerc (Dijon, France). This study was approved by the IRB and the French CCTIRS committee (Comité consultatif sur le traitement de l'information en matière de recherche et de santé) and CNIL (Commission nationale de l'informatique et des libertés). Characteristics of these patients are shown in Supplementary Table 1. All these patients ($n=56$) were diagnosed for locally advanced rectal tumors and characterized the Tumor Node Metastasis (TNM) classification. All human samples were obtained after approval by the institutional review board and ethics committee, with fully informed consents.

Statistical analysis. Two-way ANOVA test was used to establish statistical differences between the growth of non-irradiated and irradiated tumors in xenografted mice, Mann–Whitney *U*-test to establish statistical differences in biological activity (iNOS or NOX2 expression) and in phosphorylation (γ-H2AX or ATMS1981*) of macrophages, and in the number of infiltrated $CD11b^+$ cells between irradiated and non-irradiated tumors of xenografted mice or between tumors obtained from locally advanced rectal cancer patients who received or not 45 Gy total dose. Multivariate analysis with Wald test was used to determine statistical differences between tumors biopsies obtained from patients with locally advanced rectal tumors that respond or not to chemoradiotherapy. Statistical analysis of *in vitro* data was performed using Student's *t*-test or one-way ANOVA test (for Figures 2p,4b, d,5i, k and Supplementary Figure 2j). Statistically significant values are reported in figure legends. All experiments were independently performed at least three times. Data are expressed as mean ± S.E.M. GraphPad Prism version 6.0b (GraphPad Software, La Jolla, CA, USA) was employed to perform statistical analysis.

Conflict of Interest

The authors declare no conflict of interest.

Acknowledgements. This work was supported by funds from Agence Nationale de la Recherche (ANR-10-IBHU-0001, ANR-10-LABX33 and ANR-11-IDEX-003-01), Electricité de France, Fondation Gustave Roussy, Institut National du Cancer (INCA 9414), NATIXIS, SIDACTION and the French National Agency for Research on AIDS and viral Hepatitis (ANRSH) (to J-LP.), Electricité de France and Fondation Gustave Roussy (to ED). QW is recipient of PhD fellowship of China Scholarship Council. AP and AA are, respectively, recipient of PhD fellowship and post-doc fellowship from Agence Nationale de Recherche sur le Sida et sur les Hépatites (ANRSH). LV and FL are recipient of PhD fellowships from Fondation pour la Recherche Médicale and CIFRE. HD, EM and MT are supported by the Laboratory of Excellence LERMIT with a grant from ANR (ANR-10-LABX-33) under the program 'Investissements d'Avenir' ANR-11-IDEX-0003-01. IM is funded by INCA (INCA-DGOS-INSERM 6043). CM work was supported by the 'Cancéropôle Grand Est', and the 'Conseils Régionaux de Bourgogne, de Franche Comté et de Lorraine'. We gratefully acknowledge S Solier, Y Lecluse and S Salome-Desnoulez for technical support.

Author contributions

QW, AA, AP, CL, CM, IM, LV, FL, HD, EM, ZM, MT, MG, OC and FM performed experiments. J-LP designed the study. QW, ED and J-LP analyzed the results, assembled the figures and wrote the paper. QW and CM performed statistical analysis. QW, DMO, FR, ES and NM provided advices and edited the paper.

1. Azzam EI, Jay-Gerin JP, Pain D. Ionizing radiation-induced metabolic oxidative stress and prolonged cell injury. *Cancer Lett* 2012; **327**: 48–60.
2. Hekim N, Cetin Z, Nikitaki Z, Cort A, Saygili EI. Radiation triggering immune response and inflammation. *Cancer Lett* 2015; **368**: 156–163.
3. Park B, Yee C, Lee KM. The effect of radiation on the immune response to cancers. *Int J Mol Sci* 2014; **15**: 927–943.
4. Kroemer G, Galluzzi L, Kepp O, Zitvogel L. Immunogenic cell death in cancer therapy. *Annu Rev Immunol* 2013; **31**: 51–72.

5. Ghiringhelli F, Apetoh L, Tesniere A, Aymeric L, Ma Y, Ortiz C *et al.* Activation of the NLRP3 inflammasome in dendritic cells induces IL-1beta-dependent adaptive immunity against tumors. *Nat Med* 2009; **15**: 1170–1178.
6. Prakash H, Klug F, Nadella V, Mazumdar V, Schmitz-Winnenthal H, Umansky L. Low doses of gamma irradiation potentially modifies immunosuppressive tumor microenvironment by retuning tumor-associated macrophages: lesson from insulinoma. *Carcinogenesis* 2016; **37**: 301–313.
7. Merrick A, Errington F, Milward K, O'Donnell D, Harrington K, Bateman A *et al.* Immunosuppressive effects of radiation on human dendritic cells: reduced IL-12 production on activation and impairment of naive T-cell priming. *Br J Cancer* 2005; **92**: 1450–1458.
8. Price JG, Idoyaga J, Salmon H, Hogstad B, Bigarella CL, Ghaffari S *et al.* CDKN1A regulates Langerhans cell survival and promotes Treg cell generation upon exposure to ionizing irradiation. *Nat Immunol* 2015; **16**: 1060–1068.
9. Klug F, Prakash H, Huber PE, Seibel T, Bender N, Halama N *et al.* Low-dose irradiation programs macrophage differentiation to an iNOS(+)/M1 phenotype that orchestrates effective T cell immunotherapy. *Cancer Cell* 2013; **24**: 589–602.
10. Chiang CS, Fu SY, Wang SC, Yu CF, Chen FH, Lin CM *et al.* Irradiation promotes an m2 macrophage phenotype in tumor hypoxia. *Front Oncol* 2012; **2**: 89.
11. Franklin RA, Liao W, Sarkar A, Kim MV, Bivona MR, Liu K *et al.* The cellular and molecular origin of tumor-associated macrophages. *Science* 2014; **344**: 921–925.
12. Mosser DM, Edwards JP. Exploring the full spectrum of macrophage activation. *Nat Rev Immunol* 2008; **8**: 958–969.
13. Weiss M, Byrne AJ, Blazek K, Saliba DG, Pease JE, Perocheau D *et al.* IRF5 controls both acute and chronic inflammation. *Proc Natl Acad Sci USA* 2015; **112**: 11001–11006.
14. Weiss M, Blazek K, Byrne AJ, Perocheau DP, Udalova IA. IRF5 is a specific marker of inflammatory macrophages *in vivo*. *Mediators Inflamm* 2013; **2013**: 245804.
15. Krausgruber T, Blazek K, Smallie T, Alzabin S, Lockstone H, Sahgal N *et al.* IRF5 promotes inflammatory macrophage polarization and TH1-TH17 responses. *Nat Immunol* 2011; **12**: 231–238.
16. Satoh T, Takeuchi O, Vandenbon A, Yasuda K, Tanaka Y, Kumagai Y *et al.* The Jmjd3-Irf4 axis regulates M2 macrophage polarization and host responses against helminth infection. *Nat Immunol* 2010; **11**: 936–944.
17. Cosin-Roger J, Ortiz-Masia D, Calatayud S, Hernandez C, Esplugues JV, Barrachina MD. The activation of Wnt signaling by a STAT6-dependent macrophage phenotype promotes mucosal repair in murine IBD. *Mucosal Immunol* 2016; **9**: 986–998.
18. Kapoor N, Niu J, Saad Y, Kumar S, Sirakova T, Becerra E *et al.* Transcription factors STAT6 and KLF4 implement macrophage polarization via the dual catalytic powers of MCPIP. *J Immunol* 2015; **194**: 6011–6023.
19. Rodriguez-Zapata M, Reyes E, Sanchez L, Espinosa A, Solera J, Alvarez-Mon M. Defective reactive oxygen metabolite generation by macrophages from acute brucellosis patients. *Infection* 1997; **25**: 187–188.
20. Colegio OR, Chu NQ, Szabo AL, Chu T, Rhebergen AM, Jairam V *et al.* Functional polarization of tumour-associated macrophages by tumour-derived lactic acid. *Nature* 2014; **513**: 559–563.
21. Wen Z, Liu H, Li M, Li B, Gao W, Shao Q *et al.* Increased metabolites of 5-lipoxygenase from hypoxic ovarian cancer cells promote tumor-associated macrophage infiltration. *Oncogene* 2015; **34**: 1241–1252.
22. Mantovani A, Sozzani S, Locati M, Allavena P, Sica A. Macrophage polarization: tumor-associated macrophages as a paradigm for polarized M2 mononuclear phagocytes. *Trends Immunol* 2002; **23**: 549–555.
23. Condeelis J, Pollard JW. Macrophages: obligate partners for tumor cell migration, invasion, and metastasis. *Cell* 2006; **124**: 263–266.
24. Coffelt SB, Hughes R, Lewis CE. Tumor-associated macrophages: effectors of angiogenesis and tumor progression. *Biochim Biophys Acta* 2009; **1796**: 11–18.
25. Lee CH, Espinosa I, Vrijaldenhoven S, Subramanian S, Montgomery KD, Zhu S *et al.* Prognostic significance of macrophage infiltration in leiomyosarcomas. *Clin Cancer Res* 2008; **14**: 1423–1430.
26. Jensen TO, Schmidt H, Moller HJ, Hoyer M, Maniecki MB, Sjoegren P *et al.* Macrophage markers in serum and tumor have prognostic impact in American Joint Committee on Cancer stage I/II melanoma. *J Clin Oncol* 2009; **27**: 3330–3337.
27. Steidl C, Lee T, Shah SP, Farinha P, Han G, Nayar T *et al.* Tumor-associated macrophages and survival in classic Hodgkin's lymphoma. *N Engl J Med* 2010; **362**: 875–885.
28. Chung FT, Lee KY, Wang CW, Heh CC, Chan YF, Chen HW *et al.* Tumor-associated macrophages correlate with response to epidermal growth factor receptor-tyrosine kinase inhibitors in advanced non-small cell lung cancer. *Int J Cancer* 2012; **131**: E227–E235.
29. Mantovani A, Allavena P. The interaction of anticancer therapies with tumor-associated macrophages. *J Exp Med* 2015; **212**: 435–445.
30. De Palma M, Lewis CE. Macrophage regulation of tumor responses to anticancer therapies. *Cancer Cell* 2013; **23**: 277–286.
31. Burma S, Chen BP, Murphy M, Kurimasa A, Chen DJ. ATM phosphorylates histone H2AX in response to DNA double-strand breaks. *J Biol Chem* 2001; **276**: 42462–42467.
32. Murray PJ, Allen JE, Biswas SK, Fisher EA, Gilroy DW, Goerdt S *et al.* Macrophage activation and polarization: nomenclature and experimental guidelines. *Immunity* 2014; **41**: 14–20.
33. Guo Z, Kozlov S, Lavin MF, Person MD, Paull TT. ATM activation by oxidative stress. *Science* 2010; **330**: 517–521.
34. Zhang Y, Choksi S, Chen K, Pobezinskaya Y, Linnoila I, Liu ZG. ROS play a critical role in the differentiation of alternatively activated macrophages and the occurrence of tumor-associated macrophages. *Cell Res* 2013; **23**: 898–914.
35. Bedard K, Krause KH. The NOX family of ROS-generating NADPH oxidases: physiology and pathophysiology. *Physiol Rev* 2007; **87**: 245–313.
36. Lambeth JD. NOX enzymes and the biology of reactive oxygen. *Nat Rev Immunol* 2004; **4**: 181–189.
37. Trakarnsanga A, Ithimakin S, Weiser MR. Treatment of locally advanced rectal cancer: controversies and questions. *World J Gastroenterol* 2012; **18**: 5521–5532.
38. Galli SJ, Borregaard N, Wynn TA. Phenotypic and functional plasticity of cells of innate immunity: macrophages, mast cells and neutrophils. *Nat Immunol* 2011; **12**: 1035–1044.
39. Mantovani A, Locati M. Tumor-associated macrophages as a paradigm of macrophage plasticity, diversity, and polarization: lessons and open questions. *Arterioscler Thromb Vasc Biol* 2013; **33**: 1478–1483.
40. Georgoudaki AM, Prokopec KE, Boura VF, Hellqvist E, Sohn S, Ostling J *et al.* Reprogramming tumor-associated macrophages by antibody targeting inhibits cancer progression and metastasis. *Cell Rep* 2016; **15**: 2000–2011.
41. Tan HY, Wang N, Man K, Tsao SW, Che CM, Feng Y. Autophagy-induced RelB/p52 activation mediates tumour-associated macrophage repolarisation and suppression of hepatocellular carcinoma by natural compound baicalin. *Cell Death Dis* 2015; **6**: e1942.
42. Rolny C, Mazzone M, Tugues S, Laoui D, Johansson I, Coulon C *et al.* HRG inhibits tumor growth and metastasis by inducing macrophage polarization and vessel normalization through downregulation of PlGF. *Cancer Cell* 2011; **19**: 31–44.
43. Buhtoiarov IN, Sondel PM, Wigginton JM, Buhtoiarova TN, Yanke EM, Mahvi DA *et al.* Anti-tumour synergy of cytotoxic chemotherapy and anti-CD40 plus CpG-ODN immunotherapy through repolarization of tumour-associated macrophages. *Immunology* 2011; **132**: 226–239.
44. Coscia M, Quaglino E, Iezzi M, Curcio C, Pantaleoni F, Riganti C *et al.* Zoledronic acid repolarizes tumour-associated macrophages and inhibits mammary carcinogenesis by targeting the mevalonate pathway. *J Cell Mol Med* 2010; **14**: 2803–2815.
45. Saliba DG, Heger A, Eames HL, Oikonomopoulos S, Teixeira A, Blazek K *et al.* IRF5:RelA interaction targets inflammatory genes in macrophages. *Cell Rep* 2014; **8**: 1308–1317.
46. Bowdridge S, Gause WC. Regulation of alternative macrophage activation by chromatin remodeling. *Nat Immunol* 2010; **11**: 879–881.
47. Krausgruber T, Saliba D, Ryzhakov G, Lanfrancotti A, Blazek K, Udalova IA. IRF5 is required for late-phase TNF secretion by human dendritic cells. *Blood* 2010; **115**: 4421–4430.
48. Lien C, Fang CM, Huso D, Livak F, Lu R, Pitha PM. Critical role of IRF-5 in regulation of B-cell differentiation. *Proc Natl Acad Sci USA* 2010; **107**: 4664–4668.
49. Jia X, Hu M, Lin Q, Ren H. Association of the IRF5 rs2004640 polymorphism with rheumatoid arthritis: a meta-analysis. *Rheumatol Int* 2013; **33**: 2757–2761.
50. Graham RR, Kozyrev SV, Baechler EC, Reddy MV, Plenge RM, Bauer JW *et al.* A common haplotype of interferon regulatory factor 5 (IRF5) regulates splicing and expression and is associated with increased risk of systemic lupus erythematosus. *Nat Genet* 2006; **38**: 550–555.
51. Carmona FD, Martin JE, Beretta L, Simeon CP, Carreira PE, Callejas JL *et al.* The systemic lupus erythematosus IRF5 risk haplotype is associated with systemic sclerosis. *PLoS ONE* 2013; **8**: e54419.
52. Baskar R, Lee KA, Yeo R, Yeoh KW. Cancer and radiation therapy: current advances and future directions. *Int J Med Sci* 2012; **9**: 193–199.
53. Eriksson D, Stigbrand T. Radiation-induced cell death mechanisms. *Tumour Biol* 2010; **31**: 363–372.
54. Matei IR, Guidos CJ, Danska JS. ATM-dependent DNA damage surveillance in T-cell development and leukemogenesis: the DSB connection. *Immunol Rev* 2006; **209**: 142–158.
55. So EY, Ouchi T. Translational initiation regulated by ATM in dendritic cells development. *Cell Death Dis* 2014; **5**: e1418.
56. So EY, Kozicki M, Ouchi T. Roles of DNA damage response proteins in mitogen-induced Thp-1 differentiation into macrophage. *J Cancer Biol Res* 2013; **1**: 1–3.
57. Hartlova A, Erttmann SF, Raffi FA, Schmalz AM, Resch U, Anugula S *et al.* DNA damage primes the type I interferon system via the cytosolic DNA sensor STING to promote anti-microbial innate immunity. *Immunity* 2015; **42**: 332–343.
58. Pereira-Lopes S, Tur J, Calatayud-Subias JA, Lloberas J, Stracker TH, Celada A. NBS1 is required for macrophage homeostasis and functional activity in mice. *Blood* 2015; **126**: 2502–2510.
59. Allouch A, David A, Amie SM, Lahouassa H, Chartier L, Margottin-Goguet F *et al.* p21-mediated RNR2 repression restricts HIV-1 replication in macrophages by inhibiting dNTP biosynthesis pathway. *Proc Natl Acad Sci USA* 2013; **110**: E3997–E4006.
60. Solier S, Ryan MC, Martin SE, Varma S, Kohn KW, Liu H *et al.* Transcription poisoning by topoisomerase I is controlled by gene length, splice sites, and miR-142-3p. *Cancer Res* 2013; **73**: 4830–4839.

Supplementary Information accompanies this paper on *Cell Death and Differentiation* website (http://www.nature.com/cdd)

Article

Cell Reports

HIV-1 Envelope Overcomes NLRP3-Mediated Inhibition of F-Actin Polymerization for Viral Entry

Graphical Abstract

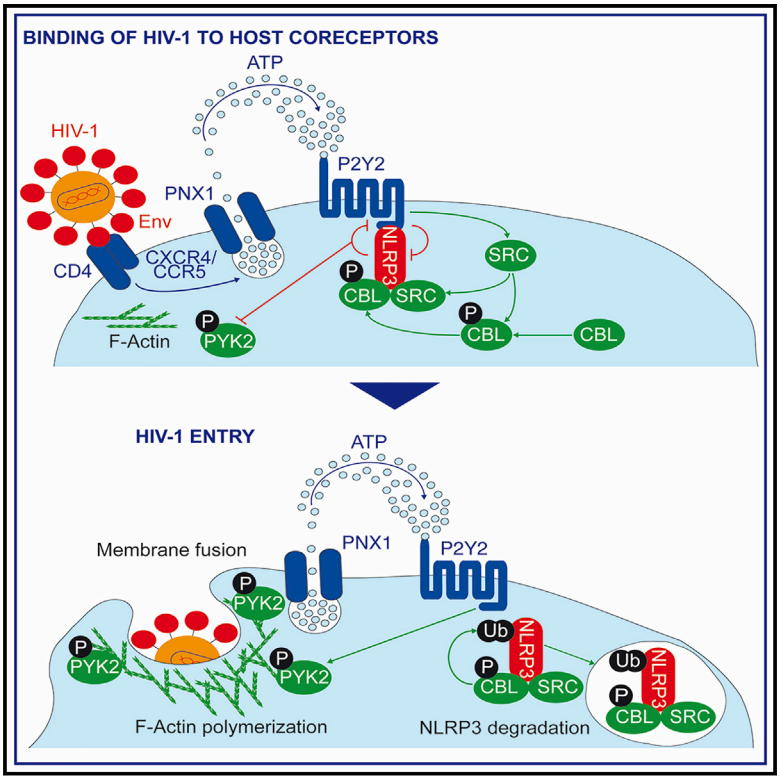

Highlights

- NLRP3 and P2Y2 interact and regulate susceptibility to HIV-1 infection
- NLRP3 is an intrinsic inhibitory factor for HIV-1 that represses F-actin remodeling
- HIV-1 Env binding to host receptors overcomes NLRP3 restriction by activating P2Y2
- P2Y2 activation leads to CBL-mediated NLRP3 degradation and favors viral entry

Authors

Audrey Paoletti, Awatef Allouch, Marina Caillet, ..., Marie-Lise Gougeon, Guido Kroemer, Jean-Luc Perfettini

Correspondence

perfettini@orange.fr

In Brief

Paoletti et al. identified a constitutive interaction between NLRP3 and P2Y2 that regulates HIV-1 entry into target cells. They revealed that NLRP3 represses viral entry by impairing F-actin reorganization. HIV-1 overcomes this host cellular resistance by inducing NLRP3 degradation through the activation of P2Y2-dependent signaling pathway.

Paoletti et al., 2019, Cell Reports *28*, 3381–3394
September 24, 2019
https://doi.org/10.1016/j.celrep.2019.02.095

CellPress

Cell Reports
Article

HIV-1 Envelope Overcomes NLRP3-Mediated Inhibition of F-Actin Polymerization for Viral Entry

Audrey Paoletti,[1,2,3,4,24] Awatef Allouch,[1,2,3,4,24] Marina Caillet,[3,4,5] Hela Saïdi,[6] Frédéric Subra,[7] Roberta Nardacci,[8] Qiuji Wu,[1,2,3,4] Zeinaf Muradova,[1,2,3,4] Laurent Voisin,[1,2,3,4] Syed Qasim Raza,[1,2,3,4] Frédéric Law,[1,2,3,4] Maxime Thoreau,[1,2,3,4] Haithem Dakhli,[1,2,3,4] Olivier Delelis,[7] Béatrice Poirier-Beaudouin,[6] Nathalie Dereuddre-Bosquet,[9,10,11] Roger Le Grand,[9,10,11] Olivier Lambotte,[9,11,12] Asier Saez-Cirion,[13] Gianfranco Pancino,[13] David M. Ojcius,[14,15] Eric Solary,[16] Eric Deutsch,[2,3,4] Mauro Piacentini,[8,17] Marie-Lise Gougeon,[6] Guido Kroemer,[5,18,19,20,21,22,23,25] and Jean-Luc Perfettini[1,2,3,4,14,25,26,*]

[1]Cell Death and Aging Team, Gustave Roussy, 114 rue Edouard Vaillant, F-94805 Villejuif, France
[2]Laboratory of Molecular Radiotherapy, INSERM U1030, Gustave Roussy, 114 rue Edouard Vaillant, F-94805 Villejuif, France
[3]Gustave Roussy, 114 rue Edouard Vaillant, F-94805 Villejuif, France
[4]Université Paris Sud - Paris 11, 114 rue Edouard Vaillant, F-94805 Villejuif, France
[5]INSERM U848, Gustave Roussy, 114 rue Edouard Vaillant, F-94805 Villejuif, France
[6]Institut Pasteur, Antiviral Immunity, Biotherapy and Vaccine Unit, Infection and Epidemiology Department, 25 rue du Dr. Roux, F-75015 Paris, France
[7]CNRS UMR 8113 LBPA, Ecole Normale Supérieure de Cachan, 61 avenue du Président Wilson, F-94230 Cachan, France
[8]National Institute for Infectious Diseases "Lazzaro Spallanzani,", Via Portuense 292, 00149 Rome, Italy
[9]INSERM U1184, Center for Immunology of Viral Infections and Autoimmune Diseases, Fontenay-aux-Roses, France
[10]Université Paris Sud, UMR 1184, Fontenay-aux-Roses, France
[11]CEA, DSV/iMETI, Division of Immunology-Virology, IDMIT, Fontenay-aux-Roses, France
[12]APHP, Service de Médecine Interne – Immunologie Clinique, Hôpitaux Universitaires Paris Sud, F-94270 Le Kremlin-Bicêtre, France
[13]Unité HIV, Inflammation et Persistance, Institut Pasteur, 25 rue du Dr. Roux, F-75025 Paris, France
[14]Department of Biomedical Sciences, University of the Pacific, Arthur A. Dugoni School of Dentistry, 155 Fifth Street, San Francisco, CA 94103, USA
[15]Université Paris Diderot, Sorbonne Paris Cité, 75013 Paris, France
[16]INSERM U1009, Gustave Roussy, 114 rue Edouard Vaillant, F-94805 Villejuif, France
[17]Department of Biology, University of Rome "Tor Vergata,", Via della Ricerca Scientifica 1, 00133 Rome, Italy
[18]Metabolomics Platform, Gustave Roussy, 114 rue Edouard Vaillant, Villejuif, France
[19]Equipe 11 labellisée Ligue contre le Cancer, Centre de Recherche des Cordeliers, INSERM U1138, Paris, France
[20]Université Paris Descartes, Sorbonne Paris Cité, Paris, France
[21]Université Pierre et Marie Curie, Paris, France
[22]Pôle de Biologie, Hôpital Européen Georges Pompidou, AP-HP, Paris, France
[23]Karolinska Institute, Department of Women's and Children's Health, Karolinska University Hospital, Stockholm, Sweden
[24]These authors contributed equally
[25]Senior author
[26]Lead Contact
*Correspondence: perfettini@orange.fr
https://doi.org/10.1016/j.celrep.2019.02.095

SUMMARY

Purinergic receptors and nucleotide-binding domain leucine-rich repeat containing (NLR) proteins have been shown to control viral infection. Here, we show that the NLR family member NLRP3 and the purinergic receptor P2Y2 constitutively interact and regulate susceptibility to HIV-1 infection. We found that NLRP3 acts as an inhibitory factor of viral entry that represses F-actin remodeling. The binding of the HIV-1 envelope to its host cell receptors (CD4, CXCR4, and/or CCR5) overcomes this restriction by stimulating P2Y2. Once activated, P2Y2 enhances its interaction with NLRP3 and stimulates the recruitment of the E3 ubiquitin ligase CBL to NLRP3, ultimately leading to NLRP3 degradation. NLRP3 degradation is permissive for PYK2 phosphorylation (PYK2Y402*) and subsequent F-actin polymerization, which is required for the entry of HIV-1 into host cells. Taken together, our results uncover a mechanism by which HIV-1 overcomes NLRP3 restriction that appears essential for the accomplishment of the early steps of HIV-1 entry.

INTRODUCTION

Although the stimulation of innate immunity with vaccine adjuvants has been extensively and efficiently harnessed for the control of major infectious diseases (such as diphtheria, tetanus, and poliomyelitis), the cellular and molecular mechanisms that orchestrate immune responses against pathogens remain largely elusive, especially with respect to the early steps of infection. Immune sensing of HIV-1 by pathogen recognition receptors (PPRs) and cytoplasmic DNA sensors may partially hinder

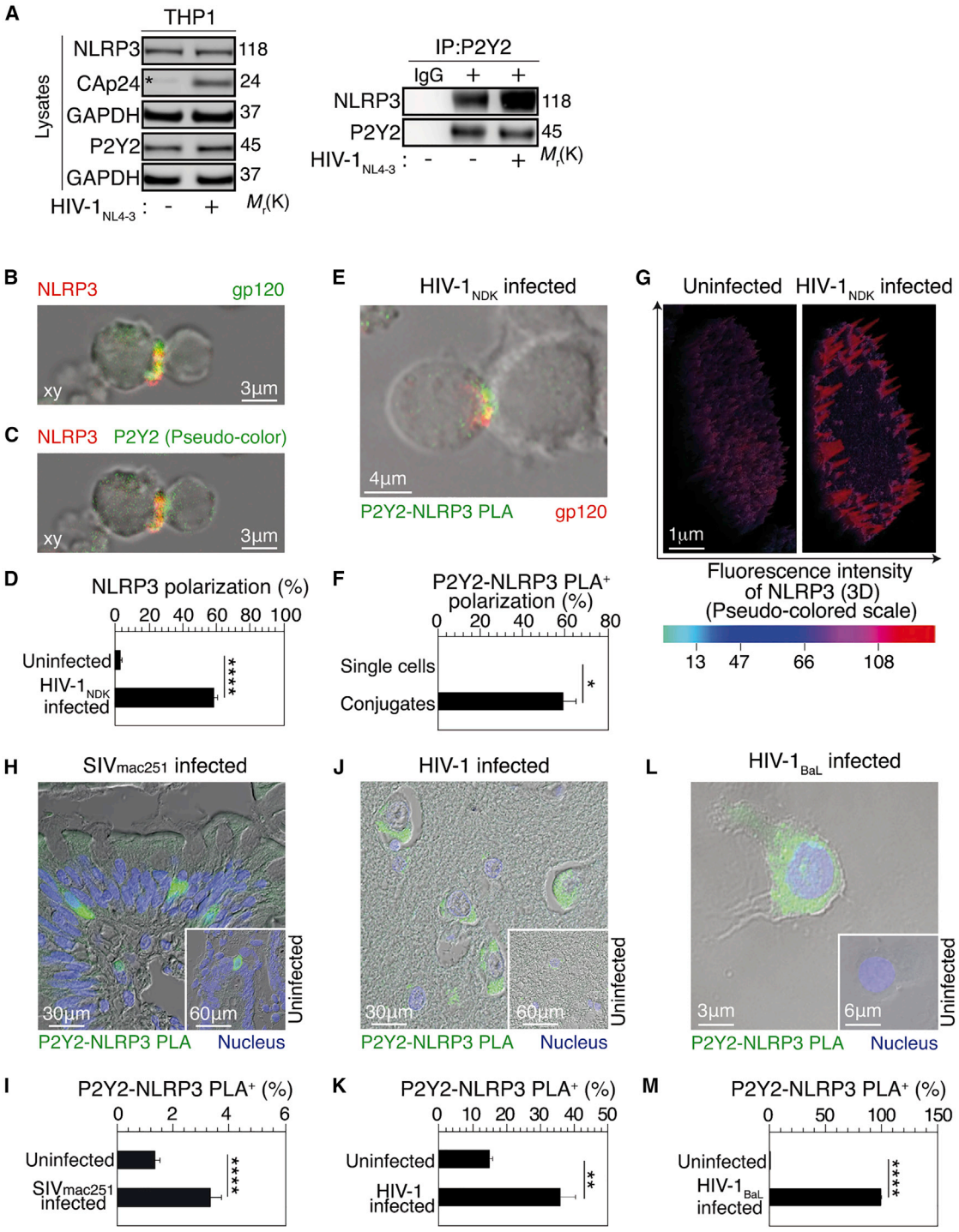

Figure 1. NLRP3 and P2Y2 Interaction Is Enhanced during HIV-1 and SIV Infections

(A) Immunoprecipitations were performed in THP1 cells after 3 h of X4-tropic HIV-1_{NL4-3} infection and analyzed by western blot. The asterisk indicates an unspecific band. Representative western blots of three independent experiments are shown. See also Figure S1A.

(B–D) Confocal microscopy images of NLRP3 (B and C), gp120 (B), and P2Y2 (C) polarizations during HIV-1-infected and uninfected lymphocyte interactions. Images are representative of three different donors. The frequency of NLRP3 polarization (D) is shown. Data are presented as means ± SEM, and significance is ****$p \leq 0.0001$ (n = 366 virological synapses from 3 independent experiments), unpaired Mann-Whitney test.

(legend continued on next page)

HIV-1 replication through the production of type-1 interferon (IFN) and the expression of restriction factors such as APOBEC3 cytidine desaminases, tetherin, and SAM domain and HD domain-containing protein 1 (SAMHD1) (Towers and Noursadeghi, 2014). Despite the beneficial impact of the cell-autonomous innate immune system on HIV-1 replication, innate signals, converging on the DNA sensing interferon gamma inducible 16 protein (IFI16) inflammasome, can contribute to chronic immune activation and eventually to pyroptosis of uninfected $CD4^+$ T cells, thereby enhancing disease progression (Doitsh et al., 2010, 2014; Monroe et al., 2014). Given the ambiguous effects of innate immune signals on HIV-1 replication and disease progression, further exploration of the innate signaling molecular pathways that govern HIV-1 infection is needed.

Most studies on HIV-1 infection have explored innate mechanisms acting before or after viral entry. Little is known about innate signaling pathways elicited during viral entry. We previously reported that purinergic receptors, which are membrane-anchored PPRs, promote the entry of HIV-1 into immune cells (Séror et al., 2011). The binding of HIV-1 envelope (Env) to its cellular receptors (CD4, CXCR4, and/or CCR5) causes the release of adenosine triphosphate (ATP) from host cells through the opening of pannexin-1 hemichannels (PNX1). Once released, extracellular ATP stimulates purinergic receptors (including the purinergic receptor P2Y2) and facilitates the membrane fusion process through the activation of the proline-rich tyrosine kinase 2 (PYK2) that is required for viral entry (Séror et al., 2011). The activation of the purinergic signaling pathway is indispensable for cell-free HIV-1 infection (Hazleton et al., 2012; Séror et al., 2011; Swartz et al., 2014), as well as for cell-to-cell transmission of the virus between infected lymphocytes and target cells, which is the most efficient route of HIV-1 spreading (Séror et al., 2011; Swartz et al., 2014). In this context, antagonists of purinergic receptors or pannexin-1 have emerged as a new class of HIV-1 microbicides (Séror et al., 2011).

Other PPRs, the NOD-like receptors (NLRs), have also been involved in the establishment of viral infection. Initially described as crucial for sensing and initiating host defense in viral infection through the formation of inflammasome (Chen and Ichinohe, 2015), NLRs (such as NLRX1) have recently been shown to be involved in the early innate response to simian immunodeficiency virus (SIV) infection and to contribute to viral replication by repressing the transcription of restriction factors (such as the interferon stimulated gene [ISG] 5, the myxovirus resistance 2 protein [MX2], and the tripartite motif-containing protein [TRIM] 5; Barouch et al., 2016). These results highlight the counterintuitive role of the inflammasome signaling, which indeed may facilitate (rather than repress) the early steps of HIV and SIV infections.

In this context and to further characterize cellular factors that may modulate P2Y2-dependent signaling during the early steps of HIV-1 infection, we studied the role of NLRs during viral infection. We identified the NACHT, LRR and PYD domains-containing protein 3 (NLRP3) as a P2Y2-interacting protein. Considering that NLRP3 and P2Y2 are endogenously expressed in $CD4^+$ T cells and cells from mononuclear phagocyte lineage (including monocytes and macrophages), we first studied the interaction between NLRP3 and P2Y2 during the cellular infection by HIV-1 and SIV. Then we characterized the biological consequences of the modulation of this interaction during the early steps of infection of macrophages, which are, together with T lymphocytes, the major target cells of HIV-1.

RESULTS

Enhancement of the Interaction between NLRP3 and P2Y2 during SIV and HIV Infection

Based on our previous work showing that the purinergic receptor P2Y2 contributes to the early steps of HIV-1 infection (Séror et al., 2011), we searched for potential P2Y2-interacting NLR proteins, identifying NLRP3 as an interactor of P2Y2 (Figure 1A). The endogenous NLRP3 and P2Y2 proteins co-immunoprecipitated in human THP1 monocytes (Figure 1A), indicating that both proteins constitutively interact. Of note, this interaction increased after 3 h of infection of human THP1 monocytes with CXCR4-tropic (X4-tropic) HIV-1_{NL4-3} (Figures 1A and S1A). We then studied the subcellular localization of NLRP3 during the early steps of HIV-1 infection obtained by co-culturing of uninfected peripheral blood lymphocytes (PBLs) with X4-tropic HIV-1_{NDK}-infected PBLs. NLRP3 polarized toward the contact sites formed between HIV-1_{NDK}-infected and uninfected host cells (Figures 1B and 1C). At these contact sites, NLRP3 colocalized with the glycoprotein gp120 (Figure 1B) and the purinergic receptor P2Y2 (Figure 1C). Thus, NLRP3 accumulated at the virological synapse that is formed between HIV-1_{NDK} -infected and uninfected PBLs (Figure 1D).

(E and F) PLA between P2Y2 and NLRP3 (E) and frequencies of positive signals (F) detected on interacting HIV-1-infected and uninfected lymphocytes are shown. The image is representative of three different donors. Data are presented as means ± SEM, and significance is *$p \leq 0.05$ (n = 29 virological synapses from three independent experiments), unpaired Mann-Whitney test.

(G) Fluorescence intensities of NLRP3 in HIV-1-infected and uninfected lymphocytes obtained from confocal microscopy are shown a three-dimensional (3D) Z-projection. Representative experiment of three different donors is shown.

(H and I) PLA between P2Y2 and NLRP3 (H) and frequencies of positive signals detected on ileum sections (I) obtained from SIV_{mac251}-infected and uninfected *Macaca fascicularis* are shown. Images are representative of four SIV_{mac251}-infected and three uninfected *Macaca fascicularis*. Data are presented as means ± SEM, and significance is ****$p \leq 0.0001$ (n = 3 uninfected, n = 4 uninfected), unpaired Mann-Whitney test.

(J and K) PLA between P2Y2 and NLRP3 (J) and frequencies of positive signals detected on brain autopsies (K) from HIV-1-infected and uninfected individuals are shown. Images are representative of nine HIV-1-infected and two uninfected donors. Data are presented as means ± SEM, and significance is **$p \leq 0.01$ (n = 2 uninfected, n = 9 infected), unpaired Mann-Whitney test.

(L and M) PLA between P2Y2 and NLRP3 (L) and frequencies of positive signals (M) detected during MDMs infection are shown. The image is representative of three different donors. Data are presented as means ± SEM, and significance is ****$p \leq 0.0001$ (n = 1,075 and 1,133 for uninfected and HIV-1_{BaL} infected MDMs, respectively), unpaired Mann-Whitney test.

See also Figure S1.

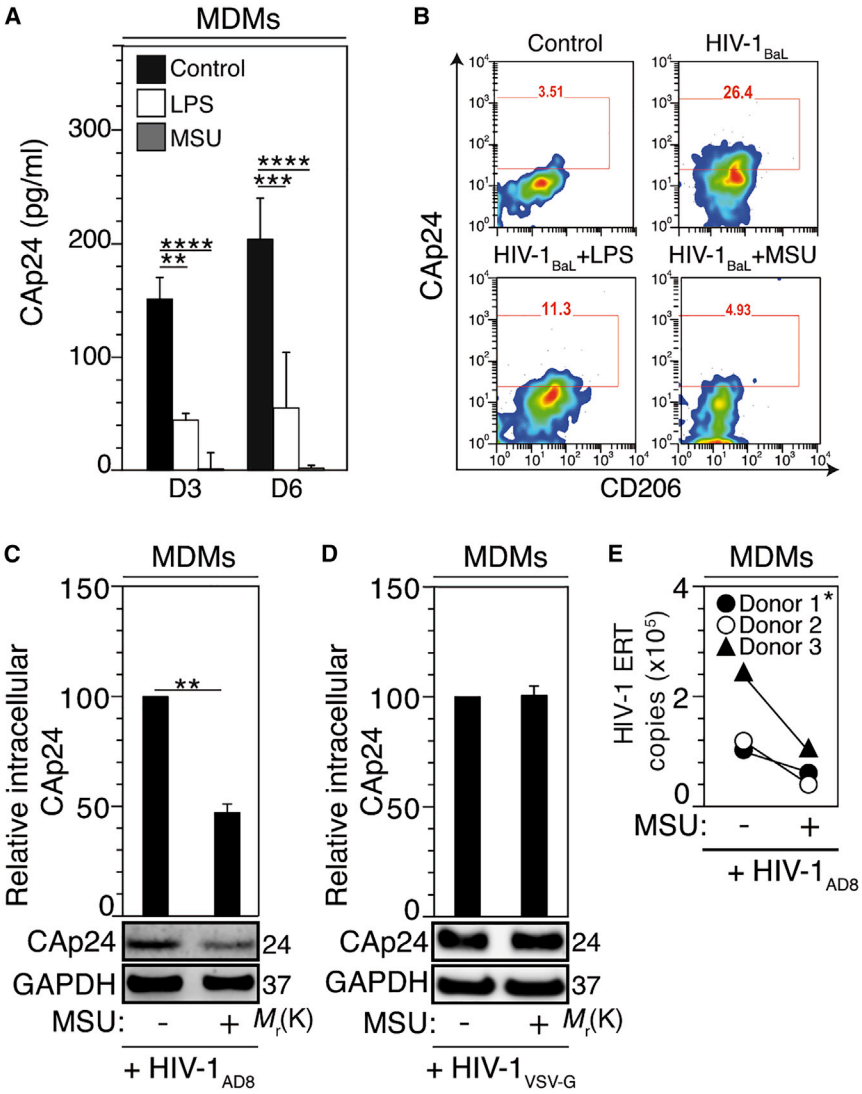

Figure 2. NLRP3 Inflammasome Activation Impairs HIV-1 Entry

(A and B) HIV-1 CAp24 content in cell supernatant analyzed by ELISA at 3 and 6 days (A) and intracellular CAp24 analyzed by flow cytometry at 6 days (B) after R5-tropic HIV-1_{BaL} infection of LPS- or MSU-treated MDMs. Data obtained from n = 3 independent experiments are presented in (A) as means ± SEM. Significance levels are **p ≤ 0.01, ***p ≤ 0.001, and ****p ≤ 0.0001, unpaired Mann-Whitney test. Representative flow cytometry analyses of three independent experiments are shown in (B).

(C and D) Intracellular CAp24 analyzed by western blot and the corresponding quantifications of control or MSU-treated MDMs that were infected for 6 h with R5-tropic HIV-1_{AD8} (C) or HIV-1_{VSV-G} (D). Representative western blots from three independent donors are shown. Data are obtained from three independent experiments presented as means ± SEM. Significance levels are **p ≤ 0.01 (n = 3 donors), unpaired t test.

(E) The number of copies of early reverse transcripts of HIV-1 (HIV-1 ERT) analyzed by qPCR in MDMs pretreated with 100 μM MSU for 18 h and infected for 6 h with HIV-1_{AD8} in the presence of MSU. ERT data were determined for three donors at 24 h after infection. Significance is *p ≤ 0.05 (n = 3 donors), Wilcoxon signed rank test.

See also Figures S2A, S2B, and S2C.

We determined the ability of NLRP3 to directly interact with P2Y2 by means of a proximity ligation assay (PLA). During the early steps of HIV-1 infection, the interaction between NLRP3 and P2Y2 mostly occurred at the contact sites between HIV-1_{NDK}-infected and uninfected T lymphocytes (Figures 1E and 1F). These results suggest that the interaction between NLRP3 and P2Y2 may regulate the viral entry into target cells. We also studied the subcellular localization of NLRP3 after chronic infection of PBLs with X4-tropic HIV-1_{NDK} for 72 h (Figures 1G and S1B–S1D) or that of monocyte-derived macrophages (MDMs) with R5-tropic HIV-1_{AD8} for 6 days (Figures S1E and S1F). While NLRP3 presented a diffuse cytosolic expression pattern in uninfected target cells, it aggregated in the cytoplasm and at the membrane of infected PBLs (Figures 1G and S1B–S1D) or MDMs (Figures S1E and S1F). Using PLA, we also evaluated the ability of NLRP3 to interact with P2Y2 during chronic infection and revealed that the interaction between NLRP3 and P2Y2 increased in chronically infected tissues (e.g., ileum [Figures 1H and 1I] and colon [Figures S1G and S1H] from SIV-1_{mac251}-infected non-human primate *Macaca fascicularis*, the frontal cortex from untreated HIV-1 carriers [as compared with uninfected controls; Figures 1J and 1K]), as well as in chronically infected PBLs (Figures S1I and S1J) or MDMs (Figures 1L and 1M). Altogether, these findings indicate that the interaction between NLRP3 and P2Y2 increased during acute and chronic steps of viral infection.

NLRP3 Inflammasome Activation Impairs HIV-1 Entry into Host Cells

To characterize the role of NLRP3-P2Y2 interaction and related signaling pathways during the early steps of HIV-1 infection, we first evaluated the possibility that the NLRP3 might affect viral replication through the formation of the inflammasome. Considering that sterile particulates such as monosodium urate (MSU) crystals are capable of activating the NLRP3 inflammasome (Shi et al., 2010), we incubated MDMs with 100 μM MSU before infection with R5-tropic HIV-1_{BaL} and then analyzed their viral permissiveness. The activation of the NLRP3 inflammasome by MSU reduced the release of CAp24 capsid from human MDMs (Figure 2A) and its intracellular detection (Figure 2B) after 3 days (Figure 2A) and 6 days (Figures 2A and 2B) of infection with R5-tropic HIV-1_{BaL}. This

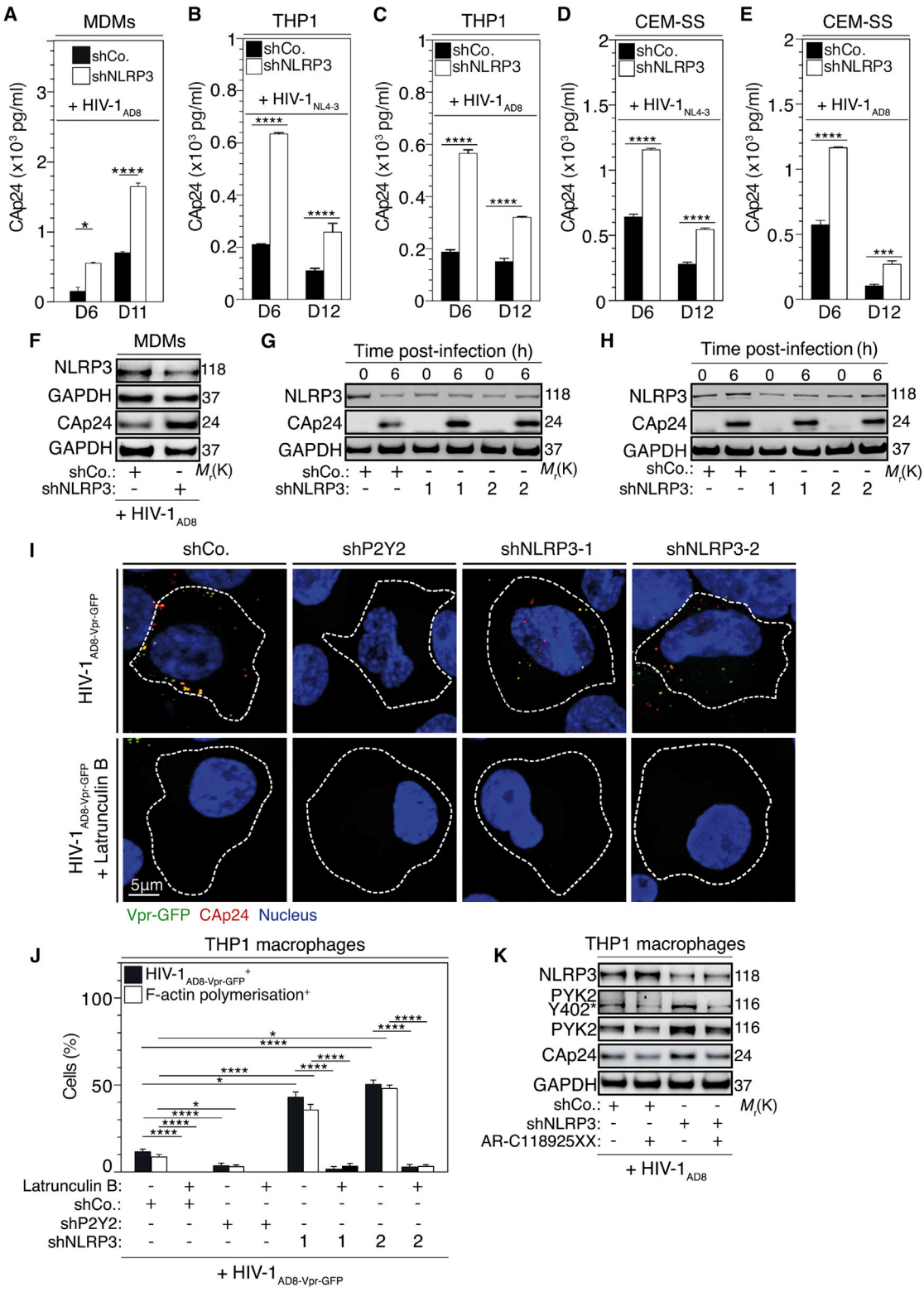

(legend on next page)

MSU-mediated inhibition of HIV-1 was more efficient than the one detected with lipopolysaccharide (LPS) (Figures 2A and 2B). To further characterize the impact of NLRP3 inflammasome activation on the early steps of HIV-1 infection, we monitored the effects of MSU treatment on intracellular HIV-1 CAp24 capsid levels (after removal of membrane bound non-internalized virus with trypsin treatment) and on the early reverse transcripts that are detected after 6 and 24 h, respectively, of infection of human MDMs with R5-tropic HIV-1_{AD8}. These data revealed that NLRP3 inflammasome activation impaired the accumulation of intracellular HIV-1 CAp24 capsid (Figure 2C) and subsequently reduced the early reverse transcripts (Figure 2E) without affecting cell viability (Figure S2A) nor the membrane expression of the viral receptors CD4 (Figure S2B) and CXCR5 (Figure S2C). Accordingly, MSU did not impair the accumulation of intracellular HIV-1 CAp24 capsid in human MDMs that were infected by the HIV-$1_{NL4\text{-}3\Delta ENV}$ variant (defective in viral envelope) pseudotyped with the vesicular stomatitis virus G protein (VSV-G) envelope, HIV-$1_{VSV\text{-}G}$ (Figure 2D). Altogether, these results demonstrate that NLRP3 inflammasome activation inhibits HIV-1 entry into host cells.

NLRP3 Protein Inhibits HIV-1 Infection by Repressing the Cytoskeletal Remodeling Required for HIV-1 Entry

We determined the role of NLRP3 inflammasome protein during the early steps of HIV-1 infection through the knockdown of NLRP3 using specific short hairpin RNA (shRNA). We observed that the depletion of NLRP3 increased the release of CAp24 capsid from human MDMs (Figure 3A and S3A), THP1 monocytes (Figures 3B, 3C, and S3B), and CEM-SS T cells (Figures 3D, 3E, and S3C) after 6, 11, or 12 days of infection with R5-tropic HIV-1_{AD8} (Figures 3A, 3C, and 3E) or X4-tropic HIV-$1_{NL4\text{-}3}$ (Figures 3B and 3D). After removing membrane-bound non-internalized HIV-1 particles by trypsinizing the cells, western blot detection of intracellular CAp24 capsid corroborated that the depletion of NLRP3 in MDMs increased cellular susceptibility to HIV-1 infection after 6 h of infection (Figure 3F). These data were confirmed by the depletion of NLRP3 in THP1 monocytes that were then infected with X4-tropic HIV-$1_{NL4\text{-}3}$ for 6 h (Figures 3G and S3D). To rule out the possibility that NLRP3 protein may also act at post-entry levels, we evaluated the effects of NLRP3 overexpression on viral yields after transfection of X4-tropic HIV-$1_{NL4\text{-}3}$ (Figure S3E) or R5-tropic HIV-1_{AD8} (Figure S3F) DNA constructs that subsequently produce infectious virions. NLRP3 overexpression (Figures S3E and S3F) did not impact the amount and infectivity of X4-tropic HIV-$1_{NL4\text{-}3}$ (Figures S3G and S3I) and R5-tropic HIV-1_{AD8} (Figures S3H and S3J) produced 48 h post transfection. Consistently, the depletion of NLRP3 failed to increase infection of target cells by HIV-$1_{VSV\text{-}G}$ (Figures 3H and S3K). These results imply that NLRP3 protein selectively inhibits receptor-mediated entry of HIV-1.

Emerging evidence has revealed important inflammasome-independent roles for ASC and CASP1 in controlling immune responses through the modulation of F-actin polymerization (Caution et al., 2015; Ippagunta et al., 2011). In our previous report (Séror et al., 2011), we demonstrated that following HIV-1 infection, P2Y2 enhances plasma membrane depolarization through the activating autophosphorylation of the proline-tyrosine kinase 2 (PYK2) on tyrosine residue 402 (PYK2Y402*) to favor the early fusion of the HIV-1 membrane and the target cell. Importantly, activated PYK2 is known to broadly modulate the F-actin rearrangement and polymerization to regulate immune cells migration, morphology or growth (Collins et al., 2010; Du et al., 2001; Okigaki et al., 2003; Ren et al., 2001; Wang et al., 2003). F-actin remodeling is also required for HIV-1 membrane fusion with target cells and entry (Jiménez-Baranda et al., 2007; Stolp and Fackler, 2011). Considering that F-actin cytoskeletal remodeling and the associated PYK2 activation both contribute to HIV-1 early viral entry (Jiménez-Baranda et al., 2007; Séror et al., 2011; Stolp and Fackler, 2011),

Figure 3. NLRP3 Inhibits HIV-1 Entry by Repressing F-Actin Polymerization

(A) HIV-1 CAp24 in cell supernatant analyzed by ELISA of control and NLRP3-depleted MDMs infected with HIV-1_{AD8} after 6 and 11 days of infection. Data are presented as means ± SEM, and significance levels are *p ≤ 0.05 and ****p ≤ 0.0001 (n = 3 independent donors), unpaired Mann-Whitney test. See also Figure S3A.

(B and C) HIV-1 CAp24 in cell supernatant analyzed by ELISA of control and NLRP3-depleted THP1 monocytes infected with X4-tropic HIV-$1_{NL4\text{-}3}$ (B) and R5-tropic HIV-1_{AD8} (C) after 6 and 12 days of infection. Data are presented as means ± SEM, and significance is ****p ≤ 0.0001 (n = 3 independent experiments), unpaired t test. See also Figure S3B.

(D and E) HIV-1 CAp24 in cell supernatant analyzed by ELISA of control and NLRP3-depleted CEM-SS T cells infected with X4-tropic HIV-$1_{NL4\text{-}3}$ (D) and R5-tropic HIV-1_{AD8} (E) after 6 and 12 days of infection. Data are presented as means ± SEM, and significance is ****p ≤ 0.0001 (n = 3 independent experiments), ANOVA test. See also Figure S3C.

(F) Intracellular CAp24 analyzed by western blot in control and NLRP3-depleted MDMs, which were infected for 6 h with R5-tropic HIV-1_{AD8}. Representative western blots of three independent donors are shown. See also Figures S3D and S3K.

(G and H) Intracellular HIV-1 CAp24 analyzed by western blot in control and NLRP3-depleted THP1 cells infected for 6 h with X4-tropic HIV-$1_{NL4\text{-}3}$ (G) or HIV-$1_{NL4\text{-}3\Delta Env}$ pseudotyped with VSV-G envelope (H). Representative western blots of three independent experiments are shown.

(I) Confocal microscopy images of HIV-1 entry (detected with CAp24 and Vpr-GFP signals) in THP1 macrophages control and depleted for P2Y2 (shP2Y2) or for NLRP3 (shNLRP3-1 and 2) and infected for 6 h with R5-tropic HIV-$1_{AD8\text{-}Vpr\text{-}GFP}$ in the presence or absence of latrunculin B (10 μM). Dashed lines indicate the cellular perimeters. The corresponding F-actin polymerization staining (with phalloidin) is shown in Figure S3L. Images are representative of three independent experiments.

(J) Cell percentage of HIV-$1_{AD8\text{-}Vpr\text{-}GFP}$ and F-actin polymerization positive cells determined by confocal microscopy as shown in (I) and in Figure S3L. Data obtained from three independent experiments are presented as means ± SEM (n = 300 cells). Significance levels are *p ≤ 0.05 and ****p ≤ 0.0001, ANOVA test.

(K) NLRP3, PYK2Y402*, PYK2, and intracellular CAp24 analyzed by western blot of control and NLRP3-depleted THP1 macrophages pretreated 18 h with AR-C118925XX (100 μM) and infected with R5-tropic HIV-1_{AD8} for 6 h treated in the presence of the drug. Western blots are representative of three independent experiments.

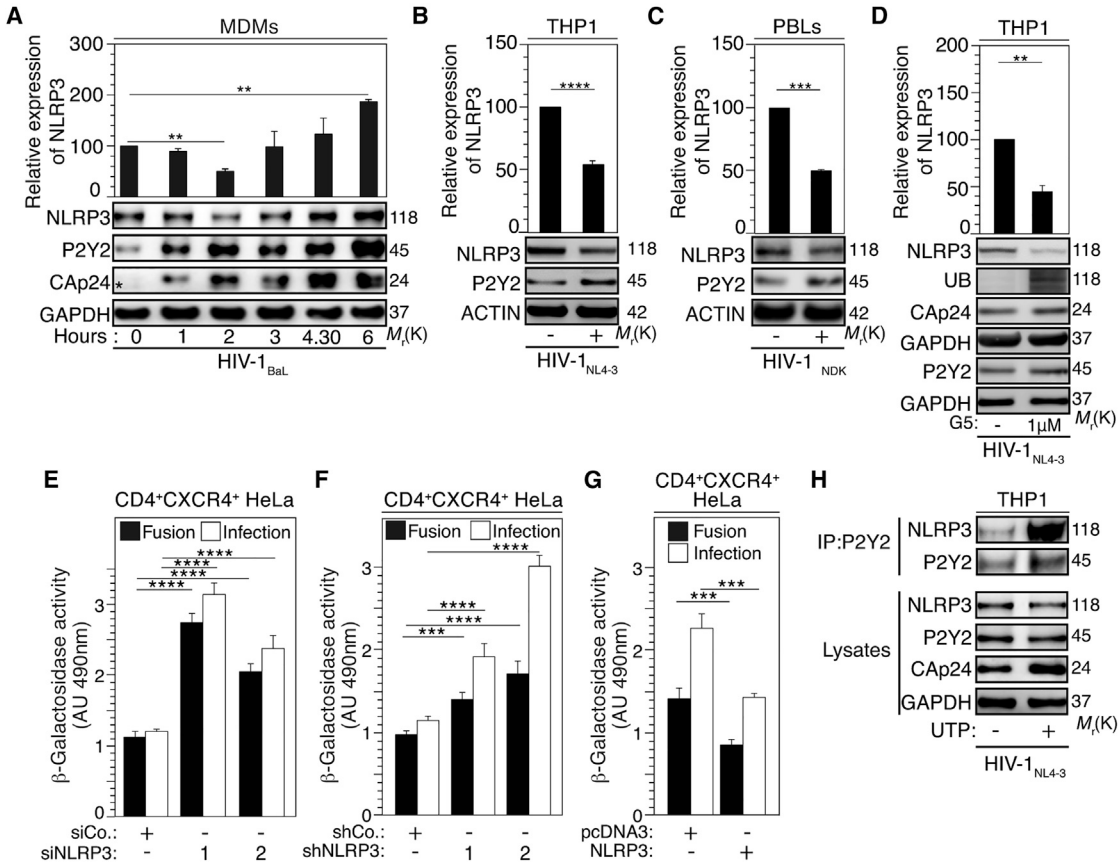

Figure 4. NLRP3 Expression Is Decreased during the Early Steps of HIV-1 Infection

(A–C) NLRP3 and P2Y2 expressions in MDMs (A), THP1 cells (B), and PHA/IL-2-stimulated human lymphocytes (C) that were infected, respectively, during indicated times (A), 6 h (B), or 3 h (C) with indicated viruses. Intracellular CAp24 level is also shown in (A). Representative western blots of three independent experiments are shown. The relative NLRP3 expression data from n = 3 independent experiments are presented as means ± SEM. Significance levels are $^{**}p \leq 0.01$, $^{***}p \leq 0.001$, and $^{****}p \leq 0.0001$, unpaired t test.

(D) THP1 cells were infected for 6 h with X4-tropic HIV-1_{NL4-3} in the presence of 1 μM G5 and analyzed by western blot for NLRP3, ubiquitinylation (UB), P2Y2, intracellular CAp24, and GAPDH expressions. Data obtained from n = 3 independent experiments are presented as means ± SEM. Significance level is $^{**}p \leq 0.01$, unpaired t test.

(E–G) Tat-inducible β-Galactosidase reporter gene expressing HeLa CD4$^+$CXCR4$^+$ cells were depleted (E and F) or transfected (G) for NLRP3 for, respectively, 48 h (E and F) or 24 h (G), co-cultured with fusogenic HIV-1 envelope (Env) expressing HeLa cells (E–G), or infected with X4-tropic HIV-1_{NL4-3} (E–G) and evaluated for HIV-1 Env-mediated fusion and for infection (E–G). Data obtained from n = 3 independent experiments are presented as means ± SEM. Significance levels are $^{***}p \leq 0.001$ and $^{****}p \leq 0.0001$, unpaired t test. See also Figures S5A, S5B, and S5C.

(H) Immunoprecipitations were performed in THP1 monocytes that were stimulated for 2 h with UTP and then infected with X4-tropic HIV-1_{NL4-3} for 6 h in the presence of UTP. Representative western blots of two independent experiments are shown. See also Figures S5L and S5M.

we hypothesized that NLRP3 may antagonize the effects of activated P2Y2 and PYK2 on F-actin remodeling upon HIV-1 infection, thereby inhibiting HIV-1 entry. Confocal microscopy analysis revealed that NLRP3 depletion increased the entry of GFP-fused viral protein (Vpr) containing viral particles (HIV-$1_{AD8\text{-}Vpr\text{-}GFP}$) (McDonald et al., 2002) into PMA-THP1 macrophages, as revealed by the intracellular detection of HIV-$1_{AD8\text{-}Vpr\text{-}GFP}$ and CAp24 (Figures 3I and 3J). The enhanced viral entry into NLRP3-depleted cells was associated with an increase of F-actin cytoskeletal polymerization (Figures 3J and S3L). Moreover, inhibition of F-actin polymerization by latrunculin B abrogated the stimulation of HIV-1 infection by NLRP3 depletion (Figures 3I, 3J, and S3L). Consistently, the selective P2Y2 antagonist AR-C118925XX abrogated the NLRP3 depletion-driven signaling pathway (as revealed by the decreased of PYK2402* and intracellular CAp24 level [Figure 3K]) in NLRP3-depleted THP1 macrophages that were infected with R5-tropic HIV-1_{AD8} for 6 h. Altogether, these results demonstrate that, independently from its contribution to the inflammasome, NLRP3 protein acts as an endogenous repressor of F-actin cytoskeletal polymerization that facilitates the P2Y2-dependent entry of HIV-1 into target cells.

NLRP3 Is Degraded during the Early Steps of HIV-1 Infection

To determine how HIV-1 may overcome the NLRP3-mediated inhibition of its entry into host cells, we simultaneously measured NLRP3 and P2Y2 expressions during infection.

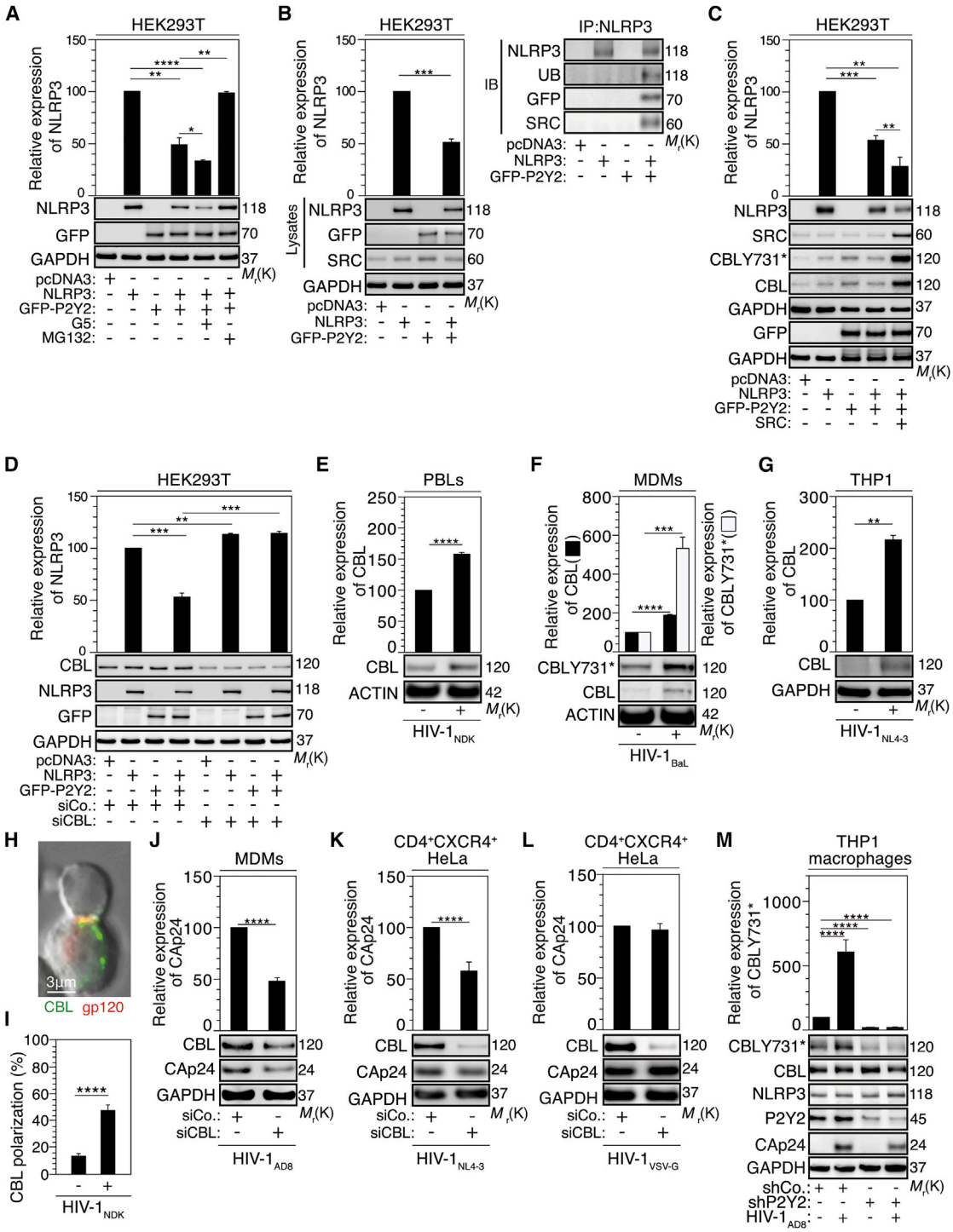

Figure 5. HIV-1 Viral Entry Is Controlled by E3 Ubiquitin Ligase CBL-Dependent Modulation of NLRP3 Expression

(A) NLRP3 and/or GFP-P2Y2 expressing cells were treated with 1 μM G5 or 10 μM MG132 and analyzed for NLRP3 and P2Y2 expressions.

(B) HEK293T cells expressing NLRP3 and GFP-P2Y2 were immunoprecipitated for NLRP3 and analyzed for ubiquitinylation (UB), SRC, NLRP3, and P2Y2 expressions.

(C) HEK293T cells expressing NLRP3, GFP-P2Y2, and/or SRC were analyzed for NLRP3, P2Y2, SRC, CBLY731*, and CBL expressions.

(D) NLRP3 and/or GFP-P2Y2 expressing cells were silenced for CBL and analyzed for NLRP3, P2Y2, and CBL expression. All protein expressions are performed using western blot. Representative western blots of three independent experiments are shown in (A)–(D). Relative expression of NLRP3 data from n = 3 independent experiments are presented as means ± SEM. Significance levels are *p ≤ 0.05, **p ≤ 0.01, ***p ≤ 0.001, and ****p ≤ 0.0001, unpaired t test.

(legend continued on next page)

Despite the fact that P2Y2 protein levels increased, NLRP3 protein levels rapidly decreased after cell-free infection of MDMs with R5-tropic HIV-1_{BaL} (Figure 4A), THP1 monocytes (Figures 4B, S4A, S4B, and S4E–S4H) and CEM-SS T cells (Figures S4C, S4D, and S4I–S4L) with X4-tropic HIV-1_{NL4-3} (Figures 4B, S4A, S4C, S4E, S4F, S4I, and S4J) or R5-tropic HIV-1_{AD8} (Figures S4B, S4D, S4G, S4H, S4K, and S4L), and PBLs with X4-tropic HIV-1_{NDK} (Figure 4C). However, NLRP3 mRNA expressions were not altered after infection of THP1 monocytes (Figures S4M and S4N) and CEM-SS T cells (Figures S4O and S4P) with X4-tropic HIV-1_{NL4-3} (Figures S4M and S4O) and R5-tropic HIV-1_{AD8} (Figures S4N and S4P). The ubiquitin isopeptidase inhibitor G5 that was previously described as an inducer of NLRP3 degradation (Py et al., 2013) decreased the protein levels of NLRP3 (Figure 4D), thus suggesting that the reduction of NLRP3 protein expression induced by HIV-1 infection must occur through post-transcriptional mechanisms. This process is associated with the enhancement of P2Y2 expression and HIV-1 permissiveness of THP1 monocytes (as indicated by the increased intracellular accumulation of HIV-1 capsid CAp24) (Figure 4D), in line with the hypothesis that NLRP3 and P2Y2 control HIV-1 entry into target cells. Consistently, we observed that the depletion or the overexpression of NLRP3 (Figures S5A–S5C) enhanced or reduced, respectively, HIV-1 Env-elicited fusion (Figures 4E–4G), the intracellular accumulation of HIV-1 CAp24 capsid (Figures S5D–S5F), and the susceptibility to HIV-1 infection (Figure 4E–4G), without affecting the expression of the HIV-1 receptor CD4 and that of its co-receptor CXCR4 (Figures S5G–S5I). Consistent with our previous report (Séror et al., 2011), we confirmed that the P2Y2 inhibitor AR-C118925XX (Figure S5J) and shRNA-mediated P2Y2 depletion (Figure S5K) impaired the entry of R5-tropic HIV-1_{AD8} into MDMs (Figure S5J) or of X4-tropic HIV-1_{NL4-3} into THP1 monocytes (Figure S5K). This effect is associated with the increased expression of NLRP3 in target cells (Figure S5K). We also evaluated the impact of the selective activation of P2Y2 by uridine triphosphate (UTP) in THP1 cells infected with X4-tropic HIV-1_{NL4-3} for 6 h on the NLRP3 and P2Y2 interaction and on the levels of NLRP3. P2Y2 activation led to a significant enhancement of the NLRP3-P2Y2 interaction associated with the degradation of NLRP3 and an increase of HIV-1 entry into cells (Figures 4H, S5L, and S5M). Altogether, these data indicate that the activation of P2Y2 occurring shortly after HIV-1 infection increases the susceptibility of cells to viral entry by inducing NLRP3 protein degradation.

HIV-1 Envelope Overcomes NLRP3 Inhibition through the Activation of the E3 Ubiquitin Ligase CBL

To define the molecular mechanisms accounting for the degradation of NLRP3 during the early steps of infection, HEK293T cells were transfected with full-length NLRP3, with GFP-tagged full-length P2Y2, or with both constructs. Co-expression of GFP-P2Y2 with NLRP3 reduced the expression of NLRP3 protein, while co-expression of NLRP3 failed to reduce the expression of GFP-P2Y2 (Figure 5A). The downregulation of NLRP3 by P2Y2 was increased by the ubiquitin isopeptidase inhibitor G5 and fully blocked by the proteasome inhibitor MG132 (Figures 5A and S6A), thus demonstrating that upon P2Y2 activation, NLRP3 is ubiquitinylated and degraded by the proteasome. Considering that the ubiquitinylation and subsequent degradation of NLRP3 can be initiated by ubiquitin ligases such as E3 ubiquitin ligase CBL through its SRC kinase-dependent phosphorylation (on tyrosine 731, CBLY731*) (Kankkunen et al., 2014; Py et al., 2013), we checked whether the kinase SRC that was previously described as a downstream target of P2Y2-dependent signaling pathway (Liu et al., 2004) may interact with NLRP3 and control its degradation through the activation of CBL. Indeed, the kinase SRC co-immunoprecipitated with NLRP3 when NLRP3 was ubiquitinylated and degraded (Figure 5B). Moreover, pharmacological inhibition of SRC with PP1 or PP2 impaired the interaction between NLRP3 and P2Y2 (Figure S6B) and favored NLRP3 accumulation in THP1 cells (Figure S6B). Moreover, in HEK293T cells, transfection of full-length SRC together with full-length NLRP3 and GFP-tagged full-length P2Y2 led to an increased expression and phosphorylation of CBL on tyrosine 731 (CBLY731*) as well as to NLRP3 degradation (Figure 5C). Since the SRC kinase is a candidate for proteasomal degradation through a CBL-dependent process (Sandilands et al., 2012), we next investigated the role of CBL in P2Y2-induced degradation of NLRP3. Indeed, CBL depletion abolished the negative effect of GFP-P2Y2 on the overall abundance of the NLRP3 protein (Figure 5D). Altogether, these results suggest that P2Y2 controls NLRP3

(E–G) PHA/IL-2-stimulated human lymphocytes (E), MDMs (F), and THP1 cells (G) were infected, respectively, for 3, 3, or 6 h with X4-tropic HIV-1_{NDK} (E), R5-tropic HIV-1_{BaL} (F), or X4-tropic HIV-1_{NL4-3} (G) and analyzed by western blot for CBLY731* and CBL relative expressions. Representative western blots of three independent experiments are shown. Relative expressions data from n = 3 independent experiments are presented as means ± SEM. Significances are **$p \leq 0.01$, ***$p \leq 0.001$, and ****$p \leq 0.0001$, unpaired t test.

(H and I) Confocal microscopy image (H) of CBL and gp120 polarization during HIV-1-infected and uninfected lymphocyte interactions. Frequencies of CBL polarization during HIV-1-infected and uninfected lymphocyte interactions are shown (I). Images are representative of three different donors. Data are presented as means ± SEM, and significance is ****$p \leq 0.0001$ (n = 3 independent donors), unpaired t test.

(J) Intracellular CAp24 analyzed by western blot and its relative expression in control and CBL-depleted MDMs were infected for 6 h with HIV-1_{AD8}. Representative western blots of three independent experiments are shown. Relative expression data from three independent experiments are presented as means ± SEM. Significance is ****$p \leq 0.0001$ (n = 3 independent donors), unpaired t test.

(K and L) Intracellular CAp24 analyzed by western blot of CBL-depleted $CD4^+CXCR4^+$ cells were infected with HIV-1_{NL4-3} (K) or HIV-1_{VSV-G} (L) for 6 h. Representative western blots of three independent experiments are shown. Relative expression from n = 3 independent experiments are presented as means ± SEM. Significance is ****$p \leq 0.0001$, unpaired t test.

(M) Expressions of CBLY731*, CBL, P2Y2, and intracellular CAp24 analyzed by western blot in control and P2Y2-depleted THP1 macrophages infected for 6 h with R5-tropic HIV-1_{AD8}. Representative western blots of three independent experiments are shown. Relative expression of CBLY731* from n = 3 independent experiments are presented as means ± SEM. Significance is ****$p \leq 0.0001$, unpaired t test.

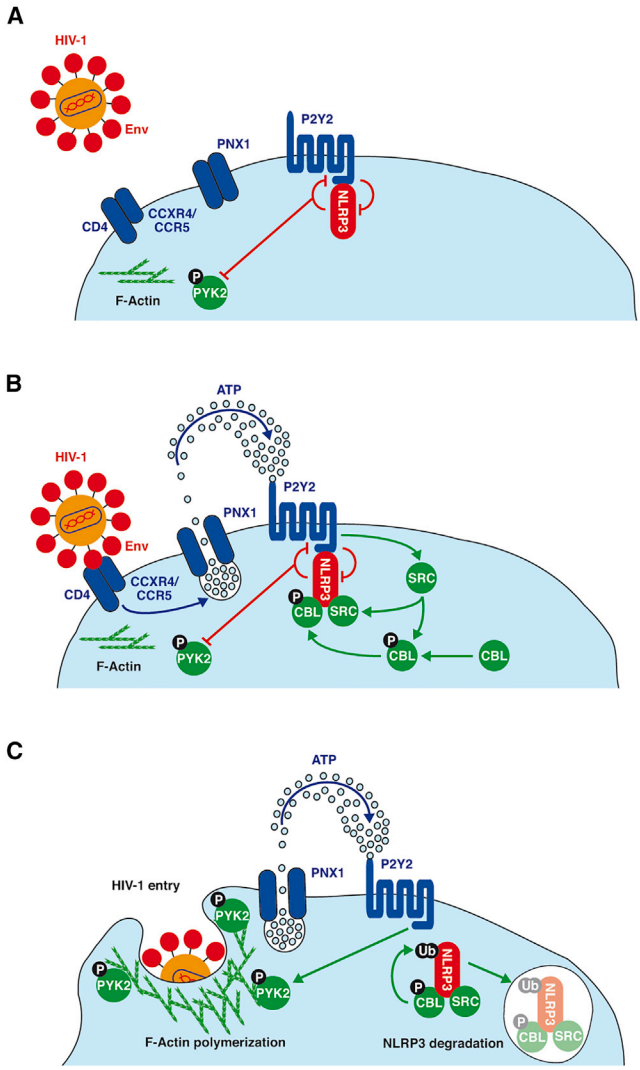

Figure 6. Model of HIV-1 Escape to NLRP3 Inhibition during the Early Steps of Viral Entry

(A–C) NLRP3 interacts constitutively with P2Y2 and suppresses the phosphorylation of PYK2 (PYK2Y402*) and F-actin polymerization in host cells (A). The binding of HIV-1 envelope to its receptor (CD4) and co-receptors (CXCR4 or CCR5) leads to rapid ATP release from host cells through pannexin-1 (PNX1) and activates P2Y2. Once activated, P2Y2 enhances its interaction with NLRP3 and activates and favors the recruitment of SRC and CBL to NLRP3 (B), leading to NLRP3 ubiquitinylation and degradation. NLRP3 degradation leads to PYK2 phosphorylation (PYK2Y402*) and subsequent F-actin polymerization, which is required for the entry of HIV-1 into host cells (C).

degradation through a pathway involving the CBL ubiquitin ligase.

Next, we studied the role of the E3 ubiquitin ligase CBL during the early steps of HIV-1 infection. We detected increased CBL expression during cell-free infection of PBLs (Figure 5E), MDMs (Figure 5F), and THP1 monocytes (Figure 5G). This process was associated with the activating phosphorylation of CBL on tyrosine 731 (CBLY731*) 3 h post-infection of macrophages with R5-tropic HIV-1_{BaL} (Figure 5F). We also studied the subcellular localization of CBL after co-culture of X4-tropic HIV-1_{NDK}-infected and uninfected PBLs. CBL polarized toward the contact sites formed between HIV-1-infected and uninfected cells (Figures 5H and 5I), where it colocalized with the HIV-1 glycoprotein gp120 (Figure 5H). Immunofluorescence microscopy confirmed that the NLRP3/P2Y2 interaction occurs at sites of viral entry during virological synapse formation between HIV-1_{NDK}-infected and uninfected lymphoblasts (Figures 1C–1E), as well as upon cell-free infection of PBLs (Figures S1I and S1J) or MDMs (Figures 1L and 1M). We finally determined whether the E3 ubiquitin ligase CBL that is involved in the regulation of NLRP3 expression (Figure 5D) and relocalizes to the HIV-1-induced virological synapse (Figures 5H and 5I) might control viral entry. MDMs (Figure 5J) or $CD4^+CXCR4^+$ HeLa cells (Figure 5K) were depleted of CBL and infected for 6 h with R5-HIV-1_{AD8} or X4-tropic HIV-1_{NL4-3}, respectively. The depletion of CBL inhibited HIV-1 entry into target cells (as indicated by reduced intracellular HIV-1 CAp24 capsid; Figures 5J and 5K). Moreover, CBL depletion failed to reduce cell permissiveness to HIV-1_{VSV-G} (Figure 5L), again suggesting that the E3 ubiquitin ligase CBL controls P2Y2-dependent viral entry mediated by the viral envelope. To demonstrate the functional link between CBL function and P2Y2 activation during HIV-1 infection, P2Y2-depleted THP1 macrophages and control cells were infected with R5-tropic HIV-1_{AD8} for 6 h. P2Y2 depletion impaired the activating phosphorylation of CBL on tyrosine 731 (CBLY731*) (Figure 5M). This effect was associated with increased expression of NLRP3 and reduced entry of HIV-1 into target cells (Figure 5M). Altogether these results suggest that the binding between HIV-1 Env and its host cell receptors (CD4 and chemokine co-receptors) induces the recruitment of the E3 ubiquitin ligase CBL to viral entry sites for modulating the functional interaction between NLRP3 and P2Y2 interaction, thus facilitating viral entry.

DISCUSSION

Deciphering the complex network of innate signaling pathways is crucial for understanding the function of immune cells (such as monocytes, macrophages, and dendritic cells) that might constitute prime targets for prophylactic or therapeutic intervention in various human pathologies (such as autoinflammatory, autoimmune, infectious, and neoplastic diseases). Innate immune signals reportedly play contrasting roles during the acute and chronic phases of HIV-1 infection (Doitsh et al., 2014). Recently, rapid inflammasome activation was reported following SIV infection of Rhesus monkeys (Barouch et al., 2016). During early SIV pathogenesis, NLRX1-mediated inhibition of inflammasome activation represses the transcription of antiviral restriction factors (such as ISG5, MX2, APOBEC3, and TRIM5) and facilitates early viral replication (Barouch et al., 2016). Here, we report that the expression of NLRP3 proteins is modulated through post-translational modifications during the early steps of HIV-1 infection and controls target cell susceptibility. We observed that following the binding of HIV-1 envelope to its host receptors (CD4, CXCR4, and/or CCR5), the interaction between NLRP3 and P2Y2 rapidly increased after HIV-1 infection, leading to the degradation of NLRP3 by

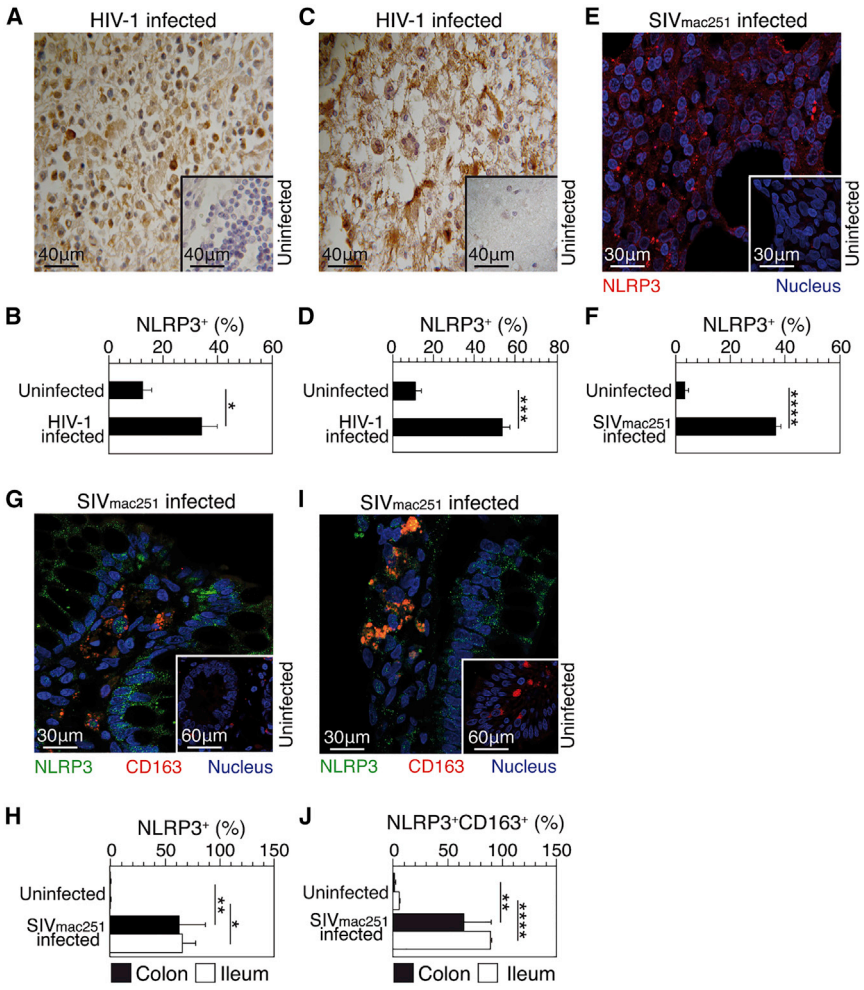

Figure 7. NLRP3 Expression Is Increased in Chronic HIV-1 and SIV Infection

(A–J) Quantification of NLRP3 and/or CD163 positive cells in lymph nodes (A, B, E, and F), brain (C and D), colon (G and H), and ileum (I and J) sections obtained from HIV-1-infected and uninfected patients (A–D) or from SIVmac251-infected and uninfected *Macaca fascicularis* (E–J) are shown. Images are representative of n = 6 HIV-1-infected and n = 4 uninfected persons in (A), of n = 3 HIV-1-infected and n = 3 uninfected persons in (C), of n = 3 SIVmac251-infected and n = 3 uninfected *Macaca fascicularis* in (G), and of n = 4 SIVmac251-infected and n = 3 uninfected *Macaca fascicularis* in (E) and (I). In (G), (H), (I), and (J), the NLRP3 expression was analyzed in CD163 positive macrophages. Data are presented in (B), (D), (F), (H), and (J) as means ± SEM. Significance levels are *$p \leq 0.05$, **$p \leq 0.01$, ***$p \leq 0.001$, and ****$p \leq 0.0001$, unpaired Mann-Whitney test.

the E3 ubiquitin ligase CBL, thus favoring P2Y2-dependent viral entry into target cells through PYK2-dependent F-actin polymerization. Indeed, the interaction between HIV-1 Env and its co-receptors enhances the interaction between NLRP3 and P2Y2 and subsequently induces the degradation of NLRP3 by CBL, favoring the activation (phosphorylation) of PYK2 (PYK2Y402*) and subsequent cytoskeletal rearrangement (through F-actin polymerization) that facilitates HIV-1 early membrane fusion with target cells (Jiménez-Baranda et al., 2007; Stolp and Fackler, 2011; Vorster et al., 2011) and hence viral entry (Figure 6).

Our results are in agreement with published works supporting the notion that polymorphisms affecting the *NLRP3* gene could influence the susceptibility to HIV-1 infection (Pontillo et al., 2010, 2012) and coinfection with *Mycobacterium tuberculosis* (Pontillo et al., 2013). Altogether, our results suggest that HIV-1 (through its envelope protein) hijacks the functional crosstalk between NLRP3 and P2Y2 to optimize its viral life cycle.

The observation that the depletion of NLRP3 enhanced the infectivity of host cells by HIV-1 suggests that NLRP3 proteins function as intrinsic inhibitory factors for HIV-1 infection. In sharp contrast to the vast majority of identified inhibitory factors that impair viral infection at post-entry steps (Harris et al., 2012), NLRP3 proteins limit HIV-1 infection by interfering with viral entry, suggesting that the NLRP3-P2Y2 interaction could be targeted for the prevention and treatment of HIV-1 infection. NLRP3 inflammasome activators (such as LPS or MSU crystals) reduce the susceptibility of HIV-1 target cells through the modulation of P2Y2-dependent F-actin remodeling. Thus, strategies designed to alter the functional interaction between NLRP3 and P2Y2 could effectively block HIV-1 infection. Nevertheless, the identification of the inflammasome inhibitor NLRX1 as transcriptional repressor of restriction factors that impair viral replication (Barouch et al., 2016) underlines the complexity of signaling pathways elicited by NLRP3 family members during the early steps of HIV-1 infection. Further molecular investigations are required to fully understand the role of NLRP3 family members during these viral steps. Future investigations must address the impact of the functional NLRP3-P2Y2 interaction on cellular regulators that are known to affect cortical F-actin rearrangement and to HIV-1 infection such as LIM domain kinase 1 (Vorster et al., 2011), moesin (Barrero-Villar et al., 2009), filamin-A (Jiménez-Baranda et al., 2007), and cofilin (Yoder et al., 2008).

There may be differences between the acute and the prolonged effects of HIV-1 on the aforementioned regulatory system. Indeed, immunoreactive NLRP3 was detected at higher levels in lymph nodes (Figures 7A and 7B) and in the frontal cortex (Figures 7C and 7D) from untreated HIV-1 carriers, as compared with uninfected specimens. Similar results were obtained when comparing control tissues from the non-human primate *Macaca fascicularis* with lymph nodes (Figures 7E and 7F) or intestinal tissues (colon in Figures 7G and 7H; ileum in Figures 7I and 7J) from macaques infected with SIV_{mac251}.

NLRP3 expression was preferentially observed in CD163$^+$ macrophages (Figures 7G, 7I, and 7J) that are known to express P2Y2 (Elliott et al., 2009). After 21 days of infection of THP1 monocytes and CEM-SS T cells with X4- and R5-tropic viruses, respectively, NLRP3 protein expression was increased (Figures S7A–S7F, S7I, and S7J), although no modification of NLRP3 mRNA levels was detectable (Figures S7M–S7P). P2Y2 protein expression did not change in CEM-SS T cells but increased after 21 days of infection of THP1 monocytes (Figures S7G, S7H, S7K, and S7L). Altogether, these results suggest that the molecular mechanisms involved in the enhanced interaction between NLRP3 and P2Y2 that is detected during chronic infection with HIV-1 may be distinct from those detected in the early steps of HIV-1 infection. The increased NLRP3 expression during chronic HIV-1 infection is consistent with recent findings showing that HIV-1 activates NLRP3 inflammasome through Tat and Vpr proteins in lymphocytes, microglial cells, and macrophages (Bandera et al., 2018; Chivero et al., 2017; Haque et al., 2016; Mamik et al., 2017). Thus, NLRP3 may play a dual opposite role during early steps of infection by inhibiting viral entry and at the later post-entry steps by contributing to neuroinflammation and immune activation associated with HIV-1 infection.

The blockade of immune checkpoints in lymphocytes has recently emerged as a new and promising approach for treating both chronic viral infection and cancer. Here, we identified a functional interaction that acts on myeloid cells and that could be exploited for the development of HIV vaccines or therapeutic combinations to cure HIV infection (Barouch et al., 2016) and potentially other viral infections (such as hepatitis B and C). In addition, it appears likely that the NLRP3-P2Y2 interaction could be manipulated for the treatment of HIV-1-associated brain disease, which is also associated with strong activation of the NLRP3 inflammasome (Walsh et al., 2014). Future studies should explore the possibility of modulating the NLRP3-P2Y2 functional interaction with the aim of treating human diseases that are triggered by excessive activation of the NLRP3 inflammasome, such as cryopyrin-associated periodic syndromes (Agostini et al., 2004), rheumatoid arthritis (Vande Walle et al., 2014), obesity (Vandanmagsar et al., 2011), or Alzheimer's disease (Halle et al., 2008).

Thus, our data demonstrate a constitutive interaction between NLRP3 and P2Y2 that could be targeted to reduce viral propagation and improve the immune response against HIV infection.

STAR★METHODS

Detailed methods are provided in the online version of this paper and include the following:

- KEY RESOURCES TABLE
- LEAD CONTACT AND MATERIALS AVAILABILITY
- EXPERIMENTAL MODEL AND SUBJECT DETAILS
  - Cell lines
  - Primary Cells
  - Non-Human primates
  - Human autopsies
- METHODS DETAILS
  - Plasmids and transfections
  - siRNA- and shRNA-mediated knockdowns
  - Virus productions
  - Viral infections
  - Immunofluorescence
  - Western blots and immunoprecipitations
  - Flow cytometry
  - Quantitative PCR (qPCR)
- QUANTIFICATION AND STATISTICAL ANALYSIS
- DATA AND CODE AVAILABILITY

SUPPLEMENTAL INFORMATION

Supplemental Information can be found online at https://doi.org/10.1016/j.celrep.2019.02.095.

ACKNOWLEDGMENTS

This work was supported by funds from Agence Nationale de la Recherche (ANR-10-IBHU-0001, ANR-10-LABX33, and ANR-11-IDEX-003-01), Electricité de France, Fondation Gustave Roussy, Institut National du Cancer (INCA 9414), NATIXIS, Sidaction, and the French National Agency for Research on AIDS and Viral Hepatitis (ANRSH) (to J.-L.P.); Ligue contre le Cancer (équipe labellisée), Agence National de la Recherche (ANR) – Projets blancs, Cancéropôle Ile-de-France, Institut National du Cancer (INCa), Institut Universitaire de France, the LabEx Immuno-Oncology, the RHU Torino Lumière, the SIRIC Stratified Oncology Cell DNA Repair and Tumor Immune Elimination (SOCRATE), and the SIRIC Cancer Research and Personalized Medicine (CARPEM) (to G.K.); MIUR (PRIN 2012 and FIRB), the Ministry of Health of Italy "Ricerca Corrente" and "Ricerca Finalizzata," AIRC and European Commission "Transpath" Marie Curie Project (to M.P.); and Electricité de France and Fondation Gustave Roussy (to E.D.). A.P. and A.A. are recipients of PhD fellowships and a post-doc fellowship, respectively, from Agence Nationale de Recherche sur le Sida et sur les Hépatites (ANRSH). S.Q.R. is supported by Higher Education Commission (Pakistan) and by the Laboratory of Excellence LERMIT with a grant from ANR (ANR-10-LABX-33) under the program "Investissements d'Avenir" ANR-11-IDEX-0003-01. M.C. is funded by a postdoctoral fellowship from Sidaction. We gratefully acknowledge Y. Lecluse and S. Salome-Desnoulez for technical support.

AUTHOR CONTRIBUTIONS

Conceptualization, J.-L.P.; Methodology, J.-L.P., A.P., and A.A.; Investigation, A.P., A.A., M.C., H.S., F.S., R.N., Q.W., Z.M., L.V., S.Q.R., F.L., M.T., H.D., B.P.-B., and N.D.-B.; Validation, J.-L.P.; Formal Analysis, A.P. and A.A.; Writing – Original Draft, J.-L.P., A.P., and A.A.; Writing – Review & Editing, J.-L.P., A.A., G.K., and D.M.O.; Resources, O.D., R.L.G., O.L., A.S.-C., G.P., E.S., E.D., M.P., M.-L.G., and G.K.; Supervision, J.-L.P.

DECLARATION OF INTERESTS

The authors declare no competing interests.

Received: June 27, 2018
Revised: January 8, 2019
Accepted: February 22, 2019
Published: September 24, 2019

REFERENCES

Agostini, L., Martinon, F., Burns, K., McDermott, M.F., Hawkins, P.N., and Tschopp, J. (2004). NALP3 forms an IL-1beta-processing inflammasome with increased activity in Muckle-Wells autoinflammatory disorder. Immunity *20*, 319–325.

Allouch, A., Di Primio, C., Alpi, E., Lusic, M., Arosio, D., Giacca, M., and Cereseto, A. (2011). The TRIM family protein KAP1 inhibits HIV-1 integration. Cell Host Microbe *9*, 484–495.

Allouch, A., David, A., Amie, S.M., Lahouassa, H., Chartier, L., Margottin-Goguet, F., Barré-Sinoussi, F., Kim, B., Sáez-Cirión, A., and Pancino, G. (2013). p21-mediated RNR2 repression restricts HIV-1 replication in macrophages by inhibiting dNTP biosynthesis pathway. Proc. Natl. Acad. Sci. USA *110*, E3997–E4006.

Bandera, A., Masetti, M., Fabbiani, M., Biasin, M., Muscatello, A., Squillace, N., Clerici, M., Gori, A., and Trabattoni, D. (2018). The NLRP3 Inflammasome Is Upregulated in HIV-Infected Antiretroviral Therapy-Treated Individuals with Defective Immune Recovery. Front. Immunol. *9*, 214.

Barouch, D.H., Ghneim, K., Bosche, W.J., Li, Y., Berkemeier, B., Hull, M., Bhattacharyya, S., Cameron, M., Liu, J., Smith, K., et al. (2016). Rapid Inflammasome Activation following Mucosal SIV Infection of Rhesus Monkeys. Cell *165*, 656–667.

Barrero-Villar, M., Cabrero, J.R., Gordón-Alonso, M., Barroso-González, J., Alvarez-Losada, S., Muñoz-Fernández, M.A., Sánchez-Madrid, F., and Valenzuela-Fernández, A. (2009). Moesin is required for HIV-1-induced CD4-CXCR4 interaction, F-actin redistribution, membrane fusion and viral infection in lymphocytes. J. Cell Sci. *122*, 103–113.

Caillet, M., Janvier, K., Pelchen-Matthews, A., Delcroix-Genête, D., Camus, G., Marsh, M., and Berlioz-Torrent, C. (2011). Rab7A is required for efficient production of infectious HIV-1. PLoS Pathog. *7*, e1002347.

Caution, K., Gavrilin, M.A., Tazi, M., Kanneganti, A., Layman, D., Hoque, S., Krause, K., and Amer, A.O. (2015). Caspase-11 and caspase-1 differentially modulate actin polymerization via RhoA and Slingshot proteins to promote bacterial clearance. Sci. Rep. *5*, 18479.

Chen, I.Y., and Ichinohe, T. (2015). Response of host inflammasomes to viral infection. Trends Microbiol. *23*, 55–63.

Chivero, E.T., Guo, M.L., Periyasamy, P., Liao, K., Callen, S.E., and Buch, S. (2017). HIV-1 Tat Primes and Activates Microglial NLRP3 Inflammasome-Mediated Neuroinflammation. J. Neurosci. *37*, 3599–3609.

Collins, M., Bartelt, R.R., and Houtman, J.C. (2010). T cell receptor activation leads to two distinct phases of Pyk2 activation and actin cytoskeletal rearrangement in human T cells. Mol. Immunol. *47*, 1665–1674.

David, A., Sáez-Cirión, A., Versmisse, P., Malbec, O., Iannascoli, B., Herschke, F., Lucas, M., Barré-Sinoussi, F., Mouscadet, J.F., Daëron, M., and Pancino, G. (2006). The engagement of activating FcgammaRs inhibits primate lentivirus replication in human macrophages. J. Immunol. *177*, 6291–6300.

Delelis, O., Malet, I., Na, L., Tchertanov, L., Calvez, V., Marcelin, A.G., Subra, F., Deprez, E., and Mouscadet, J.F. (2009). The G140S mutation in HIV integrases from raltegravir-resistant patients rescues catalytic defect due to the resistance Q148H mutation. Nucleic Acids Res. *37*, 1193–1201.

Dioszeghy, V., Benlhassan-Chahour, K., Delache, B., Dereuddre-Bosquet, N., Aubenque, C., Gras, G., Le Grand, R., and Vaslin, B. (2006). Changes in soluble factor-mediated CD8+ cell-derived antiviral activity in cynomolgus macaques infected with simian immunodeficiency virus SIVmac251: relationship to biological markers of progression. J. Virol. *80*, 236–245.

Doitsh, G., Cavrois, M., Lassen, K.G., Zepeda, O., Yang, Z., Santiago, M.L., Hebbeler, A.M., and Greene, W.C. (2010). Abortive HIV infection mediates CD4 T cell depletion and inflammation in human lymphoid tissue. Cell *143*, 789–801.

Doitsh, G., Galloway, N.L., Geng, X., Yang, Z., Monroe, K.M., Zepeda, O., Hunt, P.W., Hatano, H., Sowinski, S., Muñoz-Arias, I., and Greene, W.C. (2014). Cell death by pyroptosis drives CD4 T-cell depletion in HIV-1 infection. Nature *505*, 509–514.

Du, Q.S., Ren, X.R., Xie, Y., Wang, Q., Mei, L., and Xiong, W.C. (2001). Inhibition of PYK2-induced actin cytoskeleton reorganization, PYK2 autophosphorylation and focal adhesion targeting by FAK. J. Cell Sci. *114*, 2977–2987.

Elliott, M.R., Chekeni, F.B., Trampont, P.C., Lazarowski, E.R., Kadl, A., Walk, S.F., Park, D., Woodson, R.I., Ostankovich, M., Sharma, P., et al. (2009). Nucleotides released by apoptotic cells act as a find-me signal to promote phagocytic clearance. Nature *461*, 282–286.

Halle, A., Hornung, V., Petzold, G.C., Stewart, C.R., Monks, B.G., Reinheckel, T., Fitzgerald, K.A., Latz, E., Moore, K.J., and Golenbock, D.T. (2008). The NALP3 inflammasome is involved in the innate immune response to amyloid-beta. Nat. Immunol. *9*, 857–865.

Haque, S., Lan, X., Wen, H., Lederman, R., Chawla, A., Attia, M., Bongu, R.P., Husain, M., Mikulak, J., Saleem, M.A., et al. (2016). HIV Promotes NLRP3 Inflammasome Complex Activation in Murine HIV-Associated Nephropathy. Am. J. Pathol. *186*, 347–358.

Harris, R.S., Hultquist, J.F., and Evans, D.T. (2012). The restriction factors of human immunodeficiency virus. J. Biol. Chem. *287*, 40875–40883.

Hazleton, J.E., Berman, J.W., and Eugenin, E.A. (2012). Purinergic receptors are required for HIV-1 infection of primary human macrophages. J. Immunol. *188*, 4488–4495.

He, Y., Varadarajan, S., Muñoz-Planillo, R., Burberry, A., Nakamura, Y., and Núñez, G. (2014). 3,4-methylenedioxy-β-nitrostyrene inhibits NLRP3 inflammasome activation by blocking assembly of the inflammasome. J. Biol. Chem. *289*, 1142–1150.

Ippagunta, S.K., Malireddi, R.K., Shaw, P.J., Neale, G.A., Vande Walle, L., Green, D.R., Fukui, Y., Lamkanfi, M., and Kanneganti, T.D. (2011). The inflammasome adaptor ASC regulates the function of adaptive immune cells by controlling Dock2-mediated Rac activation and actin polymerization. Nat. Immunol. *12*, 1010–1016.

Jiménez-Baranda, S., Gómez-Moutón, C., Rojas, A., Martínez-Prats, L., Mira, E., Ana Lacalle, R., Valencia, A., Dimitrov, D.S., Viola, A., Delgado, R., et al. (2007). Filamin-A regulates actin-dependent clustering of HIV receptors. Nat. Cell Biol. *9*, 838–846.

Kankkunen, P., Välimäki, E., Rintahaka, J., Palomäki, J., Nyman, T., Alenius, H., Wolff, H., and Matikainen, S. (2014). Trichothecene mycotoxins activate NLRP3 inflammasome through a P2X7 receptor and Src tyrosine kinase dependent pathway. Hum. Immunol. *75*, 134–140.

Liu, J., Liao, Z., Camden, J., Griffin, K.D., Garrad, R.C., Santiago-Pérez, L.I., González, F.A., Seye, C.I., Weisman, G.A., and Erb, L. (2004). Src homology 3 binding sites in the P2Y2 nucleotide receptor interact with Src and regulate activities of Src, proline-rich tyrosine kinase 2, and growth factor receptors. J. Biol. Chem. *279*, 8212–8218.

Mamik, M.K., Hui, E., Branton, W.G., McKenzie, B.A., Chisholm, J., Cohen, E.A., and Power, C. (2017). HIV-1 Viral Protein R Activates NLRP3 Inflammasome in Microglia: implications for HIV-1 Associated Neuroinflammation. J. Neuroimmune Pharmacol. *12*, 233–248.

McDonald, D., Vodicka, M.A., Lucero, G., Svitkina, T.M., Borisy, G.G., Emerman, M., and Hope, T.J. (2002). Visualization of the intracellular behavior of HIV in living cells. J. Cell Biol. *159*, 441–452.

Monroe, K.M., Yang, Z., Johnson, J.R., Geng, X., Doitsh, G., Krogan, N.J., and Greene, W.C. (2014). IFI16 DNA sensor is required for death of lymphoid CD4 T cells abortively infected with HIV. Science *343*, 428–432.

Okigaki, M., Davis, C., Falasca, M., Harroch, S., Felsenfeld, D.P., Sheetz, M.P., and Schlessinger, J. (2003). Pyk2 regulates multiple signaling events crucial for macrophage morphology and migration. Proc. Natl. Acad. Sci. USA *100*, 10740–10745.

Perfettini, J.L., Roumier, T., Castedo, M., Larochette, N., Boya, P., Raynal, B., Lazar, V., Ciccosanti, F., Nardacci, R., Penninger, J., et al. (2004). NF-kappaB and p53 are the dominant apoptosis-inducing transcription factors elicited by the HIV-1 envelope. J. Exp. Med. *199*, 629–640.

Perfettini, J.L., Castedo, M., Nardacci, R., Ciccosanti, F., Boya, P., Roumier, T., Larochette, N., Piacentini, M., and Kroemer, G. (2005). Essential role of p53 phosphorylation by p38 MAPK in apoptosis induction by the HIV-1 envelope. J. Exp. Med. *201*, 279–289.

Pontillo, A., Brandão, L.A., Guimarães, R.L., Segat, L., Athanasakis, E., and Crovella, S. (2010). A 3'UTR SNP in NLRP3 gene is associated with susceptibility to HIV-1 infection. J. Acquir. Immune Defic. Syndr. *54*, 236–240.

Pontillo, A., Oshiro, T.M., Girardelli, M., Kamada, A.J., Crovella, S., and Duarte, A.J. (2012). Polymorphisms in inflammasome' genes and susceptibility to HIV-1 infection. J. Acquir. Immune Defic. Syndr. *59*, 121–125.

Pontillo, A., Carvalho, M.S., Kamada, A.J., Moura, R., Schindler, H.C., Duarte, A.J., and Crovella, S. (2013). Susceptibility to Mycobacterium tuberculosis infection in HIV-positive patients is associated with CARD8 genetic variant. J. Acquir. Immune Defic. Syndr. *63*, 147–151.

Py, B.F., Kim, M.S., Vakifahmetoglu-Norberg, H., and Yuan, J. (2013). Deubiquitination of NLRP3 by BRCC3 critically regulates inflammasome activity. Mol. Cell *49*, 331–338.

Ren, X.R., Du, Q.S., Huang, Y.Z., Ao, S.Z., Mei, L., and Xiong, W.C. (2001). Regulation of CDC42 GTPase by proline-rich tyrosine kinase 2 interacting with PSGAP, a novel pleckstrin homology and Src homology 3 domain containing rhoGAP protein. J. Cell Biol. *152*, 971–984.

Saïdi, H., Melki, M.T., and Gougeon, M.L. (2008). HMGB1-dependent triggering of HIV-1 replication and persistence in dendritic cells as a consequence of NK-DC cross-talk. PLoS ONE *3*, e3601.

Sandilands, E., Serrels, B., Wilkinson, S., and Frame, M.C. (2012). Src-dependent autophagic degradation of Ret in FAK-signalling-defective cancer cells. EMBO Rep. *13*, 733–740.

Séror, C., Melki, M.T., Subra, F., Raza, S.Q., Bras, M., Saïdi, H., Nardacci, R., Voisin, L., Paoletti, A., Law, F., et al. (2011). Extracellular ATP acts on P2Y2 purinergic receptors to facilitate HIV-1 infection. J. Exp. Med. *208*, 1823–1834.

Seye, C.I., Yu, N., González, F.A., Erb, L., and Weisman, G.A. (2004). The P2Y2 nucleotide receptor mediates vascular cell adhesion molecule-1 expression through interaction with VEGF receptor-2 (KDR/Flk-1). J. Biol. Chem. *279*, 35679–35686.

Shi, Y., Mucsi, A.D., and Ng, G. (2010). Monosodium urate crystals in inflammation and immunity. Immunol. Rev. *233*, 203–217.

Stolp, B., and Fackler, O.T. (2011). How HIV takes advantage of the cytoskeleton in entry and replication. Viruses *3*, 293–311.

Swartz, T.H., Esposito, A.M., Durham, N.D., Hartmann, B.M., and Chen, B.K. (2014). P2X-selective purinergic antagonists are strong inhibitors of HIV-1 fusion during both cell-to-cell and cell-free infection. J. Virol. *88*, 11504–11515.

Towers, G.J., and Noursadeghi, M. (2014). Interactions between HIV-1 and the cell-autonomous innate immune system. Cell Host Microbe *16*, 10–18.

Vandanmagsar, B., Youm, Y.H., Ravussin, A., Galgani, J.E., Stadler, K., Mynatt, R.L., Ravussin, E., Stephens, J.M., and Dixit, V.D. (2011). The NLRP3 inflammasome instigates obesity-induced inflammation and insulin resistance. Nat. Med. *17*, 179–188.

Vande Walle, L., Van Opdenbosch, N., Jacques, P., Fossoul, A., Verheugen, E., Vogel, P., Beyaert, R., Elewaut, D., Kanneganti, T.D., van Loo, G., and Lamkanfi, M. (2014). Negative regulation of the NLRP3 inflammasome by A20 protects against arthritis. Nature *512*, 69–73.

Vorster, P.J., Guo, J., Yoder, A., Wang, W., Zheng, Y., Xu, X., Yu, D., Spear, M., and Wu, Y. (2011). LIM kinase 1 modulates cortical actin and CXCR4 cycling and is activated by HIV-1 to initiate viral infection. J. Biol. Chem. *286*, 12554–12564.

Walsh, J.G., Reinke, S.N., Mamik, M.K., McKenzie, B.A., Maingat, F., Branton, W.G., Broadhurst, D.I., and Power, C. (2014). Rapid inflammasome activation in microglia contributes to brain disease in HIV/AIDS. Retrovirology *11*, 35.

Wang, Q., Xie, Y., Du, Q.S., Wu, X.J., Feng, X., Mei, L., McDonald, J.M., and Xiong, W.C. (2003). Regulation of the formation of osteoclastic actin rings by proline-rich tyrosine kinase 2 interacting with gelsolin. J. Cell Biol. *160*, 565–575.

Yoder, A., Yu, D., Dong, L., Iyer, S.R., Xu, X., Kelly, J., Liu, J., Wang, W., Vorster, P.J., Agulto, L., et al. (2008). HIV envelope-CXCR4 signaling activates cofilin to overcome cortical actin restriction in resting CD4 T cells. Cell *134*, 782–792.

STAR★METHODS

KEY RESOURCES TABLE

REAGENT or RESOURCE	SOURCE	IDENTIFIER
Antibodies		
CD71 (PE)	BD Pharmingen	555537; RRID: AB_395921
CD184 (CXCR4) (PE-Cy^{tm}5)	BD Pharmingen	555975; RRID: AB_396268
CD206 (FITC)	BD Pharmingen	551135; RRID: AB_394065
CD206 (Alexa Fluor 647)	ABD Serotec	MCA2235A647; RRID: AB_324890
CD4 (FITC)	BD Pharmingen	555346; RRID: AB_395751
CD163 (Alexa Fuor 647)	BD Pharmingen	562669; RRID: AB_2737710
CD163	BD Pharmingen	556017; RRID: AB_396295
CD11b (APC-Cy7)	BD Pharmingen	557657; RRID: AB_396772
CD163 (FITC)	BioLegend	333617; RRID: AB_2563093
CD14 (PE)	ebioscience	12-0149-42; RRID: AB_10598367
Mouse and Rabbit TrueBlot® ULTRA	ebioscience	18-8817 and 18-8816; RRID: AB_2610849 and AB_2610847
HIV-1 p24 (clone KC57)(FITC)	Beckman Coulter	CO6604665; RRID: AB_1575987
c-CBL (clone D4E10)	Cell Signaling	#8447; RRID: AB_10860763
Phospho-c-CBL Tyr731 (c-CBLY731*)	Cell Signaling	#3554; RRID: AB_2070452
GFP XP® (clone D5.1)	Cell Signaling	#2956; RRID: AB_1196615
PYK2 (clone 5E2)	Cell Signaling	#3480; RRID: AB_2174093
Pospho-PYK2 (Tyr402) (PYK2Y402*)	Cell Signaling	#3291; RRID: AB_2300530
SRC (clone 36D10)	Cell Signaling	#2109; RRID: AB_2106059
Phospho-SRC (Tyr416) (SRCY416*)	Cell Signaling	#2101; RRID: AB_331697
Beta-Actin (HRP)	Abcam	ab49900; RRID: AB_867494
NLRP3 (Cryo-2)	Adipogen	AG-20B-0014-C100; RRID: AB_2490202
NLRP3	Sigma-Aldrich	HPA017374; RRID: AB_1846750
P2Y2	Alomone	#APR-010; RRID: AB_2040078
Ubiquitin (clone P4D1)	Santa Cruz	sc-8017; RRID: AB_628423
FLAG ™	Sigma-Aldrich	F7425; RRID: AB_439687
GAPDH	Millipore	MAB374; RRID: AB_2107445
CAp24 (42-50)	NIH AIDS Reagent Program	4250
CAp24	Abcam	ab9044; RRID: AB_306962
gp120 (2G12)	NIH AIDS Reagent Program	1476
Bacterial and Virus Strains		
HIV-1_{NL4-3}	J.-L. Perfettini	(Séror et al., 2011)
HIV-$1_{NL4-3\Delta ENV}$	J.-L. Perfettini	(Séror et al., 2011)
HIV-1_{AD8}	NIH AIDS Reagent program	11346
HIV-1_{NDK}	M-L. Gougeon	(Saïdi et al., 2008)
HIV-1_{BaL}	NIH AIDS Reagent program	510
Biological Samples		
Human brain and lymph nodes tissues	National Institute for Infectious diseases Lazzaro Spallanzani http://www.inmi.it/index.htm	N/A
Macaca fascicularis lymph nodes, colon and ileum tissues	CEA, DSV/iMETI, Division of Immunology-Virology, IDMIT, France http://jacob.cea.fr/drf/ifrancoisjacob/Pages/Departements/IDMIT/laboratoires.aspx	N/A

(*Continued on next page*)

Continued

REAGENT or RESOURCE	SOURCE	IDENTIFIER
Human Blood Buffy coats	French blood bank (Etablissement Français du sang (EFS)) https://dondesang.efs.sante.fr/	B31111
Chemicals, Peptides, and Recombinant Proteins		
Alexa Fluor 594 phalloidin	Invitrogen	A12381
Recombinant Human and mouse M-CSF	PeproTech	300-25, 315-02
Recombinant human IL-2	PeproTech	200-02
PHA	Sigma	L8754
X-Gal	Sigma-Aldrich	B4252
Z-Leu-Leu-Leu-al (MG132)	Sigma-Aldrich	C2211
Anti-FLAG®M2 Affinity Gel	Sigma-Aldrich	A2220
Benzonase	Novagen®	71206-3
AR-C118925XX	Tocris	4890
Latrunculin B	Sigma-Aldrich	L5288
Oligofectamine	Invitrogen	58303
Puromycin	Invivogen	ant-pr-1
PMA	Invivogen	tlrl-pma
MSU	Invivogen	tlrl-msu
INTERFERin	Polyplus Transfection	409-10
UTP	Sigma	U6875
PP1	Sigma-Aldrich	P0040
PP2	Sigma-Aldrich	P0042
G5	Calbiochem	#662125
Fugene	Promega	E2312
PHA	Sigma	L8754
Critical Commercial Assays		
ELISA p24	Perkin Elmer	NEK050A
eta-galactosidase assay kit	Roche	10745731001
LDH assay kit	Roche	04744926001
Taqman universal Master Mix II, no UNG	ThermoFisher Scientific	4440040
Deposited data		
Western blot source data	This paper	Mendeley data https://doi.org/10.17632/6bxgc4h4m2.1
Experimental Models: Cell Lines		
HeLa $CD4^+$-$CXCR4^+$	J.-L. Perfettini	(Séror et al., 2011)
HeLa Env^+	J.-L. Perfettini	(Séror et al., 2011)
TZM-bl	NIH AIDS Reagent Program	8129
HEK293T	M. Caillet	(Caillet et al., 2011)
CEM-SS	A. Allouch	(Allouch et al., 2011)
THP1	ATCC	ATCC TIB202
THP1 PLKO empty control	This paper	N/A
THP1 PLKO shNLRP3.1	This paper	N/A
THP1 PLKO shNLRP3.2	This paper	N/A
THP1 PLKO shP2Y2	This paper	N/A
Human Blood Buffy coats	French blood bank (Etablissement Français du sang (EFS)) https://dondesang.efs.sante.fr/	B31111
Experimental Models: Organisms/Strains		
Macaca fascicularis	CEA, DSV/iMETI, Division of Immunology-Virology, IDMIT, France http://jacob.cea.fr/drf/ifrancoisjacob/Pages/Departements/IDMIT/laboratoires.aspx	N/A

(*Continued on next page*)

Continued

REAGENT or RESOURCE	SOURCE	IDENTIFIER
Oligonucleotides		
NLRP3 Taqman predesigned probe	ThermoFisher scientific	4331182 (Hs00918082_m1)
GAPDH TaqMan predesigned probe	ThermoFisher scientific	4331182 (Hs02758991_g1)
siRNA control for siNLRP3 1 and 2	This paper (Table S1)	N/A
siNLRP3 1 and 2 siRNAs	This paper (Table S1)	N/A
siGenome Non Targeting SMART siRNA Pool for SMART pool siRNA	Dharmacon (Table S1)	D-001206-13-20
siGENOME SMART pool human CBL siRNA	Dharmacon (Table S1)	M-003003-02-0005
Early Reverse transcripts primers and probes	G. Pancino (Table S1)	(David et al., 2006)
PLKO.1- shRNAs	This paper (Table S1)	N/A
Recombinant DNA		
pUNO-NLRP3	InvivoGen	puno1-hnalp3
pFlag-Luciferase	A. Allouch	(Allouch et al., 2011)
3×Flag-pcDNA3	G. Nunez	(He et al., 2014)
3×Flag-pcDNA3 NLRP3	G. Nunez	(He et al., 2014)
pEFGP-N1-P2Y2	L. Erb	(Seye et al., 2004)
pGFP-Vpr	G. Pancino	NA
pHIV-1_{NL4-3}	J.-L. Perfettini	(Séror et al., 2011)
pHIV-$1_{NL4-3\Delta ENV}$	J.-L. Perfettini	(Séror et al., 2011)
pHIV-1_{AD8}	NIH AIDS Reagent program	(Séror et al., 2011)
pMDG-VSV-G	J.-L. Perfettini	(Séror et al., 2011)
pCMV GAG-POL-HIV	M. Caillet	(Caillet et al., 2011)
Software and Algorithms		
Image J	https://imagej.nih.gov/ij/	N/A
Icy	http://icy.bioimageanalysis.org/download	N/A
GraphPad Prism version 6.0	https://www.graphpad.com/	N/A
Other		
AB human serum Male HIV tested	Biowest	S4190-100
Hoechst 33342	Invitrogen	H3570
Protein G Sepharose 4 Fast Flow	GE healthcare	17-0618-01

LEAD CONTACT AND MATERIALS AVAILABILITY

Further information for resources and reagents should be directed to and will be provided by the Lead Contact, Jean-Luc Perfettini (perfettini@orange.fr).

EXPERIMENTAL MODEL AND SUBJECT DETAILS

Cell lines

The monocyte THP1 cells and CEM-SS T cells were maintained in RMPI-1640-Glutamax medium supplemented with 10% heat inactivated fetal bovine serum (FBS) and 100 UI/mL penicillin-streptomycin (Life technology). THP1 cells were obtained from ATCC. THP1 macrophages were obtained by treatment for 3 hours with 100 nM phorbol-12-myristate-13-acetate (PMA, Invivogen) of THP1 monocytes and after extensive washings were let to differentiate for 72 hours before experimentation. HeLa cells stably transfected with the Env gene of HIV-$1_{LAI/IIIB}$ (HeLa Env^+), HeLa cells transfected with CD4 (HeLa $CD4^+CXCR4^+$), HeLa TZM-bl and HEK293T cells were cultured in Dulbecco's modified Eagle's medium (DMEM)-Glutamax supplemented with 10% FBS and 100 UI/ml penicillin-streptomycin, in the absence or presence of the indicated concentrations of inhibitors. All cell lines used were mycoplasma-free.

Primary Cells

To generate Monocytes Derived Macrophages (MDMs) for HIV-1 infections with HIV-1_{BaL}, $CD14^+$ monocytes were isolated from peripheral blood mononuclear cells (PBMCs) by positive selection using anti-CD14 beads (Miltenyi Biotec). Buffy coats from healthy

donors were obtained from the French blood bank (Etablissement Français du Sang (EFS)). In accordance with French law, written informed consent to use the cells for clinical research was obtained from each donor. Purified monocytes were incubated in RMPI-1640-Glutamax medium supplemented with 100 UI/ml penicillin-streptomycin and with 10% FBS in the presence of 10 ng/ml recombinant human (rh) M-CSF (PeproTech). After 6 days of culture, adherent cells corresponding to the macrophages enriched fraction were harvested, washed and used for HIV-1_{BaL} infection experiments. For macrophage silencing and infections with HIV-1_{AD8}, monocytes were separated from PBMCs by adherence to the plastic, detached and cultured for 6 days in hydrophobic Teflon dishes (Lumox Duthsher) in macrophage medium (RPMI 1640 supplemented with 200 mM L-glutamine, 100 U of penicillin, 100 μg streptomycin, 10 mM HEPES, 10 mM sodium pyruvate, 50 μM β-mercaptoethanol, 1% minimum essential medium vitamins, 1% non-essential amino acids (Life technology)) supplemented with 15% of heat inactivated human serum AB (Life technology or Biowest). For experiments, MDMs were harvested and resuspended in macrophage medium containing 10% of FBS. MDMs obtained with this method are 91 to 96% $CD14^+$, they express: the differentiation markers (CD11b and CD71) and the M2 macrophage polarization markers (CD163 and CD206) (Allouch et al., 2013).

T cells were prepared from the monocyte depleted cell fraction of PBMCs. Peripheral blood lymphocytes (PBLs) were activated for 48 hours in fresh medium supplemented with 2.5 μg/ml PHA (Sigma-Aldrich) and 1 μg/ml rhIL-2 (PeproTech). PBLs were then washed and cultured in growth medium containing 1 μg/mL rhIL-2 for 24 hours before HIV-1 infections.

Non-Human primates

Adult cynomolgus macaques (*Macaca fascicularis*) (four males and three females) were imported from Mauritius and housed in the facilities of the ''Commissariat à l'Energie Atomique et aux Energies Alternatives'' (CEA, Fontenay-aux-Roses, France). The protocols employed were approved by the ethical committee of the CEA ''Comité d'Ethique en Experimentation Animale'' registered in the French Research Ministry under number 44. Samples from lymph nodes, ileum and colon tissues were obtained from *Macaca fascicularis* that have been infected at the age of 5 years old by intrarectal inoculation with a single dose of 50 50% animal infectious doses (AID_{50}) of SIV_{mac251}. Tissues were collected during animal necropsy (for SIV_{mac251}-infected animals, on days 701 to 738 after SIV infection) after sedation of the animals (ketamine chlorhydrate 10 mg/kg) followed by euthanasia (injection of sodium pentobarbital 180 mg/kg). Non-human primates (NHP, which includes *M. fascicularis*) were used at the CEA in accordance with French national regulation and under national veterinary inspectors (CEA Permit Number A 92-032-02). The CEA is in compliance with Standards for Human Care and Use of Laboratory of the Office for Laboratory Animal Welfare (OLAW, USA) under OLAW Assurance number #A5826-01. The use of NHP at CEA is also in accordance with recommendation of the European Directive (2010/63, recommendation N°9). Animals were housed in adjoining individual cages allowing social interactions, under controlled conditions of humidity, temperature and light (12-hour light/12-hour dark cycles). Water was available *ad libitum*. Animals were monitored and fed 1-2 times daily with commercial monkey chow and fruits by trained personnel. Macaques were provided with environmental enrichment including toys, novel foodstuffs and music under the supervision of the CEA Animal Welfare Body. The animals were used under the supervision of the veterinarians in charge of the animal facility. Experimental procedures were conducted after animal sedation with ketamine chlorydrate (Rhone-Merieux, Lyon, France, 10 mg/kg) as previously described (Dioszeghy et al., 2006).

Human autopsies

Human autopsies from axillary lymph nodes and frontal cortex were obtained in accordance with the Italian and EU legislations, after approval by the Institutional Review Board of the Lazzaro Spallanzani National Institute for Infectious Disease (Ethics Committee approval number 40/2006). Axillary lymph nodes and post-mortem frontal cortex sections were obtained from healthy (6 and 5, respectively) and HIV-1- infected individuals (6 and 11, respectively) (all men, mean age 36 years, the median values of HIV-1 viral load was 4.5 ± 0.6 $\log_{10}$ cp/ml and < 500 CD4 T cells/μl). Frontal cortex sections were obtained from patients with HIV-1-associated dementia.

METHODS DETAILS

Plasmids and transfections

NLRP3 coding sequence in the pUNO vector was purchased from Invivogen. The Flag-tagged NLRP3 full-length coding sequence was inserted in the 3xFlag-pcDNA3 and are a kind of gift from Gabriel Nunez (He et al., 2014). The sequence coding for P2Y2 (in the pEFGP-N1 vector) is gift from Laura Erb (Seye et al., 2004). Transient transfections of HeLa $CD4^+CXCR4^+$ cells ($2.4x10^5$) or HEK293T ($3x10^5$) cells with mammalian expression vectors (1-5 μg) were performed using Fugene transfection reagent (Promega), following the manufacturer's instructions. Western blot, immunoprecipitation analyses and experiences of HIV-1 infection or cell fusion were performed 24 hours after transfection. The transfection of pHIV-1_{AD8} and pHIV-1_{NL4-3} in HEK293T were performed 48 hours after transfection of pFlag-Luciferase or p3xFlag-NLRP3.

siRNA- and shRNA-mediated knockdowns

For HeLa $CD4^+CXCR4^+$ knockdown the small interfering RNAs (siRNAs) used against NLRP3 were purchased from Sigma and had the following sequences: NLRP3, siRNA-1, 5′-GGAUCAAACUACUCUGUGA-3′; siRNA-2, 5′-UGCAAGAUCUCUCAGCAAA-3′ and the corresponding control siRNA, 5′-UUCAAUAAAUUCUUGAGGU-3′. The siRNAs against CBL used for primary MDMs and

HEK293T cells are siGenome (Dharmacon) smart pool selected composed of a pool of four siRNAs having the following sequences for CBL (siRNA1, 5′-GGAGACACAUUUCGGAUUA-3′; siRNA2, 5′-GAUCUGACCUGCAAUGAUU-3′; siRNA3, 5′-GACAAUCCCUCA CAAUAAA-3′; siRNA4, 5′-CCAGAAAGCUUUGGUCAUU-3′). The siRNAs used as control with siGenome smart pool are a pool of four on target plus non-targeting siRNAs (Dharmacon). siRNAs transfection of HeLa $CD4^+CXCR4^+$ or HEK293T cells were performed with 20 nM siRNA using Oligofectamine (Invitrogen) according to the manufacturer's instructions. Western blot analyses and experiences of HIV-1 infections or cell fusions were performed 48 hours after siRNA transfection. For siRNA transfection of MDMs, the protocol was previously described (Allouch et al., 2013): MDMs were seeded ($0.5x10^6$ MDMs/0.5 ml/ well of 12-well plate in macrophages medium + 10% FBS) and let to be attached at 37°C for 2 hours prior siRNAs transfection. The siRNAs transfections were performed with the INTERFERin (Polyplus Transfection). Different amounts of siRNAs were pre-diluted in 1 mL of Opti-MEM in which 20 μL of INTERFERin were added and the transfection mix was let to incubate at room temperature for 10 minutes. The transfection mix (250 μl) was added to $0.5x10^6$ MDMs at the final concentrations of 50 nM of siRNAs against CBL. Equal amounts of the on target plus non-targeting siRNAs were added to the control MDMs. The MDMs were then incubated at 37°C for overnight. The medium was replaced with fresh macrophage medium supplemented with 10% FBS prior to the infections. At 72 hours post-CBL siRNA transfection MDMs were infected with $HIV\text{-}1_{AD8}$ (MOI of 1) for 6 hours, cell lysates were assayed for protein expression by western blot.

For short hairpin RNA (shRNA) lentiviral particles transduction, the pLKO.1 shRNA expression lentiviral vector coding for each targeted gene was purchased from Thermo Scientific. The shRNAs used in knockdown experiments had the following sequences for P2Y2 (shRNA1, 5′-ATGTTCCACCTGGCTGTGTCTGATGCACT-3′), for NLRP3 (shRNA1, 5′-TTCTTGAAGTGTTTCTAACGC-3′, shRNA2, 5′-AAACAGTAGAACAATTCCAGC-3′) and pLKO.1 empty vector control. Lentiviral vector particles were generated by cotransfection of three plasmids coding for the gag-pol HIV-1 genes (pCMV- HIV-1-GAG-POL), for the vector genome carrying shRNA of interest (pLKO.1 shRNA) and for the plasmid coding for an envelope of VSVG (pMDG-VSV-G). Co-transfection was performed in HEK293T cells using Fugene transfection reagent (Promega) according to the manufacturer's protocol. Two days after transfection, supernatants were filtered using 0.45-μm cellulose acetate filters (Sartorius stedim), aliquoted and frozen at −80°C. For transduction, lentivirus productions were added to the monocytic THP1 cell line ($4x10^6$) or into $CD4^+CXR4^+$ HeLa cells (10^6) and 24 hours after transduction the medium was replaced with fresh growth medium containing 1 μg/mL puromycin (Invivogen). MDMs, CEM-SS T Cells or THP1 cells ($1x10^6$) were transduced with 2 μg CAp24 of a pool of LKO.1 shNLRP3 (shRNA1 and shRNA2) for 48 hours before infections with $HIV\text{-}1_{NL4\text{-}3}$ or $HIV\text{-}1_{AD8}$ (MOI of 1).

Virus productions

To produce stocks of wild-type $HIV\text{-}1_{NL4\text{-}3}$ or $HIV\text{-}1_{AD8}$, HEK293T cells ($2x10^6$) were transfected with 20 μg of the corresponding proviral DNA ($pHIV\text{-}1_{NL4\text{-}3}$ or $pHIV\text{-}1_{AD8}$) and for Env-deleted VSV-G pseudotyped NL4-3 viruses ($pHIV\text{-}1_{NL4\text{-}3\Delta Env}$), HEK293T cells ($2x10^6$) cells were transfected with 4 μg of VSV-G expression vector (pVSV-G) and 16 μg of HIV-1 proviral DNA ($pHIV\text{-}1_{NL4\text{-}3\Delta Env}$) by the calcium phosphate method. After 12 hours, the transfection mixture was replaced with 8 mL of fresh growth medium. Then, 24 hours later, the media containing the first batch of virus was harvested and 8 mL of fresh growth medium was added to the cells for additional 24 hours. $HIV\text{-}1_{NDK}$ and $HIV\text{-}1_{BaL}$ were obtained after infection of activated PBLs and MDM with $HIV\text{-}1_{NDK}$ and $HIV\text{-}1_{BaL}$ viral stocks, respectively and harvesting the corresponding supernatants at three and six days after infections (Saïdi et al., 2008). $HIV\text{-}1_{AD8\text{-}Vpr\text{-}GFP}$ was obtained through the transfection of $3x10^6$ HEK293T cells with 10 μg $pHIV\text{-}1_{AD8}$ (NIH AIDS research reagents), 2.5 μg pGFP-Vpr expression vectors using Fugene (Promega) following manufacturer's instructions.

Upon collection, all virus-containing media was low-speed centrifuged, filtered through a 0.45 μm pore size filter (Sartorius stedim), to remove cell debris, treated with Benzonase (Novagen®) and stored in 1 mL aliquots at −80°C (Delelis et al., 2009; Perfettini et al., 2004, 2005). Viral stocks were standardized by quantification of CAp24 antigen in cell culture supernatants with an enzyme-linked immunoabsorbent assay (Perkin Elmer) and infection of TZM-bl cells (bearing the β-galactosidase gene under the control of HIV-1 LTR) with serial dilutions of the viral stocks followed by cell fixation and X-Gal staining. The multiplicity of infection (MOI) was determined at 48 hours of infection of TZM-bl based on the number of the positive X-Gal cells.

Viral infections

After 3 days of infection with $HIV\text{-}1_{NDK}$ (MOI of 1), PHA/IL-2–stimulated peripheral blood lymphocytes were cocultured with uninfected lymphoblasts or alone for 48 hours and analyzed by immunofluorescence for synapse formation. MDMs were infected with $HIV\text{-}1_{BaL}$ (with a MOI of 2) during 3 days for the analysis by Proximity Ligation Assay (PLA) (following manufacturer's instructions) and the intracellular CAp24 by FACS, as previously described (Séror et al., 2011), for MSU (100 μM) and LPS (10 ng/ml) treated cells. MDMs or PMA-THP1 macrophages infected with $HIV\text{-}1_{AD8}$ were pre-treated 18 hours with MSU (100 μM) and AR-C118925XX (100 μM) and infected during six hours with $HIV\text{-}1_{AD8}$ (MOI of 1) in the presence of the indicated drugs. The quantification of the LDH release in the cell supernatants of MSU-treated MDM was performed using the commercially available ELISA kits for LDH (Roche) according to the manufacturers' instructions at 24 hours after infection.

THP1 cells were also infected with $HIV\text{-}1_{NL4\text{-}3}$ (MOI of 1) or $HIV\text{-}1_{NL4\text{-}3\Delta Env}$ (MOI of 1) during 6 hours and analyzed for related signaling pathways by western blot. THP1 monocytes or CEM-SS T cells were infected or not for 3 hours with X4-tropic $HIV\text{-}1_{NL4\text{-}3}$ or R5-tropic $HIV\text{-}1_{AD8}$ (MOI of 1) and then were either harvest for western blot and mRNA analysis or kept for 21 days by passing cells every 3 days for the same analysis.

For THP1 monocytes or CEM-SS T cells silenced for NLRP3, through the transduction of lentiviral vectors expressing shRNA1 and shRNA2 against NLRP3 gene, and control cells were infected with HIV-1_{NL4-3} or HIV-1_{AD8} (MOI of 1) at 48 hours after shRNA transduction for 6 hours and after washings were suspended in equal medium volumes. Cell supernatants were then harvested at 6 and 12 days after infection for quantification of HIV-1 CAp24 contents. For immunoprecipitation assays, THP1 cells were treated 8 hours with PP1 (20 μM), PP2 (20 μM) or 2 hours of pretreatment with UTP (100 μM) before infection. Then, THP1 cells were infected during 6 hours with HIV-1_{NL4-3} (MOI of 1) in the presence of the indicated drugs. To remove the membrane bound non-internalized HIV-1 particles before analysis of intracellular CAp24 by western blot, cells were treated with trypsin at 37°C for 20 minutes followed by two extensive washings. Target cell infectivity was evaluated using the enhanced β-galactosidase assay kit (Roche). PMA-THP1 macrophages were infected with HIV-$1_{AD8\text{-}Vpr\text{-}GFP}$ (MOI of 1) in the presence of latrunculin B (10 μM) during 6 hours and the control cells were treated with ethanol and then were fixed with 2% PFA for immunofluorescence analysis.

Immunofluorescence

Cells were fixed in 2% paraformaldehyde-PBS for 5 minutes, permeabilized in 0.3% Triton (Sigma) in PBS or 0.1% Triton for MDMs and PBLs, and incubated with PBS-FBS 20% for 1 hour. Tissue 4-μm sections (lymph nodes, ileum and colon tissues) were cut from the paraffin blocks of the paraformaldehyde fixed tissues from *Macaca fascicularis* or humans. After paraffin removal, slides were subjected to antigen retrieval by microwave boiling in 1 mmol/l EDTA pH 9.0. Cell slides were then incubated during overnight for immunofluorescence with anti-P2Y2 (Alomone), anti-NLRP3 (Adipogen), anti-CD163 (BD laboratories) or anti-gp120 (2G12) (AIDS Research and Reference Reagent Program, Division of AIDS, NIAID) or for immunochemistry with anti-NLRP3 (Sigma) after permeabilization in 0.3% Triton for 5 minutes and saturation in PBS-FBS 20% for 1 hour. Then, cells were incubated with appropriate secondary antibodies conjugated to Alexa Fluor 488, 546 or 647 fluorochromes (Life technologies) at room temperature during 1 hour and 30 minutes. Actin was stained with Alexa Fluor 594 Phalloidin for 30 minutes at room temperature. DNA was stained with Hoechst 33342, Trihydrochloride, Trihydrate (Life technologies) and then cells were mounted with Flouromount G medium (Southern biotech). Proximity Ligation Assay (DUOLINK®, Sigma) was performed according to the manufacturer's instructions using anti-NLRP3 (Adipogen) and anti P2Y2 (Alomone) as primary antibodies. Images of cells were acquired by laser-scanning fluorescent confocal microscopy Leica SPE with LAS-X software (Leica) with 8 bits configuration and using a 63X oil objective (1.4 numerical aperture). Leica Microsystem immersion oil (11513859) was used and imaging was performed at room temperature. Confocal images were analyzed with ImageJ and exported as TIFs for figures illustration. For 3D immunofluorescence intensity image construction, images were analyzed by Icy software (in Figure 1G).

Western blots and immunoprecipitations

Cells were washed twice with PBS and lysed in appropriated buffer (250 mM NaCl, 0.1% NP-40, 5 mM EDTA, 10 mM Na3VO4, 10 mM NaF, 5 mM DTT, 3 mM Na4P2O7, 1 mM EGTA, 10 mM Glycerol phosphate, 10 mM Tris-Hcl (pH = 7.5) and the protease and phosphatase inhibitors (Roche)). 10-40 μg of protein extracts were run on 4%–12% or 10% SDS-PAGE and transferred at 4°C onto a nitrocellulose membrane (0.2 Micron). After incubation for 2 hours at room temperature with 5% nonfat milk or BSA (Bovine Serum Albumin) in Tris-buffered saline and 0.1% Tween 20 (TBS-Tween), membranes were incubated with primary antibody at 4°C overnight. Horseradish peroxidase–conjugated goat anti–mouse or anti–rabbit (SouthernBiotech) antibodies were then incubated for 1 hour 30 minutes and revealed with the enhanced ECL detection system (GE Healthcare) in the linear range. The primary antibodies for western blot against CBL (D4E10), GFP (D5.1), PYK2 (5E2), PYK2Y402*, SRC (36D10) and SRCY416* were obtained from Cell Signaling. Primary antibodies against ACTIN and GAPDH were purchased from Abcam and Millipore, respectively. The primary antibodies anti-CAp24 (42-50) and anti-gp120 (2G12) were from NIH (AIDS Research and Reference Reagent Program, Division of AIDS, NIAID). Antibody anti-NLRP3 was from Adipogen (Cryo-2), anti-P2Y2 was from Alomone, anti-ubiquitin (UB) (P4D1) was from Santa-Cruz, and anti-Flag was from Sigma. For immunoprecipitations, cell pellets were lysed at indicated times after infection or 24 hours after transfection in CHAPS buffer (50 mM Tris- HCl (pH = 7.5), 0.50 M NaCl and 0.1% CHAPS) containing protease and phosphatase inhibitors. Anti-P2Y2 (Alomone) antibodies were incubated overnight at 4°C with 500 μg cell lysates. The complexes were precipitated by incubation with Protein G Sepharose 4 Fast Flow (GE Healthcare) for 4 hours. For relative expression quantification analyzed protein bands were quantified by ImageJ software and normalized on the corresponding endogenous expression of GAPDH or ACTIN proteins. To determine the relative NLRP3 interacting with P2Y2, NLRP3 protein bands were normalized on the corresponding immunoprecipitated P2Y2.

Flow cytometry

For flow cytometry, THP1 cells and MDMs (10^6 cells/ml) were harvested in RPMI complete medium, washed twice with PBS, saturated at 4°C for 20 min with PBS-FBS 10% and incubated with anti-CD4 (FITC) and anti-CD184 (CXCR4) (PE-Cy5) antibodies. The indicated antibodies and isotype-matched antibodies used were obtained from BD PharMingen. Phenotypic analyses on primary human MDMs infected by HIV-1_{BaL} were realized by flow cytometry using mAb anti-CD163 (FITC) (BioLegend), anti-CD206 (Alexa Fluor®647 (AbD Serotec) and anti-p24 (PE) (Beckman Coulter).

Quantitative PCR (qPCR)

The quantification of the HIV-1 early reverse transcripts (ERT) was based on the quantification of HIV-1 R-U5 DNA and performed as previously described (David et al., 2006). DNA was extracted with the DNeasy Tissue Kit (QIAGEN) at 24 h.p.i for ERT detection in MDMs. The quantitative PCR analysis was carried on an ABI prism 7000 Sequence Detection System. The amounts of HIV-1 cDNA copies were normalized to the endogenous reference gene albumin. Standard curve were generated by serial dilutions of a commercial human genomic DNA (Roche).

For the detection of NLRP3 mRNA, total RNA from $0.25x20^6$ THP1 monocytes or CEM-SS T cells were extracted using RNeasy kit (QIAGEN). RNA was transcribed using SuperScript II RT (Invitrogen). The predesigned Applied Biosystems probes for NLRP3 gene (Hs00918082 m1) and GAPDH (Hs02758991 g1) (for normalization) were used. These probes were included in the premade TaqMan Gene expression mixes obtained from thermofisher scientific. The results were analyzed with the cycle threshold method (CT) and each sample was normalized to the quantity of endogenous GAPDH mRNA.

QUANTIFICATION AND STATISTICAL ANALYSIS

Statistical parameters including exact values of n, precisions measures (mean ± SEM), statistical significances and the tests used for each analysis are reported in the Figures and Figures legends. All values were expressed as the mean ± SEM of cell individual samples. Samples values were analyzed using two-tailed unpaired Student's t test for two groups, ANOVA for multiple comparisons groups, Mann-Whitney test for human MDMs and PBLs donors not normalized data and Wilcoxon signed rank test for MDMs donors analyzed for early reverse transcripts. Significance levels are * $p \leq 0.05$, ** $p \leq 0.01$, *** $p \leq 0.001$ and **** $p \leq 0.0001$. Statistical analysis was performed in GraphPad Prism version 6.0b (GraphPad Software). No statistical test was used to determine sample size. No samples were excluded for analysis. The experiments were not randomized. Investigators were not blinded to allocation during experiments and outcome assessments.

DATA AND CODE AVAILABILITY

The western blot data reported in this paper have been deposited on Mendeley Data (Mendeley data https://doi.org/10.17632/6bxgc4h4m2.1) and are accessible to readers upon request.

REFERENCES

1. Gordon S. Phagocytosis: The Legacy of Metchnikoff. *Cell*. 2016;166(5):1065-1068. doi:10.1016/j.cell.2016.08.017
2. Cavaillon JM, Legout S. Centenary of the death of Elie Metchnikoff: a visionary and an outstanding team leader. *Microbes Infect*. 2016;18(10):577-594. doi:10.1016/j.micinf.2016.05.008
3. Munro DAD, Hughes J. The Origins and Functions of Tissue-Resident Macrophages in Kidney Development. *Front Physiol*. 2017;8:837. Published 2017 Oct 25. doi:10.3389/fphys.2017.00837
4. Ginhoux F, Schultze JL, Murray PJ, Ochando J, Biswas SK. New insights into the multidimensional concept of macrophage ontogeny, activation and function. *Nat Immunol*. 2016;17(1):34-40. doi:10.1038/ni.3324
5. Mikkola HKA, Orkin SH. The journey of developing hematopoietic stem cells. *Development*. 2006;133(19):3733-3744. doi:10.1242/dev.02568
6. Epelman S, Lavine KJ, Randolph GJ. Origin and functions of tissue macrophages. *Immunity*. 2014;41(1):21-35. doi:10.1016/j.immuni.2014.06.013
7. Varol C, Mildner A, Jung S. Macrophages: development and tissue specialization. *Annu Rev Immunol*. 2015;33:643-675. doi:10.1146/annurev-immunol-032414-112220
8. Sevenich L. Brain-resident microglia and blood-borne macrophages orchestrate central nervous system inflammation in neurodegenerative disorders and brain cancer. *Front Immunol*. 2018;9:697. Published 2018 Apr 6. doi:10.3389/fimmu.2018.00697
9. Mak KS, Funnell AP, Pearson RC, Crossley M. PU.1 and Haematopoietic Cell Fate: Dosage Matters. *Int J Cell Biol*. 2011;2011:808524. doi:10.1155/2011/808524
10. T'Jonck W, Guilliams M, Bonnardel J. Niche signals and transcription factors involved in tissue-resident macrophage development. *Cell Immunol.* 2018;330:43-53. doi:10.1016/j.cellimm.2018.02.005
11. Khazen W, M'bika J-P, Tomkiewicz C, et al. Expression of macrophage-selective markers in human and rodent adipocytes. *FEBS Lett*. 2005;579(25):5631-5634. doi:10.1016/j.febslet.2005.09.032
12. Akinrinmade OA, Chetty S, Daramola AK, Islam MU, Thepen T, Barth S. CD64: An Attractive Immunotherapeutic Target for M1-type Macrophage Mediated Chronic Inflammatory Diseases. *Biomedicines.* 2017;5(3):56. Published 2017 Sep 12. doi:10.3390/biomedicines5030056
13. Hoeksema MA, Glass CK. Nature and nurture of tissue-specific macrophage phenotypes. *Atherosclerosis*. 2019;281:159-167.

doi:10.1016/j.atherosclerosis.2018.10.005

14. Kurotaki D, Uede T, Tamura T. Functions and development of red pulp macrophages. *Microbiol Immunol*. 2015;59(2):55-62. doi:10.1111/1348-0421.12228
15. Lopez-Atalaya JP, Askew KE, Sierra A, Gomez-Nicola D. Development and maintenance of the brain's immune toolkit: Microglia and non-parenchymal brain macrophages. *Dev Neurobiol*. 2018;78(6):561-579. doi:10.1002/dneu.22545
16. Yu JS, Ramasamy TS, Murphy N, et al. PI3K/mTORC2 regulates TGF-β/Activin signalling by modulating Smad2/3 activity via linker phosphorylation. *Nat Commun*. 2015;6:7212. Published 2015 May 22. doi:10.1038/ncomms8212
17. Stanley ER, Chitu V. CSF-1 receptor signaling in myeloid cells. *Cold Spring Harb Perspect Biol*. 2014;6(6):a021857. Published 2014 Jun 2. doi:10.1101/cshperspect.a021857
18. Bain CC, Schridde A. Origin, Differentiation, and Function of Intestinal Macrophages. *Front Immunol.* 2018;9:2733. Published 2018 Nov 27. doi:10.3389/fimmu.2018.02733
19. Chang PV, Hao L, Offermanns S, Medzhitov R. The microbial metabolite butyrate regulates intestinal macrophage function via histone deacetylase inhibition. *Proc Natl Acad Sci U S A.* 2014;111(6):2247-2252. doi:10.1073/pnas.1322269111
20. Okabe Y, Medzhitov R. Tissue-specific signals control reversible program of localization and functional polarization of macrophages. *Cell*. 2014;157(4):832-844. doi:10.1016/j.cell.2014.04.016
21. Wolf AA, Yáñez A, Barman PK, Goodridge HS. The Ontogeny of Monocyte Subsets. *Front Immunol.* 2019;10:1642. Published 2019 Jul 17. doi:10.3389/fimmu.2019.01642
22. Teh YC, Ding JL, Ng LG, Chong SZ. Capturing the Fantastic Voyage of Monocytes Through Time and Space. *Front Immunol.* 2019;10:834. Published 2019 Apr 16. doi:10.3389/fimmu.2019.00834
23. Cheng H, Zheng Z, Cheng T. New paradigms on hematopoietic stem cell differentiation. *Protein Cell*. 2020;11(1):34-44. doi:10.1007/s13238-019-0633-0
24. Terry RL, Miller SD. Molecular control of monocyte development. *Cell Immunol*. 2014;291(1-2):16-21. doi:10.1016/j.cellimm.2014.02.008
25. Yáñez A, Coetzee SG, Olsson A, et al. Granulocyte-Monocyte Progenitors and Monocyte-Dendritic Cell Progenitors Independently Produce Functionally Distinct Monocytes. *Immunity*. 2017;47(5):890-902.e4. doi:10.1016/j.immuni.2017.10.021
26. Auffray C, Sieweke MH, Geissmann F. Blood monocytes: development, heterogeneity, and relationship with dendritic cells. *Annu Rev Immunol.* 2009;27:669-

692. doi:10.1146/annurev.immunol.021908.132557

27. Kurotaki D, Sasaki H, Tamura T. Transcriptional control of monocyte and macrophage development. *Int Immunol*. 2017;29(3):97-107. doi:10.1093/intimm/dxx016
28. Tamura T, Kurotaki D, Koizumi S. Regulation of myelopoiesis by the transcription factor IRF8. *Int J Hematol.* 2015;101(4):342-351. doi:10.1007/s12185-015-1761-9
29. Kurotaki D, Osato N, Nishiyama A, et al. Essential role of the IRF8-KLF4 transcription factor cascade in murine monocyte differentiation. *Blood*. 2013;121(10):1839-1849. doi:10.1182/blood-2012-06-437863
30. Spooner CJ, Cheng JX, Pujadas E, Laslo P, Singh H. A Recurrent Network Involving the Transcription Factors PU.1 and Gfi1 Orchestrates Innate and Adaptive Immune Cell Fates. *Immunity*. 2009;31(4):576-586. doi:10.1016/j.immuni.2009.07.011
31. Ziegler-Heitbrock L, Hofer TP. Toward a refined definition of monocyte subsets. *Front Immunol.* 2013;4:23. Published 2013 Feb 4. doi:10.3389/fimmu.2013.00023
32. Sampath P, Moideen K, Ranganathan UD, Bethunaickan R. Monocyte Subsets: Phenotypes and Function in Tuberculosis Infection. *Front Immunol.* 2018;9:1726. Published 2018 Jul 30. doi:10.3389/fimmu.2018.01726
33. Sprangers S, de Vries TJ, Everts V. Monocyte Heterogeneity: Consequences for Monocyte-Derived Immune Cells. *J Immunol Res.* 2016;2016:1475435. doi:10.1155/2016/1475435
34. Patel AA, Zhang Y, Fullerton JN, et al. The fate and lifespan of human monocyte subsets in steady state and systemic inflammation. *J Exp Med*. 2017;214(7):1913-1923. doi:10.1084/jem.20170355
35. Gordon S, Taylor PR. Monocyte and macrophage heterogeneity. *Nat Rev Immunol*. 2005;5(12):953-964. doi:10.1038/nri1733
36. Hoeffel G, Ginhoux F. Ontogeny of Tissue-Resident Macrophages. *Front Immunol.* 2015;6:486. Published 2015 Sep 22. doi:10.3389/fimmu.2015.00486
37. Sieweke MH, Allen JE. Beyond stem cells: self-renewal of differentiated macrophages. *Science.* 2013;342(6161):1242974. doi:10.1126/science.1242974
38. Guilliams M, Mildner A, Yona S. Developmental and Functional Heterogeneity of Monocytes. *Immunity*. 2018;49(4):595-613. doi:10.1016/j.immuni.2018.10.005
39. Epelman S, Lavine KJ, Beaudin AE, et al. Embryonic and adult-derived resident cardiac macrophages are maintained through distinct mechanisms at steady state and during inflammation. *Immunity*. 2014;40(1):91-104. doi:10.1016/j.immuni.2013.11.019

40. Ma Y, Mouton AJ, Lindsey ML. Cardiac macrophage biology in the steady-state heart, the aging heart, and following myocardial infarction. *Transl Res*. 2018;191:15-28. doi:10.1016/j.trsl.2017.10.001
41. Dutta P, Sager HB, Stengel KR, et al. Myocardial Infarction Activates CCR2(+) Hematopoietic Stem and Progenitor Cells. *Cell Stem Cell.* 2015;16(5):477-487. doi:10.1016/j.stem.2015.04.008
42. Yao Y, Xu XH, Jin L. Macrophage Polarization in Physiological and Pathological Pregnancy. *Front Immunol.* 2019;10:792. Published 2019 Apr 15. doi:10.3389/fimmu.2019.00792
43. Chen Z, Klein T, Murray RZ, et al. Osteoimmunomodulation for the development of advanced bone biomaterials. *Mater Today*. 2016;19(6):304-321. doi:10.1016/j.mattod.2015.11.004
44. Mantovani A, Sica A, Sozzani S, Allavena P, Vecchi A, Locati M. The chemokine system in diverse forms of macrophage activation and polarization. *Trends Immunol*. 2004;25(12):677-686. doi:10.1016/j.it.2004.09.015
45. Dos Anjos Cassado A. F4/80 as a Major Macrophage Marker: The Case of the Peritoneum and Spleen. *Results Probl Cell Differ*. 2017;62:161-179. doi:10.1007/978-3-319-54090-0_7
46. Nielsen MC, Hvidbjerg Gantzel R, Clària J, Trebicka J, Møller HJ, Grønbæk H. Macrophage Activation Markers, CD163 and CD206, in Acute-on-Chronic Liver Failure. *Cells.* 2020;9(5):1175. Published 2020 May 9. doi:10.3390/cells9051175
47. Svendsen P, Etzerodt A, Deleuran BW, Moestrup SK. Mouse CD163 deficiency strongly enhances experimental collagen-induced arthritis. *Sci Rep.* 2020;10(1):12447. Published 2020 Jul 24. doi:10.1038/s41598-020-69018-7
48. Mukherjee S, Darzi S, Paul K, Werkmeister JA, Gargett CE. Mesenchymal stem cell-based bioengineered constructs: foreign body response, cross-talk with macrophages and impact of biomaterial design strategies for pelvic floor disorders. *Interface Focus.* 2019;9(4):20180089. doi:10.1098/rsfs.2018.0089
49. Fingleton B. Matrix metalloproteinases as regulators of inflammatory processes. *Biochim Biophys Acta Mol Cell Res.* 2017;1864(11 Pt A):2036-2042. doi:10.1016/j.bbamcr.2017.05.010
50. Hesketh M, Sahin KB, West ZE, Murray RZ. Macrophage Phenotypes Regulate Scar Formation and Chronic Wound Healing. *Int J Mol Sci.* 2017;18(7):1545. Published 2017 Jul 17. doi:10.3390/ijms18071545

51. Fan X, Zhang H, Cheng Y, Jiang X, Zhu J, Jin T. Double Roles of Macrophages in Human Neuroimmune Diseases and Their Animal Models. *Mediators Inflamm.* 2016;2016:8489251. doi:10.1155/2016/8489251
52. Mosser DM, Edwards JP. Exploring the full spectrum of macrophage activation [published correction appears in Nat Rev Immunol.2010 Jun;10(6):460]. *Nat Rev Immunol.* 2008;8(12):958-969. doi:10.1038/nri2448
53. Rath M, Müller I, Kropf P, Closs EI, Munder M. Metabolism via Arginase or Nitric Oxide Synthase: Two Competing Arginine Pathways in Macrophages. *Front Immunol.* 2014;5:532. Published 2014 Oct 27. doi:10.3389/fimmu.2014.00532
54. Bertani FR, Mozetic P, Fioramonti M, et al. Classification of M1/M2-polarized human macrophages by label-free hyperspectral reflectance confocal microscopy and multivariate analysis. *Sci Rep.* 2017;7(1):8965. Published 2017 Aug 21. doi:10.1038/s41598-017-08121-8
55. Klopfleisch R. Macrophage reaction against biomaterials in the mouse model - Phenotypes, functions and markers. *Acta Biomater.* 2016;43:3-13. doi:10.1016/j.actbio.2016.07.003
56. Watanabe S, Alexander M, Misharin AV, Budinger GRS. The role of macrophages in the resolution of inflammation. *J Clin Invest.* 2019;129(7):2619-2628. Published 2019 May 20. doi:10.1172/JCI124615
57. Sun SC. Non-canonical NF-κB signaling pathway. *Cell Res*. 2011;21(1):71-85. doi:10.1038/cr.2010.177
58. Liu T, Zhang L, Joo D, Sun SC. NF-κB signaling in inflammation. *Signal Transduct Target Ther.* 2017;2:17023-. doi:10.1038/sigtrans.2017.23
59. Dorrington MG, Fraser IDC. NF-κB Signaling in Macrophages: Dynamics, Crosstalk, and Signal Integration. *Front Immunol.* 2019;10:705. Published 2019 Apr 9. doi:10.3389/fimmu.2019.00705
60. Yu H, Lin L, Zhang Z, Zhang H, Hu H. Targeting NF-κB pathway for the therapy of diseases: mechanism and clinical study. *Signal Transduct Target Ther.* 2020;5(1):209. Published 2020 Sep 21. doi:10.1038/s41392-020-00312-6
61. Amarante-Mendes GP, Adjemian S, Branco LM, Zanetti LC, Weinlich R, Bortoluci KR. Pattern Recognition Receptors and the Host Cell Death Molecular Machinery. *Front Immunol.* 2018;9:2379. Published 2018 Oct 16. doi:10.3389/fimmu.2018.02379
62. Shih VFS, Tsui R, Caldwell A, Hoffmann A. A single NFκB system for both canonical and non-canonical signaling. *Cell Res*. 2011;21(1):86-102. doi:10.1038/cr.2010.161

63. Wu Y, Bressette D, Carrell JA, et al. Tumor necrosis factor (TNF) receptor superfamily member TACI is a high affinity receptor for TNF family members APRIL and BLyS. *J Biol Chem*. 2000;275(45):35478-35485. doi:10.1074/jbc.M005224200
64. Cildir G, Low KC, Tergaonkar V. Noncanonical NF-κB Signaling in Health and Disease. *Trends Mol Med*. 2016;22(5):414-429. doi:10.1016/j.molmed.2016.03.002
65. Huxford T, Ghosh G. A structural guide to proteins of the NF-kappaB signaling module. *Cold Spring Harb Perspect Biol.* 2009;1(3):a000075. doi:10.1101/cshperspect.a000075
66. Wang N, Liang H, Zen K. Molecular mechanisms that influence the macrophage m1-m2 polarization balance. *Front Immunol.* 2014;5:614. Published 2014 Nov 28. doi:10.3389/fimmu.2014.00614
67. Vasanthakumar A, Liao Y, Teh P, et al. The TNF Receptor Superfamily-NF-κB Axis Is Critical to Maintain Effector Regulatory T Cells in Lymphoid and Non-lymphoid Tissues. *Cell Rep*. 2017;20(12):2906-2920. doi:10.1016/j.celrep.2017.08.068
68. Lawrence T, Natoli G. Transcriptional regulation of macrophage polarization: enabling diversity with identity. *Nat Rev Immunol.* 2011;11(11):750-761. Published 2011 Oct 25. doi:10.1038/nri3088
69. Platanitis E, Decker T. Regulatory Networks Involving STATs, IRFs, and NFκB in Inflammation. *Front Immunol.* 2018;9:2542. Published 2018 Nov 13. doi:10.3389/fimmu.2018.02542
70. Mogensen TH. IRF and STAT Transcription Factors - From Basic Biology to Roles in Infection, Protective Immunity, and Primary Immunodeficiencies. *Front Immunol.* 2019;9:3047. Published 2019 Jan 8. doi:10.3389/fimmu.2018.03047
71. Abdolvahab MH, Darvishi B, Zarei M, Majidzadeh-A K, Farahmand L. Interferons: Role in cancer therapy. *Immunotherapy*. 2020;12(11):833-855. doi:10.2217/imt-2019-0217
72. Schoggins JW. Interferon-Stimulated Genes: What Do They All Do?. *Annu Rev Virol.* 2019;6(1):567-584. doi:10.1146/annurev-virology-092818-015756
73. Liu S, Imani S, Deng Y, et al. Targeting IFN/STAT1 Pathway as a Promising Strategy to Overcome Radioresistance. *Onco Targets Ther.* 2020;13:6037-6050. Published 2020 Jun 24. doi:10.2147/OTT.S256708
74. Twum DY, Colligan SH, Hoffend NC, et al. IFN regulatory factor-8 expression in macrophages governs an antimetastatic program [published online ahead of print, 2019 Feb 7]. *JCI Insight*. 2019;4(3):e124267. doi:10.1172/jci.insight.124267

75. Waqas SFH, Ampem G, Röszer T. Analysis of IL-4/STAT6 signaling in macrophages. *Methods Mol Biol*. 2019;1966:211-224. doi:10.1007/978-1-4939-9195-2_17
76. Czimmerer Z, Daniel B, Horvath A, et al. The Transcription Factor STAT6 Mediates Direct Repression of Inflammatory Enhancers and Limits Activation of Alternatively Polarized Macrophages. *Immunity*. 2018;48(1):75-90.e6. doi:10.1016/j.immuni.2017.12.010
77. Martinez-Nunez RT, Louafi F, Sanchez-Elsner T. The interleukin 13 (IL-13) pathway in human macrophages is modulated by microRNA-155 via direct targeting of interleukin 13 receptor α1 (IL13Rα1). *J Biol Chem*. 2011;286(3):1786-1794. doi:10.1074/jbc.M110.169367
78. Nakamura R, Sene A, Santeford A, et al. IL10-driven STAT3 signalling in senescent macrophages promotes pathological eye angiogenesis. *Nat Commun.* 2015;6:7847. Published 2015 Aug 11. doi:10.1038/ncomms8847
79. Hume DA, Himes SR. Transcription Factors That Regulate Macrophage Development and Function. In: Gordon S, ed. *The Macrophage as Therapeutic Target.* Berlin, Heidelberg: Springer Berlin Heidelberg; 2003:11-40. doi:10.1007/978-3-642-55742-2_2
80. Yanai H, Negishi H, Taniguchi T. The IRF family of transcription factors inception, impact and implications in oncogenesis. *Oncoimmunology*. 2012;1(8):1376-1386. doi:10.4161/onci.22475
81. Jefferies CA. Regulating IRFs in IFN Driven Disease. *Front Immunol.* 2019;10:325. Published 2019 Mar 29. doi:10.3389/fimmu.2019.00325
82. Zhang Y, Li H. Reprogramming Interferon Regulatory Factor Signaling in Cardiometabolic Diseases. *Physiology (Bethesda)*. 2017;32(3):210-223. doi:10.1152/physiol.00038.2016
83. Günthner R, Anders HJ. Interferon-regulatory factors determine macrophage phenotype polarization. *Mediators Inflamm.* 2013;2013:731023. doi:10.1155/2013/731023
84. Yanai H, Chiba S, Hangai S, et al. Revisiting the role of IRF3 in inflammation and immunity by conditional and specifically targeted gene ablation in mice. *Proc Natl Acad Sci U S A*. 2018;115(20):5253-5258. doi:10.1073/pnas.1803936115
85. Ban T, Sato GR, Tamura T. Regulation and role of the transcription factor IRF5 in innate immune responses and systemic lupus erythematosus. *Int Immunol*. 2018;30(11):529-536. doi:10.1093/intimm/dxy032

86. Krausgruber T, Blazek K, Smallie T, et al. IRF5 promotes inflammatory macrophage polarization and T H1-TH17 responses. *Nat Immunol*. 2011;12(3):231-238. doi:10.1038/ni.1990
87. Feng D, Sangster-Guity N, Stone R, et al. Differential requirement of histone acetylase and deacetylase activities for IRF5-mediated proinflammatory cytokine expression. *J Immunol*. 2010;185(10):6003-6012. doi:10.4049/jimmunol.1000482
88. Karki R, Lee E, Place D, et al. IRF8 Regulates Transcription of Naips for NLRC4 Inflammasome Activation. *Cell*. 2018;173(4):920-933.e13. doi:10.1016/j.cell.2018.02.055
89. El Chartouni C, Schwarzfischer L, Rehli M. Interleukin-4 induced interferon regulatory factor (Irf) 4 participates in the regulation of alternative macrophage priming. *Immunobiology*. 2010;215(9-10):821-825. doi:10.1016/j.imbio.2010.05.031
90. Liu YC, Zou XB, Chai YF, Yao YM. Macrophage polarization in inflammatory diseases. *Int J Biol Sci.* 2014;10(5):520-529. Published 2014 May 1. doi:10.7150/ijbs.8879
91. Satoh T, Takeuchi O, Vandenbon A, et al. The Jmjd3-Irf4 axis regulates M2 macrophage polarization and host responses against helminth infection. *Nat Immunol*. 2010;11(10):936-944. doi:10.1038/ni.1920
92. Achuthan A, Cook AD, Lee M-C, et al. Granulocyte macrophage colony-stimulating factor induces CCL17 production via IRF4 to mediate inflammation. *J Clin Invest*. 2016;126(9):3453-3466. doi:10.1172/JCI87828
93. Rengarajan J, Mowen KA, McBride KD, Smith ED, Singh H, Glimcher LH. Interferon regulatory factor 4 (IRF4) interacts with NFATc2 to modulate interleukin 4 gene expression. *J Exp Med*. 2002;195(8):1003-1012. doi:10.1084/jem.20011128
94. Li H, Jiang T, Li MQ, Zheng XL, Zhao GJ. Transcriptional Regulation of Macrophages Polarization by MicroRNAs. *Front Immunol.* 2018;9:1175. Published 2018 May 28. doi:10.3389/fimmu.2018.01175
95. Albina JE, Mahoney EJ, Daley JM, Wesche DE, Morris SMJ, Reichner JS. Macrophage arginase regulation by CCAAT/enhancer-binding protein beta. *Shock*. 2005;23(2):168-172. doi:10.1097/01.shk.0000148054.74268.e2
96. Lee B, Qiao L, Lu M, et al. C/EBPα regulates macrophage activation and systemic metabolism. *Am J Physiol Endocrinol Metab*. 2014;306(10):E1144-54. doi:10.1152/ajpendo.00002.2014
97. Ruffell D, Mourkioti F, Gambardella A, et al. A CREB-C/EBPbeta cascade induces

M2 macrophage-specific gene expression and promotes muscle injury repair. *Proc Natl Acad Sci U S A*. 2009;106(41):17475-17480. doi:10.1073/pnas.0908641106

98. Curtale G, Rubino M, Locati M. MicroRNAs as Molecular Switches in Macrophage Activation. *Front Immunol.* 2019;10:799. Published 2019 Apr 17. doi:10.3389/fimmu.2019.00799
99. Essandoh K, Li Y, Huo J, Fan GC. MiRNA-mediated macrophage polarization and its potential role in the regulation of inflammatory response. *Shock*. 2016;46(2):122-131. doi:10.1097/SHK.0000000000000604
100. Zhang L, Huang C, Guo Y, et al. MicroRNA-26b Modulates the NF- B Pathway in Alveolar Macrophages by Regulating PTEN. *J Immunol*. 2015;195(11):5404-5414. doi:10.4049/jimmunol.1402933
101. Lu Z, Li Y, Takwi A, et al. miR-301a as an NF-κB activator in pancreatic cancer cells. *EMBO J*. 2011;30(1):57-67. doi:10.1038/emboj.2010.296
102. Kohanbash G, Okada H. MicroRNAs and STAT interplay. *Semin Cancer Biol*. 2012;22(1):70-75. doi:10.1016/j.semcancer.2011.12.010
103. Mann M, Mehta A, Zhao JL, et al. An NF-κB-microRNA regulatory network tunes macrophage inflammatory responses [published correction appears in Nat Commun. 2018 Aug 16;9(1):3338]. *Nat Commun.* 2017;8(1):851. Published 2017 Oct 11. doi:10.1038/s41467-017-00972-z
104. Bala S, Marcos M, Kodys K, et al. Up-regulation of microRNA-155 in macrophages contributes to increased Tumor Necrosis Factor α (TNFα) production via increased mRNA half-life in alcoholic liver disease. *J Biol Chem*. 2011;286(2):1436-1444. doi:10.1074/jbc.M110.145870
105. McCoy CE, Sheedy FJ, Qualls JE, et al. IL-10 inhibits miR-155 induction by toll-like receptors. *J Biol Chem*. 2010;285(27):20492-20498. doi:10.1074/jbc.M110.102111
106. Peng L, Zhang H, Hao Y, et al. Reprogramming macrophage orientation by microRNA 146b targeting transcription factor IRF5. *EBioMedicine*. 2016;14:83-96. doi:10.1016/j.ebiom.2016.10.041
107. Fang H, Yang M, Pan Q, et al. MicroRNA-22-3p alleviates spinal cord ischemia/reperfusion injury by modulating M2 macrophage polarization via IRF5. *J Neurochem*. 2021;156(1):106-120. doi:10.1111/jnc.15042
108. So AY, Sookram R, Chaudhuri AA, et al. Dual mechanisms by which miR-125b represses IRF4 to induce myeloid and B-cell leukemias. *Blood.* 2014;124(9):1502-1512. doi:10.1182/blood-2014-02-553842

109. Ikeda S, Kitadate A, Abe F, et al. Hypoxia-inducible microRNA-210 regulates the DIMT1-IRF4 oncogenic axis in multiple myeloma. *Cancer Sci*. 2017;108(4):641-652. doi:10.1111/cas.13183
110. Qin Z, Wang PY, Su DF, Liu X. miRNA-124 in Immune System and Immune Disorders. *Front Immunol.* 2016;7:406. Published 2016 Oct 4. doi:10.3389/fimmu.2016.00406
111. Bi J, Zeng X, Zhao L, et al. miR-181a Induces Macrophage Polarized to M2 Phenotype and Promotes M2 Macrophage-mediated Tumor Cell Metastasis by Targeting KLF6 and C/EBPα. *Mol Ther Nucleic Acids.* 2016;5(9):e368. Published 2016 Sep 27. doi:10.1038/mtna.2016.71
112. Stunault MI, Bories G, Guinamard RR, Ivanov S. Metabolism Plays a Key Role during Macrophage Activation. *Mediators Inflamm.* 2018;2018:2426138. Published 2018 Dec 10. doi:10.1155/2018/2426138
113. Geeraerts X, Bolli E, Fendt SM, Van Ginderachter JA. Macrophage Metabolism As Therapeutic Target for Cancer, Atherosclerosis, and Obesity. *Front Immunol.* 2017;8:289. Published 2017 Mar 15. doi:10.3389/fimmu.2017.00289
114. Viola A, Munari F, Sánchez-Rodríguez R, Scolaro T, Castegna A. The Metabolic Signature of Macrophage Responses. *Front Immunol.* 2019;10:1462. Published 2019 Jul 3. doi:10.3389/fimmu.2019.01462
115. Thapa B, Lee K. Metabolic influence on macrophage polarization and pathogenesis. *BMB Rep*. 2019;52(6):360-372. doi:10.5483/BMBRep.2019.52.6.140
116. Galván-Peña S, O'Neill LA. Metabolic reprograming in macrophage polarization. *Front Immunol.* 2014;5:420. Published 2014 Sep 2. doi:10.3389/fimmu.2014.00420
117. Diskin C, Pålsson-McDermott EM. Metabolic Modulation in Macrophage Effector Function. *Front Immunol.* 2018;9:270. Published 2018 Feb 19. doi:10.3389/fimmu.2018.00270
118. Roberts J, G. Fallon P, Hams E. The Pivotal Role of Macrophages in Metabolic Distress. *Macrophage Act Biol Dis*. 2020;(Il). doi:10.5772/intechopen.86474
119. Rodriguez PC, Ochoa AC, Al-Khami AA. Arginine Metabolism in Myeloid Cells Shapes Innate and Adaptive Immunity. *Front Immunol.* 2017;8:93. Published 2017 Feb 7. doi:10.3389/fimmu.2017.00093
120. Cheng DL, Fang HX, Liang Y, Zhao Y, Shi CS. MicroRNA-34a promotes iNOS secretion from pulmonary macrophages in septic suckling rats through activating STAT3 pathway. *Biomed Pharmacother.* 2018;105:1276-1282.

doi:10.1016/j.biopha.2018.06.063

121. Yeramian A, Martin L, Serrat N, et al. Arginine Transport via Cationic Amino Acid Transporter 2 Plays a Critical Regulatory Role in Classical or Alternative Activation of Macrophages. *J Immunol*. 2006;176(10):5918-5924. doi:10.4049/jimmunol.176.10.5918
122. Fang HY, Hughes R, Murdoch C, et al. Hypoxia-inducible factors 1 and 2 are important transcriptional effectors in primary macrophages experiencing hypoxia. *Blood*. 2009;114(4):844-859. doi:10.1182/blood-2008-12-195941
123. Murdoch C, Muthana M, Lewis CE. Hypoxia Regulates Macrophage Functions in Inflammation. *J Immunol*. 2005;175(10):6257-6263. doi:10.4049/jimmunol.175.10.6257
124. Kierans SJ, Taylor CT. Regulation of glycolysis by the hypoxia-inducible factor (HIF): implications for cellular physiology. *J Physiol*. 2021;599(1):23-37. doi:10.1113/JP280572
125. Rahat MA, Bitterman H, Lahat N. Molecular mechanisms regulating macrophage response to hypoxia. *Front Immunol.* 2011;2:45. Published 2011 Sep 16. doi:10.3389/fimmu.2011.00045
126. Takeda N, O'Dea EL, Doedens A, et al. Differential activation and antagonistic function of HIF-α isoforms in macrophages are essential for NO homeostasis. *Genes Dev*. 2010;24(5):491-501. doi:10.1101/gad.1881410
127. Matrone C, Pignataro G, Molinaro P, et al. HIF-1α reveals a binding activity to the promoter of iNOS gene after permanent middle cerebral artery occlusion. *J Neurochem*. 2004;90(2):368-378. doi:10.1111/j.1471-4159.2004.02483.x
128. Choe SS, Shin KC, Ka S, Lee YK, Chun JS, Kim JB. Macrophage HIF-2α ameliorates adipose tissue inflammation and insulin resistance in obesity. *Diabetes*. 2014;63(10):3359-3371. doi:10.2337/db13-1965
129. Watts ER, Walmsley SR. Inflammation and Hypoxia: HIF and PHD Isoform Selectivity. *Trends Mol Med*. 2019;25(1):33-46. doi:10.1016/j.molmed.2018.10.006
130. Youle RJ, van der Bliek AM. Mitochondrial fission, fusion, and stress. *Science*. 2012;337(6098):1062-1065. doi:10.1126/science.1219855
131. Vakifahmetoglu-Norberg H, Ouchida AT, Norberg E. The role of mitochondria in metabolism and cell death. *Biochem Biophys Res Commun*. 2017;482(3):426-431. doi:10.1016/j.bbrc.2016.11.088
132. Bordi M, Nazio F, Campello S. The Close Interconnection between Mitochondrial

Dynamics and Mitophagy in Cancer. *Front Oncol.* 2017;7:81. Published 2017 May 2. doi:10.3389/fonc.2017.00081

133. An HJ, Cho G, Lee JO, Paik SG, Kim YS, Lee H. Higd-1a interacts with Opa1 and is required for the morphological and functional integrity of mitochondria. *Proc Natl Acad Sci U S A*. 2013;110(32):13014-13019. doi:10.1073/pnas.1307170110
134. Ren L, Chen X, Chen X, Li J, Cheng B, Xia J. Mitochondrial Dynamics: Fission and Fusion in Fate Determination of Mesenchymal Stem Cells. *Front Cell Dev Biol.* 2020;8:580070. Published 2020 Oct 15. doi:10.3389/fcell.2020.580070
135. Benard G, Karbowski M. Mitochondrial fusion and division: Regulation and role in cell viability. *Semin Cell Dev Biol*. 2009;20(3):365-374. doi:10.1016/j.semcdb.2008.12.012
136. Gao Z, Li Y, Wang F, et al. Mitochondrial dynamics controls anti-tumour innate immunity by regulating CHIP-IRF1 axis stability. *Nat Commun.* 2017;8(1):1805. Published 2017 Nov 27. doi:10.1038/s41467-017-01919-0
137. Youle RJ, van der Bliek AM. Mitochondrial fission, fusion, and stress. *Science.* 2012;337(6098):1062-1065. doi:10.1126/science.1219855
138. Li Y, He Y, Miao K, Zheng Y, Deng C, Liu TM. Imaging of macrophage mitochondria dynamics in vivo reveals cellular activation phenotype for diagnosis. *Theranostics.* 2020;10(7):2897-2917. Published 2020 Feb 3. doi:10.7150/thno.40495
139. Ryu SW, Han EC, Yoon J, Choi C. The mitochondrial fusion-related proteins Mfn2 and OPA1 are transcriptionally induced during differentiation of bone marrow progenitors to immature dendritic cells. *Mol Cells*. 2014;38(1):89-94. doi:10.14348/molcells.2015.2285
140. Lloberas J, Muñoz JP, Hernández-Álvarez MI, Cardona PJ, Zorzano A, Celada A. Macrophage mitochondrial MFN2 (mitofusin 2) links immune stress and immune response through reactive oxygen species (ROS) production. *Autophagy*. 2020;16(12):2307-2309. doi:10.1080/15548627.2020.1839191
141. Tur J, Pereira-Lopes S, Vico T, et al. Mitofusin 2 in Macrophages Links Mitochondrial ROS Production, Cytokine Release, Phagocytosis, Autophagy, and Bactericidal Activity. *Cell Rep.* 2020;32(8):108079. doi:10.1016/j.celrep.2020.108079
142. Westermann B. Mitochondrial fusion and fission in cell life and death. *Nat Rev Mol Cell Biol*. 2010;11(12):872-884. doi:10.1038/nrm3013
143. Qing J, Zhang Z, Novák P, Zhao G, Yin K. Mitochondrial metabolism in regulating macrophage polarization: An emerging regulator of metabolic inflammatory diseases.

Acta Biochim Biophys Sin (Shanghai). 2020;52(9):917-926. doi:10.1093/abbs/gmaa081

144. Guido C, Whitaker-Menezes D, Lin Z, et al. Mitochondrial fission induces glycolytic reprogramming in cancer-associated myofibroblasts, driving stromal lactate production, and early tumor growth. *Oncotarget*. 2012;3(8):798-810. doi:10.18632/oncotarget.574
145. Kapetanovic R, Afroz SF, Ramnath D, et al. Lipopolysaccharide promotes Drp1-dependent mitochondrial fission and associated inflammatory responses in macrophages. *Immunol Cell Biol*. 2020;98(7):528-539. doi:10.1111/imcb.12363
146. Yu W, Wang X, Zhao J, et al. Stat2-Drp1 mediated mitochondrial mass increase is necessary for pro-inflammatory differentiation of macrophages [published correction appears in Redox Biol. 2021 Feb;39:101786]. *Redox Biol.* 2020;37:101761. doi:10.1016/j.redox.2020.101761
147. Formentini L, Santacatterina F, Núñez de Arenas C, et al. Mitochondrial ROS Production Protects the Intestine from Inflammation through Functional M2 Macrophage Polarization. *Cell Rep*. 2017;19(6):1202-1213. doi:10.1016/j.celrep.2017.04.036
148. Bhatia D, Chung KP, Nakahira K, et al. Mitophagy-dependent macrophage reprogramming protects against kidney fibrosis. *JCI Insight.* 2019;4(23):e132826. Published 2019 Dec 5. doi:10.1172/jci.insight.132826
149. Ding WX, Yin XM. Mitophagy: Mechanisms, pathophysiological roles, and analysis. *Biol Chem*. 2012;393(7):547-564. doi:10.1515/hsz-2012-0119
150. Aparicio-Trejo OE, Tapia E, Sánchez-Lozada LG, Pedraza-Chaverri J. Mitochondrial bioenergetics, redox state, dynamics and turnover alterations in renal mass reduction models of chronic kidney diseases and their possible implications in the progression of this illness. *Pharmacol Res.* 2018;135:1-11. doi:10.1016/j.phrs.2018.07.015
151. Zhong Z, Umemura A, Sanchez-Lopez E, et al. NF-κB Restricts Inflammasome Activation via Elimination of Damaged Mitochondria. *Cell*. 2016;164(5):896-910. doi:10.1016/j.cell.2015.12.057
152. Liu Z, Kuang W, Zhou Q, Zhang Y. TGF-β1 secreted by M2 phenotype macrophages enhances the stemness and migration of glioma cells via the SMAD2/3 signalling pathway. *Int J Mol Med*. 2018;42(6):3395-3403. doi:10.3892/ijmm.2018.3923
153. Calabrese MF, Rajamohan F, Harris MS, et al. Structural basis for AMPK activation: Natural and synthetic ligands regulate kinase activity from opposite poles by different

molecular mechanisms. *Structure*. 2014;22(8):1161-1172. doi:10.1016/j.str.2014.06.009

154. Novikova DS, Garabadzhiu AV, Melino G, Barlev NA, Tribulovich VG. AMP-activated protein kinase: structure, function, and role in pathological processes. *Biochemistry (Mosc)*. 2015;80(2):127-144. doi:10.1134/S0006297915020017
155. Xiao B, Sanders MJ, Underwood E, et al. Structure of mammalian AMPK and its regulation by ADP. *Nature*. 2011;472(7342):230-233. doi:10.1038/nature09932
156. Theret M, Mounier R, Rossi F. The origins and non-canonical functions of macrophages in development and regeneration. *Development.* 2019;146(9):dev156000. Published 2019 May 2. doi:10.1242/dev.156000
157. Sag D, Carling D, Stout RD, Suttles J. Adenosine 5′-Monophosphate-Activated Protein Kinase Promotes Macrophage Polarization to an Anti-Inflammatory Functional Phenotype. *J Immunol*. 2008;181(12):8633-8641. doi:10.4049/jimmunol.181.12.8633
158. Garcia D, Shaw RJ. AMPK: Mechanisms of Cellular Energy Sensing and Restoration of Metabolic Balance. *Mol Cell*. 2017;66(6):789-800. doi:10.1016/j.molcel.2017.05.032
159. Yan Y, Zhou XE, Xu HE, Melcher K. Structure and Physiological Regulation of AMPK. *Int J Mol Sci.* 2018;19(11):3534. Published 2018 Nov 9. doi:10.3390/ijms19113534
160. Herzig S, Shaw RJ. AMPK: Guardian of metabolism and mitochondrial homeostasis. *Nat Rev Mol Cell Biol*. 2018;19(2):121-135. doi:10.1038/nrm.2017.95
161. Zhu YP, Brown JR, Sag D, Zhang L, Suttles J. Adenosine 5′-Monophosphate–Activated Protein Kinase Regulates IL-10–Mediated Anti-Inflammatory Signaling Pathways in Macrophages. *J Immunol*. 2015;194(2):584-594. doi:10.4049/jimmunol.1401024
162. Niemand C, Nimmesgern A, Haan S, et al. Activation of STAT3 by IL-6 and IL-10 in primary human macrophages is differentially modulated by suppressor of cytokine signaling 3. *J Immunol.* 2003;170(6):3263-3272. doi:10.4049/jimmunol.170.6.3263
163. Fredman G, Tabas I. Macrophages Govern the Progression and Termination of Inflammation in Atherosclerosis and Metabolic Diseases. In: Biswas SK, Mantovani A, eds. *Macrophages: Biology and Role in the Pathology of Diseases*. New York: Springer New York; 2014:387-403. doi:10.1007/978-1-4939-1311-4_18
164. Gordon S, Plüddemann A. Tissue macrophages: heterogeneity and functions. *BMC Biol.* 2017;15(1):53. Published 2017 Jun 29. doi:10.1186/s12915-017-0392-4

165. Murray PJ, Wynn TA. Protective and pathogenic functions of macrophage subsets. *Nat Rev Immunol.* 2011;11(11):723-737. Published 2011 Oct 14. doi:10.1038/nri3073
166. Theret M, Mounier R, Rossi F. The origins and non-canonical functions of macrophages in development and regeneration. *Development.* 2019;146(9):dev156000. Published 2019 May 2. doi:10.1242/dev.156000
167. Lavin Y, Mortha A, Rahman A, Merad M. Regulation of macrophage development and function in peripheral tissues. *Nat Rev Immunol*. 2015;15(12):731-744. doi:10.1038/nri3920
168. Davies LC, Jenkins SJ, Allen JE, Taylor PR. Tissue-resident macrophages. *Nat Immunol.* 2013;14(10):986-995. doi:10.1038/ni.2705
169. Russo L, Lumeng CN. Properties and functions of adipose tissue macrophages in obesity. *Immunology*. 2018;155(4):407-417. doi:10.1111/imm.13002
170. Odegaard JI, Ricardo-Gonzalez RR, Goforth MH, et al. Macrophage-specific PPARgamma controls alternative activation and improves insulin resistance. *Nature.* 2007;447(7148):1116-1120. doi:10.1038/nature05894
171. Nguyen KD, Qiu Y, Cui X, et al. Alternatively activated macrophages produce catecholamines to sustain adaptive thermogenesis. *Nature.* 2011;480(7375):104-108. Published 2011 Nov 20. doi:10.1038/nature10653
172. Yin J, Valin KL, Dixon ML, Leavenworth JW. The Role of Microglia and Macrophages in CNS Homeostasis, Autoimmunity, and Cancer. *J Immunol Res.* 2017;2017:5150678. doi:10.1155/2017/5150678
173. Perry VH, Teeling J. Microglia and macrophages of the central nervous system: The contribution of microglia priming and systemic inflammation to chronic neurodegeneration. *Semin Immunopathol*. 2013;35(5):601-612. doi:10.1007/s00281-013-0382-8
174. Nayak D, Roth TL, McGavern DB. Microglia development and function. *Annu Rev Immunol*. 2014;32:367-402. doi:10.1146/annurev-immunol-032713-120240
175. Konishi H, Kiyama H. Microglial TREM2/DAP12 Signaling: A Double-Edged Sword in Neural Diseases. *Front Cell Neurosci.* 2018;12:206. Published 2018 Aug 6. doi:10.3389/fncel.2018.00206
176. Labandeira-Garcia JL, Costa-Besada MA, Labandeira CM, Villar-Cheda B, Rodríguez-Perez AI. Insulin-Like Growth Factor-1 and Neuroinflammation. *Front Aging Neurosci.* 2017;9:365. Published 2017 Nov 3. doi:10.3389/fnagi.2017.00365
177. Smith JA, Das A, Ray SK, Banik NL. Role of pro-inflammatory cytokines released

from microglia in neurodegenerative diseases. *Brain Res Bull*. 2012;87(1):10-20. doi:https://doi.org/10.1016/j.brainresbull.2011.10.004

178. Bachiller S, Jiménez-Ferrer I, Paulus A, et al. Microglia in Neurological Diseases: A Road Map to Brain-Disease Dependent-Inflammatory Response. *Front Cell Neurosci.* 2018;12:488. Published 2018 Dec 18. doi:10.3389/fncel.2018.00488
179. Borges da Silva H, Fonseca R, Pereira RM, Cassado Ados A, Álvarez JM, D'Império Lima MR. Splenic Macrophage Subsets and Their Function during Blood-Borne Infections. *Front Immunol.* 2015;6:480. Published 2015 Sep 22. doi:10.3389/fimmu.2015.00480
180. A-Gonzalez N, Castrillo A. Origin and specialization of splenic macrophages. *Cell Immunol.* 2018;330:151-158. doi:10.1016/j.cellimm.2018.05.005
181. Backer R, Schwandt T, Greuter M, et al. Effective collaboration between marginal metallophilic macrophages and CD8+ dendritic cells in the generation of cytotoxic T cells. *Proc Natl Acad Sci U S A*. 2010;107(1):216-221. doi:10.1073/pnas.0909541107
182. Sasai M, Linehan MM, Iwasaki A. Bifurcation of Toll-like receptor 9 signaling by adaptor protein 3. *Science.* 2010;329(5998):1530-1534. doi:10.1126/science.1187029
183. Kurotaki D, Uede T, Tamura T. Functions and development of red pulp macrophages. *Microbiol Immunol*. 2015;59(2):55-62. doi:10.1111/1348-0421.12228
184. Nguyen-Lefebvre AT, Horuzsko A. Kupffer Cell Metabolism and Function. *J Enzymol Metab.* 2015;1(1):101.
185. Ma Y, Yang M, He Z, Wei Q, Li J. The Biological Function of Kupffer Cells in Liver Disease. *Biol Myelomonocytic Cells*. 2017. doi:10.5772/67673
186. Doherty DG. Immunity, tolerance and autoimmunity in the liver: A comprehensive review. *J Autoimmun.* 2016;66:60-75. doi:10.1016/j.jaut.2015.08.020
187. You Q, Cheng L, Kedl RM, Ju C. Mechanism of T cell tolerance induction by murine hepatic Kupffer cells. *Hepatology*. 2008;48(3):978-990. doi:10.1002/hep.22395
188. Bilzer M, Roggel F, Gerbes AL. Role of Kupffer cells in host defense and liver disease. *Liver Int.* 2006;26(10):1175-1186. doi:10.1111/j.1478-3231.2006.01342.x
189. Crispe IN, Dao T, Klugewitz K, Mehal WZ, Metz DP. The liver as a site of T-cell apoptosis: graveyard, or killing field?. *Immunol Rev*. 2000;174:47-62. doi:10.1034/j.1600-0528.2002.017412.x
190. Louie DAP, Liao S. Lymph Node Subcapsular Sinus Macrophages as the Frontline of Lymphatic Immune Defense. *Front Immunol.* 2019;10:347. Published 2019 Feb 28. doi:10.3389/fimmu.2019.00347

191. Moran I, Grootveld AK, Nguyen A, Phan TG. Subcapsular Sinus Macrophages: The Seat of Innate and Adaptive Memory in Murine Lymph Nodes. *Trends Immunol*. 2019;40(1):35-48. doi:10.1016/j.it.2018.11.004
192. Gray EE, Cyster JG. Lymph node macrophages. *J Innate Immun*. 2012;4(5-6):424-436. doi:10.1159/000337007
193. Junt T, Moseman EA, Iannacone M, et al. Subcapsular sinus macrophages in lymph nodes clear lymph-borne viruses and present them to antiviral B cells. *Nature*. 2007;450(7166):110-114. doi:10.1038/nature06287
194. Sinder BP, Pettit AR, McCauley LK. Macrophages: Their Emerging Roles in Bone. *J Bone Miner Res*. 2015;30(12):2140-2149. doi:10.1002/jbmr.2735
195. Kaur S, Raggatt LJ, Batoon L, Hume DA, Levesque JP, Pettit AR. Role of bone marrow macrophages in controlling homeostasis and repair in bone and bone marrow niches. *Semin Cell Dev Biol*. 2017;61:12-21. doi:10.1016/j.semcdb.2016.08.009
196. Boyce B, Yao Z, Xing L. Osteoclasts have multiple roles in bone in addition to bone resorption. *Crit Rev Eukaryot Gene Expr*. 2009;19(3):171-180. doi:10.1615/CritRevEukarGeneExpr.v19.i3.10
197. Cho SW. Role of osteal macrophages in bone metabolism. *J Pathol Transl Med*. 2015;49(2):102-104. doi:10.4132/jptm.2015.02.02
198. Klei TR, Meinderts SM, van den Berg TK, van Bruggen R. From the Cradle to the Grave: The Role of Macrophages in Erythropoiesis and Erythrophagocytosis. *Front Immunol.* 2017;8:73. Published 2017 Feb 2. doi:10.3389/fimmu.2017.00073
199. Boulais PE, Frenette PS. Making sense of hematopoietic stem cell niches. *Blood*. 2015;125(17):2621-2629. doi:10.1182/blood-2014-09-570192
200. Janssens R, Struyf S, Proost P. The unique structural and functional features of CXCL12. *Cell Mol Immunol*. 2018;15(4):299-311. doi:10.1038/cmi.2017.107
201. Kopf M, Schneider C, Nobs SP. The development and function of lung-resident macrophages and dendritic cells. *Nat Immunol*. 2015;16(1):36-44. doi:10.1038/ni.3052
202. Lohmann-Matthes ML, Steinmüller C, Franke-Ullmann G. Pulmonary macrophages. *Eur Respir J*. 1994;7(9):1678-1689.
203. Schneberger D, Aharonson-Raz K, Singh B. Monocyte and macrophage heterogeneity and Toll-like receptors in the lung. *Cell Tissue Res*. 2011;343(1):97-106. doi:10.1007/s00441-010-1032-2
204. Hussell T, Bell TJ. Alveolar macrophages: Plasticity in a tissue-specific context. *Nat Rev Immunol*. 2014;14(2):81-93. doi:10.1038/nri3600

205. Maris NA, Dessing MC, de Vos AF, et al. Toll-like receptor mRNA levels in alveolar macrophages after inhalation of endotoxin. *Eur Respir J*. 2006;28(3):622-626. doi:10.1183/09031936.06.00010806
206. Allard B, Panariti A, Martin JG. Alveolar Macrophages in the Resolution of Inflammation, Tissue Repair, and Tolerance to Infection. *Front Immunol.* 2018;9:1777. Published 2018 Jul 31. doi:10.3389/fimmu.2018.01777
207. Soroosh P, Doherty TA, Duan W, et al. Lung-resident tissue macrophages generate Foxp3+ regulatory T cells and promote airway tolerance. *J Exp Med*. 2013;210(4):775-788. doi:10.1084/jem.20121849
208. Kawano H, Kayama H, Nakama T, Hashimoto T, Umemoto E, Takeda K. IL-10-producing lung interstitial macrophages prevent neutrophilic asthma. *Int Immunol*. 2016;28(10):489-501. doi:10.1093/intimm/dxw012
209. Schyns J, Bureau F, Marichal T. Lung Interstitial Macrophages: Past, Present, and Future. *J Immunol Res.* 2018;2018:5160794. Published 2018 Apr 30. doi:10.1155/2018/5160794
210. Atri C, Guerfali FZ, Laouini D. Role of Human Macrophage Polarization in Inflammation during Infectious Diseases. *Int J Mol Sci.* 2018;19(6):1801. Published 2018 Jun 19. doi:10.3390/ijms19061801
211. Berrington WR, Hawn TR. Mycobacterium tuberculosis, macrophages, and the innate immune response: does common variation matter?. *Immunol Rev.* 2007;219:167-186. doi:10.1111/j.1600-065X.2007.00545.x
212. Bhat KH, Yaseen I. Mycobacterium tuberculosis: Macrophage Takeover and Modulation of Innate Effector Responses. *Mycobacterium Res Dev*. 2018. doi:10.5772/intechopen.75003
213. Huang Z, Luo Q, Guo Y, et al. Mycobacterium tuberculosis-Induced Polarization of Human Macrophage Orchestrates the Formation and Development of Tuberculous Granulomas In Vitro. *PLoS One.* 2015;10(6):e0129744. Published 2015 Jun 19. doi:10.1371/journal.pone.0129744
214. Nikitina E, Larionova I, Choinzonov E, Kzhyshkowska J. Monocytes and Macrophages as Viral Targets and Reservoirs. *Int J Mol Sci.* 2018;19(9):2821. Published 2018 Sep 18. doi:10.3390/ijms19092821
215. Wong ME, Jaworowski A, Hearps AC. The HIV Reservoir in Monocytes and Macrophages [published correction appears in Front Immunol. 2019 Oct 22;10:2517]. *Front Immunol.* 2019;10:1435. Published 2019 Jun 26.

doi:10.3389/fimmu.2019.01435

216. Gordon S, Plüddemann A. Role of Macrophages in Autoimmunity. In: Rose NR, Mackay IR eds. *Autoimmune Diseases Fifth Ed*. Elsevier; 2014:161-174. doi:10.1016/B978-0-12-384929-8.00011-3
217. Tas SW, Quartier P, Botto M, Fossati-Jimack L. Macrophages from patients with SLE and rheumatoid arthritis have defective adhesion in vitro, while only SLE macrophages have impaired uptake of apoptotic cells. *Ann Rheum Dis*. 2006;65(2):216-221. doi:10.1136/ard.2005.037143
218. Herrada AA, Escobedo N, Iruretagoyena M, et al. Innate Immune Cells' Contribution to Systemic Lupus Erythematosus. *Front Immunol.* 2019;10:772. Published 2019 Apr 15. doi:10.3389/fimmu.2019.00772
219. Ma C, Xia Y, Yang Q, Zhao Y. The contribution of macrophages to systemic lupus erythematosus. *Clin Immunol.* 2019;207:1-9. doi:10.1016/j.clim.2019.06.009
220. Funes SC, Rios M, Escobar-Vera J, Kalergis AM. Implications of macrophage polarization in autoimmunity. *Immunology*. 2018;154(2):186-195. doi:10.1111/imm.12910
221. Siouti E, Andreakos E. The many facets of macrophages in rheumatoid arthritis. *Biochem Pharmacol.* 2019;165:152-169. doi:10.1016/j.bcp.2019.03.029
222. Kinne RW, Bräuer R, Stuhlmüller B, Palombo-Kinne E, Burmester GR. Macrophages in rheumatoid arthritis. *Arthritis Res*. 2000;2(3):189-202. doi:10.1186/ar86
223. Udalova IA, Mantovani A, Feldmann M. Macrophage heterogeneity in the context of rheumatoid arthritis. *Nat Rev Rheumatol*. 2016;12(8):472-485. doi:10.1038/nrrheum.2016.91
224. Chawla A, Nguyen KD, Goh YP. Macrophage-mediated inflammation in metabolic disease. *Nat Rev Immunol.* 2011;11(11):738-749. Published 2011 Oct 10. doi:10.1038/nri3071
225. De Lorenzo A, Gratteri S, Gualtieri P, Cammarano A, Bertucci P, Di Renzo L. Why primary obesity is a disease?. *J Transl Med.* 2019;17(1):169. Published 2019 May 22. doi:10.1186/s12967-019-1919-y
226. Castoldi A, Naffah de Souza C, Câmara NO, Moraes-Vieira PM. The Macrophage Switch in Obesity Development. *Front Immunol.* 2016;6:637. Published 2016 Jan 5. doi:10.3389/fimmu.2015.00637
227. Lauterbach MA, Wunderlich FT. Macrophage function in obesity-induced inflammation and insulin resistance. *Pflugers Arch.* 2017;469(3-4):385-396.

doi:10.1007/s00424-017-1955-5

228. Labani-Motlagh A, Ashja-Mahdavi M, Loskog A. The Tumor Microenvironment: A Milieu Hindering and Obstructing Antitumor Immune Responses. *Front Immunol.* 2020;11:940. Published 2020 May 15. doi:10.3389/fimmu.2020.00940
229. Jin MZ, Jin WL. The updated landscape of tumor microenvironment and drug repurposing. *Signal Transduct Target Ther.* 2020;5(1):166. Published 2020 Aug 25. doi:10.1038/s41392-020-00280-x
230. Son B, Lee S, Youn H, Kim E, Kim W, Youn B. The role of tumor microenvironment in therapeutic resistance. *Oncotarget*. 2017;8(3):3933-3945. doi:10.18632/oncotarget.13907
231. Audrito V, Managò A, Gaudino F, et al. NAD-Biosynthetic and Consuming Enzymes as Central Players of Metabolic Regulation of Innate and Adaptive Immune Responses in Cancer. *Front Immunol.* 2019;10:1720. Published 2019 Jul 25. doi:10.3389/fimmu.2019.01720
232. Lin JY, Li XY, Tadashi N, Dong P. Clinical significance of tumor-associated macrophage infiltration in supraglottic laryngeal carcinoma. *Chin J Cancer*. 2011;30(4):280-286. doi:10.5732/cjc.010.10336
233. Sica A, Straus L, Allavena P. Tumor-Associated Macrophages. In: Biswas SK, Mantovani A, eds. *Macrophages: Biology and Role in the Pathology of Diseases*. New York: Springer New York; 2014:425-443. doi:10.1007/978-1-4939-1311-4_20
234. Li J, Li L, Li Y, et al. Tumor-associated macrophage infiltration and prognosis in colorectal cancer: systematic review and meta-analysis. *Int J Colorectal Dis*. 2020;35(7):1203-1210. doi:10.1007/s00384-020-03593-z
235. Noy R, Pollard JW. Tumor-associated macrophages: from mechanisms to therapy [published correction appears in Immunity. 2014 Nov 20;41(5):866]. *Immunity.* 2014;41(1):49-61. doi:10.1016/j.immuni.2014.06.010
236. Nielsen SR, Schmid MC. Macrophages as Key Drivers of Cancer Progression and Metastasis. *Mediators Inflamm.* 2017;2017:9624760. doi:10.1155/2017/9624760
237. Ginhoux F, Jung S. Monocytes and macrophages: Developmental pathways and tissue homeostasis. *Nat Rev Immunol*. 2014;14(6):392-404. doi:10.1038/nri3671
238. Gschwandtner M, Derler R, Midwood KS. More Than Just Attractive: How CCL2 Influences Myeloid Cell Behavior Beyond Chemotaxis. *Front Immunol.* 2019;10:2759. Published 2019 Dec 13. doi:10.3389/fimmu.2019.02759
239. Liu Y, Cao X. The origin and function of tumor-associated macrophages. *Cell Mol*

Immunol. 2015;12(1):1-4. doi:10.1038/cmi.2014.83

240. Zhu Y, Herndon JM, Sojka DK, et al. Tissue-Resident Macrophages in Pancreatic Ductal Adenocarcinoma Originate from Embryonic Hematopoiesis and Promote Tumor Progression. *Immunity.* 2017;47(3):597. doi:10.1016/j.immuni.2017.08.018
241. Loyher PL, Hamon P, Laviron M, et al. Macrophages of distinct origins contribute to tumor development in the lung. *J Exp Med.* 2018;215(10):2536-2553. doi:10.1084/jem.20180534
242. Subimerb C, Pinlaor S, Lulitanond V, et al. Circulating CD14(+) CD16(+) monocyte levels predict tissue invasive character of cholangiocarcinoma. *Clin Exp Immunol.* 2010;161(3):471-479. doi:10.1111/j.1365-2249.2010.04200.x
243. Feng AL, Zhu JK, Sun JT, et al. CD16+ monocytes in breast cancer patients: Expanded by monocyte chemoattractant protein-1 and may be useful for early diagnosis. *Clin Exp Immunol*. 2011;164(1):57-65. doi:10.1111/j.1365-2249.2011.04321.x
244. Murdoch C, Giannoudis A, Lewis CE. Mechanisms regulating the recruitment of macrophages into hypoxic areas of tumors and other ischemic tissues. *Blood*. 2004;104(8):2224-2234. doi:10.1182/blood-2004-03-1109
245. Xu R, Li Y, Yan H, et al. CCL2 promotes macrophages-associated chemoresistance via MCPIP1 dual catalytic activities in multiple myeloma. *Cell Death Dis.* 2019;10(10):781. Published 2019 Oct 14. doi:10.1038/s41419-019-2012-4
246. An G, Wu F, Huang S, et al. Effects of CCL5 on the biological behavior of breast cancer and the mechanisms of its interaction with tumor-associated macrophages. *Oncol Rep*. 2019;42(6):2499-2511. doi:10.3892/or.2019.7344
247. Kranjc MK, Novak M, Pestell RG, Lah TT. Cytokine CCL5 and receptor CCR5 axis in glioblastoma multiforme. *Radiol Oncol.* 2019;53(4):397-406. Published 2019 Nov 20. doi:10.2478/raon-2019-0057
248. Ding H, Zhao L, Dai S, Li L, Wang F, Shan B. CCL5 secreted by tumor associated macrophages may be a new target in treatment of gastric cancer. *Biomed Pharmacother*. 2016;77:142-149. doi:10.1016/j.biopha.2015.12.004
249. Aldinucci D, Borghese C, Casagrande N. Formation of the Immunosuppressive Microenvironment of Classic Hodgkin Lymphoma and Therapeutic Approaches to Counter It. *Int J Mol Sci.* 2019;20(10):2416. Published 2019 May 15. doi:10.3390/ijms20102416
250. Casagrande N, Borghese C, Visser L, Mongiat M, Colombatti A, Aldinucci D. CCR5

antagonism by maraviroc inhibits Hodgkin lymphoma microenvironment interactions and xenograft growth. *Haematologica.* 2019;104(3):564-575. doi:10.3324/haematol.2018.196725

251. Hume DA, MacDonald KPA. Therapeutic applications of macrophage colony-stimulating factor-1 (CSF-1) and antagonists of CSF-1 receptor (CSF-1R) signaling. *Blood*. 2012;119(8):1810-1820. doi:10.1182/blood-2011-09-379214
252. Barbera-Guillem E, Nyhus JK, Wolford CC, Friece CR, Sampsel JW. Vascular endothelial growth factor secretion by tumor-infiltrating macrophages essentially supports tumor angiogenesis, and IgG immune complexes potentiate the process. *Cancer Res*. 2002;62(23):7042-7049.
253. Wheeler KC, Jena MK, Pradhan BS, et al. VEGF may contribute to macrophage recruitment and M2 polarization in the decidua. *PLoS One.* 2018;13(1):e0191040. Published 2018 Jan 11. doi:10.1371/journal.pone.0191040
254. Sekiguchi K, Ito Y, Hattori K, et al. VEGF Receptor 1-Expressing Macrophages Recruited from Bone Marrow Enhances Angiogenesis in Endometrial Tissues. *Sci Rep.* 2019;9(1):7037. Published 2019 May 7. doi:10.1038/s41598-019-43185-8
255. Weddell JC, Chen S, Imoukhuede PI. VEGFR1 promotes cell migration and proliferation through PLCγ and PI3K pathways. *NPJ Syst Biol Appl.* 2017;4:1. Published 2017 Dec 19. doi:10.1038/s41540-017-0037-9
256. Yasuda S, Sho M, Yamato I, et al. Simultaneous blockade of programmed death 1 and vascular endothelial growth factor receptor 2 (VEGFR2) induces synergistic anti-tumour effect in vivo. *Clin Exp Immunol*. 2013;172(3):500-506. doi:10.1111/cei.12069
257. Lai YS, Wahyuningtyas R, Aui SP, Chang KT. Autocrine VEGF signalling on M2 macrophages regulates PD-L1 expression for immunomodulation of T cells. *J Cell Mol Med*. 2019;23(2):1257-1267. doi:10.1111/jcmm.14027
258. Bagnato A, Spinella F, Rosanò L. The endothelin axis in cancer: the promise and the challenges of molecularly targeted therapy. *Can J Physiol Pharmacol.* 2008;86(8):473-484. doi:10.1139/Y08-058
259. Grimshaw MJ, Wilson JL, Balkwill FR. Endothelin-2 is a macrophage chemoattractant: implications for macrophage distribution in tumors. *Eur J Immunol.* 2002;32(9):2393-2400. doi:10.1002/1521-4141(200209)32:9<2393::AID-IMMU2393>3.0.CO;2-4
260. Chen CC, Chen LL, Hsu YT, Liu KJ, Fan CS, Huang TS. The endothelin-integrin axis is involved in macrophage-induced breast cancer cell chemotactic interactions with

endothelial cells. *J Biol Chem*. 2014;289(14):10029-10044. doi:10.1074/jbc.M113.528406

261. Puthenveetil A, Dubey S. Metabolic reprograming of tumor-associated macrophages. *Ann Transl Med.* 2020;8(16):1030. doi:10.21037/atm-20-2037
262. Ivashkiv LB. The hypoxia–lactate axis tempers inflammation. *Nat Rev Immunol*. 2020;20(2):85-86. doi:10.1038/s41577-019-0259-8
263. Zheng X, Mansouri S, Krager A, et al. Metabolism in tumour-associated macrophages: a quid pro quo with the tumour microenvironment. *Eur Respir Rev.* 2020;29(157):200134. Published 2020 Oct 1. doi:10.1183/16000617.0134-2020
264. Colegio OR, Chu NQ, Szabo AL, et al. Functional polarization of tumour-associated macrophages by tumour-derived lactic acid. *Nature*. 2014;513(7519):559-563. doi:10.1038/nature13490
265. Pokrývková B, Šmahelová J, Dalewská N, et al. ARG1 mRNA Level Is a Promising Prognostic Marker in Head and Neck Squamous Cell Carcinomas. *Diagnostics (Basel)*. 2021;11(4):628. Published 2021 Mar 31. doi:10.3390/diagnostics11040628
266. Rabold K, Netea MG, Adema GJ, Netea-Maier RT. Cellular metabolism of tumor-associated macrophages – functional impact and consequences. *FEBS Lett*. 2017;591(19):3022-3041. doi:10.1002/1873-3468.12771
267. Kusmartsev S. Enhanced 15-lipoxygenase activity and elevated eicosanoid production in kidney tumor microenvironment contribute to the inflammation and immune suppression. *Oncoimmunology*. 2012;1(2):249-251. doi:10.4161/onci.1.2.18502
268. Li H, Yang B, Huang J, et al. Cyclooxygenase-2 in tumor-associated macrophages promotes breast cancer cell survival by triggering a positive-feedback loop between macrophages and cancer cells. *Oncotarget*. 2015;6(30):29637-29650. doi:10.18632/oncotarget.4936
269. Mizuno R, Kawada K, Sakai Y. Prostaglandin E2/EP Signaling in the Tumor Microenvironment of Colorectal Cancer. *Int J Mol Sci.* 2019;20(24):6254. Published 2019 Dec 11. doi:10.3390/ijms20246254
270. Prima V, Kaliberova LN, Kaliberov S, Curiel DT, Kusmartsev S. COX2/mPGES1/PGE2 pathway regulates PD-L1 expression in tumor-associated macrophages and myeloid-derived suppressor cells. *Proc Natl Acad Sci U S A*. 2017;114(5):1117-1122. doi:10.1073/pnas.1612920114
271. Wei Z, Liu X, Cheng C, Yu W, Yi P. Metabolism of Amino Acids in Cancer. *Front Cell Dev Biol.* 2021;8:603837. Published 2021 Jan 12. doi:10.3389/fcell.2020.603837

272. Ren W, Xia Y, Chen S, et al. Glutamine Metabolism in Macrophages: A Novel Target for Obesity/Type 2 Diabetes. *Adv Nutr*. 2019;10(2):221-230. doi:10.1093/advances/nmy084
273. Oh MH, Sun IH, Zhao L, et al. Targeting glutamine metabolism enhances tumor-specific immunity by modulating suppressive myeloid cells. *J Clin Invest*. 2020;130(7):3865-3884. doi:10.1172/JCI131859
274. Chen Y, Song Y, Du W, Gong L, Chang H, Zou Z. Tumor-associated macrophages: an accomplice in solid tumor progression. *J Biomed Sci.* 2019;26(1):78. Published 2019 Oct 20. doi:10.1186/s12929-019-0568-z
275. Zeng XY, Xie H, Yuan J, et al. M2-like tumor-associated macrophages-secreted EGF promotes epithelial ovarian cancer metastasis via activating EGFR-ERK signaling and suppressing lncRNA LIMT expression. *Cancer Biol Ther*. 2019;20(7):956-966. doi:10.1080/15384047.2018.1564567
276. Hosono M, Koma YI, Takase N, et al. CXCL8 derived from tumor-associated macrophages and esophageal squamous cell carcinomas contributes to tumor progression by promoting migration and invasion of cancer cells. *Oncotarget.* 2017;8(62):106071-106088. Published 2017 Nov 20. doi:10.18632/oncotarget.22526
277. Tong H, Ke JQ, Jiang FZ, et al. Tumor-associated macrophage-derived CXCL8 could induce ERα suppression via HOXB13 in endometrial cancer. *Cancer Lett*. 2016;376(1):127-136. doi:10.1016/j.canlet.2016.03.036
278. Zhou J, Tang Z, Gao S, Li C, Feng Y, Zhou X. Tumor-Associated Macrophages: Recent Insights and Therapies. *Front Oncol.* 2020;10:188. Published 2020 Feb 25. doi:10.3389/fonc.2020.00188
279. Lin Y, Xu J, Lan H. Tumor-associated macrophages in tumor metastasis: biological roles and clinical therapeutic applications. *J Hematol Oncol.* 2019;12(1):76. Published 2019 Jul 12. doi:10.1186/s13045-019-0760-3
280. Chanmee T, Ontong P, Konno K, Itano N. Tumor-associated macrophages as major players in the tumor microenvironment. *Cancers (Basel).* 2014;6(3):1670-1690. Published 2014 Aug 13. doi:10.3390/cancers6031670
281. Chen Q, Zhang XH, Massagué J. Macrophage binding to receptor VCAM-1 transmits survival signals in breast cancer cells that invade the lungs. *Cancer Cell.* 2011;20(4):538-549. doi:10.1016/j.ccr.2011.08.025
282. Doak GR, Schwertfeger KL, Wood DK. Distant Relations: Macrophage Functions in the Metastatic Niche. *Trends in Cancer*. 2018;4(6):445-459.

doi:10.1016/j.trecan.2018.03.011

283. Maimela NR, Liu S, Zhang Y. Fates of CD8+ T cells in Tumor Microenvironment. *Comput Struct Biotechnol J.* 2018;17:1-13. Published 2018 Nov 22. doi:10.1016/j.csbj.2018.11.004

284. Fridlender ZG, Buchlis G, Kapoor V, et al. CCL2 blockade augments cancer immunotherapy [published correction appears in Cancer Res. 2010 Mar 15;70(6):2569. Crisanti, Cecilia [corrected to Crisanti, M Cecilia]]. *Cancer Res.* 2010;70(1):109-118. doi:10.1158/0008-5472.CAN-09-2326

285. Quaranta V, Schmid MC. Macrophage-Mediated Subversion of Anti-Tumour Immunity. *Cells.* 2019;8(7):747. Published 2019 Jul 19. doi:10.3390/cells8070747

286. Seidel JA, Otsuka A, Kabashima K. Anti-PD-1 and Anti-CTLA-4 Therapies in Cancer: Mechanisms of Action, Efficacy, and Limitations. *Front Oncol.* 2018;8:86. Published 2018 Mar 28. doi:10.3389/fonc.2018.00086

287. Tay RE, Richardson EK, Toh HC. Revisiting the role of CD4+ T cells in cancer immunotherapy-new insights into old paradigms. *Cancer Gene Ther.* 2021;28(1-2):5-17. doi:10.1038/s41417-020-0183-x

288. Henry CJ, Ornelles DA, Mitchell LM, Brzoza-Lewis KL, Hiltbold EM. IL-12 produced by dendritic cells augments CD8+ T cell activation through the production of the chemokines CCL1 and CCL17. *J Immunol.* 2008;181(12):8576-8584. doi:10.4049/jimmunol.181.12.8576

289. Ruffell B, Chang-Strachan D, Chan V, et al. Macrophage IL-10 blocks CD8+ T cell-dependent responses to chemotherapy by suppressing IL-12 expression in intratumoral dendritic cells. *Cancer Cell.* 2014;26(5):623-637. doi:10.1016/j.ccell.2014.09.006

290. Marchesi M, Andersson E, Villabona L, et al. HLA-dependent tumour development: a role for tumour associate macrophages?. *J Transl Med.* 2013;11:247. Published 2013 Oct 6. doi:10.1186/1479-5876-11-247

291. Contini P, Ghio M, Poggi A, et al. Soluble HLA-A,-B,-C and -G molecules induce apoptosis in T and NK CD8+ cells and inhibit cytotoxic T cell activity through CD8 ligation. *Eur J Immunol*. 2003;33(1):125-134. doi:10.1002/immu.200390015

292. Halenius A, Gerke C, Hengel H. Classical and non-classical MHC I molecule manipulation by human cytomegalovirus: so many targets—but how many arrows in the quiver?. *Cell Mol Immunol.* 2015;12(2):139-153. doi:10.1038/cmi.2014.105

293. Kochan G, Escors D, Breckpot K, Guerrero-Setas D. Role of non-classical MHC class I molecules in cancer immunosuppression. *Oncoimmunology*. 2013;2(11):e26491.

doi:10.4161/onci.26491

294. Abd Hamid M, Wang RZ, Yao X, et al. Enriched HLA-E and CD94/NKG2A Interaction Limits Antitumor CD8+ Tumor-Infiltrating T Lymphocyte Responses. *Cancer Immunol Res.* 2019;7(8):1293-1306. doi:10.1158/2326-6066.CIR-18-0885
295. Harada A, Ishigami S, Kijima Y, et al. Clinical implication of human leukocyte antigen (HLA)-F expression in breast cancer. *Pathol Int*. 2015;65(11):569-574. doi:10.1111/pin.12343
296. Ribatti D, Nico B, Crivellato E, Roccaro AM, Vacca A. The history of the angiogenic switch concept. *Leukemia*. 2007;21(1):44-52. doi:10.1038/sj.leu.2404402
297. Riabov V, Gudima A, Wang N, Mickley A, Orekhov A, Kzhyshkowska J. Role of tumor associated macrophages in tumor angiogenesis and lymphangiogenesis. *Front Physiol.* 2014;5:75. Published 2014 Mar 5. doi:10.3389/fphys.2014.00075
298. Kerjaschki D. The crucial role of macrophages in lymphangiogenesis. *J Clin Invest*. 2005;115(9):2316-2319. doi:10.1172/JCI26354
299. He Y, Rajantie I, Ilmonen M, et al. Preexisting lymphatic endothelium but not endothelial progenitor cells are essential for tumor lymphangiogenesis and lymphatic metastasis. *Cancer Res*. 2004;64(11):3737-3740. doi:10.1158/0008-5472.CAN-04-0088
300. Hsu MC, Pan MR, Hung WC. Two Birds, One Stone: Double Hits on Tumor Growth and Lymphangiogenesis by Targeting Vascular Endothelial Growth Factor Receptor 3. *Cells.* 2019;8(3):270. Published 2019 Mar 21. doi:10.3390/cells8030270
301. Ran S, Montgomery KE. Macrophage-mediated lymphangiogenesis: the emerging role of macrophages as lymphatic endothelial progenitors. *Cancers (Basel).* 2012;4(3):618-657. doi:10.3390/cancers4030618
302. Mantovani A, Marchesi F, Malesci A, Laghi L, Allavena P. Tumour-associated macrophages as treatment targets in oncology. *Nat Rev Clin Oncol*. 2017;14(7):399-416. doi:10.1038/nrclinonc.2016.217
303. Dijkgraaf EM, Heusinkveld M, Tummers B, et al. Chemotherapy alters monocyte differentiation to favor generation of cancer-supporting M2 macrophages in the tumor microenvironment. *Cancer Res*. 2013;73(8):2480-2492. doi:10.1158/0008-5472.CAN-12-3542
304. Shree T, Olson OC, Elie BT, et al. Macrophages and cathepsin proteases blunt chemotherapeutic response in breast cancer. *Genes Dev*. 2011;25(23):2465-2479. doi:10.1101/gad.180331.111

305. Jones KI, Tiersma J, Yuzhalin AE, et al. Radiation combined with macrophage depletion promotes adaptive immunity and potentiates checkpoint blockade. *EMBO Mol Med.* 2018;10(12):e9342. doi:10.15252/emmm.201809342
306. Grégoire H, Roncali L, Rousseau A, et al. Targeting Tumor Associated Macrophages to Overcome Conventional Treatment Resistance in Glioblastoma. *Front Pharmacol.* 2020;11:368. Published 2020 Apr 8. doi:10.3389/fphar.2020.00368
307. Leblond MM, Pérès EA, Helaine C, et al. M2 macrophages are more resistant than M1 macrophages following radiation therapy in the context of glioblastoma. *Oncotarget.* 2017;8(42):72597-72612. Published 2017 Aug 7. doi:10.18632/oncotarget.19994
308. Tabatabaei P, Visse E, Bergström P, Brännström T, Siesjö P, Bergenheim AT. Radiotherapy induces an immediate inflammatory reaction in malignant glioma: a clinical microdialysis study. *J Neurooncol*. 2017;131(1):83-92. doi:10.1007/s11060-016-2271-1
309. Bian Z, Shi L, Kidder K, Zen K, Garnett-Benson C, Liu Y. Intratumoral SIRPα-deficient macrophages activate tumor antigen-specific cytotoxic T cells under radiotherapy. *Nat Commun.* 2021;12(1):3229. Published 2021 May 28. doi:10.1038/s41467-021-23442-z
310. Xiang X, Wang J, Lu D, Xu X. Targeting tumor-associated macrophages to synergize tumor immunotherapy. *Signal Transduct Target Ther.* 2021;6(1):75. Published 2021 Feb 23. doi:10.1038/s41392-021-00484-9
311. Pathria P, Louis TL, Varner JA. Targeting Tumor-Associated Macrophages in Cancer. *Trends Immunol*. 2019;40(4):310-327. doi:10.1016/j.it.2019.02.003
312. Laplagne C, Domagala M, Le Naour A, et al. Latest Advances in Targeting the Tumor Microenvironment for Tumor Suppression. *Int J Mol Sci.* 2019;20(19):4719. Published 2019 Sep 23. doi:10.3390/ijms20194719
313. Anfray C, Ummarino A, Andón FT, Allavena P. Current Strategies to Target Tumor-Associated-Macrophages to Improve Anti-Tumor Immune Responses. *Cells.* 2019;9(1):46. Published 2019 Dec 23. doi:10.3390/cells9010046
314. Karapetyan L, Luke JJ, Davar D. Toll-Like Receptor 9 Agonists in Cancer. *Onco Targets Ther.* 2020;13:10039-10060. Published 2020 Oct 9. doi:10.2147/OTT.S247050
315. Lee BL, Barton GM. Trafficking of endosomal Toll-like receptors. *Trends Cell Biol.* 2014;24(6):360-369. doi:10.1016/j.tcb.2013.12.002
316. Le Naour J, Galluzzi L, Zitvogel L, Kroemer G, Vacchelli E. Trial watch: TLR3

agonists in cancer therapy. *Oncoimmunology.* 2020;9(1):1771143. Published 2020 Jun 2. doi:10.1080/2162402X.2020.1771143

317. Frega G, Wu Q, Le Naour J, et al. Trial Watch: experimental TLR7/TLR8 agonists for oncological indications. *Oncoimmunology.* 2020;9(1):1796002. Published 2020 Jul 21. doi:10.1080/2162402X.2020.1796002
318. Chi H, Li C, Zhao FS, et al. Anti-tumor Activity of Toll-Like Receptor 7 Agonists. *Front Pharmacol.* 2017;8:304. Published 2017 May 31. doi:10.3389/fphar.2017.00304
319. Ernst O, Failayev H, Athamna M, He H, Tsfadia Y, Zor T. A dual and conflicting role for imiquimod in inflammation: A TLR7 agonist and a cAMP phosphodiesterase inhibitor. *Biochem Pharmacol*. 2020;182:114206. doi:https://doi.org/10.1016/j.bcp.2020.114206
320. Chen Y, Jin H, Song Y, et al. Targeting tumor-associated macrophages: A potential treatment for solid tumors. *J Cell Physiol*. 2021;236(5):3445-3465. doi:10.1002/jcp.30139
321. Ngambenjawong C, Gustafson HH, Pun SH. Progress in tumor-associated macrophage (TAM)-targeted therapeutics. *Adv Drug Deliv Rev*. 2017;114:206-221. doi:10.1016/j.addr.2017.04.010
322. Benner B, Good L, Quiroga D, et al. Pexidartinib, a Novel Small Molecule CSF-1R Inhibitor in Use for Tenosynovial Giant Cell Tumor: A Systematic Review of Pre-Clinical and Clinical Development. *Drug Des Devel Ther.* 2020;14:1693-1704. Published 2020 May 4. doi:10.2147/DDDT.S253232
323. Opperman KS, Vandyke K, Clark KC, et al. Clodronate-Liposome Mediated Macrophage Depletion Abrogates Multiple Myeloma Tumor Establishment In Vivo. *Neoplasia (United States)*. 2019;21(8):777-787. doi:10.1016/j.neo.2019.05.006
324. Rogers TL, Holen I. Tumour macrophages as potential targets of bisphosphonates. *J Transl Med.* 2011;9:177. Published 2011 Oct 17. doi:10.1186/1479-5876-9-177
325. Comito G, Segura CP, Taddei ML, et al. Zoledronic acid impairs stromal reactivity by inhibiting M2-macrophages polarization and prostate cancer-associated fibroblasts. *Oncotarget*. 2017;8(1):118-132. doi:10.18632/oncotarget.9497
326. Cassier PA, Italiano A, Gomez-Roca CA, et al. CSF1R inhibition with emactuzumab in locally advanced diffuse-type tenosynovial giant cell tumours of the soft tissue: a dose-escalation and dose-expansion phase 1 study. *Lancet Oncol*. 2015;16(8):949-956. doi:10.1016/S1470-2045(15)00132-1
327. Bendell JC, Tolcher AW, Jones SF, et al. Abstract A252: A phase 1 study of ARRY-

382, an oral inhibitor of colony-stimulating factor-1 receptor (CSF1R), in patients with advanced or metastatic cancers. *Mol Cancer Ther*. 2013;12(11 Supplement):A252. doi:10.1158/1535-7163.TARG-13-A252

328. Cannarile MA, Weisser M, Jacob W, Jegg AM, Ries CH, Rüttinger D. Colony-stimulating factor 1 receptor (CSF1R) inhibitors in cancer therapy. *J Immunother Cancer*. 2017;5(1):53. Published 2017 Jul 18. doi:10.1186/s40425-017-0257-y
329. Quail DF, Bowman RL, Akkari L, et al. The tumor microenvironment underlies acquired resistance to CSF-1R inhibition in gliomas. *Science*. 2016;352(6288):aad3018. doi:10.1126/science.aad3018
330. Kumar V, Donthireddy L, Marvel D, et al. Cancer-Associated Fibroblasts Neutralize the Anti-tumor Effect of CSF1 Receptor Blockade by Inducing PMN-MDSC Infiltration of Tumors. *Cancer Cell*. 2017;32(5):654-668.e5. doi:10.1016/j.ccell.2017.10.005
331. Brana I, Calles A, LoRusso PM, et al. Carlumab, an anti-C-C chemokine ligand 2 monoclonal antibody, in combination with four chemotherapy regimens for the treatment of patients with solid tumors: an open-label, multicenter phase 1b study. *Target Oncol*. 2015;10(1):111-123. doi:10.1007/s11523-014-0320-2
332. Noel M, O'Reilly EM, Wolpin BM, et al. Phase 1b study of a small molecule antagonist of human chemokine (C-C motif) receptor 2 (PF-04136309) in combination with nab-paclitaxel/gemcitabine in first-line treatment of metastatic pancreatic ductal adenocarcinoma. *Invest New Drugs*. 2020;38(3):800-811. doi:10.1007/s10637-019-00830-3
333. Jalil AAR, Andrechak JC, Discher DE. Macrophage checkpoint blockade: Results from initial clinical trials, binding analyses, and CD47-SIRPα structure-function. *Antib Ther*. 2021;3(2):80-94. doi:10.1093/ABT/TBAA006
334. Advani R, Flinn I, Popplewell L, et al. CD47 Blockade by Hu5F9-G4 and Rituximab in Non-Hodgkin's Lymphoma. *N Engl J Med*. 2018;379(18):1711-1721. doi:10.1056/NEJMoa1807315
335. Kargozar S, Mozafari M. Nanotechnology and Nanomedicine: Start small, think big. *Mater Today Proc*. 2018;5(7):15492-15500. doi:10.1016/j.matpr.2018.04.155
336. Chen G, Roy I, Yang C, Prasad PN. Nanochemistry and Nanomedicine for Nanoparticle-based Diagnostics and Therapy. *Chem Rev*. 2016;116(5):2826-2885. doi:10.1021/acs.chemrev.5b00148
337. Kinnear C, Moore TL, Rodriguez-Lorenzo L, Rothen-Rutishauser B, Petri-Fink A.

Form Follows Function: Nanoparticle Shape and Its Implications for Nanomedicine. *Chem Rev*. 2017;117(17):11476-11521. doi:10.1021/acs.chemrev.7b00194

338. Astruc D. Introduction to nanomedicine. *Molecules*. 2016;21(1). doi:10.3390/molecules21010004
339. Khan I, Saeed K, Khan I. Nanoparticles: Properties, applications and toxicities. *Arab J Chem*. 2019;12(7):908-931. doi:10.1016/j.arabjc.2017.05.011
340. Christian P, Von Der Kammer F, Baalousha M, Hofmann T. Nanoparticles: Structure, properties, preparation and behaviour in environmental media. *Ecotoxicology*. 2008;17(5):326-343. doi:10.1007/s10646-008-0213-1
341. Wang EC, Wang AZ. Nanoparticles and their applications in cell and molecular biology. *Integr Biol (Camb)*. 2014;6(1):9-26. doi:10.1039/c3ib40165k
342. Jiang F, Fu Y, Zhu Y, Tang Z, Sheng P. Fabrication of iron oxide/silica core-shell nanoparticles and their magnetic characteristics. *J Alloys Compd*. 2012;543:43-48. doi:10.1016/j.jallcom.2012.07.079
343. Zielińska A, Carreiró F, Oliveira AM, et al. Polymeric Nanoparticles: Production, Characterization, Toxicology and Ecotoxicology. *Molecules.* 2020;25(16):3731. Published 2020 Aug 15. doi:10.3390/molecules25163731
344. Begines B, Ortiz T, Pérez-Aranda M, et al. Polymeric Nanoparticles for Drug Delivery: Recent Developments and Future Prospects. *Nanomaterials (Basel).* 2020;10(7):1403. Published 2020 Jul 19. doi:10.3390/nano10071403
345. Avramović N, Mandić B, Savić-Radojević A, Simić T. Polymeric Nanocarriers of Drug Delivery Systems in Cancer Therapy. *Pharmaceutics.* 2020;12(4):298. Published 2020 Mar 25. doi:10.3390/pharmaceutics12040298
346. Chaplot SP, Rupenthal ID. Dendrimers for gene delivery--a potential approach for ocular therapy?. *J Pharm Pharmacol.* 2014;66(4):542-556. doi:10.1111/jphp.12104
347. Dias AP, da Silva Santos S, da Silva JV, et al. Dendrimers in the context of nanomedicine. *Int J Pharm*. 2020;573:118814. doi:10.1016/j.ijpharm.2019.118814
348. Tarach P, Janaszewska A. Recent Advances in Preclinical Research Using PAMAM Dendrimers for Cancer Gene Therapy. *Int J Mol Sci.* 2021;22(6):2912. Published 2021 Mar 13. doi:10.3390/ijms22062912
349. Duan Y, Dhar A, Patel C, et al. A brief review on solid lipid nanoparticles: Part and parcel of contemporary drug delivery systems. *RSC Adv*. 2020;10(45):26777-26791. doi:10.1039/d0ra03491f
350. Mirahadi M, Ghanbarzadeh S, Ghorbani M, Gholizadeh A, Hamishehkar H. A review

on the role of lipid-based nanoparticles in medical diagnosis and imaging. *Ther Deliv*. 2018;9(8):557-569. doi:10.4155/tde-2018-0020

351. García-Pinel B, Porras-Alcalá C, Ortega-Rodríguez A, et al. Lipid-Based Nanoparticles: Application and Recent Advances in Cancer Treatment. *Nanomaterials (Basel)*. 2019;9(4):638. Published 2019 Apr 19. doi:10.3390/nano9040638
352. Puri A, Loomis K, Smith B, et al. Lipid-based nanoparticles as pharmaceutical drug carriers: From concepts to clinic. *Crit Rev Ther Drug Carrier Syst*. 2009;26(6):523-580. doi:10.1615/CritRevTherDrugCarrierSyst.v26.i6.10
353. Bulbake U, Doppalapudi S, Kommineni N, Khan W. Liposomal Formulations in Clinical Use: An Updated Review. *Pharmaceutics.* 2017;9(2):12. Published 2017 Mar 27. doi:10.3390/pharmaceutics9020012
354. Núñez C, Estévez SV, del Pilar Chantada M. Inorganic nanoparticles in diagnosis and treatment of breast cancer. *J Biol Inorg Chem*. 2018;23(3):331-345. doi:10.1007/s00775-018-1542-z
355. Matea CT, Mocan T, Tabaran F, et al. Quantum dots in imaging, drug delivery and sensor applications. *Int J Nanomedicine.* 2017;12:5421-5431. Published 2017 Jul 28. doi:10.2147/IJN.S138624
356. Barroso MM. Quantum dots in cell biology. *J Histochem Cytochem*. 2011;59(3):237-251. doi:10.1369/0022155411398487
357. Kim M, Lee JH, Nam JM. Plasmonic Photothermal Nanoparticles for Biomedical Applications. *Adv Sci (Weinh).* 2019;6(17):1900471. Published 2019 Jul 22. doi:10.1002/advs.201900471
358. Sui M, Kunwar S, Pandey P, Lee J. Strongly confined localized surface plasmon resonance (LSPR) bands of Pt, AgPt, AgAuPt nanoparticles. *Sci Rep*. 2019;9(1):1-14. Published 2021 May 10. doi:10.1038/s41598-019-53292-1
359. Petryayeva E, Krull UJ. Localized surface plasmon resonance: nanostructures, bioassays and biosensing--a review. *Anal Chim Acta.* 2011;706(1):8-24. doi:10.1016/j.aca.2011.08.020
360. Wu K, Su D, Liu J, Saha R, Wang JP. Magnetic nanoparticles in nanomedicine: a review of recent advances. *Nanotechnology.* 2019;30(50):502003. doi:10.1088/1361-6528/ab4241
361. Wang F, Banerjee D, Liu Y, Chen X, Liu X. Upconversion nanoparticles in biological labeling, imaging, and therapy. *Analyst*. 2010;135(8):1839-1854. doi:10.1039/c0an00144a

362. Stevanović M, Lukić MJ, Stanković A, Filipović N, Kuzmanović M, Janićijević Ž. Chapter 1 - Biomedical inorganic nanoparticles: preparation, properties, and perspectives. In: Grumezescu V, Grumezescu AM, eds. *Materials for Biomedical Engineering: Inorganic Micro- and Nanostructures*. Elsevier; 2019:1-46. doi:10.1016/B978-0-08-102814-8.00001-9
363. Bayda S, Hadla M, Palazzolo S, et al. Inorganic Nanoparticles for Cancer Therapy: A Transition from Lab to Clinic. *Curr Med Chem*. 2017;25(34):4269-4303. doi:10.2174/0929867325666171229141156
364. Huang H, Feng W, Chen Y, Shi J. Inorganic nanoparticles in clinical trials and translations. *Nano Today*. 2020;35:100972. doi:10.1016/j.nantod.2020.100972
365. Verma J, Lal S, Van Noorden CJF. Inorganic nanoparticles for the theranostics of cancer. *Eur J Nanomedicine*. 2015;7(4):271-287. doi:10.1515/ejnm-2015-0024
366. Gobbo OL, Sjaastad K, Radomski MW, Volkov Y, Prina-Mello A. Magnetic nanoparticles in cancer theranostics. *Theranostics*. 2015;5(11):1249-1263. doi:10.7150/thno.11544
367. Evans ER, Bugga P, Asthana V, Drezek R. Metallic Nanoparticles for Cancer Immunotherapy. *Mater Today (Kidlington)*. 2018;21(6):673-685. doi:10.1016/j.mattod.2017.11.022
368. Weissig V, Guzman-Villanueva D. Nanopharmaceuticals (part 2): products in the pipeline. *Int J Nanomedicine.* 2015;10:1245-1257. Published 2015 Feb 11. doi:10.2147/IJN.S65526
369. Kim D, Kim J, Park Y Il, Lee N, Hyeon T. Recent Development of Inorganic Nanoparticles for Biomedical Imaging. *ACS Cent Sci*. 2018;4(3):324-336. doi:10.1021/acscentsci.7b00574
370. Lee SH, Kim BH, Na H Bin, Hyeon T. Paramagnetic inorganic nanoparticles as T1 MRI contrast agents. *Wiley Interdiscip Rev Nanomedicine Nanobiotechnology*. 2014;6(2):196-209. doi:10.1002/wnan.1243
371. Estelrich J, Sánchez-Martín MJ, Busquets MA. Nanoparticles in magnetic resonance imaging: from simple to dual contrast agents. *Int J Nanomedicine.* 2015;10:1727-1741. Published 2015 Mar 6. doi:10.2147/IJN.S76501
372. Xiao YD, Paudel R, Liu J, Ma C, Zhang ZS, Zhou SK. MRI contrast agents: Classification and application (Review). *Int J Mol Med*. 2016;38(5):1319-1326. doi:10.3892/ijmm.2016.2744
373. Kim HK, Lee GH, Chang Y. Gadolinium as an MRI contrast agent. *Future Med Chem*.

2018;10(6):639-661. doi:10.4155/fmc-2017-0215

374. Alphandéry E. Iron oxide nanoparticles as multimodal imaging tools. *RSC Adv*. 2019;9(69):40577-40587. doi:10.1039/c9ra08612a

375. Du J, Zhang Y, Ming J, et al. Evaluation of the tracing effect of carbon nanoparticle and carbon nanoparticleepirubicin suspension in axillary lymph node dissection for breast cancer treatment. *World J Surg Oncol*. 2016;14(1):1-8. doi:10.1186/s12957-016-0925-2

376. Lu Y, Wei JY, Yao DS, Pan ZM, Yao Y. Application of carbon nanoparticles in laparoscopic sentinel lymph node detection in patients with early-stage cervical cancer. *PLoS One.* 2017;12(9):e0183834. Published 2017 Sep 5. doi:10.1371/journal.pone.0183834

377. Sun SP, Zhang Y, Cui ZQ, et al. Clinical application of carbon nanoparticle lymph node tracer in the VI region lymph node dissection of differentiated thyroid cancer. *Genet Mol Res.* 2014;13(2):3432-3437. Published 2014 Apr 30. doi:10.4238/2014.April.30.4

378. Xue S, Ren P, Wang P, Chen G. Short and Long-Term Potential Role of Carbon Nanoparticles in Total Thyroidectomy with Central Lymph Node Dissection. *Sci Rep.* 2018;8(1):11936. Published 2018 Aug 9. doi:10.1038/s41598-018-30299-8

379. Ni JS, Li Y, Yue W, Liu B, Li K. Nanoparticle-based Cell Trackers for Biomedical Applications. *Theranostics.* 2020;10(4):1923-1947. Published 2020 Jan 12. doi:10.7150/thno.39915

380. Chen F, Ehlerding EB, Cai W. Theranostic nanoparticles. *J Nucl Med*. 2014;55(12):1919-1922. doi:10.2967/jnumed.114.146019

381. M SM, Veeranarayanan S, Maekawa T, D SK. External stimulus responsive inorganic nanomaterials for cancer theranostics. *Adv Drug Deliv Rev*. 2019;138:18-40. doi:10.1016/j.addr.2018.10.007

382. Madamsetty VS, Mukherjee A, Mukherjee S. Recent Trends of the Bio-Inspired Nanoparticles in Cancer Theranostics. *Front Pharmacol.* 2019;10:1264. Published 2019 Oct 25. doi:10.3389/fphar.2019.01264

383. Blumfield E, Swenson DW, Iyer RS, Stanescu AL. Gadolinium-based contrast agents — review of recent literature on magnetic resonance imaging signal intensity changes and tissue deposits, with emphasis on pediatric patients. *Pediatr Radiol*. 2019;49(4):448-457. doi:10.1007/s00247-018-4304-8

384. Scher N, Bonvalot S, Le Tourneau C, et al. Review of clinical applications of

radiation-enhancing nanoparticles. *Biotechnol Rep (Amst).* 2020;28:e00548. Published 2020 Oct 28. doi:10.1016/j.btre.2020.e00548

385. Sancey L, Lux F, Kotb S, et al. The use of theranostic gadolinium-based nanoprobes to improve radiotherapy efficacy. *Br J Radiol.* 2014;87(1041):20140134. doi:10.1259/bjr.20140134
386. Bottrill M, Kwok L, Long NJ. Lanthanides in magnetic resonance imaging. *Chem Soc Rev*. 2006;35(6):557-571. doi:10.1039/b516376p
387. Pyykkö P. Magically magnetic gadolinium. *Nat Chem*. 2015;7(8):680. doi:10.1038/nchem.2287
388. Ali MY, Oliva CR, Noman ASM, et al. Radioresistance in Glioblastoma and the Development of Radiosensitizers. *Cancers (Basel).* 2020;12(9):2511. Published 2020 Sep 3. doi:10.3390/cancers12092511
389. Hu P, Fu Z, Liu G, et al. Gadolinium-Based Nanoparticles for Theranostic MRI-Guided Radiosensitization in Hepatocellular Carcinoma. *Front Bioeng Biotechnol.* 2019;7:368. Published 2019 Nov 27. doi:10.3389/fbioe.2019.00368
390. Detappe A, Kunjachan S, Rottmann J, et al. AGuIX nanoparticles as a promising platform for image-guided radiation therapy. *Cancer Nanotechnol*. 2015;6(1):4. doi:10.1186/s12645-015-0012-3
391. Mignot A, Truillet C, Lux F, et al. A top-down synthesis route to ultrasmall multifunctional Gd-based silica nanoparticles for theranostic applications. *Chemistry.* 2013;19(19):6122-6136. doi:10.1002/chem.201203003
392. Lux F, Tran VL, Thomas E, et al. AGuIX(®) from bench to bedside-Transfer of an ultrasmall theranostic gadolinium-based nanoparticle to clinical medicine. *Br J Radiol*. 2019;92(1093):20180365. doi:10.1259/bjr.20180365
393. Bazzi R, Flores MA, Louis C, et al. Synthesis and properties of europium-based phosphors on the nanometer scale: Eu2O3, Gd2O3:Eu, and Y 2O3:Eu. *J Colloid Interface Sci*. 2004;273(1):191-197. doi:10.1016/j.jcis.2003.10.031
394. Le Duc G, Roux S, Paruta-Tuarez A, et al. Advantages of gadolinium based ultrasmall nanoparticles vs molecular gadolinium chelates for radiotherapy guided by MRI for glioma treatment. *Cancer Nanotechnol.* 2014;5(1):4. doi:10.1186/s12645-014-0004-8
395. Kryza D, Taleb J, Janier M, et al. Biodistribution study of nanometric hybrid gadolinium oxide particles as a multimodal SPECT/MR/optical imaging and theragnostic agent. *Bioconjug Chem*. 2011;22(6):1145-1152. doi:10.1021/bc1005976
396. Kotb S, Piraquive J, Lamberton F, et al. Safety Evaluation and Imaging Properties of

Gadolinium-Based Nanoparticles in nonhuman primates. *Sci Rep.* 2016;6:35053. Published 2016 Oct 11. doi:10.1038/srep35053

397. Rima W, Sancey L, Aloy MT, et al. Internalization pathways into cancer cells of gadolinium-based radiosensitizing nanoparticles. *Biomaterials*. 2013;34(1):181-195. doi:10.1016/j.biomaterials.2012.09.029
398. Luchette M, Korideck H, Makrigiorgos M, Tillement O, Berbeco R. Radiation dose enhancement of gadolinium-based AGuIX nanoparticles on HeLa cells. *Nanomedicine.* 2014;10(8):1751-1755. doi:10.1016/j.nano.2014.06.004
399. Stefančíková L, Porcel E, Eustache P, et al. Cell localisation of gadolinium-based nanoparticles and related radiosensitising efficacy in glioblastoma cells. *Cancer Nanotechnol.* 2014;5(1):6. doi:10.1186/s12645-014-0006-6
400. Kotb S, Detappe A, Lux F, et al. Gadolinium-Based Nanoparticles and Radiation Therapy for Multiple Brain Melanoma Metastases: Proof of Concept before Phase I Trial. *Theranostics.* 2016;6(3):418-427. Published 2016 Jan 20. doi:10.7150/thno.14018
401. Mowat P, Mignot A, Rima W, et al. In vitro radiosensitizing effects of ultrasmall gadolinium based particles on tumour cells. *J Nanosci Nanotechnol*. 2011;11(9):7833-7839. doi:10.1166/jnn.2011.4725
402. Dentamaro M, Lux F, Vander Elst L, et al. Chemical and in vitro characterizations of a promising bimodal AGuIX probe able to target apoptotic cells for applications in MRI and optical imaging. *Contrast Media Mol Imaging*. 2016;11(5):381-395. doi:10.1002/cmmi.1702
403. Detappe A, Kunjachan S, Rottmann J, et al. AGuIX nanoparticles as a promising platform for image-guided radiation therapy. *Cancer Nanotechnol.* 2015;6(1):4. doi:10.1186/s12645-015-0012-3
404. Simonet S, Rodriguez-Lafrasse C, Beal D, et al. Gadolinium-Based Nanoparticles Can Overcome the Radioresistance of Head and Neck Squamous Cell Carcinoma Through the Induction of Autophagy. *J Biomed Nanotechnol*. 2020;16(1):111-124. doi:10.1166/jbn.2020.2871
405. Roeske JC, Nuñez L, Hoggarth M, Labay E, Weichselbaum RR. Characterization of the theorectical radiation dose enhancement from nanoparticles. *Technol Cancer Res Treat*. 2007;6(5):395-401. doi:10.1177/153303460700600504
406. Miladi I, Aloy MT, Armandy E, et al. Combining ultrasmall gadolinium-based nanoparticles with photon irradiation overcomes radioresistance of head and neck

squamous cell carcinoma. *Nanomedicine Nanotechnology, Biol Med*. 2015;11(1):247-257. doi:10.1016/j.nano.2014.06.013

407. Porcel E, Tillement O, Lux F, et al. Gadolinium-based nanoparticles to improve the hadrontherapy performances. *Nanomedicine.* 2014;10(8):1601-1608. doi:10.1016/j.nano.2014.05.005
408. Wozny AS, Aloy MT, Alphonse G, et al. Gadolinium-based nanoparticles as sensitizing agents to carbon ions in head and neck tumor cells. *Nanomedicine.* 2017;13(8):2655-2660. doi:10.1016/j.nano.2017.07.015
409. Sancey L, Kotb S, Truillet C, et al. Long-term in Vivo clearance of gadolinium-based AGuIX nanoparticles and their biocompatibility after systemic injection. *ACS Nano*. 2015;9(3):2477-2488. doi:10.1021/acsnano.5b00552
410. Lux F, Mignot A, Mowat P, et al. Ultrasmall rigid particles as multimodal probes for medical applications. *Angew Chem Int Ed Engl.* 2011;50(51):12299-12303. doi:10.1002/anie.201104104
411. Shi Y, van der Meel R, Chen X, Lammers T. The EPR effect and beyond: Strategies to improve tumor targeting and cancer nanomedicine treatment efficacy. *Theranostics.* 2020;10(17):7921-7924. Published 2020 Jun 25. doi:10.7150/thno.49577
412. Bort G, Lux F, Dufort S, Crémillieux Y, Verry C, Tillement O. EPR-mediated tumor targeting using ultrasmall-hybrid nanoparticles: From animal to human with theranostic AGuIX nanoparticles. *Theranostics.* 2020;10(3):1319-1331. Published 2020 Jan 1. doi:10.7150/thno.37543
413. Verry C, Dufort S, Barbier EL, et al. MRI-guided clinical 6-MV radiosensitization of glioma using a unique gadolinium-based nanoparticles injection. *Nanomedicine (Lond)*. 2016;11(18):2405-2417. doi:10.2217/nnm-2016-0203
414. Truillet C, Thomas E, Lux F, Huynh LT, Tillement O, Evans MJ. Synthesis and Characterization of (89)Zr-Labeled Ultrasmall Nanoparticles. *Mol Pharm.* 2016;13(7):2596-2601. doi:10.1021/acs.molpharmaceut.6b00264
415. Bouziotis P, Stellas D, Thomas E, et al. ^{68}Ga-radiolabeled AGuIX nanoparticles as dual-modality imaging agents for PET/MRI-guided radiation therapy. *Nanomedicine (Lond)*. 2017;12(13):1561-1574. doi:10.2217/nnm-2017-0032
416. Bianchi A, Moncelet D, Lux F, et al. Orotracheal administration of contrast agents: A new protocol for brain tumor targeting. *NMR Biomed*. 2015;28(6):738-746. doi:10.1002/nbm.3295
417. Fries P, Morr D, Müller A, et al. Evaluation of a Gadolinium-Based Nanoparticle

(AGuIX) for Contrast-Enhanced MRI of the Liver in a Rat Model of Hepatic Colorectal Cancer Metastases at 9.4 Tesla. *Rofo*. 2015;187(12):1108-1115. doi:10.1055/s-0035-1553500

418. Verry C, Sancey L, Dufort S, et al. Treatment of multiple brain metastases using gadolinium nanoparticles and radiotherapy: NANO-RAD, a phase I study protocol. *BMJ Open.* 2019;9(2):e023591. Published 2019 Feb 11. doi:10.1136/bmjopen-2018-023591
419. Verry C, Dufort S, Villa J, et al. Theranostic AGuIX nanoparticles as radiosensitizer: A phase I, dose-escalation study in patients with multiple brain metastases (NANO-RAD trial). *Radiother Oncol*. 2021;160:159-165. doi:10.1016/j.radonc.2021.04.021
420. Donya M, Radford M, ElGuindy A, Firmin D, Yacoub MH. Radiation in medicine: Origins, risks and aspirations. *Glob Cardiol Sci Pract.* 2014;2014(4):437-448. Published 2014 Dec 31. doi:10.5339/gcsp.2014.57
421. Reisz JA, Bansal N, Qian J, Zhao W, Furdui CM. Effects of ionizing radiation on biological molecules - mechanisms of damage and emerging methods of detection. *Antioxidants Redox Signal*. 2014;21(2):260-292. doi:10.1089/ars.2013.5489
422. Ziegelberger G, van Rongen E, Croft R, et al. Principles for non-ionizing radiation protection. *Health Phys*. 2020;118(5):477-482. doi:10.1097/HP.0000000000001252
423. Furdui CM. Ionizing radiation: Mechanisms and therapeutics. *Antioxidants Redox Signal*. 2014;21(2):218-220. doi:10.1089/ars.2014.5935
424. Sung H, Ferlay J, Siegel RL, et al. Global Cancer Statistics 2020: GLOBOCAN Estimates of Incidence and Mortality Worldwide for 36 Cancers in 185 Countries. *CA Cancer J Clin*. 2021;71(3):209-249. doi:10.3322/caac.21660
425. Baskar R, Lee KA, Yeo R, Yeoh KW. Cancer and radiation therapy: Current advances and future directions. *Int J Med Sci*. 2012;9(3):193-199. doi:10.7150/ijms.3635
426. Pucci C, Martinelli C, Ciofani G. Innovative approaches for cancer treatment: current perspectives and new challenges. *Ecancermedicalscience.* 2019;13:961. doi:10.3332/ecancer.2019.961
427. Gardner SJ, Kim J, Chetty IJ. Modern Radiation Therapy Planning and Delivery. *Hematol Oncol Clin North Am*. 2019;33(6):947-962. doi:10.1016/j.hoc.2019.08.005
428. Wardman P. The importance of radiation chemistry to radiation and free radical biology (The 2008 Silvanus Thompson Memorial Lecture). *Br J Radiol.* 2009;82(974):89-104. doi:10.1259/bjr/60186130
429. Desouky O, Ding N, Zhou G. Targeted and non-targeted effects of ionizing radiation. *J*

Radiat Res Appl Sci. 2015;8(2):247-254. doi:10.1016/j.jrras.2015.03.003

430. Ravanat JL, Douki T, Cadet J. Direct and indirect effects of UV radiation on DNA and its components. *J Photochem Photobiol B.* 2001;63(1-3):88-102. doi:10.1016/s1011-1344(01)00206-8
431. Saha GB. Radiation Biology. In: Saha GB, ed. *Physics and Radiobiology of Nuclear Medicine.* New York: Springer New York; 2013:263-299. doi:10.1007/978-1-4614-4012-3_15
432. Mirza-Aghazadeh-Attari M, Darband SG, Kaviani M, et al. DNA damage response and repair in colorectal cancer: Defects, regulation and therapeutic implications. *DNA Repair (Amst)*. 2018;69:34-52. doi:10.1016/j.dnarep.2018.07.005
433. Shiloh Y. ATM and related protein kinases: safeguarding genome integrity. *Nat Rev Cancer*. 2003;3(3):155-168. doi:10.1038/nrc1011
434. Sulli G, Di Micco R, Di Fagagna FDA. Crosstalk between chromatin state and DNA damage response in cellular senescence and cancer. *Nat Rev Cancer*. 2012;12(10):709-720. doi:10.1038/nrc3344
435. Blanpain C, Mohrin M, Sotiropoulou PA, Passegué E. DNA-damage response in tissue-specific and cancer stem cells. *Cell Stem Cell*. 2011;8(1):16-29. doi:10.1016/j.stem.2010.12.012
436. Burrows AE, Elledge SJ. How ATR turns on: TopBP1 goes on ATRIP with ATR. *Genes Dev*. 2008;22(11):1416-1421. doi:10.1101/gad.1685108
437. López-Contreras AJ, Fernandez-Capetillo O. The ATR barrier to replication-born DNA damage. *DNA Repair (Amst)*. 2010;9(12):1249-1255. doi:10.1016/j.dnarep.2010.09.012
438. Caldecott KW. Single-strand break repair and genetic disease. *Nat Rev Genet*. 2008;9(8):619-631. doi:10.1038/nrg2380
439. Delacroix S, Wagner JM, Kobayashi M, Yamamoto KI, Karnitz LM. The Rad9-Hus1-Rad1 (9-1-1) clamp activates checkpoint signaling via TopBP1. *Genes Dev*. 2007;21(12):1472-1477. doi:10.1101/gad.1547007
440. Patil M, Pabla N, Dong Z. Checkpoint kinase 1 in DNA damage response and cell cycle regulation. *Cell Mol Life Sci*. 2013;70(21):4009-4021. doi:10.1007/s00018-013-1307-3
441. Tapia-Alveal C, Calonge TM, O'Connell MJ. Regulation of chk1. *Cell Div.* 2009;4:8. Published 2009 Apr 29. doi:10.1186/1747-1028-4-8
442. Urist M, Tanaka T, Poyurovsky M V., Prives C. p73 induction after DNA damage is

regulated by checkpoint kinases Chk1 and Chk2. *Genes Dev*. 2004;18(24):3041-3054. doi:10.1101/gad.1221004

443. Azenha D, Lopes MC, Martins TC. Claspin functions in cell homeostasis—A link to cancer?. *DNA Repair (Amst)*. 2017;59:27-33. doi:10.1016/j.dnarep.2017.09.002
444. Burma S, Chen BP, Murphy M, Kurimasa A, Chen DJ. ATM Phosphorylates Histone H2AX in Response to DNA Double-strand Breaks. *J Biol Chem*. 2001;276(45):42462-42467. doi:10.1074/jbc.C100466200
445. Dahl ES, Aird KM. Ataxia-Telangiectasia Mutated Modulation of Carbon Metabolism in Cancer. *Front Oncol.* 2017;7:291. Published 2017 Nov 29. doi:10.3389/fonc.2017.00291
446. Uziel T, Lerenthal Y, Moyal L, Andegeko Y, Mittelman L, Shiloh Y. Requirement of the MRN complex for ATM activation by DNA damage. *EMBO J*. 2003;22(20):5612-5621. doi:10.1093/emboj/cdg541
447. Paull TT. Mechanisms of ATM activation. *Annu Rev Biochem*. 2015;84:711-738. doi:10.1146/annurev-biochem-060614-034335
448. Lee JH, Paull TT. Mitochondria at the crossroads of ATM-mediated stress signaling and regulation of reactive oxygen species. *Redox Biol.* 2020;32:101511. doi:10.1016/j.redox.2020.101511
449. So S, Davis AJ, Chen DJ. Autophosphorylation at serine 1981 stabilizes ATM at DNA damage sites [published correction appears in J Cell Biol. 2010 Feb 8;188(3):443]. *J Cell Biol.* 2009;187(7):977-990. doi:10.1083/jcb.200906064
450. Kozlov S V., Graham ME, Jakob B, et al. Autophosphorylation and ATM activation: Additional sites add to the complexity. *J Biol Chem*. 2011;286(11):9107-9119. doi:10.1074/jbc.M110.204065
451. Ernst Schmid T, Zlobinskaya O, Multhoff G. Differences in Phosphorylated Histone H2AX Foci Formation and Removal of Cells Exposed to Low and High Linear Energy Transfer Radiation. *Curr Genomics*. 2012;13(6):418-425. doi:10.2174/138920212802510501
452. Podhorecka M, Skladanowski A, Bozko P. H2AX Phosphorylation: Its Role in DNA Damage Response and Cancer Therapy. *J Nucleic Acids.* 2010;2010:920161. Published 2010 Aug 3. doi:10.4061/2010/920161
453. Dickey JS, Redon CE, Nakamura AJ, Baird BJ, Sedelnikova OA, Bonner WM. H2AX: Functional roles and potential applications. *Chromosoma*. 2009;118(6):683-692. doi:10.1007/s00412-009-0234-4

454. Lowndes NF, Toh GW-L. DNA repair: the importance of phosphorylating histone H2AX. *Curr Biol*. 2005;15(3):R99-R102. doi:10.1016/j.cub.2005.01.029
455. Mizutani S, Takagi M. XCIND as a genetic disease of X-irradiation hypersensitivity and cancer susceptibility. *Int J Hematol*. 2013;97(1):37-42. doi:10.1007/s12185-012-1240-5
456. Blignaut M, Loos B, Botchway SW, Parker AW, Huisamen B. Ataxia-Telangiectasia Mutated is located in cardiac mitochondria and impacts oxidative phosphorylation. *Sci Rep.* 2019;9(1):4782. Published 2019 Mar 18. doi:10.1038/s41598-019-41108-1
457. Cheng Q, Chen J. Mechanism of p53 stabilization by ATM after DNA damage. *Cell Cycle*. 2010;9(3):472-478. doi:10.4161/cc.9.3.10556
458. Brady CA, Attardi LD. p53 at a glance. *J Cell Sci.* 2010;123(Pt 15):2527-2532. doi:10.1242/jcs.064501
459. Banin S, Moyal L, Shieh S, et al. Enhanced phosphorylation of p53 by ATM in response to DNA damage. *Science.* 1998;281(5383):1674-1677. doi:10.1126/science.281.5383.1674
460. Chehab NH, Malikzay A, Appel M, Halazonetis TD. Chk2/hCds1 functions as a DNA damage checkpoint in G1 by stabilizing p53. *Genes Dev*. 2000;14(3):278-288. doi:10.1101/gad.14.3.278
461. De Toledo SM, Azzam EI, Dahlberg WK, Gooding TB, Little JB. ATM complexes with HDM2 and promotes its rapid phosphorylation in a p53-independent manner in normal and tumor human cells exposed to ionizing radiation. *Oncogene*. 2000;19(54):6185-6193. doi:10.1038/sj.onc.1204020
462. Bouska A, Eischen CM. Murine double minute 2: p53-independent roads lead to genome instability or death. *Trends Biochem Sci*. 2009;34(6):279-286. doi:10.1016/j.tibs.2009.02.006
463. Zannini L, Delia D, Buscemi G. CHK2 kinase in the DNA damage response and beyond. *J Mol Cell Biol*. 2014;6(6):442-457. doi:10.1093/jmcb/mju045
464. Ahmed KM, Li JJ. NF-kappa B-mediated adaptive resistance to ionizing radiation. *Free Radic Biol Med*. 2008;44(1):1-13. doi:10.1016/j.freeradbiomed.2007.09.022
465. Li N, Banin S, Ouyang H, et al. ATM is required for IkappaB kinase (IKKk) activation in response to DNA double strand breaks. *J Biol Chem*. 2001;276(12):8898-8903. doi:10.1074/jbc.M009809200
466. Basu S, Rosenzweig KR, Youmell M, Price BD. The DNA-dependent protein kinase participates in the activation of NF kappa B following DNA damage. *Biochem Biophys*

Res Commun. 1998;247(1):79-83. doi:10.1006/bbrc.1998.8741

467. Eaton JS, Lin ZP, Sartorelli AC, Bonawitz ND, Shadel GS. Ataxia-telangiectasia mutated kinase regulates ribonucleotide reductase and mitochondrial homeostasis. *J Clin Invest*. 2007;117(9):2723-2734. doi:10.1172/JCI31604
468. Ambrose M, Goldstine J V., Gatti RA. Intrinsic mitochondrial dysfunction in ATM-deficient lymphoblastoid cells. *Hum Mol Genet*. 2007;16(18):2154-2164. doi:10.1093/hmg/ddm166
469. Valentin-Vega YA, MacLean KH, Tait-Mulder J, et al. Mitochondrial dysfunction in ataxia-telangiectasia. *Blood*. 2012;119(6):1490-1500. doi:10.1182/blood-2011-08-373639
470. Rustom A, Saffrich R, Markovic I, Walther P, Gerdes HH. Nanotubular highways for intercellular organelle transport. *Science*. 2004;303(5660):1007-1010. doi:10.1126/science.1093133
471. Vignais ML, Caicedo A, Brondello JM, Jorgensen C. Cell Connections by Tunneling Nanotubes: Effects of Mitochondrial Trafficking on Target Cell Metabolism, Homeostasis, and Response to Therapy. *Stem Cells Int.* 2017;2017:6917941. doi:10.1155/2017/6917941
472. Jin S, Cordes N. ATM controls DNA repair and mitochondria transfer between neighboring cells. *Cell Commun Signal.* 2019;17(1):144. Published 2019 Nov 8. doi:10.1186/s12964-019-0472-x
473. Kolberg M, Strand KR, Graff P, Andersson KK. Structure, function, and mechanism of ribonucleotide reductases. *Biochim Biophys Acta.* 2004;1699(1-2):1-34. doi:10.1016/j.bbapap.2004.02.007
474. Baghban R, Roshangar L, Jahanban-Esfahlan R, et al. Tumor microenvironment complexity and therapeutic implications at a glance. *Cell Commun Signal.* 2020;18(1):59. Published 2020 Apr 7. doi:10.1186/s12964-020-0530-4
475. Jarosz-Biej M, Smolarczyk R, Cichoń T, Kułach N. Tumor Microenvironment as A "Game Changer" in Cancer Radiotherapy. *Int J Mol Sci.* 2019;20(13):3212. Published 2019 Jun 29. doi:10.3390/ijms20133212
476. Giraldo NA, Sanchez-Salas R, Peske JD, et al. The clinical role of the TME in solid cancer. *Br J Cancer.* 2019;120(1):45-53. doi:10.1038/s41416-018-0327-z
477. Patel H, Nilendu P, Jahagirdar D, Pal JK, Sharma NK. Modulating secreted components of tumor microenvironment: A masterstroke in tumor therapeutics. *Cancer Biol Ther*. 2018;19(1):3-12. doi:10.1080/15384047.2017.1394538

478. Galon J, Bruni D. Approaches to treat immune hot, altered and cold tumours with combination immunotherapies. *Nat Rev Drug Discov*. 2019;18(3):197-218. doi:10.1038/s41573-018-0007-y
479. Liu YT, Sun ZJ. Turning cold tumors into hot tumors by improving T-cell infiltration. *Theranostics*. 2021;11(11):5365-5386. Published 2021 Mar 11. doi:10.7150/thno.58390
480. Formenti SC, Rudqvist N-P, Golden E, et al. Radiotherapy induces responses of lung cancer to CTLA-4 blockade. *Nat Med*. 2018;24(12):1845-1851. doi:10.1038/s41591-018-0232-2
481. Portella L, Scala S. Ionizing radiation effects on the tumor microenvironment. *Semin Oncol*. 2019;46(3):254-260. doi:10.1053/j.seminoncol.2019.07.003
482. Martins I, Raza SQ, Voisin L, et al. Anticancer chemotherapy and radiotherapy trigger both non-cell-autonomous and cell-autonomous death. *Cell Death Dis*. 2018;9(7):716. Published 2018 Jun 18. doi:10.1038/s41419-018-0747-y
483. Barker HE, Paget JT, Khan AA, Harrington KJ. The tumour microenvironment after radiotherapy: mechanisms of resistance and recurrence [published correction appears in Nat Rev Cancer. 2015 Aug;15(8):509]. *Nat Rev Cancer*. 2015;15(7):409-425. doi:10.1038/nrc3958
484. Martins I, Raza SQ, Voisin L, et al. Entosis: The emerging face of non-cell-autonomous type IV programmed death. *Biomed J*. 2017;40(3):133-140. doi:10.1016/j.bj.2017.05.001
485. Galluzzi L, Maiuri MC, Vitale I, et al. Cell death modalities: classification and pathophysiological implications. *Cell Death Differ*. 2007;14(7):1237-1243. doi:10.1038/sj.cdd.4402148
486. Green DR, Llambi F. Cell Death Signaling. *Cold Spring Harb Perspect Biol*. 2015;7(12):a006080. Published 2015 Dec 1. doi:10.1101/cshperspect.a006080
487. Jorgensen I, Miao EA. Pyroptotic cell death defends against intracellular pathogens. *Immunol Rev*. 2015;265(1):130-142. doi:10.1111/imr.12287
488. Vakifahmetoglu H, Olsson M, Zhivotovsky B. Death through a tragedy: mitotic catastrophe. *Cell Death Differ*. 2008;15(7):1153-1162. doi:10.1038/cdd.2008.47
489. Kaczmarek A, Vandenabeele P, Krysko DV. Necroptosis: the release of damage-associated molecular patterns and its physiological relevance. *Immunity*. 2013;38(2):209-223. doi:10.1016/j.immuni.2013.02.003
490. Berghe T Vanden, Vanlangenakker N, Parthoens E, et al. Necroptosis, necrosis and

secondary necrosis converge on similar cellular disintegration features. *Cell Death Differ*. 2010;17(6):922-930. doi:10.1038/cdd.2009.184

491. Adjemian S, Oltean T, Martens S, et al. Ionizing radiation results in a mixture of cellular outcomes including mitotic catastrophe, senescence, methuosis, and iron-dependent cell death. *Cell Death Dis.* 2020;11(11):1003. Published 2020 Nov 23. doi:10.1038/s41419-020-03209-y
492. Gupta N, Jadhav K, Shah V. Emperipolesis, entosis and cell cannibalism: Demystifying the cloud. *J Oral Maxillofac Pathol*. 2017;21(1):92-98. doi:10.4103/0973-029X.203763
493. Rastogi V, Sharma R, Misra SR, Yadav L, Sharma V. Emperipolesis - a review. *J Clin Diagn Res*. 2014;8(12):ZM01-2. doi:10.7860/JCDR/2014/10361.5299
494. Wang X, Li Y, Li J, et al. Cell-in-Cell Phenomenon and Its Relationship With Tumor Microenvironment and Tumor Progression: A Review. *Front Cell Dev Biol.* 2019;7:311. Published 2019 Dec 3. doi:10.3389/fcell.2019.00311
495. Sun Q, Cibas ES, Huang H, Hodgson L, Overholtzer M. Induction of entosis by epithelial cadherin expression. *Cell Res*. 2014;24(11):1288-1298. doi:10.1038/cr.2014.137
496. Hamann JC, Surcel A, Chen R, et al. Entosis Is Induced by Glucose Starvation. *Cell Rep*. 2017;20(1):201-210. doi:10.1016/j.celrep.2017.06.037
497. Overholtzer M, Mailleux AA, Mouneimne G, et al. A nonapoptotic cell death process, entosis, that occurs by cell-in-cell invasion. *Cell*. 2007;131(5):966-979. doi:10.1016/j.cell.2007.10.040
498. Fais S, Overholtzer M. Cell-in-cell phenomena, cannibalism, and autophagy: is there a relationship?. *Cell Death Dis.* 2018;9(2):95. Published 2018 Jan 24. doi:10.1038/s41419-017-0111-7
499. Fais S. Cannibalism: a way to feed on metastatic tumors. *Cancer Lett*. 2007;258(2):155-164. doi:10.1016/j.canlet.2007.09.014
500. Kroemer G, Galluzzi L, Kepp O, Zitvogel L. Immunogenic cell death in cancer therapy. *Annu Rev Immunol*. 2013;31:51-72. doi:10.1146/annurev-immunol-032712-100008
501. Galluzzi L, Kepp O, Kroemer G. Immunogenic cell death in radiation therapy. *Oncoimmunology*. 2013;2(10):e26536. doi:10.4161/onci.26536
502. Zhou J, Wang G, Chen Y, Wang H, Hua Y, Cai Z. Immunogenic cell death in cancer therapy: Present and emerging inducers. *J Cell Mol Med*. 2019;23(8):4854-4865.

doi:10.1111/jcmm.14356

503. Panaretakis T, Joza N, Modjtahedi N, et al. The co-translocation of ERp57 and calreticulin determines the immunogenicity of cell death. *Cell Death Differ*. 2008;15(9):1499-1509. doi:10.1038/cdd.2008.67

504. Obeid M. ERP57 membrane translocation dictates the immunogenicity of tumor cell death by controlling the membrane translocation of calreticulin. *J Immunol.* 2008;181(4):2533-2543. doi:10.4049/jimmunol.181.4.2533

505. van Mierlo GJ, Boonman ZF, Dumortier HM, et al. Activation of dendritic cells that cross-present tumor-derived antigen licenses CD8+ CTL to cause tumor eradication. *J Immunol.* 2004;173(11):6753-6759. doi:10.4049/jimmunol.173.11.6753

506. Wang D, Wang H, Gao H, et al. P2X7 receptor mediates NLRP3 inflammasome activation in depression and diabetes. *Cell Biosci.* 2020;10:28. Published 2020 Mar 5. doi:10.1186/s13578-020-00388-1

507. Savio LEB, de Andrade Mello P, da Silva CG, Coutinho-Silva R. The P2X7 Receptor in Inflammatory Diseases: Angel or Demon?. *Front Pharmacol*. 2018;9:52. Published 2018 Feb 6. doi:10.3389/fphar.2018.00052

508. Sáez PJ, Vargas P, Shoji KF, Harcha PA, Lennon-Duménil AM, Sáez JC. ATP promotes the fast migration of dendritic cells through the activity of pannexin 1 channels and P2X7 receptors. *Sci Signal.* 2017;10(506):eaah7107. Published 2017 Nov 21. doi:10.1126/scisignal.aah7107

509. Apetoh L, Ghiringhelli F, Tesniere A, et al. The interaction between HMGB1 and TLR4 dictates the outcome of anticancer chemotherapy and radiotherapy. *Immunol Rev.* 2007;220:47-59. doi:10.1111/j.1600-065X.2007.00573.x

510. Kono K, Mimura K, Kiessling R. Immunogenic tumor cell death induced by chemoradiotherapy: molecular mechanisms and a clinical translation. *Cell Death Dis.* 2013;4(6):e688. Published 2013 Jun 20. doi:10.1038/cddis.2013.207

511. McNulty S, Colaco CA, Blandford LE, Bailey CR, Baschieri S, Todryk S. Heat-shock proteins as dendritic cell-targeting vaccines--getting warmer. *Immunology.* 2013;139(4):407-415. doi:10.1111/imm.12104

512. Zhu H, Fang X, Zhang D, et al. Membrane-bound heat shock proteins facilitate the uptake of dying cells and cross-presentation of cellular antigen. *Apoptosis*. 2016;21(1):96-109. doi:10.1007/s10495-015-1187-0

513. Basu S, Binder RJ, Ramalingam T, Srivastava PK. CD91 is a common receptor for heat shock proteins gp96, hsp90, hsp70, and calreticulin. *Immunity*. 2001;14(3):303-

313. doi:10.1016/S1074-7613(01)00111-X

514. Hart JP, Gunn MD, Pizzo SV. A CD91-positive subset of CD11c+ blood dendritic cells: characterization of the APC that functions to enhance adaptive immune responses against CD91-targeted antigens. *J Immunol.* 2004;172(1):70-78. doi:10.4049/jimmunol.172.1.70

515. Zininga T, Ramatsui L, Shonhai A. Heat Shock Proteins as Immunomodulants. *Molecules.* 2018;23(11):2846. Published 2018 Nov 1. doi:10.3390/molecules23112846

516. Ciocca DR, Calderwood SK. Heat shock proteins in cancer: diagnostic, prognostic, predictive, and treatment implications. *Cell Stress Chaperones*. 2005;10(2):86-103. doi:10.1379/csc-99r.1

517. Burnette BC, Liang H, Lee Y, et al. The efficacy of radiotherapy relies upon induction of type i interferon-dependent innate and adaptive immunity. *Cancer Res*. 2011;71(7):2488-2496. doi:10.1158/0008-5472.CAN-10-2820

518. Daguenet E, Louati S, Wozny A-S, et al. Radiation-induced bystander and abscopal effects: important lessons from preclinical models. *Br J Cancer*. 2020;123(3):339-348. doi:10.1038/s41416-020-0942-3

519. Picaud S, Bardot B, De Maeyer E, Seif I. Enhanced tumor development in mice lacking a functional type I interferon receptor. *J Interferon Cytokine Res.* 2002;22(4):457-462. doi:10.1089/10799900252952244

520. Deng L, Liang H, Xu M, et al. STING-Dependent Cytosolic DNA Sensing Promotes Radiation-Induced Type I Interferon-Dependent Antitumor Immunity in Immunogenic Tumors. *Immunity*. 2014;41(5):843-852. doi:10.1016/j.immuni.2014.10.019

521. Vanpouille-Box C, Alard A, Aryankalayil MJ, et al. DNA exonuclease Trex1 regulates radiotherapy-induced tumour immunogenicity. *Nat Commun.* 2017;8:15618. Published 2017 Jun 9. doi:10.1038/ncomms15618

522. Grieves JL, Fye JM, Harvey S, Grayson JM, Hollis T, Perrino FW. Exonuclease TREX1 degrades double-stranded DNA to prevent spontaneous lupus-like inflammatory disease. *Proc Natl Acad Sci U S A.* 2015;112(16):5117-5122. doi:10.1073/pnas.1423804112

523. Demaria S, Formenti SC. Role of T lymphocytes in tumor response to radiotherapy. *Front Oncol.* 2012;2:95. Published 2012 Aug 24. doi:10.3389/fonc.2012.00095

524. Lee Y, Auh SL, Wang Y, et al. Therapeutic effects of ablative radiation on local tumor require CD8+ T cells: changing strategies for cancer treatment. *Blood*.

2009;114(3):589-595. doi:10.1182/blood-2009-02-206870

525. Arina A, Beckett M, Fernandez C, et al. Tumor-reprogrammed resident T cells resist radiation to control tumors. *Nat Commun.* 2019;10(1):3959. Published 2019 Sep 2. doi:10.1038/s41467-019-11906-2
526. Matsumura S, Wang B, Kawashima N, et al. Radiation-induced CXCL16 release by breast cancer cells attracts effector T cells. *J Immunol*. 2008;181(5):3099-3107. doi:10.4049/jimmunol.181.5.3099
527. Reits EA, Hodge JW, Herberts CA, et al. Radiation modulates the peptide repertoire, enhances MHC class I expression, and induces successful antitumor immunotherapy. *J Exp Med*. 2006;203(5):1259-1271. doi:10.1084/jem.20052494
528. Chakraborty M, Abrams SI, Camphausen K, et al. Irradiation of tumor cells up-regulates Fas and enhances CTL lytic activity and CTL adoptive immunotherapy. *J Immunol*. 2003;170(12):6338-6347. doi:10.4049/jimmunol.170.12.6338
529. Venkatesulu BP, Mahadevan LS, Aliru ML, et al. Radiation-Induced Endothelial Vascular Injury: A Review of Possible Mechanisms. *JACC Basic Transl Sci.* 2018;3(4):563-572. Published 2018 Aug 28. doi:10.1016/j.jacbts.2018.01.014
530. Wijerathne H, Langston JC, Yang Q, et al. Mechanisms of radiation-induced endothelium damage: Emerging models and technologies. *Radiother Oncol*. 2021;158:21-32. doi:10.1016/j.radonc.2021.02.007
531. Garcia-Barros M, Paris F, Cordon-Cardo C, et al. Tumor response to radiotherapy regulated by endothelial cell apoptosis. *Science.* 2003;300(5622):1155-1159. doi:10.1126/science.1082504
532. Langley RE, Bump EA, Quartuccio SG, Medeiros D, Braunhut SJ. Radiation-induced apoptosis in microvascular endothelial cells. *Br J Cancer*. 1997;75(5):666-672. doi:10.1038/bjc.1997.119
533. Seideman JH, Stancevic B, Rotolo JA, et al. Alpha particles induce apoptosis through the sphingomyelin pathway. *Radiat Res*. 2011;176(4):434-446. doi:10.1667/RR2472.1
534. Cervelli T, Panetta D, Navarra T, et al. Effects of single and fractionated low-dose irradiation on vascular endothelial cells. *Atherosclerosis*. 2014;235(2):510-518. doi:10.1016/j.atherosclerosis.2014.05.932
535. Guipaud O, Jaillet C, Clément-Colmou K, François A, Supiot S, Milliat F. The importance of the vascular endothelial barrier in the immune-inflammatory response induced by radiotherapy. *Br J Radiol.* 2018;91(1089):20170762. doi:10.1259/bjr.20170762

536. Baselet B, Sonveaux P, Baatout S, Aerts A. Pathological effects of ionizing radiation: endothelial activation and dysfunction. *Cell Mol Life Sci*. 2019;76(4):699-728. doi:10.1007/s00018-018-2956-z

537. Hellweg CE. The Nuclear Factor κB pathway: A link to the immune system in the radiation response. *Cancer Lett*. 2015;368(2):275-289. doi:https://doi.org/10.1016/j.canlet.2015.02.019

538. Surh YJ, Kundu JK, Na HK, Lee JS. Redox-sensitive transcription factors as prime targets for chemoprevention with anti-inflammatory and antioxidative phytochemicals. *J Nutr.* 2005;135(12 Suppl):2993S-3001S. doi:10.1093/jn/135.12.2993S

539. Kempe S, Kestler H, Lasar A, Wirth T. NF-kappaB controls the global pro-inflammatory response in endothelial cells: evidence for the regulation of a pro-atherogenic program. *Nucleic Acids Res.* 2005;33(16):5308-5319. Published 2005 Sep 21. doi:10.1093/nar/gki836

540. Gareus R, Kotsaki E, Xanthoulea S, et al. Endothelial cell-specific NF-kappaB inhibition protects mice from atherosclerosis. *Cell Metab.* 2008;8(5):372-383. doi:10.1016/j.cmet.2008.08.016

541. Wu Q, Allouch A, Paoletti A, et al. NOX2-dependent ATM kinase activation dictates pro-inflammatory macrophage phenotype and improves effectiveness to radiation therapy. *Cell Death Differ*. 2017;24(9):1632-1644. doi:10.1038/cdd.2017.91

542. Shigematsu A, Adachi Y, Koike-Kiriyama N, et al. Effects of low-dose irradiation on enhancement of immunity by dendritic cells. *J Radiat Res*. 2007;48(1):51-55. doi:10.1269/jrr.06048

543. Zhou Z, Zhao J, Hu K, et al. Single High-Dose Radiation Enhances Dendritic Cell Homing and T Cell Priming by Promoting Reactive Oxygen Species-Induced Cytoskeletal Reorganization. *Int J Radiat Oncol Biol Phys*. 2021;109(1):95-108. doi:10.1016/j.ijrobp.2020.07.2321

544. Falcke SE, Rühle PF, Deloch L, Fietkau R, Frey B, Gaipl US. Clinically Relevant Radiation Exposure Differentially Impacts Forms of Cell Death in Human Cells of the Innate and Adaptive Immune System. *Int J Mol Sci.* 2018;19(11):3574. Published 2018 Nov 13. doi:10.3390/ijms19113574

545. Gómez V, Mustapha R, Ng K, Ng T. Radiation therapy and the innate immune response: Clinical implications for immunotherapy approaches. *Br J Clin Pharmacol*. 2020;86(9):1726-1735. doi:10.1111/bcp.14351

546. Mavragani IV, Laskaratou DA, Frey B, et al. Key mechanisms involved in ionizing

radiation-induced systemic effects. A current review. *Toxicol Res (Camb).* 2015;5(1):12-33. Published 2015 Aug 11. doi:10.1039/c5tx00222b

547. Zelenay S, Reis e Sousa C. Adaptive immunity after cell death. *Trends Immunol*. 2013;34(7):329-335. doi:10.1016/j.it.2013.03.005
548. Jin H, Lee JS, Kim DC, Ko YS, Lee GW, Kim HJ. Increased Extracellular Adenosine in Radiotherapy-Resistant Breast Cancer Cells Enhances Tumor Progression through A2AR-Akt-β-Catenin Signaling. *Cancers (Basel).* 2021;13(9):2105. Published 2021 Apr 27. doi:10.3390/cancers13092105
549. Leclerc E, Vetter SW. The role of S100 proteins and their receptor RAGE in pancreatic cancer. *Biochim Biophys Acta.* 2015;1852(12):2706-2711. doi:10.1016/j.bbadis.2015.09.022
550. Gabrilovich DI, Nagaraj S. Myeloid-derived suppressor cells as regulators of the immune system. *Nat Rev Immunol*. 2009;9(3):162-174. doi:10.1038/nri2506
551. Pawelec G, Verschoor CP, Ostrand-Rosenberg S. Myeloid-Derived Suppressor Cells: Not Only in Tumor Immunity. *Front Immunol.* 2019;10:1099. Published 2019 May 15. doi:10.3389/fimmu.2019.01099
552. Tesi RJ. MDSC; the Most Important Cell You Have Never Heard Of. *Trends Pharmacol Sci*. 2019;40(1):4-7. doi:10.1016/j.tips.2018.10.008
553. Kho VM, Mekers VE, Span PN, Bussink J, Adema GJ. Radiotherapy and cGAS/STING signaling: Impact on MDSCs in the tumor microenvironment. *Cell Immunol*. 2021;362(January):104298. doi:10.1016/j.cellimm.2021.104298
554. Gabrilovich DI. Myeloid-derived suppressor cells. *Cancer Immunol Res*. 2017;5(1):3-8. doi:10.1158/2326-6066.CIR-16-0297
555. Ostrand-Rosenberg S, Horn LA, Ciavattone NG. Radiotherapy Both Promotes and Inhibits Myeloid-Derived Suppressor Cell Function: Novel Strategies for Preventing the Tumor-Protective Effects of Radiotherapy. *Front Oncol.* 2019;9:215. Published 2019 Apr 2. doi:10.3389/fonc.2019.00215
556. Lan J, Li R, Yin LM, et al. Targeting Myeloid-derived Suppressor Cells and Programmed Death Ligand 1 Confers Therapeutic Advantage of Ablative Hypofractionated Radiation Therapy Compared With Conventional Fractionated Radiation Therapy. *Int J Radiat Oncol Biol Phys*. 2018;101(1):74-87. doi:10.1016/j.ijrobp.2018.01.071
557. Xu J, Escamilla J, Mok S, et al. CSF1R signaling blockade stanches tumor-infiltrating myeloid cells and improves the efficacy of radiotherapy in prostate cancer. *Cancer*

Res. 2013;73(9):2782-2794. doi:10.1158/0008-5472.CAN-12-3981

558. Liang H, Deng L, Hou Y, et al. Host STING-dependent MDSC mobilization drives extrinsic radiation resistance. *Nat Commun.* 2017;8(1):1736. Published 2017 Nov 23. doi:10.1038/s41467-017-01566-5

559. Artis D, Spits H. The biology of innate lymphoid cells. *Nature*. 2015;517(7534):293-301. doi:10.1038/nature14189

560. Chen J, Liu X, Zeng Z, et al. Immunomodulation of NK Cells by Ionizing Radiation. *Front Oncol.* 2020;10:874. Published 2020 Jun 16. doi:10.3389/fonc.2020.00874

561. Shimasaki N, Jain A, Campana D. NK cells for cancer immunotherapy. *Nat Rev Drug Discov*. 2020;19(3):200-218. doi:10.1038/s41573-019-0052-1

562. Meza Guzman LG, Keating N, Nicholson SE. Natural Killer Cells: Tumor Surveillance and Signaling. *Cancers (Basel).* 2020;12(4):952. Published 2020 Apr 11. doi:10.3390/cancers12040952

563. Paul S, Lal G. The Molecular Mechanism of Natural Killer Cells Function and Its Importance in Cancer Immunotherapy. *Front Immunol.* 2017;8:1124. Published 2017 Sep 13. doi:10.3389/fimmu.2017.01124

564. Bi J, Tian Z. NK Cell Exhaustion. *Front Immunol.* 2017;8:760. Published 2017 Jun 28. doi:10.3389/fimmu.2017.00760

565. Cheda A, Wrembel-Wargocka J, Lisiak E, Nowosielska EM, Marciniak M, Janiak MK. Single low doses of X rays inhibit the development of experimental tumor metastases and trigger the activities of NK cells in mice. *Radiat Res*. 2004;161(3):335-340. doi:10.1667/RR3123

566. Yang G, Kong Q, Wang G, et al. Low-dose ionizing radiation induces direct activation of natural killer cells and provides a novel approach for adoptive cellular immunotherapy. *Cancer Biother Radiopharm*. 2014;29(10):428-434. doi:10.1089/cbr.2014.1702

567. Zhou L, Zhang X, Li H, et al. Validating the pivotal role of the immune system in low-dose radiation-induced tumor inhibition in Lewis lung cancer-bearing mice. *Cancer Med*. 2018;7(4):1338-1348. doi:10.1002/cam4.1344

568. Joffre OP, Segura E, Savina A, Amigorena S. Cross-presentation by dendritic cells. *Nat Rev Immunol.* 2012;12(8):557-569. Published 2012 Jul 13. doi:10.1038/nri3254

569. Wculek SK, Cueto FJ, Mujal AM, Melero I, Krummel MF, Sancho D. Dendritic cells in cancer immunology and immunotherapy. *Nat Rev Immunol*. 2020;20(1):7-24. doi:10.1038/s41577-019-0210-z

570. Peng X, He Y, Huang J, Tao Y, Liu S. Metabolism of Dendritic Cells in Tumor Microenvironment: For Immunotherapy. *Front Immunol.* 2021;12:613492. Published 2021 Feb 24. doi:10.3389/fimmu.2021.613492
571. Collin M, Bigley V. Human dendritic cell subsets: an update. *Immunology*. 2018;154(1):3-20. doi:10.1111/imm.12888
572. Ferris ST, Durai V, Wu R, et al. cDC1 prime and are licensed by $CD4^+$ T cells to induce anti-tumour immunity. *Nature*. 2020;584(7822):624-629. doi:10.1038/s41586-020-2611-3
573. Gardner A, de Mingo Pulido Á, Ruffell B. Dendritic Cells and Their Role in Immunotherapy. *Front Immunol.* 2020;11:924. Published 2020 May 21. doi:10.3389/fimmu.2020.00924
574. Koucký V, Bouček J, Fialová A. Immunology of Plasmacytoid Dendritic Cells in Solid Tumors: A Brief Review. *Cancers (Basel).* 2019;11(4):470. Published 2019 Apr 3. doi:10.3390/cancers11040470
575. Chow K V., Lew AM, Sutherland RM, Zhan Y. Monocyte-Derived Dendritic Cells Promote Th Polarization, whereas Conventional Dendritic Cells Promote Th Proliferation. *J Immunol*. 2016;196(2):624-636. doi:10.4049/jimmunol.1501202
576. Verneau J, Sautés-Fridman C, Sun CM. Dendritic cells in the tumor microenvironment: prognostic and theranostic impact. *Semin Immunol.* 2020;48:101410. doi:10.1016/j.smim.2020.101410
577. Fricke I, Gabrilovich DI. Dendritic cells and tumor microenvironment: a dangerous liaison. *Immunol Invest.* 2006;35(3-4):459-483. doi:10.1080/08820130600803429
578. Di Blasio S, van Wigcheren GF, Becker A, et al. The tumour microenvironment shapes dendritic cell plasticity in a human organotypic melanoma culture. *Nat Commun.* 2020;11(1):2749. Published 2020 Jun 2. doi:10.1038/s41467-020-16583-0
579. Huang C, Gan D, Luo F, et al. Interaction Mechanisms Between the NOX4/ROS and RhoA/ROCK1 Signaling Pathways as New Anti- fibrosis Targets of Ursolic Acid in Hepatic Stellate Cells. *Front Pharmacol.* 2019;10:431. Published 2019 May 3. doi:10.3389/fphar.2019.00431
580. Merrick A, Errington F, Milward K, et al. Immunosuppressive effects of radiation on human dendritic cells: reduced IL-12 production on activation and impairment of naive T-cell priming. *Br J Cancer.* 2005;92(8):1450-1458. doi:10.1038/sj.bjc.6602518
581. Blair TC, Bambina S, Alice AF, et al. Dendritic Cell Maturation Defines Immunological Responsiveness of Tumors to Radiation Therapy. *J Immunol*.

2020;204(12):3416-3424. doi:10.4049/jimmunol.2000194

582. Price JG, Idoyaga J, Salmon H, et al. CDKN1A regulates Langerhans cell survival and promotes Treg cell generation upon exposure to ionizing irradiation. *Nat Immunol*. 2015;16(10):1060-1068. doi:10.1038/ni.3270

583. Wu Q, Allouch A, Martins I, et al. Modulating Both Tumor Cell Death and Innate Immunity Is Essential for Improving Radiation Therapy Effectiveness. *Front Immunol.* 2017;8:613. Published 2017 May 26. doi:10.3389/fimmu.2017.00613

584. Wu Q, Allouch A, Martins I, Modjtahedi N, Deutsch E, Perfettini JL. Macrophage biology plays a central role during ionizing radiation-elicited tumor response. *Biomed J*. 2017;40(4):200-211. doi:10.1016/j.bj.2017.06.003

585. Lödermann B, Wunderlich R, Frey S, et al. Low dose ionising radiation leads to a NF-κB dependent decreased secretion of active IL-1β by activated macrophages with a discontinuous dose-dependency. *Int J Radiat Biol*. 2012;88(10):727-734. doi:10.3109/09553002.2012.689464

586. Teresa Pinto A, Laranjeiro Pinto M, Patrícia Cardoso A, et al. Ionizing radiation modulates human macrophages towards a pro-inflammatory phenotype preserving their pro-invasive and pro-angiogenic capacities. *Sci Rep.* 2016;6:18765. Published 2016 Jan 6. doi:10.1038/srep18765

587. McKinney LC, Aquilla EM, Coffin D, Wink DA, Vodovotz Y. Ionizing radiation potentiates the induction of nitric oxide synthase by IFN-γ/and/or LPS in murine macrophage cell lines: Role of TNF-α. *J Leukoc Biol*. 1998;64(4):459-466. doi:10.1002/jlb.64.4.459

588. Palmieri EM, Gonzalez-Cotto M, Baseler WA, et al. Nitric oxide orchestrates metabolic rewiring in M1 macrophages by targeting aconitase 2 and pyruvate dehydrogenase. *Nat Commun.* 2020;11(1):698. Published 2020 Feb 4. doi:10.1038/s41467-020-14433-7

589. Pons I, Gras G, Courberand S, Benveniste O, Dormont D. Consequences of gamma-irradiation on inflammatory cytokine regulation in human monocytes/macrophages. *Int J Radiat Biol*. 1997;71(2):157-166. doi:10.1080/095530097144274

590. Katayama I, Hotokezaka Y, Matsuyama T, Sumi T, Nakamura T. Ionizing radiation induces macrophage foam cell formation and aggregation through JNK-dependent activation of CD36 scavenger receptors. *Int J Radiat Oncol Biol Phys.* 2008;70(3):835-846. doi:10.1016/j.ijrobp.2007.10.058

591. Shin SC, Lee KM, Kang YM, et al. Alteration of cytokine profiles in mice exposed to

chronic low-dose ionizing radiation. *Biochem Biophys Res Commun*. 2010;397(4):644-649. doi:10.1016/j.bbrc.2010.05.121

592. Hildebrandt G, Radlingmayr A, Rosenthal S, et al. Low-dose radiotherapy (LD-RT) and the modulation of iNOS expression in adjuvant-induced arthritis in rats. *Int J Radiat Biol*. 2003;79(12):993-1001. doi:10.1080/09553000310001636639
593. Pandey R, Shankar BS, Sharma D, Sainis KB. Low dose radiation induced immunomodulation: effect on macrophages and CD8+ T cells. *Int J Radiat Biol.* 2005;81(11):801-812. doi:10.1080/09553000500531886
594. Okubo M, Kioi M, Nakashima H, et al. M2-polarized macrophages contribute to neovasculogenesis, leading to relapse of oral cancer following radiation. *Sci Rep.* 2016;6:27548. Published 2016 Jun 8. doi:10.1038/srep27548
595. Meng Y, Beckett MA, Liang H, et al. Blockade of tumor necrosis factor α signaling in tumor-associated macrophages as a radiosensitizing strategy. *Cancer Res*. 2010;70(4):1534-1543. doi:10.1158/0008-5472.CAN-09-2995
596. Yang J, Yan J, Liu B. Targeting VEGF/VEGFR to Modulate Antitumor Immunity. *Front Immunol.* 2018;9:978. Published 2018 May 3. doi:10.3389/fimmu.2018.00978
597. Prakash H, Klug F, Nadella V, Mazumdar V, Schmitz-Winnenthal H, Umansky L. Low doses of gamma irradiation potentially modifies immunosuppressive tumor microenvironment by retuning tumor-associated macrophages: lesson from insulinoma. *Carcinogenesis*. 2016;37(3):301-313. doi:10.1093/carcin/bgw007
598. Klug F, Prakash H, Huber PE, et al. Low-dose irradiation programs macrophage differentiation to an iNOS^{+}/M1 phenotype that orchestrates effective T cell immunotherapy. *Cancer Cell.* 2013;24(5):589-602. doi:10.1016/j.ccr.2013.09.014
599. Denkova AG, Liu H, Men Y, Eelkema R. Enhanced Cancer Therapy by Combining Radiation and Chemical Effects Mediated by Nanocarriers. *Adv Ther*. 2020;3(3):1900177. doi:10.1002/adtp.201900177
600. Bayat Mokhtari R, Homayouni TS, Baluch N, et al. Combination therapy in combating cancer. *Oncotarget*. 2017;8(23):38022-38043. doi:10.18632/oncotarget.16723
601. Wong R, Malthaner R. Combined chemotherapy and radiotherapy (without surgery) compared with radiotherapy alone in localized carcinoma of the esophagus. *Cochrane Database Syst Rev.* 2006;(1):CD002092. Published 2006 Jan 25. doi:10.1002/14651858.CD002092.pub2
602. Huszno J, Budryk M, Kołosza Z, Nowara E. The risk factors of toxicity during chemotherapy and radiotherapy in breast cancer patients according to the presence of

BRCA gene mutation. *Contemp Oncol (Pozn).* 2015;19(1):72-76. doi:10.5114/wo.2015.50014

603. Barnett GC, West CM, Dunning AM, et al. Normal tissue reactions to radiotherapy: towards tailoring treatment dose by genotype. *Nat Rev Cancer.* 2009;9(2):134-142. doi:10.1038/nrc2587
604. Rabus H, Gargioni E, Li WB, Nettelbeck H, Villagrasa C. Determining dose enhancement factors of high-Z nanoparticles from simulations where lateral secondary particle disequilibrium exists. *Phys Med Biol.* 2019;64(15):155016. Published 2019 Aug 7. doi:10.1088/1361-6560/ab31d4
605. Iyer AK, Khaled G, Fang J, Maeda H. Exploiting the enhanced permeability and retention effect for tumor targeting. *Drug Discov Today*. 2006;11(17-18):812-818. doi:10.1016/j.drudis.2006.07.005
606. Stapleton S, Jaffray D, Milosevic M. Radiation effects on the tumor microenvironment: Implications for nanomedicine delivery. *Adv Drug Deliv Rev*. 2017;109:119-130. doi:10.1016/j.addr.2016.05.021
607. Park J, Choi Y, Chang H, Um W, Ryu JH, Kwon IC. Alliance with EPR Effect: Combined Strategies to Improve the EPR Effect in the Tumor Microenvironment. *Theranostics.* 2019;9(26):8073-8090. Published 2019 Oct 17. doi:10.7150/thno.37198
608. Yang M, Li J, Gu P, Fan X. The application of nanoparticles in cancer immunotherapy: Targeting tumor microenvironment. *Bioact Mater.* 2020;6(7):1973-1987. Published 2020 Dec 26. doi:10.1016/j.bioactmat.2020.12.010
609. Liang R, Xie J, Li J, et al. Liposomes-coated gold nanocages with antigens and adjuvants targeted delivery to dendritic cells for enhancing antitumor immune response. *Biomaterials.* 2017;149:41-50. doi:10.1016/j.biomaterials.2017.09.029
610. Mardhian DF, Storm G, Bansal R, Prakash J. Nano-targeted relaxin impairs fibrosis and tumor growth in pancreatic cancer and improves the efficacy of gemcitabine in vivo. *J Control Release.* 2018;290:1-10. doi:10.1016/j.jconrel.2018.09.031
611. Daldrup-Link HE, Golovko D, Ruffell B, et al. MRI of tumor-associated macrophages with clinically applicable iron oxide nanoparticles. *Clin Cancer Res.* 2011;17(17):5695-5704. doi:10.1158/1078-0432.CCR-10-3420
612. Zanganeh S, Hutter G, Spitler R, et al. Iron oxide nanoparticles inhibit tumour growth by inducing pro-inflammatory macrophage polarization in tumour tissues. *Nat Nanotechnol*. 2016;11(11):986-994. doi:10.1038/nnano.2016.168
613. Bonvalot S, Rutkowski PL, Thariat J, et al. NBTXR3, a first-in-class radioenhancer

hafnium oxide nanoparticle, plus radiotherapy versus radiotherapy alone in patients with locally advanced soft-tissue sarcoma (Act.In.Sarc): a multicentre, phase 2-3, randomised, controlled trial [published correction appears in Lancet Oncol. 2019 Sep;20(9):e468]. *Lancet Oncol.* 2019;20(8):1148-1159. doi:10.1016/S1470-2045(19)30326-2

614. Scher N, Bonvalot S, Le Tourneau C, et al. Review of clinical applications of radiation-enhancing nanoparticles. *Biotechnol Rep (Amst).* 2020;28:e00548. Published 2020 Oct 28. doi:10.1016/j.btre.2020.e00548
615. Borrego-Soto G, Ortiz-López R, Rojas-Martínez A. Ionizing radiation-induced DNA injury and damage detection in patients with breast cancer. *Genet Mol Biol*. 2015;38(4):420-432. doi:10.1590/S1415-475738420150019
616. Vignard J, Mirey G, Salles B. Ionizing-radiation induced DNA double-strand breaks: a direct and indirect lighting up. *Radiother Oncol.* 2013;108(3):362-369. doi:10.1016/j.radonc.2013.06.013
617. Maréchal A, Zou L. DNA damage sensing by the ATM and ATR kinases. *Cold Spring Harb Perspect Biol.* 2013;5(9):a012716. Published 2013 Sep 1. doi:10.1101/cshperspect.a012716
618. Sahu RP, Batra S, Srivastava SK. Activation of ATM/Chk1 by curcumin causes cell cycle arrest and apoptosis in human pancreatic cancer cells. *Br J Cancer*. 2009;100(9):1425-1433. doi:10.1038/sj.bjc.6605039
619. Cremona CA, Behrens A. ATM signalling and cancer. *Oncogene.* 2014;33(26):3351-3360. doi:10.1038/onc.2013.275
620. Savitsky K, Bar-Shira A, Gilad S, et al. A single ataxia telangiectasia gene with a product similar to PI-3 kinase. *Science.* 1995;268(5218):1749-1753. doi:10.1126/science.7792600
621. Du Y, Sun H, Lux F, et al. Radiosensitization Effect of AGuIX, a Gadolinium-Based Nanoparticle, in Nonsmall Cell Lung Cancer. *ACS Appl Mater Interfaces*. 2020;12(51):56874-56885. doi:10.1021/acsami.0c16548
622. Pradhan AK, Nahar SN, Montenegro M, et al. Resonant X-ray enhancement of the Auger effect in high-Z atoms, molecules, and nanoparticles: potential biomedical applications. *J Phys Chem A.* 2009;113(45):12356-12363. doi:10.1021/jp904977z
623. Weiss M, Blazek K, Byrne AJ, Perocheau DP, Udalova IA. IRF5 is a specific marker of inflammatory macrophages in vivo. *Mediators Inflamm.* 2013;2013:245804. doi:10.1155/2013/245804

624. Miao X, Leng X, Zhang Q. The Current State of Nanoparticle-Induced Macrophage Polarization and Reprogramming Research. *Int J Mol Sci.* 2017;18(2):336. Published 2017 Feb 6. doi:10.3390/ijms18020336

625. Yen HJ, Hsu SH, Tsai CL. Cytotoxicity and immunological response of gold and silver nanoparticles of different sizes. *Small*. 2009;5(13):1553-1561. doi:10.1002/smll.200900126

626. Hashimoto M, Toshima H, Yonezawa T, et al. Responses of RAW264.7 macrophages to water-dispersible gold and silver nanoparticles stabilized by metal-carbon σ-bonds. *J Biomed Mater Res A.* 2014;102(6):1838-1849. doi:10.1002/jbm.a.34854

627. Giovanni M, Yue J, Zhang L, Xie J, Ong CN, Leong DT. Pro-inflammatory responses of RAW264.7 macrophages when treated with ultralow concentrations of silver, titanium dioxide, and zinc oxide nanoparticles. *J Hazard Mater*. 2015;297:146-152. doi:10.1016/j.jhazmat.2015.04.081

628. Friedman JR, Nunnari J. Mitochondrial form and function. *Nature*. 2014;505(7483):335-343. doi:10.1038/nature12985

629. Otera H, Wang C, Cleland MM, et al. Mff is an essential factor for mitochondrial recruitment of Drp1 during mitochondrial fission in mammalian cells. *J Cell Biol*. 2010;191(6):1141-1158. doi:10.1083/jcb.201007152

630. Toyama EQ, Herzig S, Courchet J, et al. Metabolism. AMP-activated protein kinase mediates mitochondrial fission in response to energy stress. *Science*. 2016;351(6270):275-281. doi:10.1126/science.aab4138

631. Mihaylova MM, Shaw RJ. The AMPK signalling pathway coordinates cell growth, autophagy and metabolism. *Nat Cell Biol.* 2011;13(9):1016-1023. Published 2011 Sep 2. doi:10.1038/ncb2329

632. Stein SC, Woods A, Jones NA, Davison MD, Carling D. The regulation of AMP-activated protein kinase by phosphorylation. *Biochem J.* 2000;345 Pt 3(Pt 3):437-443. doi:10.1042/0264-6021:3450437

633. Jin X, Li F, Liu B, et al. Different mitochondrial fragmentation after irradiation with X-rays and carbon ions in HeLa cells and its influence on cellular apoptosis. *Biochem Biophys Res Commun*. 2018;500(4):958-965. doi:10.1016/j.bbrc.2018.04.214

634. Zhang B, Davidson MM, Zhou H, Wang C, Walker WF, Hei TK. Cytoplasmic irradiation results in mitochondrial dysfunction and DRP1-dependent mitochondrial fission. *Cancer Res*. 2013;73(22):6700-6710. doi:10.1158/0008-5472.CAN-13-1411

635. Jugé R, Breugnot J, Da Silva C, Bordes S, Closs B, Aouacheria A. Quantification and

Characterization of UVB-Induced Mitochondrial Fragmentation in Normal Primary Human Keratinocytes. *Sci Rep.* 2016;6:35065. Published 2016 Oct 12. doi:10.1038/srep35065

636. Sanli T, Storozhuk Y, Linher-Melville K, et al. Ionizing radiation regulates the expression of AMP-activated protein kinase (AMPK) in epithelial cancer cells: Modulation of cellular signals regulating cell cycle and survival. *Radiother Oncol*. 2012;102(3):459-465. doi:10.1016/j.radonc.2011.11.014
637. Zhao H, Chen L, Zhong G, et al. Titanium dioxide nanoparticles induce mitochondrial dynamic imbalance and damage in HT22 cells. *J Nanomater*. 2019;2019. doi:10.1155/2019/4607531
638. Huang H, Zhou M, Ruan L, et al. AMPK mediates the neurotoxicity of iron oxide nanoparticles retained in mitochondria or lysosomes. *Metallomics*. 2019;11(7):1200-1206. doi:10.1039/c9mt00103d
639. Li L, Li L, Zhou X, et al. Silver nanoparticles induce protective autophagy via Ca^{2+}/CaMKKβ/AMPK/mTOR pathway in SH-SY5Y cells and rat brains. *Nanotoxicology*. 2019;13(3):369-391. doi:10.1080/17435390.2018.1550226
640. Gao F, Reynolds MB, Passalacqua KD, Sexton JZ, Abuaita BH, O'Riordan MXD. The Mitochondrial Fission Regulator DRP1 Controls Post-Transcriptional Regulation of TNF-α. *Front Cell Infect Microbiol.* 2021;10:593805. Published 2021 Jan 14. doi:10.3389/fcimb.2020.593805
641. Qiu S, Liu T, Piao C, et al. AMPKα2 knockout enhances tumour inflammation through exacerbated liver injury and energy deprivation-associated AMPKα1 activation. *J Cell Mol Med*. 2019;23(3):1687-1697. doi:10.1111/jcmm.13978
642. Mounier R, Théret M, Arnold L, et al. AMPKα1 regulates macrophage skewing at the time of resolution of inflammation during skeletal muscle regeneration. *Cell Metab*. 2013;18(2):251-264. doi:10.1016/j.cmet.2013.06.017
643. Sanli T, Rashid A, Liu C, et al. Ionizing radiation activates AMP-activated kinase (AMPK): A target for radiosensitization of human cancer cells. *Int J Radiat Oncol Biol Phys*. 2010;78(1):221-229. doi:10.1016/j.ijrobp.2010.03.005
644. Hawley SA, Boudeau J, Reid JL, et al. Complexes between the LKB1 tumor suppressor, STRADα/β and MO25α/β are upstream kinases in the AMP-activated protein kinase cascade. *J Biol*. 2003;2(4):1-16. doi:10.1186/1475-4924-2-28
645. Woods A, Dickerson K, Heath R, et al. Ca2+/calmodulin-dependent protein kinase kinase-β acts upstream of AMP-activated protein kinase in mammalian cells. *Cell*

Metab. 2005;2(1):21-33. doi:10.1016/j.cmet.2005.06.005

646. Zhang CS, Lin SC. AMPK promotes autophagy by facilitating mitochondrial fission. *Cell Metab*. 2016;23(3):399-401. doi:10.1016/j.cmet.2016.02.017
647. Deniaud A, Sharaf El Dein O, Maillier E, et al. Endoplasmic reticulum stress induces calcium-dependent permeability transition, mitochondrial outer membrane permeabilization and apoptosis. *Oncogene*. 2008;27(3):285-299. doi:10.1038/sj.onc.1210638
648. Tsai YY, Huang YH, Chao YL, et al. Identification of the nanogold particle-induced endoplasmic reticulum stress by omic techniques and systems biology analysis. *ACS Nano*. 2011;5(12):9354-9369. doi:10.1021/nn2027775
649. Christen V, Capelle M, Fent K. Silver nanoparticles induce endoplasmatic reticulum stress response in zebrafish. *Toxicol Appl Pharmacol*. 2013;272(2):519-528. doi:10.1016/j.taap.2013.06.011
650. Yang X, Shao H, Liu W, et al. Endoplasmic reticulum stress and oxidative stress are involved in ZnO nanoparticle-induced hepatotoxicity. *Toxicol Lett*. 2015;234(1):40-49. doi:10.1016/j.toxlet.2015.02.004
651. Liu Y, Zhang P, Li F, et al. Metal-based NanoEnhancers for Future Radiotherapy: Radiosensitizing and Synergistic Effects on Tumor Cells. *Theranostics*. 2018;8(7):1824-1849. Published 2018 Feb 12. doi:10.7150/thno.22172
652. Khan AA, Allemailem KS, Almatroudi A, et al. Endoplasmic Reticulum Stress Provocation by Different Nanoparticles: An Innovative Approach to Manage the Cancer and Other Common Diseases. *Molecules.* 2020;25(22):5336. Published 2020 Nov 16. doi:10.3390/molecules25225336
653. Kim J, Yang G, Kim Y, Kim J, Ha J. AMPK activators: mechanisms of action and physiological activities. *Exp Mol Med.* 2016;48(4):e224. Published 2016 Apr 1. doi:10.1038/emm.2016.16
654. Owen MR, Doran E, Halestrap AP. Evidence that metformin exerts its anti-diabetic effects through inhibition of complex 1 of the mitochondrial respiratory chain. *Biochem J*. 2000;348 Pt 3(Pt 3):607-614.
655. Brunmair B, Staniek K, Gras F, et al. Thiazolidinediones, like metformin, inhibit respiratory complex I: a common mechanism contributing to their antidiabetic actions?. *Diabetes.* 2004;53(4):1052-1059. doi:10.2337/diabetes.53.4.1052
656. Lee AJ. Metformin in noninsulin-dependent diabetes mellitus. *Pharmacotherapy*. 1996;16(3):327-351.

657. Costa CS, Ronconi JVV, Daufenbach JF, et al. In vitro effects of silver nanoparticles on the mitochondrial respiratory chain. *Mol Cell Biochem*. 2010;342(1-2):51-56. doi:10.1007/s11010-010-0467-9

658. Gallud A, Klöditz K, Ytterberg J, et al. Cationic gold nanoparticles elicit mitochondrial dysfunction: a multi-omics study. *Sci Rep.* 2019;9(1):4366. Published 2019 Mar 13. doi:10.1038/s41598-019-40579-6

659. Bianchi A, Dufort S, Lux F, et al. Targeting and in vivo imaging of non-small-cell lung cancer using nebulized multimodal contrast agents. *Proc Natl Acad Sci U S A*. 2014;111(25):9247-9252. doi:10.1073/pnas.1402196111

660. Martinez FO, Gordon S. The M1 and M2 paradigm of macrophage activation: time for reassessment. *F1000Prime Rep.* 2014;6:13. Published 2014 Mar 3. doi:10.12703/P6-13

661. Kohli K, Pillarisetty VG, Kim TS. Key chemokines direct migration of immune cells in solid tumors [published online ahead of print, 2021 Feb 18]. *Cancer Gene Ther.* 2021;10.1038/s41417-021-00303-x. doi:10.1038/s41417-021-00303-x

662. Duan Q, Zhang H, Zheng J, Zhang L. Turning Cold into Hot: Firing up the Tumor Microenvironment. *Trends Cancer.* 2020;6(7):605-618. doi:10.1016/j.trecan.2020.02.022

663. Garrido-Martin EM, Mellows TWP, Clarke J, et al. M1hot tumor-associated macrophages boost tissue-resident memory T cells infiltration and survival in human lung cancer. *J Immunother Cancer.* 2020;8(2):e000778. doi:10.1136/jitc-2020-000778

664. Menares E, Gálvez-Cancino F, Cáceres-Morgado P, et al. Tissue-resident memory $CD8^+$ T cells amplify anti-tumor immunity by triggering antigen spreading through dendritic cells. *Nat Commun.* 2019;10(1):4401. Published 2019 Sep 27. doi:10.1038/s41467-019-12319-x

665. Shi J, Hua L, Harmer D, Li P, Ren G. Cre driver mice targeting macrophages. *Methods Mol Biol*. 2018;1784(1):263-275. doi:10.1007/978-1-4939-7837-3_24

666. Kim H, Kim M, Im SK, Fang S. Mouse Cre-LoxP system: general principles to determine tissue-specific roles of target genes. *Lab Anim Res.* 2018;34(4):147-159. doi:10.5625/lar.2018.34.4.147